Characterisation of UVA-induced DNA damage responses in human skin cells

A thesis presented to the National University of Ireland, Galway,
for the degree of Doctor of Philosophy

by

Sarah Angela Conmy, BSc.

DNA Damage Response laboratory,
Centre for Chromosome Biology,
School of Natural Science, Biochemistry,
National University of Ireland, Galway.

Head of School: Prof. Vincent O'Flaherty
Head of Biochemistry Discipline: Dr. Michael P. Carty
Supervisor: Dr. Michael P. Carty

September 2013

Acknowledgements

First and foremost I want to thank my research supervisor Dr. Michael Carty for his support, guidance and encouragement over the past four years-through the ups and downs of research. I have learned a lot, and for that I am grateful.

To the DDR girls who have gone before me-Ania, Severine, Kathleen, Aine and Mitra for all your help, scientific and otherwise! For making the lab an enjoyable place to work, for teas and tears and laughs and hugs! A special thank you to my partner in crime, Ania-a true friend for life. To the girls next door, my surrogate lab-Laura, Reka, Jennifer and Rola for all the fun times. To Laura-a look is all it takes! And to the 'winesday' gang, for distractions on the hard days and celebrations on the good!

I sincerely want to thank my parents, if it was not for their encouragement and support I would not be the person I am today.

Mostly I want to thank my better half, Damien. For supporting me in every way. For the sacrifices he has made for me. For his tolerance, and mostly his love. It is done! Our life starts now…

Table of Contents

Thesis structure and declaration of contributions

Thesis structure

This thesis is presented in monograph format. It consists of an extensive literature review (Chapter 1: Introduction), followed by research objectives, and a methodology chapter (Chapter 2: Materials and Methods). Two independent results chapters are presented. The first results chapter (Chapter 3) is presented in manuscript format, with a view for submission to a peer-reviewed journal. This chapter includes a short introduction, followed by results and discussion. Supplementary information relating to the manuscript is also included in Chapter 3. The second results chapter (Chapter 4) is presented in monograph format, and includes results presented in sequential order and a discussion. The results chapters are followed by a concluding chapter (Chapter 5), which includes a general discussion, a summary of the findings presented in this research thesis, and outlines future directions. References related to all five chapters are presented in one bibliography (Chapter 6).

Declaration of contributions

I declare that I have not obtained a previous qualification from the National University of Ireland, Galway, or any other institution, based on the work presented in this thesis. I conducted the research presented here, and wrote this thesis under the supervision of Dr. Michael P. Carty.

Abbreviations

α-MSH	alpha melanocyte-stimulating hormone
4-OHT	4-hydroxytamoxifen
53BP1	p53 binding protein-1
6, 4-PP	Pyrimidine (6-4) pyrimidine photoproduct
8-oxo-G	8-oxo-7, 8-dihydro-2'-deoxyguanosine
ADP	Adenosine diphosphate
AH2	Annealing helicase 2
ANOVA	Analysis of variance
AP	Apurinic/apyrimidinic (abasic) site
APC/C	Anaphase-promoting complex/cyclosome
AT	Ataxia telangiectasia
ATM	Ataxia telangiectasia mutated
ATR	Ataxia telangiectasia mutated and Rad3-related
ATRIP	ATR-interacting protein
BCC	Basal cell carcinoma
Bcl-2	B cell lymphoma 2 protein
BER	Base excision repair
BRCA1	Breast cancer type 1 susceptibility protein
BRCT	BRCA1 C Terminus domain
BrdU	5-Bromo-2'-deoxyuridine
BSA	Bovine serum albumin
Cdc	Cell division cycle protein
CDK	Cyclin-dependent kinase
Chk1	Checkpoint kinase 1
Chk2	Checkpoint kinase 2
CIN	Chromosomal instability
CKI	CDK-inhibitor protein
CPD	Cyclobutane pyrimidine dimers
CTLA-4	Cytotoxic T-Lymphocyte Antigen 4
DAPI	4, 6 diamidino-2-phenylindole
DCF	2', 7'-dichlorofluorescin
DCFH-DA	2', 7'-dichlorofluroescein diacetate

dCMP	Deoxycytidine monophosphate
DDR	DNA damage response
DMSO	Dimethyl sulfoxide
DNA	Deoxyribonucleic acid
DNA-PK	DNA-dependent protein kinase
dNTP	deoxyribonucleotide triphosphate
DSB	Double strand break
DSE	Double strand end
DT	Delayed tanning
E2F	E2F transcription factor family
EDTA	Ethylenediaminetetraacetic acid
EdU	5-Ethynyl-2'-deoxyuridine
ERCC1	Excision Repair Cross-Complementing Rodent Repair Deficiency protein 1
ERK	Extracellular signal-regulated kinase
ET-1	Endothelian-1
FA	Fanconi anemia
FBH1	F-box DNA helicase 1
FBS	Foetal bovine serum
FITC	Fluorescein iso-thiocyanate
GAPDH	Glyceraldehyde 3-phosphate dehydrogenase
GFP	Green fluorescent protein
GGR	Global genome repair
Gy	Gray (SI unit of absorbed radiation)
H2AX	Histone protein family H2A, member X
hMOF	Males-absent on the first protein
HR	Homologous recombination
HRP	Horse radish peroxidise
HU	Hydroxyurea
IARC	International Agency for Research on Cancer
Il-2	Interleukin 2
IPD	Immediate pigment darkening
IR	Ionising radiation
MAPK	Mitogen-activated protein kinase

MCC	Mitotic checkpoint complex
MCM	Minchromosome maintenance 2
MCR-1	Melanocortin receptor 1
MDC1	Mediator of DNA damage checkpoint protein-1
MDM-2	Mouse double minute 2 homolog
MED	Minimal erythemal dose
MEF	Mouse embryonic fibroblast
MEK	Mitogen-activated protein kinase kinase
MIN	Microsatellite instability
Mre11	Meiotic recombination 11
MRN	Mre11-Rad50-Nbs1 protein complex
MSC	Melanocyte stem cell
mTOR	Mammalian target of rapamycin
NAC	*N*-acetly-cysteine
NADPH	Nicotinamide adenine dinucleotide phosphate
NBS	Nijmegen breakage syndrome
Nbs1	Nijmegen breakage syndrome protein 1
NER	Nucleotide excision repair
NHEJ	Non-homologous end joining
NHEM	Normal human epidermal melanocytes
OGG1	8-oxo-G glycosylase
PAF15	PCNA-associated factor 15
PARP	Poly (ADP-ribose) polymerase
PBS	Phosphate-buffered saline
PCNA	Proliferating cell nuclear antigen
PFA	Paraformaldehyde
PI	Propidium iodide
PIKK	Phosphoinositol 3-kinase-like kinase
PIP	PCNA-interacting peptide
PKB	Protein kinase B
PKC	Protein kinase C
PMA	Phorbol 12-Myristate 13-Acetate
PMSF	Phenylmethylsulfonyl fluoride
Polη	Polymerase eta

PP2A	Protein phosphatase 2A
PP5	Protein phosphatase 5
PREX2	Phosphoinositol-3,4,5-triphosphat-dependent RAC exchange factor 1 gene
PTCH	Protein patch homologue gene
PTM	Post-translational modification
PVDF	Polyvinylidene fluoride
RAC1	RAS-related C3 botulinum toxin substrate 1 gene
Raf	Raf proto-oncogene serine/threonine protein kinase
Rb	Retinoblastoma protein
RFC	Replication factor C protein complex
RKIP	Raf-1 kinase inhibitory protein
RNA	Ribonucleic acid
ROS	Reactive oxygen species
RPA	Replication Protein A
SAC	Spindle assembly checkpoint
SCC	Squamous cell carcinoma
SDS-PAGE	Sodium dodecyl sulphate polyacrylamide gel electrophoresis
SED	Standard erythemal dose
SMARCAL1	SWI/SNF-related matrix-associated actin-dependent regulator of chromatin subfamily A-like protein 1
SMG1	Suppressor with morphological effect on genitalia family member
SSB	Single strand break
ssDNA	Single stranded deoxyribonucleic acid
SV40	Simian virus 40
TBS	Tris buffered saline
TCR	Transcription coupled repair
Tip60	Tat-interactive protein 60 kDa
TIPIN	Timeless interacting protein
TLS	Translesion synthesis
TopBP1	Topoisomerase-II binding protein 1
TP53	p53 tumour suppressor gene
TRITC	Tetramethylrhodamine

TRP1	Tyrosinase-related protein 1
TRP2	Tyrosinase-related protein 2
TRRAP	Transformation/transcription domain-associated protein
Ub	Ubiquitin
UBM	Ubiquitin-binding motif
UBZ	Ubiquitin-binding zinc finger
USP1	Ubiquitin carboxyl-terminal hydrolase 1
UV	Ultraviolet radiation
WRN	Werner syndrome protein
XP	Xeroderma pigmentosum
XPA	Xeroderma pigmentosum group A protein
XPV	Xeroderma pigmentosum variant
XRCC4	X-ray repair cross-complementing protein 4

Abstract

Accumulating evidence indicates that exposure to long-wavelength ultraviolet A (UVA) radiation (315-400 nm), which accounts for >95% of solar UV radiation reaching the earth's surface, is a significant risk factor for the development of skin cancer, particularly melanoma. While it is well established that UVA radiation induces DNA damage, including cyclobutane pyrimidine dimers (CPDs) and 8-oxoguanosine (8-oxo-G) lesions, the response of cells to UVA-induced DNA damage is not well characterised on a molecular level. This research characterised UVA radiation-induced DNA damage response (DDR) pathways in human skin cells, including primary human melanocytes.

DNA polymerase eta (polη) is a specialised translesion synthesis polymerase which carries out error-free replication past UVC-induced dithymidine CPDs *in vitro* and *in vivo.* The data presented here provides evidence that polη plays a role in the replication of UVA-damaged DNA in human fibroblasts. Polη was localised to discrete nuclear foci following UVA exposure, exclusively in cells undergoing DNA replication. UVA exposure induced a rapid and transient decrease in DNA replication. Polη-deficient cells showed delayed recovery from UVA-induced replication arrest, and enhanced phosphorylation of checkpoint kinase 1 (Chk1). Moreover, polη-deficient cells were hypersensitive to UVA radiation in the presence of caffeine, an inhibitor of phosphoinositol 3-kinase-like kinase (PIKK)-dependent Chk1 phosphorylation. This indicates that in the absence of polη, the Chk1 pathway plays an important role in the response of cells to UVA radiation. Overall, the data provides evidence that tolerance of UVA-induced DNA damage is mediated, in part, by polη. This highlights the importance for UVA protection, especially in individuals with the xeroderma pigmentosum variant disease, lacking polη.

Exposure to UVA radiation is a specific risk factor in the development of melanoma, which arises from malignant transformation of melanocytes. However, the molecular mechanisms linking UVA exposure and melanoma development remain unclear. Here the responses of primary normal human

epidermal melanocytes (NHEM) to UVA-irradiation were characterised. UVA radiation induced PIKK-mediated DNA damage responses in NHEM, including activation of both the ATR-Chk1 and ATM-Chk2 pathways. Moreover, a key role was identified for Chk1 in the regulation of DNA replication in UVA-irradiated primary human melanocytes. Using a phospho-proteomic screen, UVA-induced alterations in the phosphorylation status of proteins involved in a number of signalling pathways, including CDK-mediated cell cycle regulation, the mitogen activated Raf-MEK-ERK pathway and the cytoskeleton-associated PKC-α-adducin pathway, were identified. This research provides insights into the cellular pathways that normally modulate the response of primary human melanocytes to UVA radiation.

1 Introduction

1.1 Cancer

Cancer is the leading cause of death worldwide, accounting for 13% of all deaths worldwide in 2008 (IARC, 2010). In 2010, Ireland had the fifth highest rate of cancer incidence in Europe, with a 56% increase in cancer rates observed between 1994 and 2010 (NCRI, 2013a). Cancer is a disease of uncontrolled cell proliferation, and arises from cells which evade the tightly regulated mechanisms controlling normal cell proliferation. Uncontrolled cell growth and division gives rise to tumours, which can be classed as benign or malignant. Malignant tumours represent a class of tumours with the capability of invading neighbouring tissues or metastasising to remote tissues, via the blood and lymph systems, and thus represent a significant health risk. Benign tumours are generally lower risk, due to lack of metastasis. Underlying cancer formation are genetic abnormalities which can be inherited or arise sporadically, resulting in inactivation of tumour suppressor genes or activation of oncogenes (Cahill et al., 1999).

Exposures to agents which damage DNA increase the risk of cancer development, by increasing the probability of mutation formation at the sites of DNA damage. Exposure to solar UV radiation is the major risk factor in the development of skin cancer, and represents one of the most well defined causative links between exposure to an environmental agent and cancer development. Skin cancer is the most common cancer diagnosed worldwide, accounting for 29% and 31% of all cancers in women and men respectively (NCRI, 2013a).

1.1.1 General characteristics of cancer

The complexity of cancer stems from the diverse forms it takes and the anatomical locations in which it can arise. However, even the most heterogeneous cancers have certain common characteristics. Six common characteristics of cancers were first defined in 2000 in a seminal review by Hanahan and Weinberg, in which they proposed six physiological capabilities of cancer cells, coined the six ‘hallmarks of cancer’, which allow cancer cells to evade the processes controlling normal cell growth

(Hanahan and Weinberg, 2000). The six hallmarks of cancer were defined as (i) self-sufficiency in growth signals, (ii) evasion of growth-inhibitory signals, (iii) resistance to cell death, (iv) limitless replicative potential, (v) sustained angiogenesis and (vi) invasion and metastasis (Hanahan and Weinberg, 2000). Following on from this ground breaking paper, in 2011 Hanahan and Weinberg updated the view of common cancer characteristics, based on the plethora of cancer research that had occurred in the intervening decade. They defined two more emerging hallmarks of cancer: (i) evasion of immune destruction and (ii) deregulation of cellular energetics (Hanahan and Weinberg, 2011). Furthermore, emphasis was placed on two enabling characteristics of cancer cells, which allow the hallmarks to come to fruition, namely: (i) the underlying genetic instability of cancer cells and (ii) tumour-associated inflammation (Hanahan and Weinberg, 2011). The work has provided an important framework to understand the links between molecular events and cancer pathology.

1.1.2 Genomic instability

Genomic instability is considered central and essential for cancer development (Cahill et al., 1999). Genomic instability has many distinct forms, including chromosomal instability (CIN), which encompasses alterations in chromosome number or structure, and microsatellite instability (MIN), which refers to changes in the nucleotide sequence. CIN is a common feature of solid tumours (Lengauer et al., 1998), resulting from chromosomal mis-segregation and recombination (Cahill et al., 1999; Shivji and Venkitaraman, 2004), recently DNA replication stress has been implicated as a driving force for CIN (Burrell et al., 2013). Defective mismatch repair and homologous recombination give rise to MIN (Cahill et al., 1999; Vo et al., 2005), a common feature of colorectal cancers (Vilar and Gruber, 2010).

As early as 1974 Loeb *et al.* proposed that errors in DNA replication could be responsible for the genomic instability associated with a malignant phenotype, and that an accumulation of replication errors in DNA resulted in malignant progression (Loeb et al., 1974). Since the spontaneous error

rate of replicative polymerases is not sufficient to account for the error rate observed in cancer cells, in 1991 Loeb proposed the idea of a 'mutator phenotype' in which spontaneous errors occur in genes controlling genome stability, resulting in deregulation of genome stability networks, and the subsequent accumulation of mutations as observed in cancer cells (Loeb, 1991). Heritable cancer-prone diseases, with mutations in genes involved in maintaining genome stability (for examples see Table 1.1), support the mutator phenotype hypothesis. Thus, at the root of cancer prevention lays a network of cellular processes aiming to ensure the integrity of the genome.

Table 1.1 Examples of inherited cancer-prone genetic syndromes (adapted from Ciccia and Elledge, (2010)).

Syndrome	Mutated gene(s)	Defective genome stability process	Common cancer(s)
Xeroderma pigmentosum (XP)	*XPA-XPG*	Nucleotide excision repair	Skin cancer
Xeroderma pigmentosum variant (XPV)	*POLH*	Translesion synthesis	Skin cancer
Ataxia telangiectasia (AT)	*ATM*	DSB repair, DDR signalling	Lymphomas, leukaemia
Nijmegen breakage syndrome (NBS)	*NBS1*	DSB repair	B cell lymphoma
Familial breast cancer	*BRCA1/BRCA2*	DSB repair, HR	Breast and ovarian cancer

1.1.3 DNA damage response acts as a barrier to carcinogenesis

The genome is constantly under threat from agents which cause DNA damage, both from endogenous and exogenous sources (Hoeijmakers, 2001). Endogenous sources of DNA damage include replication errors and reactive oxygen species (ROS) produced as a result of cellular respiration. Exogenous sources of DNA damage include ultraviolet (UV) radiation, ionising radiation (IR), and environmental chemicals, such as

benxo[a]pyrene in cigarette smoke and chemotherapeutic agents, including cisplatin.

There are a number of biochemical pathways in cells, collectively called the DNA damage response (DDR; Section 1.7), that counteract the deleterious effects of these DNA damaging agents and are essential to ensure the integrity of the genome. DNA damage is sensed by components of the DDR and this in turn signals the activation DNA repair, inhibition cell cycle progression in the presence of damage or initiation cell death if the damage is too severe (Niida and Nakanishi, 2006; Zhou and Elledge, 2000). In this way the DDR acts as a barrier to the initiation of carcinogenesis by limiting the potential for mutagenesis, the driving force of carcinogenesis (Hanahan and Weinberg, 2011). The importance of the DDR in preventing carcinogenesis is highlighted by the numerous cancer-prone genetic disorders which result from defects in DDR proteins (Table 1.1 and Ciccia and Elledge, (2010)).

As well as acting as a barrier to the initiation of carcinogenesis, the DDR is also activated during the early stages of tumourigenesis, in response to oncogene activation or loss of tumour suppressor genes (Bartek et al., 2007; Bartkova et al., 2005; Gorgoulis et al., 2005). Oncogene-induced replication stress, such as that caused by N-Ras overexpression, is considered the underlying trigger of DDR activation during the early stages of tumourigenesis (Bartkova et al., 2006; Di Micco et al., 2006). Oncogene-induced activation of the DDR can result in oncogene-induced senescence, a permanent state of growth arrest, an alternative barrier to carcinogenesis (Bartkova et al., 2006; Di Micco et al., 2006). It is proposed that DDR activation in early tumourigenesis also creates a selection pressure for cancer cells, favouring the survival of cells which have defects in the genomic maintenance machinery (Bartek et al., 2007). Thus cells with acquired mutations in genes involved in DDR signalling, for example tumour protein p53 gene (*TP53*), escape the constraints of cell cycle checkpoint activation and cell death, resulting in tumour progression (Bartek et al., 2007).

The double-edged sword of the DDR in the prevention of carcinogenesis is that the most common cancer therapies, including IR and chemotherapeutics, act by inducing of DNA damage. Thus, while the DDR acts an effective barrier to carcinogenesis and tumour progression, it also plays a role in the resistance of cells to standard anti-cancer treatments, including radiation and chemotherapy (Bao et al., 2006; Galluzzi et al., 2012). For example, enhanced repair of the DNA damage induced by radiotherapy or chemotherapeutic agents can contribute to the survival and continued proliferation of cancer cells (Zeng-Rong et al., 1995).

1.2 Solar UV radiation and skin cancer

One of the best examples of the relationship between DNA damage and cancer development is that of exposure to solar ultraviolet (UV) radiation and the development of skin cancer. Solar UV radiation is divided in to UVC (200-280 nm), UVB (280-315 nm) and UVA (315-400 nm; see Figure 1.1). Short-wavelength UVC-radiation and UVB wavelengths less than 295 nm are blocked by the atmosphere (Freeman et al., 1989). Thus UV-radiation reaching the earth's surface is composed of approximately 95% long-wavelength UVA radiation and 5% UVB radiation (Nunez et al., 1994) (Figure 1.1). The exact proportions of UV-radiation are dependent on a number of factors, including ozone composition, latitude, time of day and cloud cover, but generally there is proportionally more UVA at higher latitudes and in winter (Lubin and Jensen, 1995).

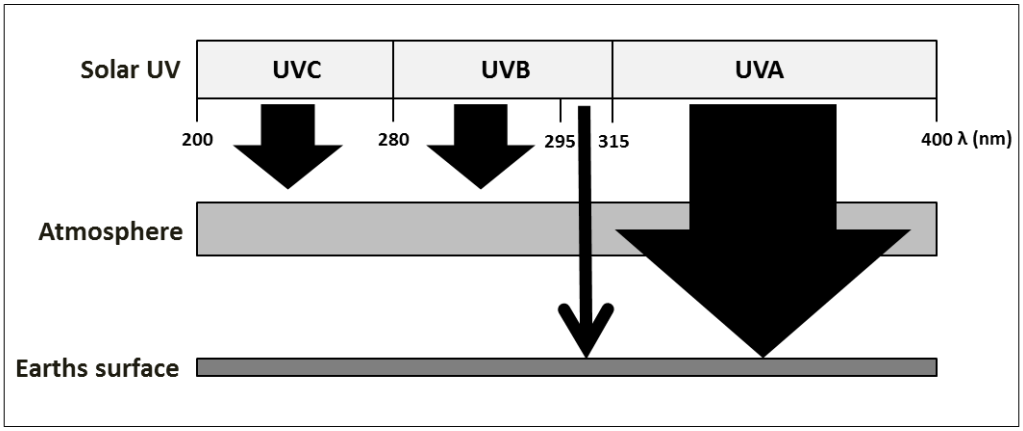

Figure 1.1 UV-radiation spectrum and transmission through the earths' atmosphere.

Exposure to solar UV radiation is the major risk factor for the development of skin cancer, the most common cancer in Ireland, with on average 6,899 cases of skin cancer diagnosed annually (NCRI, 2013a). Skin cancer is divided into two main subtypes: (i) non-melanoma, which includes squamous cell carcinoma (SCC) and basal cell carcinoma (BCC), and (ii) melanoma. SCC and BCC are keratinocyte derived cancers, while melanoma is derived from the malignant transformation of melanocytes (Section 1.6).

The molecular mechanisms linking exposure to short-wavelength UVB-radiation and the induction of non-melanoma skin cancers are quite well defined (Tornaletti and Pfeifer, 1996). UVB radiation is directly absorbed by the DNA bases, inducing the formation of DNA lesions (Piette et al., 1986). The primary UVB (and UVC)-induced lesions are cyclobutane pyrimidine dimers (CPDs), formed by the covalent attachment of two adjacent pyrimidines through saturation the 5,6 double bonds, and pyrimidine (6-4) pyrimidone photoproducts (6,4-PPs), formed by a covalent linkage between the 5,6 double bond of one pyrimidine and carbon 4 of the adjacent pyrimidine (Figure 1.2). Both CPDs and 6,4-PPs are mutagenic, with CPDs considered the primary mutagenic lesion, due to the efficient repair of 6,4-PPs (You et al., 2001). Error-prone replication past UV-induced CPDs results in the generation of C-T and CC-TT transition mutations, considered 'UV signature mutations' (Wikonkal and Brash, 1999). UV signature mutations are found in the p53 gene in the majority of non-melanoma skin cancers (Brash et al., 1991; Ziegler et al., 1993). Moreover, mutations in the *p53* gene in UV-induced carcinomas in mice were found to be UV signature mutations (Rebel et al., 2005). The important contribution of UV photoproducts to skin carcinogenesis is highlighted by the high prevalence of UV signature mutations in the *TP53* and *PTCH* genes of BCCs from XP individuals (D'Errico et al., 2000), who have defects in the repair of UV-induced photoproducts (see Section 1.10.1).

1.2.1 Units of UV radiation dose

The biological effects of UV radiation are dependent on both the quantity (dose) and quality (wavelength) of exposure. The biological effects of the different UV wavelengths will be discussed in Section 1.4. Here, the various units used to express quantities of UV radiation will be outlined.

Irradiance is the unit used to describe the amount of UV radiation emitted by a UV source, and is a measure of the power of UV radiation per unit of area incident on a surface, expressed in watt per meter squared (W/m^2). Calculated from irradiance, given that 1 W/m^2 is equal to 1 J/m^2/sec, is the radiant exposure, more commonly referred to as the dose rate, expressed in joules per meter squared (J/m^2), which takes into account the time required to achieve a quantity of irradiance from a given source (Diffey, 2002).

Biologically relevant UV radiation doses are often expressed as minimal erythemal dose (MED) or standard erythemal dose (SED), which are weighted UV doses capable of inducing an erythemal (skin reddening) response (IARC, 2005; Lucas et al., 2006). MED refers to the UV dose required to produce qualifying erythema in individuals of a specified skin type. Definition of the exact UV dose equal to 1 MED are complicated by inconsistencies in (i) the definition of erythema, as being either just-perceptible reddening or uniform redness, and (ii) the definition of skin type (see Section 1.5.1 for explanation of human skin types). One MED is approximately equal to 200 J/m^2 of biologically effective UV radiation, for an individual with skin type I (Lucas et al., 2006). To overcome the inconsistencies in MED measurements, one SED was defined as being equivalent to 100 J/m^2 of biologically effective UV radiation, and is independent of skin type (CIE Standard, 1998).

In this study the dose rate of the broadband UVA source used is expressed in kJ/m^2. An important consideration when choosing the UVA dose at which to measure cellular responses is to choose a biologically relevant dose. 75-300 kJ/m^2 UVA-radiation utilised in this study is approximately

equivalent to 25-100 minutes of mid-day sun exposure in Paris (Kuluncsics et al., 1999).

1.3 UVA radiation-induced DNA damage

While the contribution of UVB to skin carcinogenesis is relatively well defined, and is dependent on the induction of pre-mutagenic UV DNA lesions (de Gruijl et al., 2001), the role of exposure to long-wavelength UVA radiation in the induction of skin cancer is still a matter of intense debate, which stems in part from inconsistencies in the literature regarding the types of DNA damage induced by UVA radiation (Runger and Kappes, 2008). The maximal absorption of UV radiation by the DNA occurs at 300 nm, within the UVB region of the spectrum (Freeman et al., 1989). Until recently, UVA was not thought to significantly contribute to the carcinogenic effects of solar UV-exposure, since radiation in the UVA range is weakly absorbed by DNA (Girard et al., 2011). However, UVA-radiation is readily absorbed by other cellular chromophores, generating reactive oxidative species (ROS), including singlet oxygen and hydrogen peroxide (Wondrak et al., 2006). ROS, in particular singlet oxygen, can interact with DNA, primarily with guanine bases, resulting in the formation of oxidative DNA lesions, including 8-oxo-7,8-dihydro-2'-deoxyguanosine (8-oxo-G; Figure 1.2; Cadet et al., 2009). Thus, the genotoxic effects of UVA radiation were generally attributed to the induction of oxidative stress and oxidative DNA damage.

However, as early as 1973, Tyrell described the induction of CPDs in bacterial DNA following exposure to UVA (365 nm) radiation, with dithymidine dimers being the most common CPD formed (Tyrrell, 1973). More recently, there has been a surge in the number of studies focused on characterising the types of UVA-induced DNA damage. This was brought about in part by a number of publications in the early 2000's from the Cadet laboratory (Grenoble, France), describing a novel HPLC tandem mass spectrometry approach to directly quantify UV-induced photoproducts (Douki and Cadet, 2001; Douki et al., 2000). Using this sensitive HPLC tandem mass spectrometry approach, along with DNA immunoblotting

using lesion specific antibodies, UVA-induced CPDs have been detected in cultured mammalian cells and in human skin (Courdavault et al., 2004; Douki et al., 2003; Mouret et al., 2006; Perdiz et al., 2000; Rochette et al., 2003). UVA-induced CPDs predominantly form at TT sites (Douki et al., 2003; Mouret et al., 2006; Rochette et al., 2003). UVA-induced CPDs at TC and CT sites were also detected in cultured mammalian cells and whole human skin, but to a much lesser extent than TT CPDs (Douki et al., 2003; Mouret et al., 2006). Other photoproducts, including CC CPDs, 6, 4-PPs or Dewar valence isomers, were not detected following UVA exposure in these studies. However, studies employing anti-6,4-PP antibodies have reported the induction of 6,4-PPs in UVA-irradiated DNA and NER-deficient mammalian cells, albeit at a much reduced level (approximately 30 times less per kJ/m^2) compared to UVA-induced CPDs (Cortat et al., 2013; Schuch et al., 2009). While UVA induces CPDs, UVC and UVB radiation are 10^5 and 10^3 times more efficient on a per joule basis, respectively, at inducing DNA photoproducts compared to long-wavelength UVA radiation (Perdiz et al., 2000).

Due to the low absorption of UVA by DNA, there is some debate as to whether UVA-induced CPDs occur via direct absorption of UVA or through a photosensitisation mechanism. More recent studies suggest that UVA-induced CPDs occur through a direct photoabsorption of UVA, a conclusion supported by the direct induction of CPDs in UVA-irradiated isolated DNA in the absence of photosensitisers (Jiang et al., 2009; Mouret et al., 2010). Evidence strengthening a direct absorption mechanism comes from the fact that thymidine tracts absorb UVA radiation more readily when present in double-stranded DNA (dsDNA) rather than in single-stranded DNA (ssDNA; Mouret et al., 2010). Regardless of the mechanism, CPDs are the most common type of UVA-induced DNA damage (Douki et al., 2003; Mouret et al., 2006; Rochette et al., 2003). Moreover, CPDs and 8-oxo-G lesions are induced by UVA at a ratio of 10:3 in mammalian cells, suggesting that CPDs are more prominent than 8-oxo-G lesions (Douki et al., 2003). Other types of DNA damage detected following UVA exposure

include oxidised purines, oxidised pyrimidines, single strand breaks (SSBs), abasic sites and DNA-protein crosslinks (Girard et al., 2011).

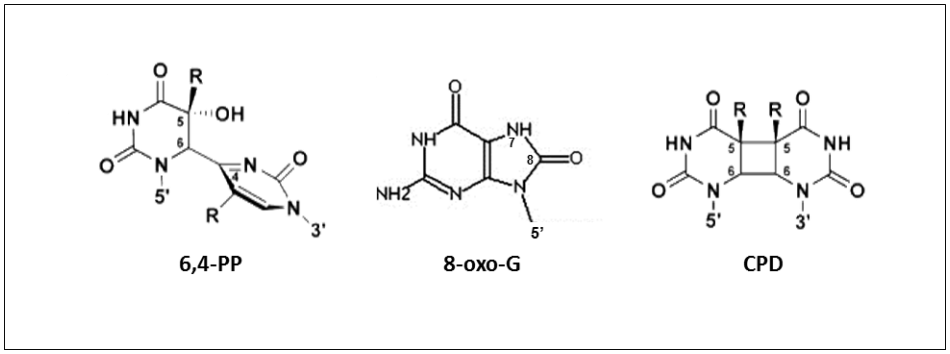

Figure 1.2 Chemical structures of the major UV-induced DNA lesions. Cyclobutane pyrimidine dimer (CPD), 8-oxo-7,8-dihydro-2'-deoxyguanosine (8-oxo-G) and pyrimidine (4–6) pyrimidone photoproduct (6,4-PP). R = H on the cytosine residue, or CH_3 on the thymidine residue. 5' and 3' represent site of attachment of the 5' and 3' bases respectively to the sugar-phosphate backbone of DNA. (Adapted from Li et al., 2006).

1.4 UVA radiation: a risk factor for skin carcinogenesis

The generally accepted model of skin carcinogenesis is based on the induction of DNA photoproducts following exposure to UV radiation. Mutations at the sites of these lesions, in particular when occurring in tumour suppressor genes or oncogenes, results in malignant transformation and skin carcinogenesis (Runger, 2007). Since short-wavelength UVB radiation is more efficient in inducing DNA damage than UVA, UVB was considered to be the primary inducer of skin cancer, particularly non-melanoma sub-types. However, based on this model there is also evidence that long-wavelength UVA radiation contributes to the induction of skin cancer. Here the evidence suggesting a general role for UVA radiation in the induction of non-melanoma skin cancer will be highlighted. The role for UVA radiation in melanoma development is discussed in detail in Section 1.6.1.

Supporting a role for UVA exposure in skin carcinogenesis, a study of the wavelength-dependence of skin cancer induction in mice, showed the peak in UV-induced skin cancer to occur following exposure to UVB radiation,

but also found a second smaller yet significant peak in skin cancer induction following exposure to UVA radiation (de Gruijl et al., 1993) and (Figure 1.3). UVA exposure was sufficient to induce squamous cell carcinomas and papillomas in a number if animal studies (de Laat et al., 1997; Kelfkens et al., 1991). Moreover, chronic UVA exposure induced the malignant transformation of human keratinocytes (He et al., 2006).

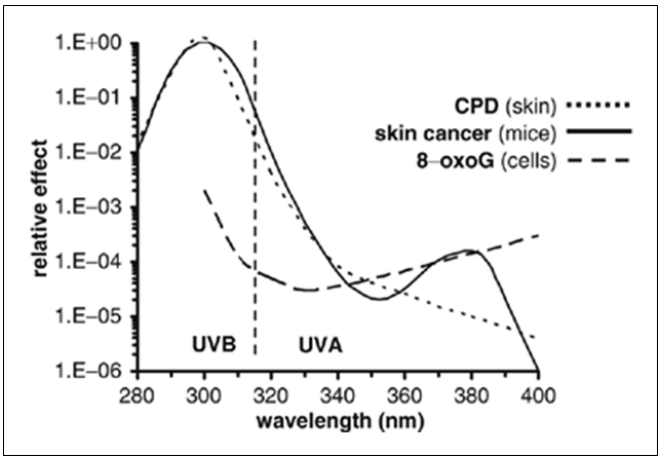

Figure 1.3 Wavelength dependence of UV-induced DNA damage and non-melanoma skin cancers in transgenic mice. A compilation of data from a number of sources shows the wavelength-dependence of UV-induced skin cancers in mice. The wavelength-dependence of UV-induced cyclobutane pyrimidine dimers (CPDs) and 8-oxo-7,8-dihydro-2'-deoxyguanosine (8-oxo-G) lesions are also shown. The vertical dashed line marks the separation of UVB and UVA wavelengths (adapted from Runger and Kappes, 2008).

1.4.1 UVA-induced mutagenesis

As mentioned above, until recently, the genotoxic effect of UVA was attributed to the induction of oxidative DNA lesions, including the most common oxidative DNA lesion 8-oxo-G (Kielbassa et al., 1997). 8-oxo-G, generally gives rise to G-T transversion mutations, as a result of incorporation of adenine opposite the 8-oxo-G, or A-C transversions, as a result of misincorporation of 8-oxo-G opposite an adenine in the template (Cheng et al., 1992). However, the mutation spectrum observed following exposure of mammalian cells to UVA-radiation does not reflect a role for 8-

oxo-G in UVA mutagenesis (Drobetsky et al., 1995; Robert et al., 1996). This is supported by studies in mouse embryonic fibroblasts (MEFs) from *OGG1* (8-oxo-G glycosylase gene)-deficient mice, which are defective in base excision repair (BER), the primary pathway in the removal of 8-oxo-G (see Section 1.10.2). *OGG1*-deficinet mice did not have increased mutation frequency following exposure to UVA radiation, suggesting that 8-oxo-G does not significantly contribute to UVA mutagenesis (Kappes and Runger, 2005). This is in contrast to the situation in *ogg1*-deficient yeast, where the mutation rate was increased following UVA exposure (Kozmin et al., 2005). However, organism specific differences in the processing of UVA-induced DNA damage could account for this.

UV photolesions most commonly give rise to C-T and CC-TT transition mutations, as a consequence of misincorporation of adenine opposite a cytosine of a DNA photolesion. A role for UVA-induced CPDs as a pre-mutagenic UVA-induced DNA lesion is supported by a study in NER-deficient Chinese hamster ovary (CHO) cells, where 65% of UVA-induced mutations detected in the *APRT* locus were C-T transition mutations (Sage et al., 1996), suggesting that in the absence of repair UVA-induced photoproducts are potentially mutagenic. C-T transition mutations were also detected in UVA-exposed NER-proficient CHO cells, but to a lesser extent, accounting for 33% of the total mutations (Sage et al., 1996). Furthermore, UVA and UVB induced a similar mutation spectrum in primary human fibroblasts, with C-T and CC-TT transition mutations being the most common mutation induced by both wavelengths (41% and 52% of the total mutations induced by UVA and UVB respectively) (Kappes et al., 2006). Also supporting a role for photolesions in UVA-induced mutagenesis, both UVA- and UVB-induced C-T and CC-TT transition mutations were most commonly found on the non-transcribed strand (Kappes et al., 2006), since photolesions are more readily repaired by NER on the transcribed strand (McGregor et al., 1991). In a study of UVA-irradiated mice, the predominant UVA-induced mutation, accounting for 55% of UVA-induced mutations, in mouse skin were C-T transition (Ikehata et al., 2008), further

supporting a role for CPDs, rather than oxidative DNA damage, in UVA-induced mutagenesis.

1.5 Melanocytes

There is increasing evidence that exposure to UVA radiation is of particular relevance to the development of melanoma (Mitchell, 2012; Moan et al., 1999; Wang et al., 2001). Melanoma arises from the malignant transformation of melanocytes, specialised pigment-producing cells. Cutaneous melanocytes refer to melanocytes located in the basal layers of the epidermis (epidermal melanocytes) and in the hair follicle, while non-cutaneous melanocytes refer to the melanocytes found in the eye, inner ear, brain and heart. The present study focuses on epidermal melanocytes and their responses to long-wavelength UVA-radiation. Melanocytes are derived from the neural crest, and retain some neuron-like properties, including distinct dendritic morphology, which allows a single melanocyte to contact many keratinocytes, and it is through these contacts that melanosomes, containing melanin, are transferred to surrounding keratinocytes (Figure 1.4). In the epidermis, melanocytes and keratinocytes, the major dermal skin cell, are found in a ratio of 1:36, known as the 'epidermal melanin unit' (Fitzpatrick and Breathnach, 1963). Melanosome transfer to keratinocytes plays an important role in photoprotection, as the melanosomes form supranuclear caps in keratinocytes, protecting the DNA from the damaging effects of UV exposure as melanin acts as a UV-absorbing chromophore (Kobayashi et al., 1998b).

Epidermal keratinocytes undergo a well-defined differentiation programme, culminating in terminal differentiation and cell death (Eckert et al., 1997). The epidermis is constantly repopulated with keratinocytes by the division of keratinocyte stem cells, located in the basal epidermis (Eckert et al., 1997). In contrast to the high turnover of keratinocytes in the basal epidermis, the melanocyte population of the basal epidermis is relatively static (Abdel-Malek and Swope, 2011). The long lifespan of epidermal melanocytes is attributed in part to their resistance to apoptosis, as a result

of overexpression of the anti-apoptotic B-cell lymphoma 2 (Bcl-2) protein (Lin and Fisher, 2007; Plettenberg, 1995).

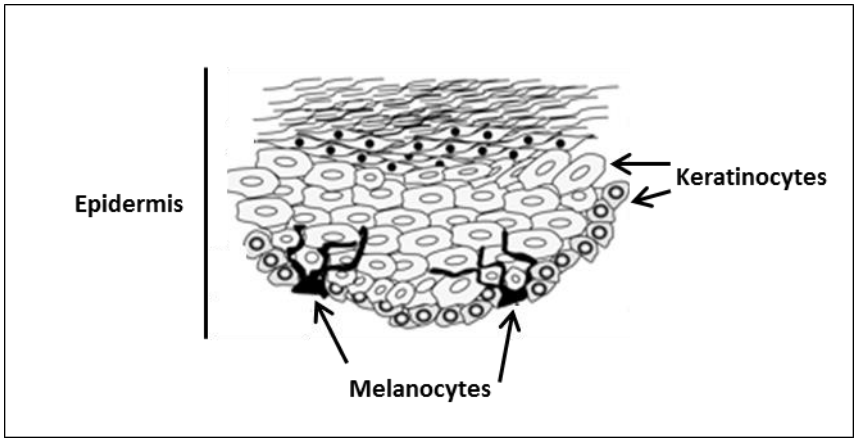

Figure 1.4 Location of melanocytes in the epidermis. Melanocytes are located in the basal epidermis, surrounded by keratinocytes. Adapted from Costin and Hearing (2007).

1.5.1 Melanogenesis and tanning response

Melanin, including both brown/black eumelanin and red/yellow pheomelanin, is the pigment responsible for skin colour and tanning. Skin colour is one of the most variable characteristic of humans. The Fitzpatrick scale is widely used to classify skin types I-VI, and is based not solely on the degree of pigmentation, but on the skin's erythema response and ability to tan (Fitzpatrick, 1988). For example, skin type I is white, has high susceptibility to sunburn and skin cancer and low tanning ability, whereas skin type VI is black with very low susceptibility to sunburn and skin cancer and very good tanning ability. Melanin is synthesised in melanocytes within specialised organelles called melanosomes, in a process called melanogenesis. However, the number of melanocytes present does not differ between the skin of low versus highly pigmented individuals (Szabó, 1954), but rather skin pigmentation is determined by the rate of melanin synthesis, the relative amounts of eumelanin and pheomelanin and the rate of transfer of melanosomes to surrounding keratinocytes (Abdel-Malek and Swope, 2011).

Melanins are complex heterogeneous biopolymers, the exact structure of which remains unknown (Watt et al., 2009). Tyrosine, the precursor in melanogenesis, is converted to L-dopa by tyrosinase, the rate limiting enzyme in melanogenesis. Other enzymes essential for melanin biogenesis are dopachrome tautomerase (also called tyrosinase-related protein 2; TRP2) and tyrosinase-related protein 1 (TRP1) (Figure 1.5) (Costin and Hearing, 2007).

Melanogenesis is a tightly regulated process. As noted above, constitutive pigmentation is controlled by the rate of synthesis of melanin. To this end tyrosinase, the rate limiting enzyme in melanogenesis, is less abundant in lightly pigmented melanocytes (Halaban et al., 1983). Moreover, tyrosinase activity is regulated by post-translational modifications, and is activated by protein kinase Cβ (PKCβ)-mediated phosphorylation (Park et al., 1993). Melanogenesis, stimulated following UV-exposure, is regulated not only by melanocyte-derived factors, but also by paracrine factors derived from neighbouring keratinocytes (Lin and Fisher, 2007). UV-exposure increases the production of proteins involved in melanogenesis including tyrosinase, TRP1, and alpha melanocyte-stimulating hormone (α-MSH) and its receptor, melanocortin 1 receptor (MC1-R) in melanocytes (Chakraborty et al., 1995; Nishioka et al., 1999). In parallel, UV-exposure stimulates the production of α-MSH and endothelin-1 (ET-1) in keratinocytes which act as paracrine factors stimulating melanogenesis (Abdel-Malek and Swope, 2011). Interestingly, DNA damage and specifically DNA repair intermediates, including thymidine dinucleotides and oligomers, considered to represent NER repair intermediates, have been shown to stimulate melanogenesis (Agar and Young, 2005; Eller et al., 1996).

The tanning response following UV-exposure can be defined in two distinct phases: immediate pigment darkening (IPD) and delayed tanning (DT). IPD which occurs as a result of exposure to UVA radiation and visible light, consists of an immediate darkening which fades rapidly within two hours of exposure (Routaboul et al., 1999). IPD is not associated with an increase in the number of melanosomes in the cells, but with chemical modification of existing melanin, morphological changes in melanocytes including

migration of melanosomes to the melanocyte dendrites and increased transfer of melanosomes to keratinocytes (Routaboul et al., 1999). More recently, UVA-induced IPD has been shown to be activated through photo activation of retinol-like receptors on the surface of melanocytes, and involve calcium mobilisation (Wicks et al., 2011). DT occurs primarily in response to UVB exposure, but also following UVA. Pigment darkening appears 48-72 hours following exposure, peaks 3-4 weeks after exposure and fades in the subsequent months (Gilchrest et al., 1996). DT is a result of an increase in melanocyte number, melanosome number, degree of melanisation, melanocyte dendricity, and transfer of melanosomes to keratinocytes (Gilchrest et al., 1996).

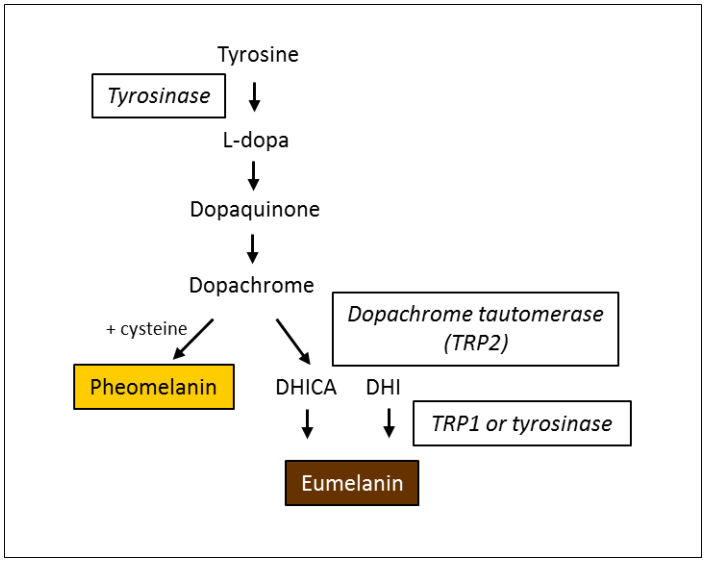

Figure 1.5 Schematic overview of melanogenesis. The key enzymes involved in melanin synthesis are shown in italics. Abbreviations: 5,6-dihydroxyindole-2-carboxylic acid (DHIAC) 5,6-dihydroxyindole (DHI) and tyrosinase-related protein (TRP). (Adapted from Costin and Hearing, 2007).

1.5.2 Melanin: the photoprotective pigment

Melanin acts as a chromophore by absorbing UV-radiation and as a scavenger of ROS. Both processes protect cellular DNA and other biomolecules from the harmful effect of UV exposure. Epidemiological evidence clearly indicates that melanin plays a key role in the prevention of

UV-induced skin cancers, since skin cancer incidence is much lower in individuals with high pigmentation compared to lightly pigmented individuals (Crombie, 1979). The melanin content of cultured cells and human skin inversely correlates with the quantity of UV-induced DNA photoproducts (Kobayashi et al., 1998a; Tadokoro et al., 2003). The photoprotective effects of melanin are somewhat abrogated by the fact that melanin also acts as a photosensitiser, absorbing UVA radiation, leading to the production of ROS which can react with and damage cellular DNA and proteins (Takeuchi et al., 2004; Wondrak et al., 2006). Thus a delicate and complex balance between the photoprotective effects of melanin against harmful UVB radiation, and the photosensitisation of melanin resulting in ROS generation following UVA exposure, determine the cellular outcome following exposure to sunlight.

One interesting study (Jablonski and Chaplin, 2000) suggests that the primary evolutionary driver of skin melanisation was not the prevention of UV-induced skin cancers, since following the Darwinian evolutionary model, skin cancer should not interfere with reproduction, as non-melanoma skin cancers occur primarily in older individuals and are rarely lethal. Instead it is proposed that melanin, by absorbing UV radiation, prevents folate photolysis, since folate is required for embryonic neural tube development and spermatogenesis (Jablonski and Chaplin, 2000). Moreover, the varying levels of melanin in individuals is suggested to be a compromise to allow sufficient UVB penetration to promote the formation of pre-vitamin D_3 in the skin, which is also required for normal development (Jablonski and Chaplin, 2000).

1.6 Melanoma

Melanoma arises from the malignant transformation of melanocytes. While exposure to solar UV-radiation, particularly UVA-radiation, is a risk factor in the development of melanoma (Mitchell, 2012; Wang et al., 2001), the exact molecular mechanisms linking UV exposure and melanoma development remain unclear. On average 568 cases of melanoma skin cancer are diagnosed annually in Ireland (NCRI, 2013b). Although the least

prevalent skin cancer subtype, accounting for approximately 8% of the total skin cancer incidence (NCRI, 2013b), melanoma is the most lethal form of skin cancer accounting for approximately 65% of all deaths from skin cancer (NCRI, 2013a). The high fatality rate of melanoma is associated with its highly metastatic nature and resistance to radiation and standard chemotherapy treatments (Bhatia et al., 2009).

Greater than 60% of melanomas contain activating mutations in the *BRAF* gene. Of these, approximately 80% are V600E mutations (Davies et al., 2002). B-Raf is a serine/threonine kinase, involved in signalling in the mitogen-activated protein kinase (MAPK) pathway, which mediates cell growth and survival. Thus constitutive activation of mutant B-Raf is thought to contribute to melanoma cell survival (Panka et al., 2006). In melanomas with wild-type B-Raf, alterations in other components of the MAPK kinase pathway have been reported, including the presence of activating mutations in N-Ras, and down-regulation of raf-1 kinase inhibitory protein (RKIP) (Alsina et al., 2003; Schuierer et al., 2004).

The most effective treatment for melanoma is early detection and surgical removal of the lesion and surrounding tissue (Garbe and Eigentler, 2007). Due to the highly metastatic nature of melanoma, removal of lymph nodes near the cancer is often carried out. Immunotherapy is widely used in melanoma treatment, including the administration of interleukin 2 (Il-2), and the recently described anti-cytotoxic T-lymphocyte antigen 4 (CTLA-4) antibody, Ipilimumab, which stimulates the immune system to eradicate melanoma cells (Lee et al., 2013). Treatment of late stage melanoma has a low success rate. Surgical removal of the lesion remains the primary course of treatment. Targeted melanoma therapies, including inhibitors of mutated B-Raf have also been developed, for example vemurafenib (Sosman et al., 2012), which prolong patient lifespan but resistance occurs in almost all cases (Kudchadkar et al., 2013).

1.6.1 UVA-radiation as a risk factor for melanoma

While the role of UVA-radiation in the pathogenesis of melanoma remains a matter of debate, the overwhelming evidence points to a role for UVA-exposure in the development of melanoma (Mitchell and Fernandez, 2012; Moan et al., 1999; Wang et al., 2001). UVA radiation accounts for >95% of the solar UV-radiation reaching the earths' surface. However, until recently most sun screens protected only against UVB radiation. It has been proposed that this use of UVB-protective sunscreens could have the effect of increasing the time in the sun before sunburn occurred, resulting in increased exposure to UVA radiation. Melanoma incidence is associated with acute sunburn and brief intense sun exposure, especially in childhood (Whiteman et al., 2001). This is recapitulated in animal models of melanoma, where acute UV-exposure in infancy is associated with melanoma induction in transgenic mice and *Xiphophorus* hybrid fish (Fernandez et al., 2012; Noonan et al., 2001). Moreover, long wavelength UVA-radiation can penetrate deeper into the skin than UVB, making melanocytes, located in the basal layers of the epidermis a target cell for UVA exposure *in vivo* (Bruls et al., 1984; Meinhardt et al., 2008). In 2009 the International Agency for Research on Cancer (IARC) described UVA radiation as a class I carcinogen (El Ghissassi et al., 2009).

Increased risk of melanoma is associated with the use of UVA-emitting sunbeds (Lazovich et al., 2010; Veierød et al., 2003). This is highlighted by the Icelandic melanoma epidemic, where a peak in melanoma incidence was observed between 1995 and 2005, particularly on the trunk of young women, that was associated with increased use of UVA-emitting sunbeds in the mid-1980s (Héry et al., 2010). Recently, the IARC classed UVA-emitting sunbeds as carcinogenic to humans. Moreover, the use of sunbeds for individuals under 18 years of age was banned in Northern Ireland in 2012 and in the US state of California in 2011.

The controversy over the role of UVA exposure in melanoma development is heightened by the discrepancies in results from animal models of melanoma. Initial experiments using the *Xiphophorus* hybrid fish model

provided evidence that UVA exposure is an initiator of melanoma (Setlow et al., 1993). However, subsequent analysis using a larger specimen number and more stringent UV filters, discredited this initial findings, showing that UVB, but not UVA, can initiate melanoma in the *Xiphophorus* hybrid fish model (Mitchell et al., 2010). Similar studies in *Monodelphis domestica* (opossum), showed that exposure to UVB but not to UVA is capable of inducing melanoma (Robinson et al., 2000). Although transgenic mouse models of cancer are widely used and very informative, transgenic mouse models of melanoma which accurately mimic human melanoma development have been lacking. While UVA radiation induces non-melanoma type skin cancers in transgenic albino hairless mice (de Laat et al., 1997; Kelfkens et al., 1991), such studies failed to demonstrate significant induction of melanoma by UVA radiation in mice (De Fabo et al., 2004). More recently, UVA radiation was found to induce melanoma in the hepatocyte growth factor (HGF) transgenic mouse, but only in black, not albino, mice, suggesting that melanin is required for the UVA-mediated initiation of melanoma (Noonan et al., 2012). This role for melanin in melanoma initiation is consistent the observation that African albinos have increased rates of non-melanoma skin cancer but are relatively resistant to melanoma (Lookingbill et al., 1995). Another confounding factor in determining the causes of melanoma is the development of melanoma on areas of the body that are not highly sun-exposed. While this argues against a role for UV in the pathogenesis of certain melanoma types, it highlights the possibility of multiple mechanisms driving melanoma progression, some of which may be UV-independent.

UVA radiation induces CPDs in cultured primary melanocytes (Mouret et al., 2012), although it should be noted that UVA-induced 8-oxo-G was significantly increased in melanocytes compared to matched keratinocytes (Mouret et al., 2012). The incidence of melanoma in repair-deficient XP individuals is 1000-times greater than that of the general population, suggesting a role for UV-induced DNA photolesions in melanoma development (Kraemer et al., 1987). If UV-induced DNA lesions are involved in the initiation of melanoma, then UV-signature mutations, C-T

transition mutations, would be expected to be found in key genes driving melanoma progression. This is not the case for the most common melanoma-associated mutation in the *BRAF* gene, which results from a T-A transversion at position 1799 (Ascierto et al., 2012). However, it has been proposed that the *BRAF* mutation could result from error-prone replication past a UV-induced photolesion at a dipyrimidine site upstream of residue 1799 (Thomas et al., 2006). More recently a number of genomic screens identified UV signature mutations in genes implicated in melanoma pathogenesis (Berger et al., 2012; Hodis et al., 2012; Krauthammer et al., 2012), including the identification of UV signature activating mutation in *RAC1* (RAS-related C3 botulinum toxin substrate 1 gene) in 9% of melanomas, which drives melanocyte proliferation and migration (Krauthammer et al., 2012), and *PREX2* (Phosphoinositol-3,4,5-triphosphat-dependent RAC exchange factor 1 gene) mutations, found in 14% of melanomas, which drives melanoma tumour formation (Berger et al., 2012). Complicating the UVA-melanoma argument is the presence of melanin in melanocytes, which as outlined above, acts as a double-edged sword, with roles in both photoprotection and photosensitisation (Menter et al., 1991).

While there is evidence that UVA exposure is involved in the pathogenesis of melanoma, the exact molecular mechanisms remain unclear. Inconsistencies in the field are also likely due to variations in UVA sources, as well as biological systems used. For example, UVA dose rate has been shown to affect cellular responses to UVA (Merwald et al., 2005; Shorrocks et al., 2007). This variation mirrors the heterogeneity of melanoma, which reflects the differences in individual sun exposure, melanin content and other possible factors contributing to melanomagenesis.

The consensus in the literature supports a role for UV exposure in the development of melanoma. The specific contribution of UVA and UVB radiation remains a matter of debate. However, the evidence suggests that while UVB may be required for initiation of melanoma, UVA exposure plays an important role in the melanoma progression (Mitchell and Fernandez, 2012). While UVA probably contributes to the mutagenic load in melanoma cells (Hodis et al., 2012), it may also influence melanoma

progression by modulating cellular signalling pathways and enhancing metastasis (McMillan et al., 2008; Pastila et al., 2011; Wang et al., 2001). The archaic view of the cancer cell as an independent self-sufficient entity is being replaced by a model in which dynamic interaction with the tumour micro-environment is essential for tumour progression (Mbeunkui and Johann, 2009). To this end, effects of UVA radiation on cells neighbouring the melanocytes, including keratinocytes, fibroblasts and immune cells, could contribute to melanoma progression through the production of stimulating paracrine signalling factors, in a similar fashion to the regulation of melanogenesis by paracrine factors.

As well as photocarcinogenesis, exposure to solar UV-radiation also has systemic effects on vitamin D production and the tanning response. While these pathways are mostly studied independently, they are likely to be interlinked as they evolved together to modulate solar UV exposure. It has been proposed that increased UVA exposure coupled with decreased vitamin D production could promote melanoma incidence (Godar et al., 2009).

1.7 DNA damage response (DDR)

In order to protect the integrity of the genome following the induction of DNA damage, cells activate a network of signalling pathways collectively termed the DNA damage response (DDR). DNA damage is sensed by components of the DDR and this in turn signals the activation DNA repair, inhibition cell cycle progression in the presence of damage or initiation cell death if the damage is too severe (Niida and Nakanishi, 2006; Zhou and Elledge, 2000). The DDR signalling network comprises sensor, transducer, mediator and effector proteins (Figure 1.6). The identity of the proteins activated in the DDR is dependent on a number of factors, including the type and quantity of DNA damage induced and the cell cycle phase in which the damage occurs. DDR signalling is mediated through post-translation modification (PTM) of the signalling proteins. Common PTMs include phosphorylation, ubiquitination, methylation, sumoylation, ADP-ribosylation and glycosylation (Huen and Chen, 2008). Phosphorylation is

the most widely studied PTM in response to DNA damage. The importance of phosphorylation in DDR signalling is highlighted by the central involvement of the phosphoinositol 3-kinase-like kinases (PIKKs) in the transduction of DDR signalling.

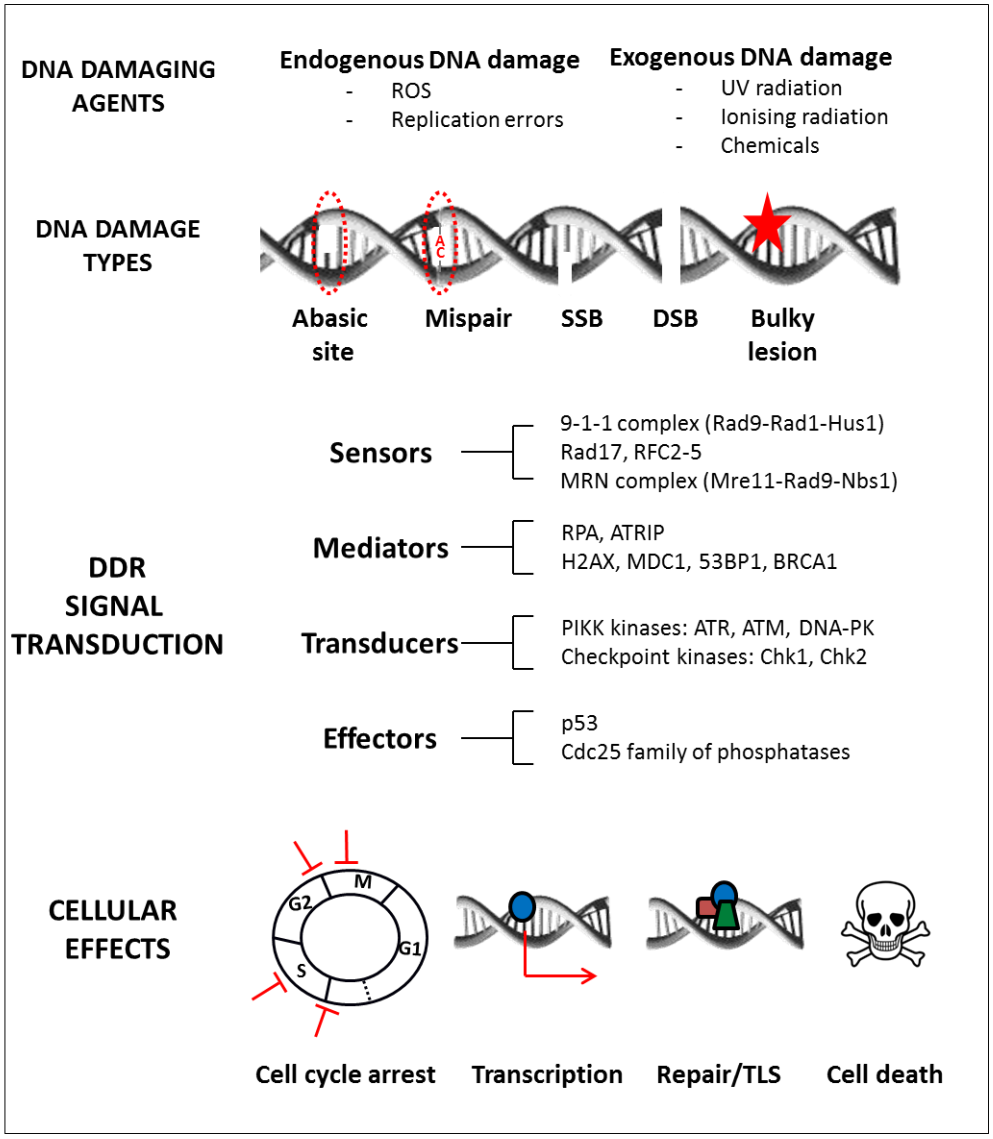

Figure 1.6 Schematic representation of the mammalian DNA damage response (DDR). Both endogenous and exogenous sources can induce a variety of DNA damage. In response to DNA damage, cells activate signalling cascades involving sensor, mediator, transducer and effector proteins, resulting in downstream cellular effects. Adapted from Niida and Nakanishi, 2006; Zhou and Elledge, 2000. (ROS=reactive oxygen species, SSB=single stand break, DSB=double strand break, RPA=replication protein A, ATRIP=ATR interacting protein, ATR=ATM and Rad3-related, ATM=ataxia telangiectasia mutated, DNA-PK=DNA-dependent protein kinase, Chk1=checkpoint kinase 1, Chk2=checkpoint kinase 2, Cdc25=cell division cycle 25, TLS=translesion synthesis).

1.7.1 Phosphoinositol 3-kinase-like kinases (PIKKs)

The primary phosphoinositol 3-kinase-like kinases (PIKKs) involved in DDR signalling are ataxia telangiectasia mutated (ATM), ATM and Rad3-related (ATR) and DNA-dependent protein kinase catalytic subunit (DNA-PK_{cs}). While ATM and DNA-PK_{cs} are primarily activated in response to DSBs, ATR is activated in response to regions of single stranded DNA (ssDNA) resulting from replication arrest (Abraham, 2001). Other members of the PIKK family include mammalian target of rapamycin (mTOR), suppressor with morphological effect on genitalia family member (SMG1) and transformation/transcription domain-associated protein (TRRAP) (McMahon et al., 1998). mTOR, a key modulator of cell growth, is activated in response to growth factors, nutrients and stress, and regulates translation, ribosome biogenesis and actin organisation (reviewed in Wullschleger et al., 2006). The role of SMG1 in mRNA surveillance and regulating nonsense-mediated mRNA decay is well characterised (Yamashita et al., 2001). More recently, a role for SMG1 in the DDR has been identified (Gehen et al., 2008). TRRAP, is highly homologous to the PIKKs, although lacking a functional kinase domain (McMahon et al., 1998). TRRAP plays a role in the recruitment of histone acetyltransferase complexes to the chromatin, which regulate transcription initiation (McMahon et al., 2000).

PIKKs are so called due the homology of the kinase domains shared with the PI3 kinases, have conserved structural elements, especially in the C-terminal (Lempiainen and Halazonetis, 2009). PIKKs are serine/threonine (S/T) kinases, which have substrate specificity for serine or threonine residues followed by glutamine (S/T-Q sites). Recent mass spectrometry screens for ATM/ATR substrates in human cells identified 900 and 570 potential S/T-Q sites on proteins that were phosphorylated in response to IR and UVC, respectively (Matsuoka et al., 2007; Stokes et al., 2007). Phosphorylation sites were identified on proteins, involved not only in DNA processing and cell cycle regulation, but also in cytoskeleton organisation and protein trafficking (Matsuoka et al., 2007; Stokes et al., 2007). These screens highlight the diversity of responses activated following exposure to

DNA damaging agents, and also the central role of the PIKKs in the cellular response to DNA damage. The following discussion will focus on ATM and ATR as transducers of the DDR.

1.7.2 Ataxia telangiectasia mutated and Rad3-related (ATR)

Human ataxia telangiectasia mutated and Rad3-related (ATR) is a large (301 kDa) protein, encoded by the *ATR* gene. *ATR* is a conserved gene and is highly homologous to *S. pombe rad3* gene and *S. cerevesiae mec1* gene (Bentley et al., 1996; Cimprich et al., 1996; Kato and Ogawa, 1994). ATR is essential and genetic abrogation of *ATR* causes embryonic lethality in mice, as a result of gross genetic instability (Brown and Baltimore, 2000). Furthermore, ATR is essential for the viability of human somatic cells (Cortez et al., 2001). A hypomorphic mutation in the *ATR* gene is responsible for the recessive genetic disorder Seckel syndrome, which is characterised by microcephaly and growth retardation (O'Driscoll et al., 2003). Furthermore a heterozygous missense mutation in *ATR* was recently identified in a group of individuals with oropharyngeal cancer syndrome (Tanaka et al., 2012)

ATR is required for efficient checkpoint activation and is activated in response to various types of DNA damage, including replication stress and DNA DSBs (Abraham, 2001). However, a single DNA structure, replication protein A (RPA)-coated ssDNA with double-stranded DNA (dsDNA) at the 5' junction, is considered to be the activating structure for ATR (MacDougall et al., 2007). RPA-coated ssDNA can form as a result of replication fork collapse, during DSB processing, and during NER (Cimprich and Cortez, 2008). ATR-interacting protein (ATRIP) is required for ATR activation, and functions to recruit ATR to sites of RPA-coated ssDNA (Zou and Elledge, 2003). The kinase activity is essential for the function of ATR in response to IR and UVC-induced DNA damage, and mutation of the ATR kinase domain results in increased sensitivity to UVC and IR coupled with abrogation of cell cycle checkpoints (Wright et al., 1998). While the ATRIP-RPA interaction is required for ATR localisation to chromatin following DNA damage, activation of ATR kinase activity

requires other factors, including interaction with topoisomerase-II binding protein 1 (TopBP1) (Kumagai et al., 2006). TopBP1 recruitment to sites of DNA damage is discussed in Section 1.8.3.1.

While Chk1 is one of the most widely studied ATR substrates, large scale screens have identified hundreds of potential ATR substrates, that have roles in divergent cellular processes (Matsuoka et al., 2007; Stokes et al., 2007). ATR-mediated phosphorylation of Chk1 is involved in cell cycle arrest and inhibition of replication origin firing (Liu et al., 2000; Zachos et al., 2003). ATR also phosphorylates other cell cycle regulators, including p53 (Tibbetts et al., 1999). In addition to signalling replication stress, ATR-mediated phosphorylation of the replication-associated protein MCM2 is required for recovery of DNA replication following arrest (Trenz et al., 2008). As well as its role in regulating cell cycle progression and DNA replication, ATR phosphorylates a number of proteins involved in DNA repair, including XPA (Wu et al., 2006) and BRCA1 (Tibbetts et al., 2000).

1.7.3 Ataxia telangiectasia mutated (ATM)

Ataxia telangiectasia mutated (ATM) is a 370 kDa protein encoded by the *ATM* gene. *ATM* was identified as the gene mutated in the genetic disorder ataxia telangiectasia (AT) (Savitsky et al., 1995a). AT patients are characterised by cerebellar ataxia associated with degeneration of the Purkinje cells, immunodeficiency, sensitivity to ionising radiation and 100-fold increase in cancer susceptibility, including to leukaemia and lymphoma (Taylor et al., 1994). At a cellular level AT cells are characterised by radioresistant DNA synthesis, cell cycle checkpoint defects, increased radiation sensitivity, and increased chromosomal instability (Lavin, 2008).

The most thoroughly characterised role of ATM is in the cellular responses to DSBs. In unperturbed cells, ATM is in an inactive state in dimers or multimeric complexes (Bakkenist and Kastan, 2003). Upon induction of DSBs, ATM is rapidly autophosphorylated on S1981, resulting in dimer dissociation and kinase activation (Bakkenist and Kastan, 2003). ATM is recruited to the site of a DSB in a Mre11-Rad50-Nbs1 (MRN) complex-

dependent manner (Uziel et al., 2003). The MRN complex acts a sensor of DSBs, binds to the ends of DSBs and recruits ATM to the break site (Mirzoeva and Petrini, 2001; Uziel et al., 2003). The retention of MRN on the chromatin is dependent on interaction with mediator of damage checkpoint-1 (MDC1) (Spycher et al., 2008). Approximately 50% of the cellular ATM was phosphorylated on S1981 in response to 0.5 Gy IR, which is estimated to induce approximately 18 DSBs, the relatively high amount of ATM that becomes phosphorylated and activated in response to very few DSBs suggests that recruitment of ATM to DSB sites is not required for ATM phosphorylation (Bakkenist and Kastan, 2003). It is suggested that rather than being directly activated by DSBs, ATM is activated by changes in higher order chromatin structure. This is supported by evidence that ATM can be activated following treatment with chloroquine or trichostatin, which alter chromatin structure without inducing DSBs (Bakkenist and Kastan, 2003).

Along with S1981, a number of other autophosphorylation sites, including S367 and S1893, are essential for ATM function in response to IR-induced DNA damage (Kozlov et al., 2006). Mutation of these residues to alanine results in impaired cell cycle checkpoint activation and ATM substrate phosphorylation in response to IR, which suggests that multiple autophosphorylation sites are required for ATM kinase function (Kozlov et al., 2006). In addition, ATM kinase activity is regulated by acetylation (Sun et al., 2005). Tat-interactive protein 60 kDa (Tip60) is the acetyl transferase responsible for ATM acetylation on K3016, which is required for efficient ATM kinase activity and conversion of ATM from dimeric to monomeric forms (Sun et al., 2005; Sun et al., 2007). Another acetyltransferase, hMOF, has been implicated in regulating ATM function in response to IR-exposure (Gupta et al., 2005).

Other regulators of ATM kinase activity include a number of protein phosphatases, including protein phosphatase 5 (PP5). Interaction of PP5 with ATM is required for ATM autophosphorylation and for phosphorylation of ATM targets following IR exposure (Ali et al., 2004). It

is possible that the phosphatase activity of PP5 may be required to dephosphorylate as yet unidentified inhibitory phosphorylation of ATM to fully activate ATM kinase activity. Moreover, protein phosphatase 2A (PP2A) acts as a negative regulator of ATM kinase activity under unperturbed conditions, but following IR-exposure, PP2A dissociates from ATM resulting in ATM autophosphorylation on S1981 and activation of ATM kinase activity (Goodarzi et al., 2004). Regulation of ATM by phosphorylation on multiple sites mirrors the regulation of the closely related PIKK, DNA-PK (Ding et al., 2003).

Activated ATM kinase phosphorylates a number of downstream substrates mediating the cellular response to DSBs. The major phenotype of AT cells is radioresistant DNA synthesis due to a failure of the intra-S checkpoint in the absence of ATM (Falck et al., 2001; Painter, 1981). ATM is required for activation of the G1/S, intra-S and G2/M checkpoints, and for the HR and NHEJ DSB repair pathways (Kastan and Lim, 2000; Shiloh and Ziv, 2013). ATM phosphorylates key proteins involved in mediating DSB-induced cell cycle arrest and apoptosis, including Chk2 and p53 (Matsuoka et al., 2000a; Maya et al., 2001). ATM-dependent phosphorylation of H2AX on S139 (generating γH2AX) in response to DSBs (Burma et al., 2001) mediates recruitment and retention of various DDR factors at the DSB site, including NBS1, MDC1, BRCA1 and 53BP1(Kobayashi et al., 2002; Stewart et al., 2003; Ward et al., 2003). A number of these proteins are also ATM substrates (Gatei et al., 2000; Lim et al., 2000).

ATM can also be activated in a DSB-independent manner in response to oxidative stress (Guo et al., 2010a; Guo et al., 2010b). Oxidative stress-induced activation of ATM is associated with autophosphorylation of ATM on S1981 (Guo et al., 2010b). However, in contrast to DSB-mediated ATM activation, under conditions of oxidative stress ATM was found to be in a dimeric state, in which the monomers are attached by an intermolecular disulphide bond at C2991 (Guo et al., 2010b). Furthermore, oxidative stress-induced activation of ATM is independent of the MRN complex (Guo et al., 2010b). Notably, while oxidative stress-induced ATM activation results in

phosphorylation of p53 and Chk2, phosphorylation of chromatin-associated ATM substrates, including H2AX and Nbs1, was not detected following oxidative stress (Guo et al., 2010b). This supports a role for ATM activation that is independent of DSB formation or repair.

Overall, the literature points to diverse roles for ATM. These include a major role in the cellular response to DSBs and other types of DNA damage. Other non-DNA damage related roles for ATM, including mediating redox homeostasis, regulating peroxisomes and synaptic signalling in neurons, have been described (Kastan and Lim, 2000; Shiloh and Ziv, 2013). Furthermore, it is likely that activation of ATM in response to various stimuli occurs through independent mechanisms (Bakkenist and Kastan, 2003; Guo et al., 2010b).

While the roles of ATM and ATR in DDR signalling have been described separately here, evidence suggests that the ATR and ATM-mediated DDR pathways are not mutually exclusive, but rather that there is considerable redundancy between the kinases. For example, under conditions of replication stress and following IR-exposure, respectively, ATR and DNA-PK also mediate H2AX phosphorylation on S139 (Stiff et al., 2004; Ward and Chen, 2001). Furthermore, ATM phosphorylates Chk1 on S317, following IR, in an Nbs1 dependent manner (Gatei et al., 2003).

1.8 DNA damage-induced cell cycle checkpoint activation

High fidelity DNA replication and error-free transmission of genetic material during cell division are essential for organism survival. Inhibition of cell cycle progression is a key outcome of DDR signalling, and is central to protecting genome integrity (Hartwell and Weinert, 1989). Checkpoint activation at the G1/S boundary prevents the onset of DNA replication in the presence of damage, while G2/M checkpoint activation prevents the onset of mitosis before DNA replication is complete. Cell cycle checkpoints can be activated during all phases of the cell cycle (Figure 1.7), and the signalling pathways leading to a specific cell cycle checkpoint is dependent on the type of DNA damage and the cell cycle phase in which the damage occurs. PIKK-mediated phosphorylation of the checkpoint kinases, Chk1

and Chk2, is central to DNA damage-induced checkpoint activation. Chk1 and Chk2 kinases phosphorylate and inactivate the Cdc25 family of phosphatases. Cdc25 activity is normally required to remove inhibitory phosphorylations from cyclin-dependent kinases (CDKs), which allow cell cycle progression.

Progression through the cell cycle under unperturbed conditions is regulated by CDK activity. Human cells express multiple CDKs involved in cell cycle regulation, including CDK1, CDK2, CDK4 and CDK6 (Vermeulen et al., 2003). While CDK protein levels remain constant during the cell cycle, the kinase activity of CDKs is only activated upon binding of the activating cyclin subunit of the CDK-cyclin complex. The level of individual cyclin proteins is regulated during the cell cycle by transcription and degradation (Arellano and Moreno, 1997). CDK activity is also controlled by inhibitory phosphorylation, for example by Wee1, which phosphorylates and inhibits CDK1 on Y15 (Parker and Piwnica-Worms, 1992), and by binding of CDK-inhibitor proteins (CKIs) (Vermeulen et al., 2003). As noted above, Cdc25 phosphatases play a critical role in removal of inhibitory phosphorylations from CDK-cyclin complexes. Once activated by cyclin binding and by dephosphorylation of inhibitory phosphorylation sites by the Cdc25 family of proteins, CDKs phosphorylate multiple substrates dependent on cell cycle phase, leading to cell cycle progression (Vermeulen et al., 2003). Given the central role of CDKs in cell cycle progression, it is not surprising that cell cycle checkpoints activated in response to DNA damage converge on CDK regulation.

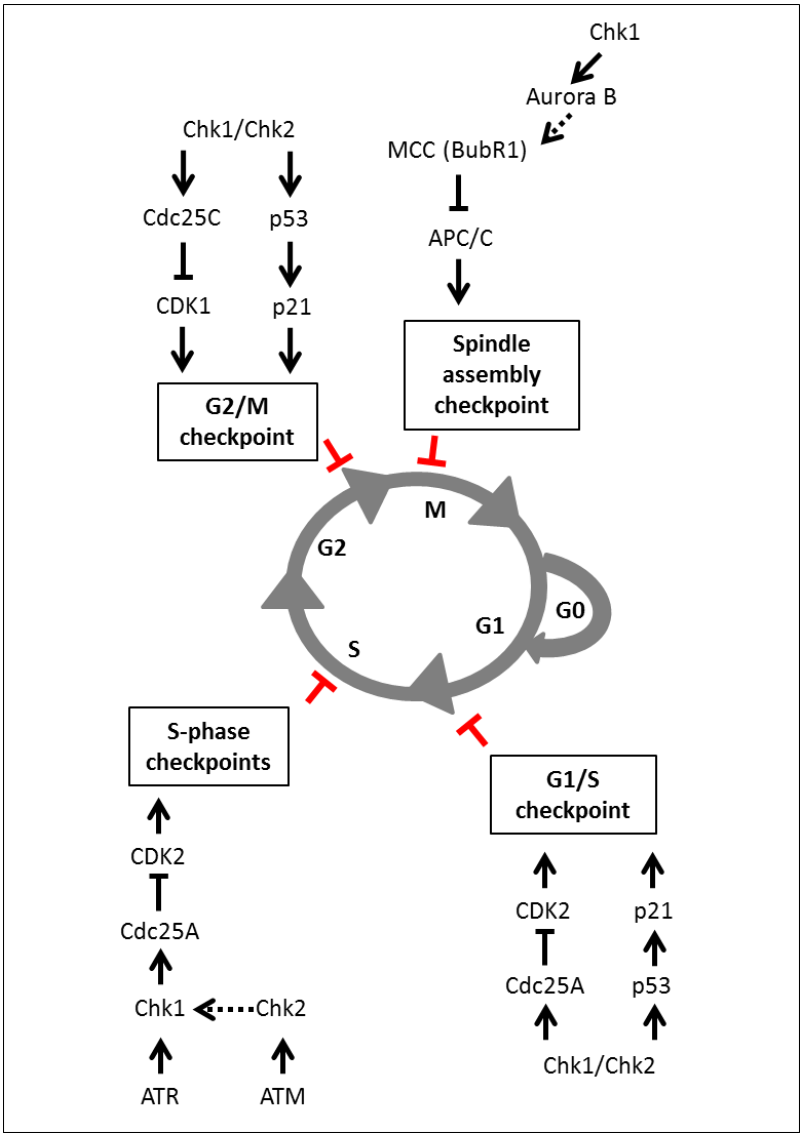

Figure 1.7 Schematic outline of mammalian DNA damage-induced cell cycle checkpoints activated at the boundary of G1/S and G2/M, during S-phase and in mitosis. Some key proteins involved in each cell cycle checkpoint are shown. (CDK=cyclin dependent kinase, Chk1=checkpoint kinase, Cdc25=cell division cycle 25, MCC=Mitotic checkpoint complex APC/C= Anaphase-promoting complex/cyclosome)

1.8.1 G1/S checkpoint

The DNA damage-induced G1/S checkpoint is central to maintenance of genome integrity, preventing the onset of DNA replication in the presence of DNA damage. The important role of the G1/S checkpoints in preventing cancer formation is highlighted by the fact that the tumour suppressor gene *TP53*, encoding a key protein in the G1 checkpoint, is the most commonly

mutated gene in cancers (Levine et al., 1991). The G1 checkpoint is mediated through two complementary pathways: (i) a rapid p53-independent pathway and (ii) a p53-mediated pathway for sustained checkpoint activation (Bartek and Lukas, 2001).

The rapidly induced G1 checkpoint is p53-independent, and proceeds through ATM-Chk2 in response to IR, or ATR-Chk1 in response to UVC irradiation (Abraham, 2001). The pathways converge on Chk1/Chk2-meidated Cdc25A phosphorylation. Chk1/Chk2-mediated phosphorylation of Cdc25A phosphatase, results in proteasome-mediated degradation of Cdc25A (Falck et al., 2001; Mailand et al., 2000). Loss of Cdc25A prevents removal of inhibitory phosphorylations from CDK2, resulting in loss of CDK2 activity. This in turn impairs loading of Cdc45 onto pre-replication complexes and therefore inhibits DNA replication in S-phase (Costanzo et al., 2000).

A slower p53-dependent response is necessary for sustained G1 checkpoint activation. p53 is a transcription factor, and under unperturbed condition is in an inactive state as a result of binding to Mouse Double Minute 2 homolog (MDM2), which promotes nuclear export and proteasome-mediated degradation of p53 (Ryan et al., 2001). Activation of p53 is a multifaceted process mediated by the ATR-Chk1 and ATM-Chk2 signalling pathways as outlined above (Figure 1.7) (Bartek and Lukas, 2001). IR-induced phosphorylation of MDM2 by ATM inhibits the interaction of MDM2 and p53, thus promoting nuclear localisation and stabilisation of p53 (Maya et al., 2001). Both Chk1 and Chk2 phosphorylate p53 on a number of sites including S20 which decreases MDM2 binding (Shieh et al., 2000). ATM and ATR phosphorylate p53 on S15 which enhances nuclear localisation (Zhang and Xiong, 2001). Activated p53 results in the transcriptional up-regulation of a number of proteins including p21 (Macleod et al., 1995). p21 binds to and inhibits CDK2-cylcinE and CDK4-cyclinD complexes resulting in inhibition of cell cycle progression (Bartek and Lukas, 2001). p21 binding inhibits the kinase activity of CDKs, preventing Retinoblastoma (Rb) protein phosphorylation. Continued

sequestration of E2F transcription factor in turn prevents E2F-mediated transcription of genes required for the G1/S transition (Wade Harper et al., 1993). p21 also functions by binding PCNA, directly inhibiting DNA synthesis (Cayrol et al., 1998).

1.8.2 G2/M checkpoint

Both ATM and ATR kinases can be activated in response to DNA damage during G2, leading to phosphorylation and activation of Chk2 and Chk1, respectively (Abraham, 2001). Both Chk1 and Chk2 kinases phosphorylate and inactivate Cdc25C, by creating a binding site for the 14-3-3 proteins, which inhibits Cdc25C phosphatase activity (Peng et al., 1997). Inhibition of Cdc25C results in a failure to activate the mitotic CDK1, preventing the onset of mitosis in the presence of DNA damage (DiPaola, 2002). Similar to the G1/S checkpoint, prolonged G2/M arrest is also mediated by activation of p53, resulting in transcriptional induction of p21 and inhibition of mitosis onset (Bunz et al., 1998)

Separate from the DNA-damage induced G2/M checkpoint, the spindle assembly checkpoint (SAC) is activated in early M-phase by the presence of unattached kinetochores (Lara-Gonzalez et al., 2012). The SAC is essential to ensure the fidelity of chromosome segregation to daughter cells, and is activated by the mitotic checkpoint complex (MCC), which includes BubR1, Cdc20, Mad2 and Bub3. The MMC acts by sequestering Cdc20, thereby preventing activation of the anaphase promoting complex or cyclosome (APC/C). Once the kinetochores are correctly attached, activated APC/C promotes ubiquitin-mediated degradation of cyclin B1 and securin. Degradation of cyclin B1 results in inactivation of CDK1 and mitotic exit. Degradation of securin promotes separase activation, resulting in separation of the sister chromatids. Chk1 has been implicated in the SAC, through Chk1-mediated phosphorylation of Aurora B, which is required for BubR1 recruitment to the kinetochores (Zachos et al., 2007).

1.8.3 The S-phase checkpoints

Faithful DNA replication during S-phase is crucial to ensure the integrity of the genome. Three S-phase checkpoints have been identified in mammalian cells, namely the replication checkpoint, the intra S-phase checkpoint and the S/M checkpoint (Bartek et al., 2004). Collectively, the general outcomes of S-phase checkpoints include slowing of replication fork progression, inhibition of origin firing and inhibition of cell cycle progression until replication is complete. There is overlap between the signalling proteins involved and the cellular outcomes (Bartek et al., 2004). Each of the S-phase checkpoints will be discussed in detail below. In contrast to both G1/S and G2/M checkpoints, all the S-phase checkpoints are p53-independent.

1.8.3.1 Replication checkpoint

The replication checkpoint is activated in response to conditions which stall replication fork progression, including DNA lesions, depletion of deoxyribonucleotide triphosphate (dNTP) pools, chemical inhibition of DNA polymerases, and collision of replication forks with transcription complexes (Branzei and Foiani, 2010). The replication checkpoint functions to inhibit the firing of inactive origins of replication, and to stabilise stalled replication forks until the stress has been alleviated (Bartek et al., 2004).

DNA replication arrest can lead to uncoupling of the DNA polymerase and helicase activities at the replication fork (Byun et al., 2005), resulting in the generation of ssDNA regions (Zou and Elledge, 2003). ssDNA is rapidly coated with replication protein A (RPA). RPA-coated ssDNA recruits and binds ATR-interacting protein (ATRIP) (Zou and Elledge, 2003). ATRIP leads to ATR recruitment to the sites of DNA damage, which is essential for ATR-mediated phosphorylation and activation of Chk1 (Zou and Elledge, 2003). Full activation of the ATR-Chk1 signalling pathway also requires a number of accessory factors including topoisomerase-II binding protein 1 (TopBP1) and claspin (Chini and Chen, 2003; Kumagai et al., 2006).

Recruitment of TopBP1 to stalled replication forks is independent of ATR-ATRIP but occurs through interaction between TopBP1 and the Rad9

subunit of the 9-1-1 complex, which is loaded onto ssDNA in a Rad17-dependent manner (Liu et al., 2006). ATR then phosphorylates Rad17, resulting in recruitment and binding of claspin, an essential factor for ATR-mediated Chk1 phosphorylation in response to replication stress (Wang et al., 2006). The Timeless-Tipin complex is also recruited to stalled replication forks via interaction of Tipin with the RPA2 subunit of trimeric RPA. This is required for efficient claspin-mediated phosphorylation of Chk1 by ATR (Kemp et al., 2010). Another protein important in activation of the ATR-mediated replication checkpoint is Protein phosphatase 5 (PP5), which binds to ATR and enhances phosphorylation of the ATR substrates Chk1 and Rad17 (Zhang et al., 2005a).

While the ATR-Chk1 pathway is essential for checkpoint activation, few Chk1 substrates have been identified to date (Blasius et al., 2011). As outlined above, the best characterised Chk1 substrate phosphorylated during the replication checkpoint is Cdc25A. Chk1-mediated phosphorylation of Cdc25A on S178 and T507 results in proteosomal-dependent degradation of Cdc25A (Chen et al., 2003; Xiao et al., 2003), which prevents cell cycle progression and origin firing, by preventing activation of CDK2-cyclin A (Falck et al., 2001; Mailand et al., 2000), and loading of Cdc45 onto replication origins (Costanzo et al., 2000).

More recently, a number of ATP-dependent annealing helicases have been reported to play a role in stabilising stalled replication forks, and mediating replication fork restart (Bansbach et al., 2009; Ciccia et al., 2009; Yuan et al., 2012). These enzymes, including SWI/SNF-related matrix-associated actin-dependent regulator of chromatin subfamily A-like protein 1 (SMARCAL1; also known as HepA-related protein (HARP)) and annealing helicase 2 (AH2; also known as Zinc finger Ran-binding domain-containing protein 3 (ZRANB3)), catalyse the rewinding of replication protein A (RPA)-coated ssDNA, thus stabilising stalled replication forks (Bansbach et al., 2009; Ciccia et al., 2009; Yuan et al., 2012). The recruitment of SMARCAL1 to RPA-coated ssDNA is dependent on interaction with RPA (Yusufzai et al., 2009), while AH2 interacts with polyubiquitinated PCNA (Ciccia et al., 2012). It is proposed that these enzymes promote replication

fork restart through disassembly of recombination intermediates and activation of a template switching mechanism (Ciccia et al., 2012), see Section 1.11.

1.8.3.2 Intra-S checkpoint

The intra-S phase checkpoint refers to a checkpoint activated in response to replication-independent DSBs occurring in S-phase (Bartek et al., 2004). IR-induced DSBs occurring in S-phase are detected by the MRN complex, which recruits ATM leading to ATM autophosphorylation and activation (Lee and Paull, 2005). ATM-mediated phosphorylation of H2AX on S319 (γH2AX) is required for efficient checkpoint activity (Rogakou et al., 1999). Other key mediators of the intra-S phase checkpoint pathway include mediator of checkpoint 1 (MDC1), p53 binding protein 1 (53BP1), and breast cancer susceptibility protein 1 (BRCA1), which are proposed to act as adaptor proteins required for efficient checkpoint activation. In addition to ATM, ATR also plays a role in the intra-S phase checkpoint. ATR is activated following DNA resection at DSB ends, which generates ssDNA, the ATR activating substrate. ATM-mediated phosphorylation of Chk2 and ATR-mediated phosphorylation of Chk1 then co-operate to prevent progression through S-phase by promoting Cdc25A degradation (Sørensen et al., 2003).

1.8.3.3 S/M checkpoint

The S/M checkpoint refers to the checkpoint activated to prevent the onset of mitosis until DNA replication is complete. While the S/M checkpoint is less well understood on a molecular level, the key substrate of the S/M checkpoint is the mitotic CDK1 (Bartek et al., 2004). The S/M checkpoint prevents activation of CDK1 through Chk1-mediated phosphorylation and degradation of Cdc25A, as described above.

Overall, the S-phase checkpoints described above are p53-independent. Thus, rather than activating a prolonged S-phase arrest, the S-phase checkpoints function to slow the rate of on-going DNA synthesis, prevent the firing of new origins of replication, and activate repair or resolution of the DNA damage.

1.8.3.4 Checkpoint recovery and replication fork restart

Activation of cell cycle checkpoints is essential to protect the integrity of the genome, and allows time for DNA damage to be repaired. However, recovery from cell cycle arrest and completion of cell division is equally important for organism survival. Thus, the mechanisms of checkpoint recovery is an emerging topic in the field of DNA damage-induced checkpoint research (Bartek and Lukas, 2007).

Central to recovery from cell cycle arrest is the ubiquitin-proteasome system. A number of proteins essential for checkpoint activation are degraded in a ubiquitin-proteasome-dependent manner when the time comes for cells to re-enter the cell cycle, including claspin (Mamely et al., 2006; Peschiaroli et al., 2006) and Wee1 (Watanabe et al., 2004b). Degradation of claspin inhibits Chk1 activation, thus allowing downstream activation of Cdc25A phosphatase, while Wee1 is a direct CDK inhibitor. Both processes result in CDK-mediated cell cycle progression.

1.9 The checkpoint kinases

As outlined above, the checkpoint kinases Chk1 and Chk2 are central to DNA-damage induced checkpoint signalling.

1.9.1 Checkpoint kinase 1 (Chk1)

Chk1 is an evolutionary conserved serine/threonine kinase (Chen and Sanchez, 2004), encoded by the *CHK1* gene. Chk1 is a 476 amino acid, 54 kDa protein with a conserved N-terminal kinase domain and a C-terminal regulatory domain, linked by a flexible region (Chen et al., 2000) (Figure 1.8(A)). Chk1 is essential as mutation of the *CHK1* gene results in embryonic lethality in mice (Liu et al., 2000). As outlined above, Chk1 plays essential roles in mediating checkpoint activation in response to DNA damage (Bartek and Lukas, 2001).

1.9.1.1 Regulation of Chk1 activity

Interacting proteins involved in DNA-damage induced Chk1 activation are outlined in Section 1.8.3.2. Here, the effect of post-translational modification on Chk1 function will be discussed. In response to DNA

damage, Chk1 kinase activity is activated by ATR-mediated phosphorylation of Chk1 on S317 and S345 (Liu et al., 2000; Zhao and Piwnica-Worms, 2001), located in the C-terminal regulatory domain of Chk1 (Figure 1.8(A)). Interestingly, deletion of the C-terminal regulatory domain of Chk1 increases its intrinsic kinase activity (Chen et al., 2000; Oe et al., 2001), suggesting the C-terminal domain acts as a negative regulator of kinase activity. Structural analysis of Chk1 provided evidence that the C-terminal regulatory domain could interact with the kinase domain, regulating kinase activity (Chen et al., 2000). Thus, phosphorylation of Chk1 has been proposed to relieve the inhibitory effect of the C-terminal domain (Figure 1.8(B)).

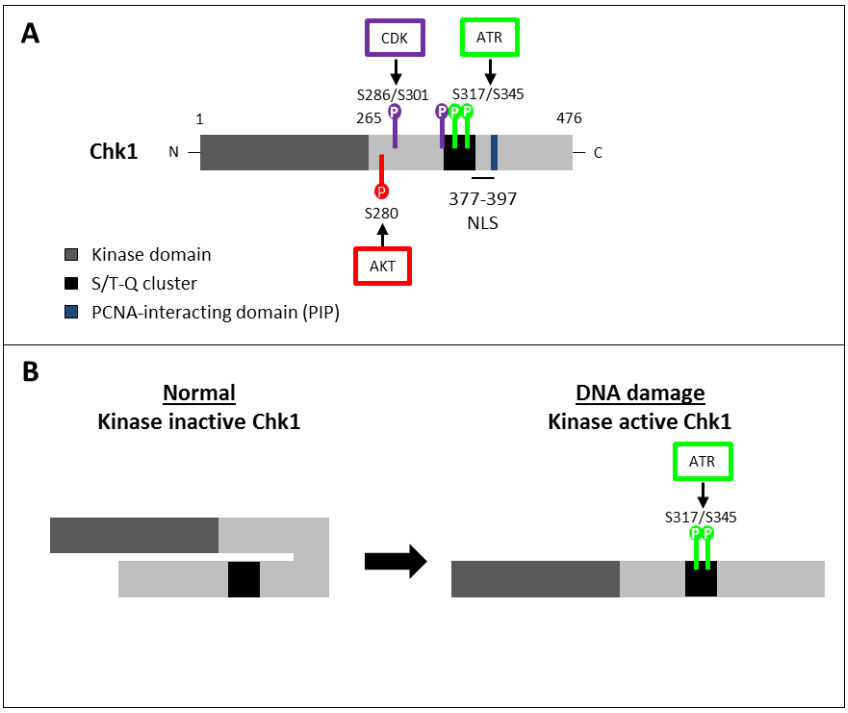

Figure 1.8 (A) Schematic outline of the domain organisation and phosphorylation sites of the human Chk1 protein. Adapted from Stracker et al., 2009. **(B) Auto-regulation model of Chk1 activity.** Colour scheme as outlined in (A). Adapted from Tapia-Alveal et al., 2009.

As well as activating Chk1 kinase activity, phosphorylation of S317 is essential for release of activated Chk1 from chromatin, allowing Chk1 to phosphorylate non-chromatin bound targets (Niida et al., 2007; Smits et al., 2006). Phosphorylation of S317 is required for S345 phosphorylation, since

mutation of S317 to alanine inhibits S345 phosphorylation in response to DNA damage (Niida et al., 2007; Walker et al., 2009; Wang et al., 2012). Furthermore, in the absence of N-terminal kinase domain, Chk1 has high levels of ATR-mediated S317 and S345 constitutive phosphorylation under unperturbed conditions, suggesting that the N-terminus functions to prevent Chk1 activation in the absence of damage (Wang et al., 2012). These observations provide a dual-regulatory mechanism preventing Chk1 activation under unperturbed conditions, whereby the C-terminus is required to inhibit Chk1 kinase activity and in parallel, the kinase domain is required to inhibit Chk1 phosphorylation (Wang et al., 2012). In addition, CDK-mediated phosphorylation of Chk1 on S286 and S301 was recently identified as playing a role in efficient IR-induced checkpoint activation (Xu et al., 2011).

As well as regulating Chk1 activation, post-translational modification of Chk1 regulates the inactivation and degradation of the protein. Phosphorylation of Chk1 on S280 by protein kinase B (PKB) inhibits Chk1 checkpoint function, resulting from impaired S345 phosphorylation, mono-ubiquitination of Chk1 and re-localisation of Chk1 to the cytosol (Puc et al., 2005). Moreover, exposure to DNA damaging agents targets Chk1 for proteosomal degradation, which is preceded by ATR-mediated phosphorylation of Chk1 on S345, and is suggested to be involved in checkpoint recovery (Zhang et al., 2005b).

Recently an additional novel regulatory mechanism for Chk1 has been identified, in which an N-terminal truncated splice variant of Chk1 (termed Chk1-S), is expressed in a panel of human cell lines, which binds to and inhibits Chk1 function (Pabla et al., 2012). Under unperturbed conditions, Chk1-S is expressed in S and G2 phases, where it binds to Chk1 and inhibits is function, thus promoting cell cycle progression from S to G2/M. Furthermore, damage-dependent phosphorylation of Chk1 interrupts the Chk1-Chk1-S interaction, resulting in Chk1 activation (Pabla et al., 2012).

1.9.1.2 DNA damage-induced Chk1 function

As outlined above, Chk1 kinase plays an essential role in activation of multiple cell cycle checkpoints. In response to DNA damage Chk1 activity slows replication fork progression, stabilises stalled replication forks, inhibits replication origin firing, as well as inhibiting the onset of mitosis before replication is complete (Liu et al., 2000; Zachos et al., 2003; Zachos et al., 2005).

Since Chk1 is an essential gene, studies of Chk1 kinase function have relied on specific small molecule inhibitors of Chk1 kinase activity, including UCN-01 (Busby et al., 2000; Syljuåsen et al., 2005) and Chir-124 (Tse et al., 2007), as well as siRNA-mediated Chk1 knockdown. More recently, the development of a viable $Chk1^{-/-}$ DT40 avian cell line (Zachos et al., 2003) has allowed more detailed analysis of Chk1 function.

Despite the central role of Chk1 in cell cycle checkpoint activation, only a limited number of Chk1 substrates have been identified. Key Chk1 substrates involved in regulating cell cycle progression are the Cdc25 family of phosphatases (described in detail in Section 1.8). As well as regulating cell cycle progression, Chk1 plays a role in activating DNA repair. Chk1-dependent phosphorylation of Rad51 on T309 is required for efficient homologous recombination (Sorensen et al., 2005). Chk1-mediated phosphorylation of FANCE, a component of the Fanconi anemia (FA) core complex, on T346 and S374 is required for activation of the Fanconi Anemia/BRCA1 DNA cross-link repair pathway (Wang et al., 2007a).

1.9.1.3 Functions of Chk1 in unperturbed cells

Chk1 is an essential protein and thus it is proposed to play a role in normal cell cycle regulation, under unperturbed conditions. Consistent with this roles for Chk1 in regulating replication initiation and replication fork stability, as well as the onset and progression of mitosis in unperturbed cells have been described (Petermann and Caldecott, 2006; Zachos and Gillespie, 2007).

Inhibition of Chk1 in unperturbed cells results in increased replication, which is associated with increased phosphorylation of ATR substrates, including Chk1, H2AX and RPA2, and increased ssDNA and formation of DSBs (Syljuåsen et al., 2005). The authors propose a mechanism whereby inhibition of Chk1 results in stabilisation of Cdc25, and activation of CDK2 which promotes loading of Cdc45 at origins of replication and promotes replication initiation. In parallel, Chk1 inhibition de-stabilises stalled replication forks, which collapse resulting in replication-associated formation of ssDNA and DSBs (Syljuåsen et al., 2005). Thus, under unperturbed conditions, Chk1 regulates origin firing and stabilisation of replication forks. It must be noted that replisomes encounter endogenous damage in the DNA template during an otherwise unperturbed cell cycle. Thus low basal levels of the DDR machinery could be activated in response to this damage. Consistent with this, certain DDR proteins, including claspin, the MRN complex and TopBP1, are localised to the chromatin during S-phase, the DDR machinery is thus 'primed' for action in the event that a replisome encounters DNA damage (Petermann and Caldecott, 2006). Furthermore, as previously noted above, (Section 1.8.2) Chk1 is also essential for activation of the spindle assembly checkpoint (SAC) and to control mitotic entry (Zachos et al., 2007).

The importance of appropriate Chk1 function is indicated by the complex mechanisms regulating Chk1 activity, under both unperturbed conditions and in response to DNA damage. While significant advances in our understanding of Chk1 regulation and function have been made, the central role of Chk1, not only regulating normal cell cycle progression, but in response to DNA damage, as well as the function of the protein in DNA repair, cell survival, transcription and possibly other pathways, suggests we have only scratched the surface of understanding the landscape of Chk1 function and regulation.

1.9.2 Checkpoint kinase 2 (Chk2)

Human Chk2 is a 60 kDa protein, encoded by the *CHK2* gene. In contrast to Chk1-deficient animals, $Chk2^{-/-}$ mice are viable, but have defects in IR-

induced G1/S checkpoint activation and in p53 stabilisation (Takai et al., 2002). Furthermore, germ-line mutations in *CHK2* have been identified in a subset of patients with the cancer prone Li Fraumeni syndrome, indicating Chk2 is a tumour suppressor (Bell et al., 1999). Activation of Chk2 kinase activity is required for the G1/S, intra-S and G2/M checkpoints (Bartek et al., 2001). Chk2 is activated by ATM-mediated phosphorylation on T68 in response to IR-induced DSBs (Matsuoka et al., 2000a). Chk2-mediated phosphorylation of Cdc25A in G1 and S-phase, results in ubiquitination and degradation of Cdc25A, inducing G1 arrest and inhibition of DNA synthesis, respectively (Falck et al., 2001; Mailand et al., 2000). In response to DNA damage in G2, Chk2 phosphorylates Cdc25C leading to 14-3-3 binding, sequestration of Cdc25C in the cytosol and inhibition of mitosis initiation (DiPaola, 2002; Peng et al., 1997). Chk2-meidated phosphorylation of p53 on S20, stabilises p53 protein and promotes sustained G1/S and G2/M checkpoint activation, as well as activation of apoptosis (Ryan et al., 2001). In addition, Chk2-mediated phosphorylation of BRCA1 on S988 regulates BRCA1 function in survival following IR (Lee et al., 2000).

1.10 DNA repair

In order to protect the integrity of the genome, cells have evolved a number of DNA repair pathways to repair various types of DNA damage, occurring as a result of normal cellular processes, such as replication or oxidative respiration, or exposure to environmental agents, such as UV radiation. The exact DNA repair pathway activated is dependent on the type of DNA damage, the location of the damage in the genome and the cell cycle phase in which the damage occurs (Hoeijmakers, 2001).

1.10.1 Nucleotide excision repair (NER)

Mutations in the genes encoding XPA-XPG proteins involved in NER gives rise to the genetic disorder xeroderma pigmentosum (XP) (Cleaver and Bootsma, 1975). XP cells are defective in the repair of UV-induced DNA lesions (Cleaver and Bootsma, 1975). The crucial role of NER in skin

cancer prevention is highlighted by the clinical phenotype of XP patients, which includes an up to 10,000-fold increase in the incidence of skin cancers (DiGiovanna and Kraemer, 2012).

The NER pathway removes helix distorting lesions, including UV-induced CPDs and 6,4-PPs, which block normal replication and transcription. Two NER sub-pathways exist, global genome repair (GGR) and transcription-coupled repair (TCR). As the name suggests, GGR surveys the entire genome for lesions, whereas TCR repairs lesions on the transcribed strand of genes (Nouspikel, 2009). The major steps in NER are lesion recognition, incision of DNA, excision of an oligonucleotide containing the lesion, gap filling and ligation. As well as the genomic loci which GGR and TCR target, the sub-pathways differ in the mechanism of lesions recognition. During GGR, helix distorting lesions are recognised by the XPC-Rad23 homologue B complex (Sugasawa et al., 1998). In contrast, stalling of RNA polymerase II at lesions during transcription provides the activating signal for TCR (Laine and Egly, 2006). The complex process of NER requires more than 25 proteins, which are assembled in a stepwise fashion at the lesion site (reviewed in Hoeijmakers (2001); Nouspikel (2009)). Following lesion recognition, the remaining steps of the two sub-pathways converge resulting in removal of a 28-32 oligonucleotide containing the lesion, gap filling by DNA polymerase δ or ε, and ligation by the ERCC1/XPE complex.

ATR regulates both NER sub-pathways through interaction and phosphorylation of XPA, the rate limiting factor for NER, that is essential for both GGR and TCR (Köberle et al., 2006). Direct interaction of ATR with XPA is required for nuclear localisation of XPA in response to UVC-induced DNA damage (Wu et al., 2006). Moreover, ATR-mediated phosphorylation of XPA on S196 stabilises XPA protein and increases retention of the protein on chromatin following DNA damage, and is required for optimal excision repair (Lee et al., 2012; Shell et al., 2009).

1.10.2 Base excision repair (BER)

The BER pathway removes chemically modified DNA bases which do not greatly distort the DNA double-helix, but which could potentially interfere with base-pairing during replication. Tens of thousands of base modifications, resulting from, for example, oxidation, alkylation or deamination, occur in normal cells every day (Zharkov, 2008). One of the lesions repaired by BER is 8-oxo-G, which if left unrepaired can result in G-T transversion mutations, as a result of incorporation of adenine opposite 8-oxo-G in the template (Cheng et al., 1992).

During BER, recognition and excision of modified bases is carried out by DNA glycosylases. There are at least 11 mammalian DNA glycosylases, each recognising a specific modified base (Robertson et al., 2009). For example, 8-oxo-G glycosylase (OGG1) recognises 8-oxo-G and cleaves the *N*-glycosidic bond between the base and the sugar-phosphate DNA backbone, resulting in the formation of an abasic site (Klungland and Bjelland, 2007). A nick in DNA backbone is then cleaved by an AP endonuclease or AP lyase, which is processed resulting in a single-nucleotide gap (Robertson et al., 2009). The nucleotide gap is filled by DNA polymerases, in particular polβ, which also cleaves the 5' deoxyribose phosphate, allowing ligation of the nick by a DNA ligases (Matsumoto and Kim, 1995). There are two BER sub-pathways, short-patch repair and long-patch repair. Short-patch repair, as outlined above, involves the re-synthesis of a single nucleotide at the damage site. Long-patch BER involves the re-synthesis of at least 2 nucleotides during strand displacement synthesis, carried out in a PCNA-dependent manner by polymerase δ, with subsequent ligation of the nick by DNA ligase I (Frosina et al., 1996).

1.10.3 DNA double strand break (DSB) repair

DNA double strand breaks (DSBs) represent an extremely genotoxic lesion, and if left unrepaired can result in gross genomic instability (Mills et al., 2003). DSBs are the primary DNA lesion formed following exposure to IR (Henner et al., 1983). However, DSBs can also be formed as an indirect

result of replication fork collapse following exposure to replication-inhibiting agents such as UVC-radiation (Yajima et al., 2009). There are two primary DSB repair pathways in mammalian cells; non-homologous end joining (NHEJ) and homologous recombination (HR).

The factors regulating the choice of DSB repair pathway remain a subject of intense study (Boulton, 2010). The cell cycle stage in which the damage occurs is a key factor in determining which DSB repair pathway is activated. HR is restricted to the S and G2 phases of the cell cycle due to a requirement for a homologous DNA sequence on a sister chromatid, while NHEJ can in principle occur during any cell cycle stage (Rothkamm et al., 2003). The structure of the DNA double-stranded ends (DSE) may also influence the choice of repair pathway, such that blunt ends being preferentially repaired by NHEJ, while 5'-3' resected structures being processed by HR (Symington and Gautier, 2011). Furthermore, the phosphorylation status of proteins, including DNA-PK (Neal et al., 2011), and recruitment of other factors to DSB sites, including BRCA1 and 53BP1 (Boulton, 2010) also regulate the choice of DSB repair pathway.

1.10.3.1 Non-homologous end joining (NHEJ)

Non-homologous end joining (NHEJ) is the primary DSB repair pathway in vertebrate cells (Wang and Lees-Miller, 2013). NHEJ is considered an error-prone DSB repair pathway, as following some processing, NHEJ ligates two DSB ends, which can result in loss of genetic information. The process of NHEJ can be divided into three stages; (i) recognition and tethering of the DSEs, (ii) processing of the DSEs and (iii) ligation (Wang and Lees-Miller, 2013). The Ku70/Ku80 complex recognises and binds the DSEs, tethering them together. Furthermore, Ku70/Ku80 recruits and binds DNA-PK_{cs}, activating the kinase activity of the DNA-PK holoenzyme (Gottlieb and Jackson, 1993). DNA-PK kinase activity is required for efficient NHEJ (Kurimasa et al., 1999). DNA processing is required to create ligatable ends. Nucleases including Artemis, Mre11 and WRN, and polymerases μ and γ are implicated in this process (Wang and Lees-Miller,

2013). DNA ends are than ligated by a DNA ligase IV in a complex with XRCC4 (Wang and Lees-Miller, 2013).

1.10.3.2 Homologous recombination (HR)

As outlined above, homologous recombination (HR) requires a homologous DNA sequence, normally from a sister chromatid, as a template for repair, and is therefore restricted to S and G2 phases of the cell cycle and is generally considered an error-free repair pathway (Jackson, 2002). Following resection of the DSB, the 3' ssDNA overhangs become coated with RPA. Rad52- and BRCA2-mediated Rad51 loading and RPA displacement from the DNA is essential for HR (Karpenshif and Bernstein, 2012; Liu et al., 2010; Sugiyama and Kowalczykowski, 2002). Rad51-coated ssDNA mediates a homology search, resulting in disruption of the base pairing of the sister chromatid and the formation of a D-loop structure. DNA polymerases δ or ε catalyse DNA synthesis from the 3' end of the damaged DNA strand, using the homologous sequence as a template (Kawamoto et al., 2005b; Maloisel et al., 2008). The ends are ligated by DNA ligase I and the DNA crossovers (Holliday junctions) resolved, releasing two undamaged sister chromatids (Jackson, 2002; Karpenshif and Bernstein, 2012).

1.11 DNA Damage Tolerance

Despite the plethora of DNA repair pathways in human cells, not all DNA lesions are repaired before cells enter S-phase. Unrepaired lesions, including UV-induced CPDs, block the progression of replicative polymerase (polymerase α, δ and γ), which can lead to stalled replication forks. Prolonged replication fork stalling can result in fork collapse and potentially DNA strand breaks (Petermann and Helleday, 2010). To overcome this threat to genome stability, cells have evolved pathways, collectively termed DNA damage tolerance or post-replicative repair pathways, which mediate replication past and beyond DNA lesions in the template, leaving the lesion to be repaired at a later stage by the classic repair pathways (Section 1.10). The two primary DNA damage tolerance pathways are translesion synthesis (TLS) and template switching. TLS will be discussed in more detail below

(Section 1.11.2). Briefly, TLS requires the recruitment of specialised TLS polymerases, which replace replicative polymerases at stalled replication forks, and carry out replication past the lesion in the template (reviewed in Ghosal and Chen, 2013; Yang et al., 2013). TLS can be either error-prone or error-free, depending on the lesion and the polymerase involved.

On the other hand, template switching is considered an error-free mechanism. Template switching involves elongation of the DNA strand using normal replicative polymerases and an undamaged template, possibly a sister chromatid, via a recombination-mediated or fork reversal process (reviewed in Branzei, 2011). Due to the use of an undamaged template and normal replicative polymerases with proof-reading ability, template switching is considered an error-free DNA damage tolerance mechanism. As is the case with DSB repair, the mechanisms controlling the choice of DNA damage tolerance pathway remains a subject of debate. Some studies suggest a role for ubiquitination of PCNA in regulating the choice, where monoubiquitination of PCNA promotes TLS, while Rad5-mediated polyubiquitination of PCNA promotes the alternative template switch pathway (Ghosal and Chen, 2013).

1.11.1 DNA polymerase eta (polη)

DNA polymerase eta (polη) is the best characterised TLS polymerase (reviewed in Cruet-Hennequart et al., 2010). Encoded by the *POLH* gene (Johnson et al., 1999a; Masutani et al., 1999b), human polη is a 78 kDa protein, the domain organisation is outlined in Figure 1.9. Mutations in the *POLH* gene can give rise to the autosomal recessive genetic disorder xeroderma pigmentosum variant (XPV) (Johnson et al., 1999a; Masutani et al., 1999b). XPV is characterised clinically by increased sun-sensitivity and elevated levels of skin cancer (Cleaver, 1972). In contrast to XP, which is caused by a defect in NER (see Section 1.10.1), XPV cells have normal levels of NER (Tung et al., 1996). At a molecular level, polη-deficient XPV cells have defects in the replication of UVC-damaged DNA and are hypermutable following UVC-exposure (Cleaver and Bootsma, 1975; Lehmann et al., 1975; Tung et al., 1996). Polη-deficient cells accumulate

mutations at CPD sites, possibly due to error-prone TLS past CPDs in the template by an alternative TLS polymerase, such polι (Stary et al., 2003; Wang et al., 2007b).

Like other TLS polymerases, polη is a low fidelity DNA polymerase, copying undamaged templates with an error rate 10^2-10^5 times higher than normal replicative polymerases (McCulloch and Kunkel, 2008). However, polη can carry out error-free replication past a dithymidine CPDs *in vitro* (Johnson et al., 1999b; Masutani et al., 1999a) inserting two adenines opposite the lesion. Structural studies have provided an explanation for the ability of polη to carry out error-free lesion bypass, the enlarged open active site of polη can accommodate the two bases of a dithymidine dimer, allowing efficient bypass of the lesion (Biertumpfel et al., 2010; Silverstein et al., 2010). The error-free bypass of dithymidine CPDs by polη provides direct evidence for a functional role of polη in the prevention of sunlight-induced skin cancers. Knockdown of the *POLH* gene in mice increases the incidence of sunlight-induced skin cancers, similar to the phenotype observed in XPV individuals (Lin et al., 2006).

While polη is not sufficient for bypass of a dithymidine 6,4-PP in template DNA, polη can insert a nucleotide opposite the 3' base of the lesion (Johnson et al., 2001; Masutani et al., 2000). A combination of polζ and polη is required for efficient bypass of a 6,4-PP *in vitro* (Johnson et al., 2001). A two-step mechanism for 6,4-PP bypass has been proposed, whereby polη catalyses the incorporation of a nucleotide opposite the 3' base of a 6,4-PP, followed by a polymerase switch to polζ which incorporates a nucleotide opposite the 5' base and extension from the lesion (Johnson et al., 2001; Shachar et al., 2009).

In addition to its role in TLS past UV photoproducts in DNA, polη plays a role in TLS past other DNA lesions, including 8-oxo-G (McCulloch et al., 2009), O^6-methylguanine (Haracska et al., 2000a), as well as lesion induced by chemotherapeutic agents cisplatin and AraC (Bassett et al., 2004; Chen et al., 2006). Furthermore, a role for polη was identified in HR (Kawamoto et

al., 2005a), somatic hypermutation (Yavuz et al., 2002) and in fragile site stability (Rey et al., 2009).

1.11.2 Translesion synthesis (TLS) and the Y-family polymerases

The process of TLS involves at least two polymerase switch events. First, the normal replicative polymerase is replaced with a TLS polymerase which replicates past the replication blocking lesion. In some cases, the TLS polymerase is replaced by another TLS polymerase which synthesises a short nucleotide tract. Finally the TLS polymerase is replaced by a normal replicative polymerase which resumes DNA synthesis (Ghosal and Chen, 2013; Lehmann et al., 2007; Sale et al., 2012).

TLS polymerases include members of the Y-family, polη, polι, polκ and REV1, the B-family, polζ, and the A-family, polθ and polν (reviewed in Waters et al., 2009). As outlined above (Section 1.11.1), polη, the focus of this research, can carry out error-free replication past dithymidine dimers *in vitro* (Johnson et al., 1999b; Masutani et al., 1999a). Polι can carry out error-free replication past 8-oxo-G lesions in DNA *in vitro* (Kirouac and Ling, 2011). Furthermore, polι is implicated in the bypass of UVC-induced DNA damage, and may account for the increased UV-mutagenesis that characterises polη-deficient cells (Dumstorf et al., 2006; Kannouche et al., 2003; Wang et al., 2007b). Polκ carries out error-free TLS past benzo[a]pyrene-guanine residues, and but is implicated in error-prone TLS past abasic sites and acetylaminofluorene-adducted guanine residues (Ogi et al., 2002). Rev1, while structurally a Y-family member, does not function as a polymerase, but rather as a deoxycytidine monophosphate (dCMP) transferase, inserting dCMP opposite guanine bases or abasic sites in the template (Nelson et al., 1996). Rev1 functions in TLS through interaction with the Rev3 subunit of polζ. Moreover, the other three Y-family polymerases interact with Rev1. The Rev1 interaction has been suggested to control switching events between polζ and other polymerases, such as during two-step TLS (Lehmann et al., 2007).

While the damaged lesion bypassed by each TLS polymerases differs (see above), TLS polymerases share some common features. In general TLS polymerases are considered error-prone polymerases due to lack 3'-5' exonuclease poof-reading activity. TLS polymerases exhibit reduced fidelity compared to normal replicative polymerases when carrying out DNA synthesis on undamaged temples. Moreover, TLS polymerases have reduced processivity compared to normal replicative polymerases limiting the extent of DNA synthesis that can be carried out by these enzymes (Sale et al., 2012; Waters et al., 2009).

Y-family polymerases share some common structural features (Figure 1.9). Within the catalytic domain, the active site of Y family TLS polymerases is bigger than normal replicative polymerases, but shares the overall 'right-hand' structure of replicative polymerases. Y-family TLS polymerases have an additional 'little finger' domain which has been implicated in mediating polymerase selectivity toward certain lesions (Boudsocq et al., 2004).

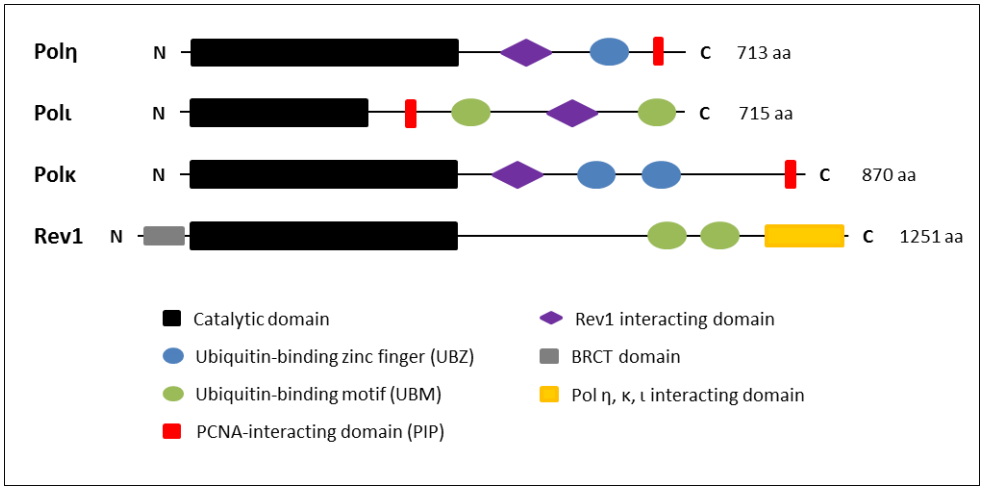

Figure 1.9 Domain organisation of human Y-family translesion synthesis DNA polymerases. Adapted from Waters et al., 2009.

1.11.3 Regulation of translesion synthesis (TLS)

In order to minimise the mutagenic risk associated with DNA replication by low-fidelity TLS polymerases, TLS is subject to tight regulation. Many levels of TLS regulation have been described, the most basic of which in

vertebrate cells is in the recruitment of TLS polymerases to replication foci following DNA damage (Sale et al., 2012). For example, polη localises to nuclear foci following exposure to UVC-radiation (Kannouche et al., 2001). The polymerase switch and TLS polymerase loading onto stalled replication forks is regulated by ubiquitination of proliferating cellular nuclear antigen (PCNA). Monoubiquitination of PCNA is critical for the recruitment of TLS polymerases to stalled replication forks (Ghosal and Chen, 2013; Lehmann et al., 2007). TLS polymerases, including polη, have a higher affinity for monoubiquitinated PCNA than replicative polymerases, such as polδ (Kannouche et al., 2004; Watanabe et al., 2004a). The ssDNA-binding protein Rad18, in conjunction with its binding partner the E2 ubiquitin-conjugating enzyme Rad6, is required for PCNA ubiquitination, and catalyses PCNA monoubiquitination on K164 in response to UVC and HU (Stelter and Ulrich, 2003; Ulrich and Jentsch, 2000; Watanabe et al., 2004a). Rad18 is recruited to stalled replication sites via interaction with RPA (Figure 1.10), although this interaction is dispensable for Rad18 recruitment and TLS function (Davies et al., 2008; Nakajima et al., 2006). Cdc7-mediated phosphorylation is required for the function of Rad18 (Day et al., 2010). Moreover, Nbs1, through its Rad6-like domain, also binds Rad18 following UV exposure and is required for Rad18-dependent PCNA ubiquitination and polη foci formation (Yanagihara et al., 2011). Recently other proteins, including FANCD2 (Fu et al., 2013) and BRCA1 (Tian et al., 2013), have been shown to regulate polη localisation following UVC. PCNA ubiquitination is also controlled by the de-ubiquitinating enzyme ubiquitin carboxyl-terminal hydrolase 1 (USP1), which normally removes monoubiquitin from PCNA (Huang et al., 2006). Following damage, USP1 is degraded by an auto-cleavage mechanism (Figure 1.10), which correlates with up-regulation of PCNA monoubiquitination (Huang et al., 2006).

Stalled replication forks lead to the generation of regions of ssDNA which activate not only TLS but ATR-Chk1-dependent DDR signalling (Section 1.8.3.1). Evidence suggests that a single stalled replication fork can accommodate both processes due to preferential loading of the DDR-related 9-1-1 clamp complex onto the 5’ end of primed RPA-coated ssDNA, while

PCNA is loaded on the 3' end (Ghosal and Chen, 2013). Thus, it is not surprising that DDR-associated proteins, including Chk1, claspin and Timeless, by mediating PCNA ubiquitination under conditions of replication stress, are involved in regulating TLS (Yang et al., 2008).

Recently, novel factors, including Spartan and PCNA-associated factor 15 (PAF15), that regulate TLS have been identified (Ghosal and Chen, 2013). Spartan interacts with monoubiquitinated PCNA through its UBZ and PIP domains, plays a key role in the regulation of TLS (Centore et al., 2012) (Figure 1.10). Spartan knockdown reduces UV-survival, and inhibits polη recruitment to foci, PCNA monoubiquitination and Rad18 chromatin association (Centore et al., 2012). Furthermore, through recruitment of p97 (AAA-ATPase), Spartan may lead to TLS polymerase extraction during DNA repair, preventing mutagenesis (Davis et al., 2012). PAF15 is another PCNA-binding protein that regulates TLS activity (Povlsen et al., 2012). During unperturbed conditions PAF15 is chromatin bound through interaction with PCNA. Following UVC-exposure PAF15 is removed from the chromatin via proteosomal-mediated degradation, which allows recruitment and binding of polη to monoubiquitinated PCNA (Povlsen et al., 2012) (Figure 1.10).

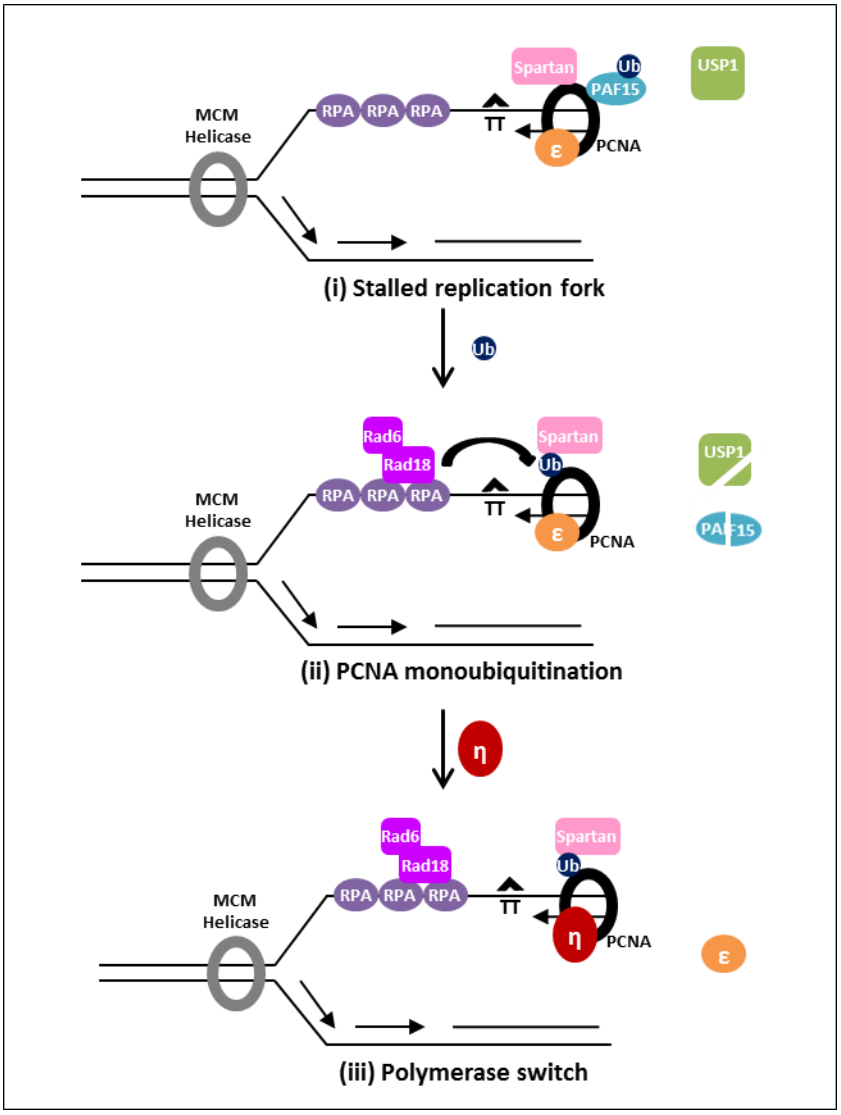

Figure 1.10 Proposed model of translesion synthesis polymerase recruitment to stalled replication forks. (i) Replication fork stalling at a DNA lesion leads to uncoupling of the replicative MCM helicase and the formation of single-stranded DNA (ssDNA), which becomes coated with replication protein A (RPA). (ii) RPA-ssDNA recruits Rad18, which, along with Rad6, monoubiquitinates PCNA on K164. Ubiquitin carboxyl-terminal hydrolase 1 (USP1), which normally de-ubiquitinates PCNA, is degraded by an auto-cleavage mechanism. PCNA-associated factor 15 (PAF15), which is normally bound to PCNA, is degraded in an ubiquitin-proteasome-dependent manner, which allows the TLS polymerase to bind monoubiquitinated PCNA. Spartan also binds monoubiquitinated PCNA, stabilising Rad18 on chromatin. (iii) The TLS polymerase (polη) replaces the replicative polymerase (polδ) by binding monoubiquitinated PCNA in a mechanism termed the polymerase switch. The subsequent steps of TLS, not depicted here, involved lesion bypass by the TLS polymerase, extension of the DNA, and another polymerase switch to replace the TLS polymerase with a replicative polymerase. Adapted from Ghosal et al., 2013.

While the involvement of PCNA monoubiquitination in the recruitment of TLS polymerases to stalled replication forks is well documented, the mechanism of TLS polymerase selection remains a subject of debate. However, some potential mechanisms for polymerase selection have been proposed (Lehmann et al., 2007; Sale et al., 2012). One such model is a dynamic model in which multiple polymerases transiently bind mono-ubiquitinated PCNA and attempt replication until the polymerase capable of bypassing the lesion is recruited (Lehmann et al., 2007; Sale et al., 2012). It should be noted that while PCNA monoubiquitination is important for efficient TLS, it is not essential for TLS in mouse embryonic fibroblasts (MEFs) (Hendel et al., 2011). However, MEFs expressing mutated PCNA which cannot be ubiquitinated on K164 have reduced efficiency of TLS past UV photolesions and altered mutagenic specificity (Hendel et al., 2011).

Another unresolved question in the field of TLS is the debate as to whether TLS occurs at the site of a stalled replication fork, or if the replication fork restarts past the lesion leaving a gap which is later filled by TLS polymerases. While the former is the general mechanism proposed, evidence for the latter mechanism exists (Lehmann et al., 2007; Sale et al., 2012). Short single-stranded regions have been detected in UVC-irradiated yeast cells, the numbers of which were elevated in mutant strains lacking TLS polymerases (Lopes et al., 2006). The issue with this model is the mechanism of fork restart past the lesion, which remains to be elucidated.

1.11.3.1 Regulation of translesion synthesis by DNA damage response proteins

It has recently been reported that recruitment of polη to sites of DNA damage requires the checkpoint protein Chk1 (Speroni et al., 2012). Independent of Chk1 kinase activity, but requiring the newly identified PCNA-interacting (PIP) motif of Chk1, Chk1 release from chromatin is required for replication fork progression and polη recruitment to nuclear foci following UVC exposure in U2OS cells (Speroni et al., 2012). Furthermore, another study identified a role for Chk1 and its accessory factors claspin and Timeless in mediating PCNA ubiquitination in response

to UVC radiation exposure (Yang et al., 2008). This suggests that Chk1, independent of kinase activity, promotes the progression of stalled replication forks, by mediating recruitment of the TLS polymerase polη. Further evidence for checkpoint-dependent regulation of polη activity comes from a study which found that DNA damage-induced ATR-mediated phosphorylation of polη on S601, is required for cell survival following UVC exposure, and mediates DNA replication behind the replication fork in human fibroblast cell lines (Göhler et al., 2011).

1.12 Research objectives

Exposure to solar UVA radiation, which accounts for >95% of solar UV radiation reaching the earth's surface, is a risk factor for the development of skin cancer, including melanoma. UVA induces DNA damage which may play a role in skin carcinogenesis. The DNA damage response (DDR) is a complex network of signalling pathways activated in cells in response to DNA damage and acts as a barrier to carcinogenesis, by initiating DNA repair, inhibiting cell cycle progression in the presence of DNA damage or activating cell death if the damage is too severe. While many studies have focused on characterising the type and quantities of UVA-induced DNA damage, little is known about the DDR pathways activated in response to UVA radiation, particularly in primary human melanocytes.

The aims of this research project were to:

(i) Investigate the role of DNA polymerase eta (polη) in the response of human cells to UVA radiation, and

(ii) Characterise UVA-induced DNA damage response pathways in primary normal human epidermal melanocytes.

2 Materials and Methods

2.1 Materials

2.1.1 Equipment

- Bench top centrifuges: Rotanta 460 centrifuge (Hettich Zentrifugen, Tuttlingen, Germany); Sigma 1-15K centrifuge (Sigma); PicoFuge™ (Stratagene)
- Cell culture incubator: AutoFlow water-jacketed CO_2 incubator with Class 100 HEPA Filtration System (NuAire Inc®, MN, USA)
- Cell culture laminar flow hood: Class II Biological Safety hood (NU-473-400E; NuAire Inc®, MN, USA)
- Chemoluminescence imager: Fujifilm LAS-3000 imager
- Cryo 1°C cell freezing container (Nalgene®, Rochester, NY, USA)
- Electrophoresis power supply: PowerPack 3000 (Bio-Rad, UK)
- Film developer: CP1000 automatic film processor (Agfa, Mortsel, Belgium)
- Flow cytometer: FACS Calibur (BD, NJ, USA)
- Fluorescent microscopes: DeltaVision Core system (Applied Precision) controlling an interline charge-coupled device camera (CoolSnap HQ2; Roper) mounted on an inverted microscope (IX-71; Olympus)
- Fume hood: 1200 standard, 4616-L (ChemFlow, CA, USA)
- Heat block: DB-2P Dri-Block (Techne® Inc., NJ, USA)
- Labnet Rocker 35A (Labnet International, Inc., NJ, USA)
- Laboratory oven: (Shaw Scientific Ltd., Ireland)
- Light microscope: Olympus CKX31 microscope
- Liquid nitrogen storage system (Jencons-PLS, Bedfordshire, UK).
- Protein electrophoresis system: Mini Protean 3® cell system (Bio-Rad, UK)
- Protein transfer system: Mini Protean 3® cell system (Bio-Rad, UK)
- Slot blot apparatus: Minifold II Slot Blot System (Schleicher and Schuell)
- Sonicator: Digital Sonifier® cell disrupter (Branson Ultrasoincs Corporation, USA)

- Spectrometers: Victor^2 1420 96-well plate multilabel counter (Wallac, MA, USA); NanoDrop-1000 spectrometer (NanoDrop Technologies Inc.)
- UV filter: Folanorm, UVUR (Folex GmbH, Dreieich, Germany)
- UV irradiance probe: UVX digital radiometer, UVX-25 probe, UVX-30 probe, UVX-35 probe (UVP Inc., CA)
- UVA source: BS-03 (Dr. Groebel UV-Electronik GmbH, Germany)
- UVB source: 302 nm, UVM-57 (UVP Inc., CA)
- UVC source: 254 nm, UVG-11 (UVP Inc., CA)
- Vacuum pump: Buchi-Vacuum pump V-700 (BUCHI Labortechnik, AG, Switzerland)
- Vacuum sealer: (Bifinett, GmbH)
- Water bath: Clifton unstirred bath (Bennett Scientific, UK)

2.1.2 Chemicals and Plastic/Glassware

- All chemicals were purchased from Sigma-Aldrich, Fisher Scientific or Merck-Millipore, unless otherwise stated.
- All sterile plasticware for use in tissue culture was from Corning, Sarstedt or Novagen, unless otherwise stated
- Glass coverslips for immunofluorescence were purchased from VWR
- All glassware was purchased from Fisher Scientific

2.1.3 Software

- CellQuest™ (BD Bioscience) – acquisition and analysis of flow cytometry data
- SoftWoRx (Applied Precision) – acquisition and analysis of fluorescent images from the DeltaVision Core system
- Image Pro Plus V 6.2 (Media Cybernetics Inc.) – quantitation of the fluorescence intensity of images acquired on the DeltaVision Core system
- Multi Gauge V 2.2 (Fujifilm) – acquisition and analysis of Chemoluminescence images

Table 2.1 Chemicals used in tissue culture

Chemical	Common name / abbreviation	Supplier	Stock conc.	Diluent	Working dose range
2', 7'-dichlorofluroescein diacetate	DCFH-DA	Sigma	10 mM	DMSO	10 µM
4-hydroxytamoxifen	4-OHT	Sigma	1 mM	EtOH	1µM
5-bromo-2'-deoxyuridine	BrdU	BD	10 mM	MEM	10 µM
5-Ethynyl-2′-deoxyuridine	EdU	Invitrogen	10 mM	DMSO	10 µM
Caffeine	Caf	Sigma	10 mM	ddH_2O	1 mM
Chir-124	CHir-124	Selleckchem	1 mM	DMSO	100 nM
cis-diammineineplatinum (II) dichloride	Cisplatin	Ebewe	1 mg/ml	ddH_2O	0 - 5 µg/ml
Gö 69833	Gö 69833	Selleckchem	10 mM	DMSO	10 µM
Hydrogen peroxide	H_2O_2	Sigma	30% (v/v)	ddH_2O	100 µM
KU-60019	ATMi	Selleckchem	10 mM	DMSO	10 µM
N-acetyl-cysteine	NAC	Sigma	1 M	ddH_2O	10 mM
Phorbol 12-Myristate 13-Acetate	PMA	Sigma	1.62 mM	DMSO	200 nM
Rottlerin	Rottlerin	Merck Millipore	10mM	DMSO	10 µM
Tetracycline	Tet	Sigma	1 mg/ml	EtOH	0.1 µg/ml
UCN-01	UCN-01	Sigma	1mM	DMSO	50-100 nM
Wortmannin	Wortmannin	Sigma	10 mM	DMSO	10 µM

2.1.4 Cells

Table 2.2 Human fibroblast cell lines

Cell line	Origin	Characteristics
XP30RO (GM0317A)	Prof. J. Cleaver, UCSF, and subsequently from the Coriell Institute for Medical Research, New Jersey, USA	Human SV40-transformed fibroblast cell line, lacking functional polη protein due to a 13-base pair deletion in exon 2 of *POLH*
TR30-2	Dr. M.P. Carty, CCB, NUIG	XP30RO-derived cell line constitutively expressing polη from a *POLH* transgene
TR30-9	Dr. M.P. Carty, CCB, NUIG	XP30RO-derived cell line expressing tetracycline-inducible V5-tagged polη
TRG-16	Dr. M.P. Carty, CCB, NUIG	XP30RO-derived cell line expressing tetracycline-inducible eGFP-tagged polη
NFF	Prof. M. Lavin, UQCCR, University of Queensland, Brisbane, Australia	Human transformed normal foreskin fibroblast cell line
XP12RO	Prof. H.P. Nasheuer, CCB, NUIG	Human SV40-transformed fibroblast cell line, lacking XPA protein due to homozygous nonsense mutation at Arg207 of *XPAC*
XP12RO-C5	Prof. H.P. Nasheuer, CCB, NUIG	XP12RO-derived cell line constitutively expressing XPA protein from *XPAC* transgene
AT fibroblasts (GM05849)	Prof. C. Morrison, CCB, NUIG	Human SV40-transformed fibroblast cell line, lacking ATM protein

Table 2.3 Melanocyte cells

Cell	Origin	Characteristics
Normal human epidermal melanocytes (NHEM)	Lonza Inc. MD, USA. (Cat No. CC-2504; Lot no. 5F0059)	Primary human Caucasian male neo-natal melanocytes
Murine melanocytes	Prof. D. Gillespie, Beatson Institute for Cancer Research, University of Glasgow, Scotland.	Spontaneously transformed murine melanocytes, isolated from a transgenic mouse in which Chk1 can be knocked down by the addition of 4-hydroxytamoxifen.

2.2 Methods

2.2.1 Cells

2.2.1.1 Human fibroblast cell lines

A list of human fibroblast cell lines utilised in this study is presented in Table 2.2. SV40-transformed XP30RO cells were originally obtained as a gift from Prof. J. Cleaver (University of California, San Francisco, USA), and subsequently purchased from the Coriell Institute for Medical Research, New Jersey, USA (Repository number GM0317A). XP30RO is a SV40-transformed fibroblast cell line derived from an XPV patient (Volpe and Cleaver, 1995) and lacks functional polη protein due to a 13-base pair deletion in exon 2 of the *POLH* gene (Johnson et al., 1999a). XP30RO cells were utilised previously to generate the polη-expressing cells lines TR30-2, TR30-9 and TRG-16 (Cruet-Hennequart et al., 2006; Cruet-Hennequart et al., 2008). Briefly, XP30RO cells were stably transfected with pcDNA6/TR® vector (Invitrogen), which expresses the tetracycline (tet) repressor under the control of a CMV promoter, and clonally selected using blasticidin, to produce the TR cell line. The TR cell line was then transfected with either (i) pMR30-V5 or (ii) pMR30-GFP vectors, and following clonal selection using zeocin, the resulting clones (i) TR30-9 and TR30-2 and (ii) TRG-16 were obtained. TR30-9 cells express a tetracycline-

inducible C-terminal V5-tagged polη as described previously (Cruet-Hennequart et al., 2006). TR30-2 cells constitutively express wild-type V5-tagged polη. TRG-16 cells express a tetracycline-inducible C-terminal GFP-tagged polη protein.

XP12RO and XP12RO-C5 obtained from Prof. H.P. Nasheuer (CCB, NUIG), were originally gifted from Prof. R.D. Wood (University of Pittsburgh, PA, USA). XP12RO cells lack functional XPA protein due to a nonsense mutation in the *XPAC* gene (Satokata et al., 1992a; Satokata et al., 1992b). XP12RO-C5 were derived from XP12RO and constitutively over-express wild-type XPA protein from an *XPAC* transgene (Köberle et al., 2006).

The GM05849 (AT fibroblast) cell line, obtained from Prof. C. Morrison (CCB, NUIG), was originally purchased from Coriell Cell Repositories. GM05849 is an SV40-transformed human fibroblast cell line derived from an AT patient, and lacks ATM protein as a result of mutation in the *ATM* gene (Savitsky et al., 1995a; Savitsky et al., 1995b).

2.2.1.2 Melanocyte cells

Melanocyte cells utilised in this study are outlined in Table 2.3.

2.2.1.2.1 Primary normal human epidermal melanocyte (NHEM)

Primary normal human epidermal melanocytes (NHEM), at passage 3, derived from a neo-natal Caucasian male, were obtained from Lonza Inc., MD, USA. According to the Lonza specifications (Lonza document No. TS-CC-50-7 11/10), NHEM were characterised based on (i) morphological observation of cells, with normal melanocytes having small cell bodies and bi- or multi-polar processes, (ii) the ability to convert L-Dopa to melanin, which requires the activity of tyrosinase (Aberdam et al., 1998), and (iii) immunofluorescence staining for Mel-5, a 75 kDa glycoprotein specifically expressed in the melanosomes of pigmented melanocytes (Bhawan, 1997).

2.2.1.2.2 Chk1-conditional knockdown murine melanocytes

Murine melanocytes, obtained from Prof. D. A. Gillespie (Beatson Institute, Glasgow, UK), were isolated from the skin of a transgenic mouse strain in

which (i) exon 2 for the *chk1* allele is flanked with LoxP sites and (ii) a Cre recombinase-estrogen receptor (Cre-ERT2) fusion protein is expressed from a transgene under the control of the skin-specific keratin 14 gene promoter, limiting Cre-ERT2 expression to the epidermis and hair follicles, and (iii) a *Rosa26-LacZ* reporter introduced to allow tracking of the recombined cells (Figure 2.1 (i) and Tho et al., (2012)). Melanocytes isolated from this mouse strain spontaneously transformed in culture due to constitutive N-Ras expression, as a result of loss of the *INK4A* locus (Prof. D. Gillespie, personal communication). The murine melanocytes express wild type Chk1 and an inactive Cre-ERT2 fusion protein (Figure 2.1 (ii)). Addition of 4-hydroxytamoxifen (4-OHT) to the culture media results in the activation of Cre recombinase, and leads to the Cre-mediated recombination of the LoxP sites flanking exon 2 of the *chk1* gene. Deletion of exon 2 of *chk1* results in complete loss of Chk1 function (Figure 2.1 (iii)). Deletion of exon 2 of *chk1* has been shown to be sufficient for complete loss of Chk1 function (Liu et al., 2000).

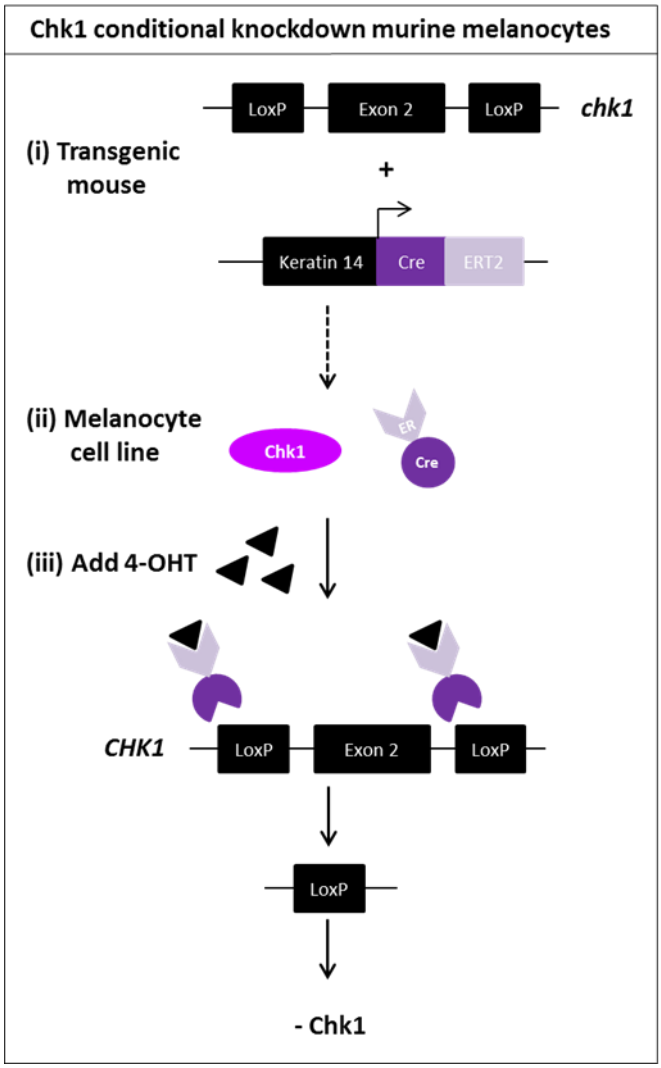

Figure 2.1 Chk1 conditional knockdown murine melanocyte cell line. The Chk1 conditional knockdown murine melanocyte cell line was generated in the laboratory of Prof. D. Gillespie, Beatson Institute, Cambridge, UK. **(i)** A FVB transgenic mouse was generated with the following genetic manipulations (a) exon 2 of *chk1* was flanked by loxP sites, (b) a transgene encoding a Cre recombinase-estrogen receptor (Cre-ERT2) fusion protein under the control of the keratin 14 gene promoter was introduced and (c) a *Rosa26-LacZ* reporter plasmid was also introduced to track recombined cells. **(ii)** Melanocytes isolated from mice expressing the N-Ras oncogene, with loss of the Ink4a locus, spontaneously transformed in culture. Untreated murine melanocytes express Chk1 protein and an inactive Cre-ERT2 fusion protein. **(iii)** Treatment with 4-hydroxytamoxifen (4-OHT) results in the binding of 4-OHT to the estrogen receptor of the Cre-ERT2 fusion protein and subsequent activation of Cre recombinase. Activated Cre catalyses recombination of the *chk1* exon2 carrying flanking loxP sites, resulting in down-regulation of Chk1 expression.

2.2.2 Cell culture

All cell culture procedures were carried out in a Class II biological safety hood (NuAire Inc.®, MN, USA). The surface of the hood and any items entering the hood were sterilised by spraying with 70% industrial methylated spirits (IMS; Fisher) before use for cell culture. Disposable sterile plasticware and pipette tips were utilised during culture procedures. Prior to cell culture, all media and trypsin solutions were pre-warmed to 37°C in a water bath. Cells were incubated in an autoflow water-jacketed CO_2 incubator (NuAire Inc.®, MN, USA) at 37°C and 5% CO_2.

2.2.2.1 Culture of human fibroblast cell lines

XP30RO, TR30-2, TRG-16, TR30-9 and AT fibroblast cell lines were routinely cultured in Minimum Essential Medium Eagle (MEM; Sigma) supplemented with 10% non-heat inactivated foetal bovine serum (FBS; Sigma), 2X essential amino acids (Gibco), 2X non-essential amino acids and 2X vitamins (Gibco), 2 mM L-glutamine (Sigma) and 1% penicillin-streptomycin (Sigma). NFF, XP12RO and XP12RO-C5 cells were cultured in Dulbeccos' Modified Eagles Medium (DMEM; Sigma) supplemented with 10% heat inactivated FBS (56°C for 30min; Gibco) and 1% penicillin-streptomycin (Sigma). Cell lines were routinely cultured in sterile 75 cm^2 tissue culture flasks (Corning) in 15 ml of the appropriate media. Media was replaced every 48-72 hrs. Cells were sub-cultured at approximately 80% confluence, as determined by observing cells using an Olympus CKX31 light microscope. Adherent cell cultures were trypsinised for approximately 5 minutes, at 37°C, in 1 ml per 25 cm^2 of 2X trypsin-EDTA (Sigma) in Hanks balanced salt solution (HBSS; Sigma). Trypsin activity was inhibited by the addition of 3 ml of media containing 10% FBS per 1 ml of trypsin solution. Cells were centrifuged at 1,200 rpm for 5 minutes in a Rotanta 460 centrifuge (Hettich Zentrifugen, Tuttlingen, Germany). The cell pellet was gently resuspended in pre-warmed media. Cell number was determined using Kova® Glasstic® Slide 10 combination coverslip-microscope slides (Hycor Biomedical Ltd., CA, USA). Seeding densities of cells are outlined in Table 2.4.

Table 2.4 Human fibroblast cell seeding densities

	Seeding density (Cell number)		
Cell	**75cm^2 flask**	**60 mm dish**	**35 mm dish**
XP30RO	8.0 x 10^5	3.5 x 10^5	8.0 x 10^4
TR30-2	1.0 x 10^6	4.0 x 10^5	1.0 x 10^5
TR30-9, TRG-16	1.5 x 10^6	5.0 x 10^5	1.5 x 10^5
NFF	5.0 x 10^5	2.0 x 10^5	8.0 x 10^4
XP12RO, XP12RO-C5	2.0 x 10^6	5.0 x 10^5	2.5 x 10^5

2.2.2.2 Tetracycline-induced polη-GFP expression in TRG-16 cells

Twenty-four hours following seeding, media was changed on TRG-16 cells, and tetracycline at a final concentration of 0.1 µg/ml was added. Polη-GFP expression was detected 24 hr following tetracycline addition, and cells were subsequently treated at this point.

2.2.2.3 Tetracycline-induced polη expression in TR30-9 cells

Twenty-four hours following seeding, media was changed on TR30-9 cells, and tetracycline at a final concentration of 0.1 µg/ml was added. Polη expression was detected 18 hr following tetracycline addition, and cells were subsequently treated at this point.

2.2.2.4 Culture of primary normal human epidermal melanocytes (NHEM)

NHEM were routinely cultured in melanocyte growth media-4 (MGM™-4; Lonza) supplemented with MGM™-4 SingleQuots™ kit (Lonza), which includes undisclosed concentrations of bovine pituitary extract, hydrocortisone, insulin, human fibroblast growth factor-basic, GA-1000, calcium chloride (final concentration: 50 µM), FBS (final concentration: 2.5% (v/v)) and phorbol 12-myristate 13-acetate (PMA; final concentration: 0.01 µg/ml). NHEM were routinely cultured in 15-20 ml of media in 75 cm^2 tissue culture flasks. 50% of the media was replaced every 48-72 hrs. NHEM were routinely subcultured using the ReagentPack™ subculture kit

(Lonza Inc.), which contains trypsin-EDTA, HEPES salt solution and Trypsin neutralising solution (TNS). Trypsin-EDTA was diluted 1:1 in HEPES salt solution before use. NHEM were sub-cultured at approximately 80% confluence. Media was removed and cells were gently washed in 8 ml of pre-warmed PBS. 4 ml of trypsin-EDTA: HEPES solution was added per 75 cm^2 flask and cells were incubated at room temperature for 30 sec to 1 min. Trypsin activity was inhibited by the addition of an equal volume of TNS and the cell solution transferred to a sterile 50 ml tube. The culture flask was washed once with double the volume of pre-warmed media. Cells were counted using Kova® Glasstic® Slide 10 combination coverslip-microscope slides (Hycor Biomedical Ltd., CA, USA). Cells were seeded at the appropriate densities outlined in Table 2.5. Prior to sub-culture of NHEM, 15 ml of pre-warmed media was added to new 75 cm^2 stock flasks and allowed to equilibrate in the incubator at 37°C and 5% CO_2 for 30 minutes.

2.2.2.5 Culture of murine melanocytes

Murine melanocytes were cultured in DMEM:F12 (Gibco) medium, supplemented with 10% (v/v) heat inactivated-FBS, 2 mM L-glutamine, 200 nM PMA and 1% penicillin-streptomycin. Murine melanocytes were routinely cultured in 20 ml of media per 75 cm^2 tissue culture flasks, 50% of the media was replaced with fresh media every 48-72 hrs. Murine melanocytes were sub-cultured as described for fibroblast cells (Section 2.2.2.1). Cells were seeded at the appropriate densities outlined in Table 2.5.

2.2.2.6 4-hydroxytamoxifen-induced Chk1 knockdown in murine melanocytes

Murine melanocytes were seeded at 3.5 x 10^5 cells in 4 ml of media on 60 mm cell culture dishes. 4-hydroxytamoxifen (4-OHT) at a final concentration of 1 µM was added at 24 hr intervals in 4 ml of fresh media. Control dishes were treated with 4 µl of ethanol. 4-OHT-induced Chk1 knockdown was monitored using western blotting using an anti-Chk1 antibody. Cells were subsequently exposed to UVA radiation 48 hr following the initial addition of 4-OHT.

Table 2.5 Melanocyte cell seeding densities

	Seeding density (Cell number)		
Cell	**T75**	**60 mm dish**	**35 mm dish**
NHEM	1.0×10^6	4.5×10^5	1.5×10^5
Murine melanocytes	1.0×10^6	3.5×10^5	1.0×10^5

2.2.3 Cryopreservation

Prior to cryopreservation, all cells were allowed to reach approximately 80% confluence. Cells were trypsinised as outlined in Sections 2.2.2.1 and 2.2.2.4. 20 µl of the cell suspension was removed and cells were counted. Cells were centrifuged at 1,200 rpm for 5 minutes and the pellet was gently resuspended in appropriate freezing media (Table 2.6) to achieve an appropriate cell density (Table 2.6). 1 ml of cell suspension was added to 1.5 ml cryovials (Nunc, Wiesbaden, Germany). Cryovials were placed in a Cryo 1°C freezing container (Nalgene®, Rochester, NY, USA) and incubated at -80° C overnight. The system allows cells to be cooled at a rate of approximately 1° C per minute, maintaining cell membrane integrity. Following overnight incubation at -80° C, cells were transferred for long-term storage to a liquid nitrogen storage system (Jencons-PLS, Bedfordshire, UK).

Table 2.6 Cell density and freezing media for cryopreservation

Cell	Freezing media	Cell density for cryopreservation (cells/ml)
XP30RO, TR30-2, TRG-16, TR30-9	MEM, 20% (v/v) non HI-FBS and 10% (v/v) DMSO	1×10^6
NFF, XP12RO, XP12RO-C5	DMEM, 20% (v/v) HI-FBS and 10% (v/v) DMSO	1×10^6
NHEM	MBM-4, 20% (v/v) HI-FBS and 10% (v/v) DMSO	5×10^5
Murine melanocytes	HI-FBS and 10% (v/v) DMSO	1.5×10^6

2.2.4 Cell resuscitation

Immediately following removal from liquid nitrogen, cells were placed in a 37°C water bath to thaw. Cells were resuspended by pipetting gently, and transferred to a 15 ml tube containing 5 ml of pre-warmed culture media. XP30RO, TR30-2 and NFF cells were centrifuged at 1,000 rpm for 3 minutes; the pellet was gently resuspended in 5 ml of fresh pre-warmed media and transferred to a 25 cm^2 culture flask. TRG-16, TR30-9, XP12RO and XP12RO-C5 cells were placed directly into a 25 cm^2 culture flask without centrifugation. NHEM and murine melanocytes were placed directly into a 75 cm^2 culture flask without centrifugation. Prior to resuscitation of NHEM, 10 ml of pre-warmed MGM-4 media was placed in a 75 cm^2 culture flask and allowed to equilibrate at 37°C for 30 minutes. All cells were incubated at 37°C and 5% CO_2. The following day, media was changed on the human fibroblast cells lines. 6 ml of fresh media was

added to NHEM and murine melanocytes the day after resuscitation, and the following day NHEM and murine melanocytes received at 50% media change.

2.2.5 UV irradiation

48 hr prior to UV-irradiation, cells were seeded on 35 mm, 60 mm or 100 mm tissue culture dishes, as indicated for individual experiments, and allowed to reach 70-80% confluence. Immediately prior to irradiation, medium was removed and placed in a sterile 50 ml tube. Cells were washed in pre-warmed sterile phosphate saline buffer (PBS; 140 mM NaCl, 2.5 mM KCl, 10 mM Na_2HPO_4, and 1.8 mM KH_2PO_4, pH 7.6). Cells were mock- or UV-irradiated in the indicated volumes of pre-warmed PBS: 1 ml of PBS per 35 mm dish, 2 ml of PBS per 60 mm dish and 6 ml of PBS per 100 mm dish. Note: for UVA irradiation of NHEM, cells were washed and irradiated in PBS containing 50 μM $CaCl_2$, a concentration equal to that in MGM-4 media.

Table 2.7 Calculated irradiance and dose rates of short wavelength UV lamps

Lamp	Peak emission wavelength (nm)	Irradiance (W/m^2)	Dose rate ($J/m^2/sec$)
UVC	254	1.67	1.67
UVB	302	2.12	2.12

Monochromatic UVC (254 nm) and UVB (302 nm) radiation was delivered from low-pressure mercury lamps (Models UVG-11 and UVM-57 respectively, UVP Inc., CA). Cells were exposed to UVC and UVB irradiation with the lids of the culture dishes removed, for the appropriate time to reach required dose, for example 12 seconds for 20 J/m^2 UVC, or 48 seconds for 100 J/m^2 UVB. To retain sterility, UVC and UVB irradiations were performed in the tissue culture hood. The irradiance of the UVC and UVB lamps was calculated using a UVX-digital radiometer fitted with UVX-25 and UVX-30 (UVP Inc., CA, USA) probes respectively. The

calculated lamp irradiance when the UVC lamp was positioned 23 cm above cells and the UVB lamp was positioned 15 cm above the cells, are shown in Table 2.7. The dose rate was calculated using the formula: 1 W/m^2 = 1 J/m^2/sec. Mock-treated samples were washed in PBS as described above but were not exposed to UV-irradiation.

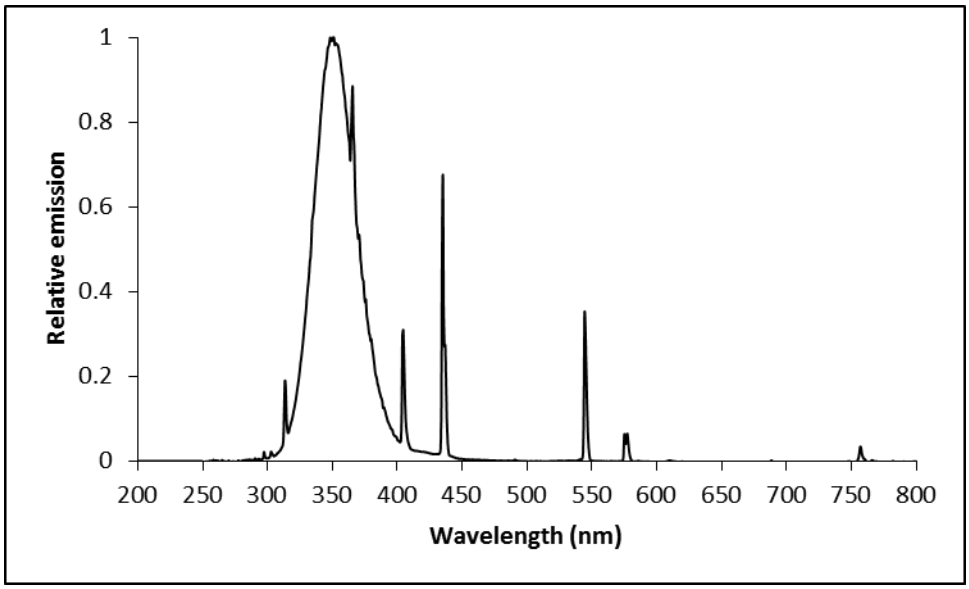

Figure 2.2 Emission spectra of UVA lamps. UV emission spectrum of UVA lamps as measured at Dr. Groebel UV-Electronik GmbH, Germany. The peak emission of the UVA lamp is 350.6 nm.

Broadband UVA radiation was delivered from 20 UVA lamps in an irradiation chamber (Model BS-03; Dr. Groebel UV-Electronik GmbH, Germany). The emission spectrum of the UVA lamps (as measured at Dr. Groebel UV-Electronik GmbH, Germany) is shown in Figure 2.2. The lamps emit UVA radiation greater than 315nm (> 98.5%) with a peak emission at 350.6 nm. The irradiance of the UVA lamps were measured using a UVX-digital radiometer connected to a UVX-36 probe (UVP Inc., CA). UVA lamp irradiances were periodically measured throughout the duration of this study and were not found to vary from initial measurements. UVA lamp irradiance should be routinely measured as lamp irradiance can decrease with use. UVA irradiation was delivered to cells in culture dishes with the lids on, to eliminate short-wavelength UV radiation. The irradiance was therefore measured through the plastic lid of a tissue culture dish. The

dose rate of the UVA lamps was 21 J/m^2/sec (Table 2.8), which corresponds to an 80 minute exposure to achieve 100 kJ/m^2 UVA. Mock-treated cells were placed in a light-proof box in the chamber for the duration of the irradiation, but were not exposed to UVA-irradiation. No difference in temperature was detected between mock-treated and UVA-irradiated samples during the UVA exposure times used in this study.

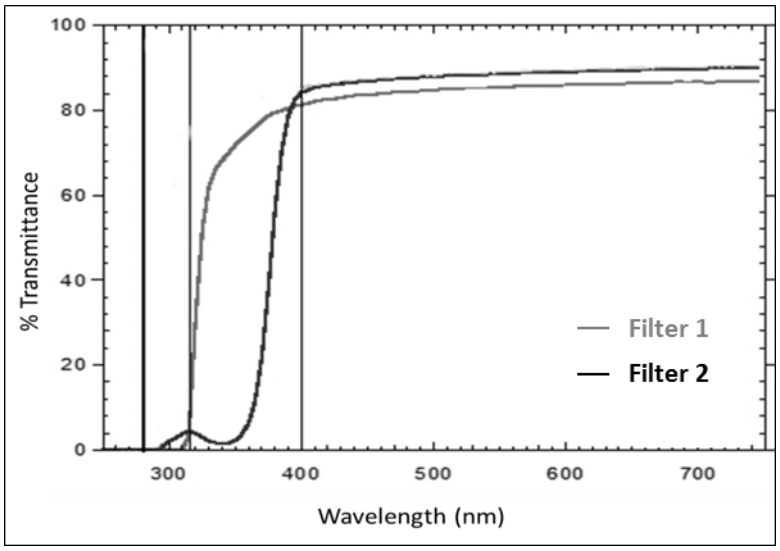

Figure 2.3 Wavelength-dependent UV transmittance through short-wavelength UV filters. The percentage transmittance of UV radiation through Filter 1 and Filter 2 short-wavelength UV filters determined using a UV-VIS Cary-50 (Varian) spectrometer in the laboratory of Dr. D. Stengel (MRI, NUIG).

Where indicated, short-wavelength UV filters, a kind gift from Dr. D. Stengel (MRI, NUIG), were placed on top of the plastic tissue culture dish lids, either separately or together, for the duration of the UVA-irradiation. The short-wavelength UV filters used in this study were Filter 1 (Folanorm; Folex GmbH, Dreieich, Germany) and Filter 2 (UVRU). Filter 1 blocks the transmission of short-wavelength UV of less than 315 nm, while filter 2 blocks the transmission of the majority of UV radiation less than 350 nm, as measured using a UV-VIS Cary-50 (Varian) instrument in the laboratory of Dr. D. Stengel (MRI, NUIG; Figure 2.3). Of note, the irradiance of the UVA lamps reaching the cells, when the tissue culture dish lids were covered with short-wavelength UV filters, was reduced significantly (Table 2.8), as

measured using a UVX-digital radiometer connected to a UVX-36 probe as described above.

Immediately following mock-treatment or UV-irradiation, PBS was removed and the previously removed media was replaced on the cells as follows: 1.5 ml per 35 mm dish, 3 ml per 60 mm dish or 10 ml per 100 mm dish. Cells were allowed to recover in the incubator, at 37°C and 5% CO_2, for the indicated times before subsequent processing as described for individual experiments below.

Table 2.8 Calculated irradiance of UVA lamps as measured through short-wavelength UV filters

Filter	Irradiance (W/m^2)	Dose rate ($J/m^2/sec$)
-	21.0	21.0
1	17.4	17.4
2	2.66	2.66
1 + 2	2.2	2.2

2.2.6 Ionising radiation

Immediately prior to ionising radiation (IR) exposure, cells were washed in pre-warmed PBS. Cells in PBS were irradiated with doses of 0-40 Gy IR in a Mainance Millennium Irradiator. Mock-irradiated samples were processed in the same manner, but not placed in the irradiator. Previously removed media was returned to the cells following mock-treatment or exposure to IR and cells were incubated at 37°C and 5% CO_2 until the time of harvest.

2.2.7 Treatment with small molecule inhibitors

Cells were seeded as outlined in Section 2.2.2. Unless otherwise stated for individual experiments, a 1/1,000 dilution of the working stock of the small molecule inhibitors, outlined in Table 2.1, was added directly to the culture media for 30 min prior to UVA-irradiation. In parallel, samples were treated with an appropriate volume of vehicle control. Following UVA-irradiation (Section 2.2.5), the previously removed media containing inhibitors or

vehicle control was returned to the cells. In certain experiments fresh pre-warmed media without inhibitors was added post-irradiation.

2.2.8 Clonogenic cell survival assay

2.2.8.1 Cell treatment and re-seeding

Cells were seeded at the indicated densities (Table 2.4) on 35mm cell culture dishes (Sarstedt) in 2ml of media. 24hr later, the media was changed. 48hr post-seeding cells were mock-treated or exposed to UV-irradiated as described in Section 2.2.5. Where indicated, 1mM caffeine (Table 2.1) was added to the medium immediately following irradiation, and an appropriate volume of ddH_2O was added to control dishes. 24hr post-irradiation and drug treatment, cells were trypsinised (as outlined in Section 2.2.2.1) and centrifuged at 1,200rpm for 5min. The cell pellet was resuspended in 3ml of pre-warmed culture media. For each sample at least 100 cells were counted using Kova® Glasstic® slides. The volume of cell suspension containing 1,000 cells was calculated and added to 60mm Cell$^+$ coated cell culture dishes (Sarstedt) containing 4ml of culture media. 1mM caffeine or an equivalent volume of ddH_2O was added to dishes, where indicated. Cells were incubated at 37°C for 9 days to allow growth of colonies.

2.2.8.2 Fixing, staining and analysis of colonies

9 days after re-seeding, colonies were fixed and stained by incubating with 1ml of staining solution (0.25% (w/v) 1,9-dimethyl-methylene blue (Sigma), 50% ethanol) for 45 minutes at room temperature, while rocking. Excess staining solution was then removed, and the dishes were washed with H_2O and allowed to dry. In some cases, due to supply shortages in dimethylene blue, colonies were fixed and stained using coomassie blue stain (40% (v/v) methanol, 10% (v/v) acetic acid and 0.2% (w/v) Brilliant Blue R (Sigma)) with rocking at 4°C overnight. Excess coomassie stain was removed using coomassie de-stain (40% (v/v) methanol and 10% (v/v) acetic acid). The dishes were dried overnight in a Class I fume hood. Visible colonies were counted manually. The survival of mock-treated samples was set at 100%,

and the survival of UV-irradiated samples was calculated as a percentage survival of the appropriate mock-treated control, using the formula:

% Survival = (Number of colonies in UVA-irradiated sample / Number of colonies in mock-treated sample) x 100

Survival curves were constructed in Microsoft Excel software. Where the effect of a drug on UV survival was to be tested, the survival of the UVA-irradiated and drug-treated samples was expressed as a percentage survival of the mock-treated and drug-treated sample, to normalise for the effects of the drug treatment alone on cell survival.

2.2.9 Trypan blue dye-exclusion assay

Cells were seeded at the indicated densities (Table 2.4 and Table 2.5) on 35mm cell culture dishes in a total volume of 2 ml media. Cells were mock-treated or exposed to UV-irradiation as outlined in Section 2.2.5. Following treatment, cells were allowed to recover at 37°C for 48hr.

2.2.9.1 Trypan blue staining

Media from the dishes, which included the floating cell population, was transferred to a 15 ml tube. Cells were detached from the dish by incubating with 0.5 ml of pre-warmed 2X trypsin: EDTA for 3 minutes. Trypsin activity was inhibited by the addition of 2 ml of pre-warmed media containing 10% (v/v) FBS, and the cell suspension was transferred to the same 15 ml tube. Dishes were further washed with 2 ml of media. The cells were centrifuged for 5 minutes at 1,200 rpm, and the cell pellet was resuspended in 1 ml of PBS. A 20 µl aliquot of cell suspension was diluted 1:1 in 0.4% (w/v) trypan blue solution (Sigma). 20 µl of the cell suspension in trypan blue solution was loaded into Kova® Glasstic® slides. Cells were counted under 40X magnification using a phase contrast filter on an Olympus CKX31 light microscope. The trypan blue dye-exclusion assay is based on the principle that viable cells with intact membranes will exclude the trypan blue dye, while the dye can readily enter non-viable cells and these cells can be visualised by light microscopy as blue cells. Both viable

(transparent) and non-viable (blue) cells were scored. At least 100 cells per sample were counted.

2.2.9.2 Analysis of the trypan blue dye-exclusion assay data

The percentage of viable cells for each sample was calculated by expressing the number of viable cells as a percentage of the total number of cells, as per the following formula:

% Viable cells = (number of viable cells/total number of cells) x 100

The percentage viability of UV-irradiated cells compared to mock-treated cells was calculated by setting the percentage of viable cells in the mock-treated sample (as calculated above) at 100%, and calculating the percentage viability of UV-irradiated cells as a percentage of the appropriate mock-treated control using the formula:

% viability = (% viable cells in treated sample x 100)/% viable cells in mock-treated sample

Data was analysed using Microsoft Excel software. Where the effect of a drug on UV viability was to be tested, the viability of the UVA-irradiated and drug-treated cells was expressed as a percentage viability of the mock-treated and drug-treated cells, to normalise for the effects of the drug treatment alone on cell viability.

2.2.10 Flow cytometry

2.2.10.1 Live cell PI-exclusion assay

Cells were seeded on 35 mm dishes as outlined in Section 2.2.2, and treated as outlined for individual experiments. Cells were trypsinised (as outlined in Section 2.2.9) at the indicated times post-treatment, washed in 1 ml of cold-PBS and centrifuged at 1,200 rcf for 5 min. Samples were placed on ice and cells were resuspended in 200 µl of ice-cold PBS. Immediately prior to FACS analysis of each sample, 100 µl of the cell suspension was placed in a FACS tube and 200 µl of PI/RNase stain (BD) was added. The assay is based on the principle that viable cells with intact plasma membranes exclude propidium iodide (PI), while non-viable cells will take up PI

resulting in increased cellular fluorescence. Samples were analysed on a FACS Calibur and data was analysed using CellQuest software.

2.2.10.2 BrdU incorporation and cell cycle analysis

2.2.10.2.1 BrdU incorporation and cell harvesting

Cells were seeded on 35 mm dishes and treated as outlined above. Cells were incubated with BrdU (10 µM) for 1 hr prior to harvest by trypsinisation, or for 1.5 hr prior to harvest in the case of NHEM. Cell pellets were resuspended in 500 µl of ice-cold PBS and transferred to a 2 ml tube. Cells were fixed by the drop-wise addition of 1.5 ml of ice-cold 100 % (v/v) ethanol. Following incubation at room temperature for 20 min, samples were stored at -20°C until the day of FACS analysis.

2.2.10.2.2 BrdU and propidium iodide staining

Staining procedures were carried out on the day of FACS analysis. Fixed cells were thawed at room temperature for 20 min, and then centrifuged at 10,000 rpm for 10 min. Following removal of the supernatant, cell pellets were loosened by scraping the tubes against a tube rack. Cells were permeabilised and DNA denatured by the dropwise addition of 500 µl 2 N HCl containing 0.5 % (v/v) Triton X-100, followed by rotation at room temperature for 30 min. In the case of NHEM, DNA was denatured by incubation for 1 hr in 4 N HCl containing 1% (v/v) Triton X-100. Cells were centrifuged at 10,000 rpm for 10 min and HCl was neutralised by the addition of 500 µl of 0.1 M $Na_2B_40_7.10H_2O$ pH 8.5. Following centrifugation at 10,000 rpm for 10 min cells were resuspended in 300 µl of blocking solution (PBS, 0.5 % (v/v) Tween-20, 1 % (w/v) BSA). 7 µl of FITC-conjugated anti-BrdU antibody (BD) was added to each sample. Samples were rotated in the dark at room temperature for 30 min. In the case of NHEM, cells were incubated with 15 µl of FITC-conjugated anti-BrdU antibody, for 45 min. Following centrifugation at 10,000 rpm for 10 min, cells were washed in 300 µl of blocking solution. Finally, cells were centrifuged at 10,000 rpm for 5 min, and incubated for at least 30 min at room temperature in 250 µl of PI-RNase stain (BD), to stain cellular DNA.

Samples were analysed by flow cytometry using a FACS Calibur (BD) and data was analysed using CellQuest™ software.

2.2.10.3 Dichlorofluorescin (DCF) oxidative stress assay

The mechanism of action of the dichlorofluorescin (DCF) oxidative stress assay is outlined in Figure 2.4. 2',7'-dichlorofluroescein diacetate (DCFH-DA) is a non-fluorescent, cell-permeable chemical. Within the cell, esterases deacetylate DCFH-DA forming non-fluorescent 2',7'-dichlorofluorescein (DCFH). Upon the induction of ROS, DCFH is oxidised to form a fluorescent product, DCF. Here, DCF fluorescence is measured using flow cytometry.

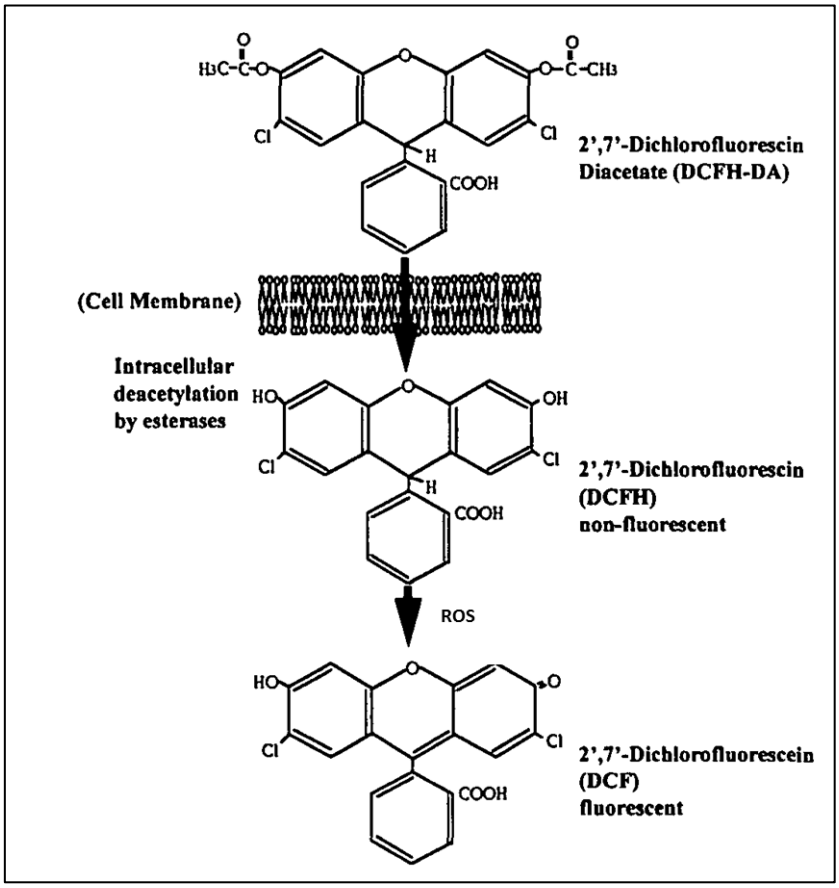

Figure 2.4 Principle of the dichlorofluroesceine (DCF) oxidative stress assay. Adapted from (Takanashi et al., 1997)

Cells were seeded on 35 mm dishes and allowed to reach 80% confluence. 10 µM 2',7'-dichlorofluorescin diacetate (DCFH-DA; Sigma) was added to the culture media for 30 min prior to treatment. DCFH-DA (10 µM) was also added to the PBS for the duration of mock-treatment or UVA-irradiation. Immediately post-UVA exposure, the previously removed media containing DCFH-DA was returned to the cells. As a positive control for oxidative stress induction, cells were treated with hydrogen peroxide (H_2O_2). Cells were washed in PBS and incubated with 100 µM H_2O_2 in PBS for 30min at 37°C, before the previously removed media was returned to the cells, as outlined above. Where indicated cells were treated with *N*-acetyl-cysteine (NAC), a widely used antioxidant (Girard et al., 2008). 10 mM NAC was added at the same time as DCFH-DA. This method of measuring UVA-induced oxidative stress by pre-incubating cells with DCFH-DA prior to UVA irradiation was adapted from Girard *et al.* (2008). However, it should be noted that DCFH-DA is a UV-sensitive chemical and it has been recently reported that pre-incubation of cells with DCHF-DA before UVA irradiation can result in increased cellular fluorescence (Boulton et al., 2011), thus in future experiments it would be preferable to incubate with DCFH-DA only post-UVA irradiation.

Following incubation at 37°C for 30 min post-treatment, cells were trypsinised and centrifuged at 1,200 rpm for 5 min at 4°C. The cell pellet was resuspended in 1ml of ice-cold 1X PBS, transferred to a 1.5 ml Eppendorf tube and centrifuged at 2,000 rcf for 5 min at 4°C. Cells pellets were resuspended in ice-cold PBS and analysed using a FACS Calibur. The fluorescence intensity of each sample was analysed in the FL1 (FITC) channel.

2.2.11 Protein lysate preparation

All steps for the preparation of protein lysates were carried out on ice. Cells were seeded on 60 mm dishes and treated as outlined for individual experiments. At the indicated times post-treatment, the dishes were placed on ice. Media was removed using a vacuum pump and cells were washed in ice-cold PBS. Dishes were placed vertically on ice to drain excess PBS

which was then removed using the pump. An appropriate volume (20-50 µl, depending on the confluence of the cells) of RIPA lysis buffer (150 mM NaCl, 1% (v/v) IGEPAL® CA-630 (Sigma), 0.25% (w/v) sodium deoxycholate, 1 mM EDTA, 30 mM Tris-HCl, pH 7.4) containing protease and phosphatase inhibitors (Table 2.9), was added to the dishes which were than scraped briefly using a 39 mm scraper (Sarstedt). Samples were incubated on ice for 5 min. Cells were than scraped and transferred to pre-labelled 1.5 ml Eppendorf tubes, vortexed for 20sec and allowed to lyse on ice for a further 15 min.

Where the floating cell fraction was required for analysis, cells were scraped into the media, rather than into lysis buffer, using a 39 mm scraper. The cell suspension was transferred to a 15 ml tube. The dish was washed with ice-cold PBS (2 ml per 60 mm dish) and added to the same 15 ml tube. The cell suspension was centrifuged at 1,200 rpm for 5 minutes at 4°C. The resulting cell pellet was resuspended in 1 ml of ice-cold PBS and transferred to a pre-labelled 1.5ml Eppendorf tube and centrifuged at 14,000 rpm for 10 sec. The cell pellet was resuspended in 25 µl of RIPA lysis buffer, containing protease and phosphatase inhibitors, vortexed for 20 sec and allowed to lyse on ice for 5 minutes. Samples were vortexed again and allowed to lyse on ice for a further 15 min. Cell lysates were stored at -20°C.

On the day of analysis lysates were thawed on ice and centrifuged at 4°C for 15min at 14,000 rpm in a Sigma 1-15K centrifuge (Sigma), to pellet the insoluble fraction. The supernatant fraction, containing soluble proteins, was transferred to a new pre-labelled 1.5ml Eppendorf tube.

Where indicated, such as for the analysis of chromatin-associated proteins in NHEM, cell lysates were sonicated on ice, three times for 10 sec at 20% amplitude using a Digital Sonifier® cell disrupter (Branson Ultrasonics Corporation, USA), with 20 sec intervals between each pulse. Whole cell lysates were then processed as outlined below.

Table 2.9 Protease and phosphatase inhibitors added to RIPA lysis buffer

Inhibitor class	Inhibitor name	Diluent	Stock concentration	Final concentration
Protease inhibitors	Aprotinin	ddH_2O	1mg/ml	2µg/ml
	Leupeptin	ddH_2O	1mg/ml	1µg/ml
	Phenylmethylsulfonyl fluoride (PMSF)	Ethanol	100mM	1mM
Phosphatase inhibitors	Sodium fluoride (NaF)	PBS	500mM	5mM
	Sodium orthovanadate (Na_3VO_4)	PBS	100mM	1mM

2.2.12 Determination of protein concentration

The concentration of protein in cell lysates was determined using the *DC*™ protein assay (BioRad Laboratories), a detergent-compatible colorimetric assay based on the Lowry method of protein determination (Lowry et al., 1951). A 2 mg/ml solution of bovine serum albumin (BSA; Fisher) in RIPA lysis buffer was utilised as the protein standard for the assay and aliquots were stored at -20°C. Immediately prior to protein determination, an aliquot of the BSA stock solution was defrosted on ice and a series of dilutions (between 0-1 mg/ml BSA) were prepared in RIPA lysis buffer. BSA solutions were mixed by vortexing, and 5 µl was added in duplicate into a flat-bottomed 96-well plate (Sarstedt). Following a brief vortex, 2 µl of protein lysate was pipetted in duplicate into the 96-well plate. *DC* Buffer A' was prepared immediately prior to use by combining 1 ml of *DC* Reagent A with 20 µl of *DC* Reagent S. 25 µl of Buffer A' was added to each well of the 96-well plate, followed by the addition of 200 µl of *DC* Reagent B. The reaction was allowed to proceed by incubating the 96-well plate at room temperature for 15 minutes. The absorbance was measured at 490 nm for 0.1 seconds on a Victor^2 1420 Multilabel Counter (Wallac, MA, USA). A standard curve was plotted using Microsoft Excel software. The coefficient of determination (R^2) statistic was utilised to estimate how well the linear trend line fitted the plotted points. Standard curves with R^2 values less than

0.95 were dismissed and the assay repeated. The concentration of protein in each samples was determined in Excel using the formula y = mx + c, where y = absorbance, m = slope of the trend line, x = protein concentration (µg/µl) and c = the y-axis intercept of the trend line.

2.2.13 Sodium dodecyl sulphate polyacrylamide gel electrophoresis (SDS-PAGE)

Protein lysates were analysed by SDS-PAGE using the Mini-PROTEAN® 3 system (Bio-Rad). SDS-PAGE gels were prepared as outlined in Table 2.10. 20 µg of protein, prepared as described in Section 2.2.11, was combined with an appropriate volume of 4 X Laemmli reducing buffer (1% (w/v) SDS, 40% (v/v) glycerol, 0.1% (w/v) bromophenol blue, 5% (v/v) β-mercaptoethanol, 250 mM Tris-HCl pH 6.8) to achieve a final concentration of 1 X Laemmli buffer. Proteins were denatured by incubating in boiling water for 5 minutes. Samples were centrifuged briefly in a bench top PicoFuge™ (Stratagene, Agilent Technologies, USA). Using Prot/Elec™ Tips (Bio-Rad), samples and pre-stained protein ladder (Thermo Scientific, Fisher, IL, USA; catalogue number 22616 or 26635) were loaded onto gels, fully immersed in 1 X running buffer (192 mM glycine, 25 mM Tris Base, 0.1% (w/v) SDS). Empty wells were filled with 1 X Laemmli buffer. Electrophoresis was carried out at 100 V for 2-6 hours until the desired protein separation was achieved, based on the migration of pre-stained protein markers.

2.2.14 Western blotting

Following separation by SDS-PAGE, proteins were transferred to polyvinylidene fluoride (PVDF) membrane (Immobilon™-P transfer membrane, 0.45 µm pore size; Millipore, MA, USA) using the Mini-TransBlot® Cell System (Bio-Rad). The SDS-PAGE gel was immersed in 1X transfer buffer (192 mM Glycine, 25 mM Tris Base) prior to transfer assembly. PVDF membrane was pre-activated by soaking in 100% methanol for 3 minutes. Excess methanol was removed by washing for 3 minutes in ddH_2O and the membranes was then immersed in 1X transfer

buffer until use. The transfer cassette was assembled with the PVDF membrane on the cathode side and the SDS-PAGE gel on the anode side, surrounded with five pieces of filter paper (pore size 11 µm; Fisher Brand) and a sponge pad (Bio-Rad), both pre-wetted in 1X transfer buffer. Transfer was carried out at 100V for 45 minutes in an electrophoresis apparatus containing pre-cooled 1X transfer buffer and an ice-pack.

Following transfer, the PVDF membrane was washed briefly in Tris-buffered saline (TBS; 10 mM Tris base, 68mM NaCl, pH 7.6) containing 0.05% (v/v) Tween®-20 (T-TBS; Fisher, NJ, USA). Non-specific protein binding sites were blocked by incubating the membrane in 20 ml of 5% blocking buffer (T-TBS, 5% (w/v) non-fat powered milk (Marvel, Premier Foods, UK)) for 1 hr at room temperature, while rocking at 30 rpm on a Labnet Rocker 35A (Labnet International, Inc., NJ, USA). Membranes to be probed with anti-GAPDH antibody were blocked in T-TBS containing 5% (w/v) BSA, under the conditions outlined above. Primary antibodies were diluted in the appropriate 5% blocking buffer as outlined in Table 2.11. Membranes were incubated with 2 ml of primary antibody solution overnight at 4°C, while rocking. Unbound primary antibody was removed by washing in 20 ml of T-TBS three times for 7 minutes at room temperature, while rocking.

Protein-bound primary antibody was achieved by probing the membrane with horseradish peroxidase (HRP)-conjugated secondary antibodies (Jackson ImmunoResearch Laboratories, Inc., PA, USA). HRP-conjugated secondary antibodies were diluted in 3% blocking solution (T-TBS, 3% (w/v) non-fat powered milk), see Table 2.11. Membranes were incubated with 20 ml of secondary antibody solution for 1 hr at room temperature while rocking. Excess secondary antibody was removed by washing in 20ml of T-TBS three times for 7 minutes at room temperature, with rocking.

HRP activity was detected using the Amersham™ ECL™ Prime western blotting detection reagent (GE Healthcare Bio-Sciences AB, Uppsala, Sweden). 1.5 ml of ECL Prime reagent was prepared per 52 cm^2 of membrane by combining Reagent A and Reagent B in a ratio of 1:1.

Table 2.10 Components of SDS-PAGS running and stacking gels

Running gel	**Volume (ml) for 1 x 1.5mm gel or 2 x 1mm gels**		
Acrylamide %	**8%**	**10%**	**12%**
ddH_2O	4.6	4	3.3
30% (w/v) Acrylamide-Bis (Bio-Rad)	2.7	3.3	4
1.5M Tris-HCl pH 8.8	2.5	2.5	2.5
10% (w/v) SDS	0.1	0.1	0.1
10% (w/v) APS	0.1	0.1	0.1
TEMED	0.006	0.004	0.004
Stacking gel	**Volume (ml) per gel**		
ddH_2O	1.4		
30% (w/v) Acrylamide-Bis (Bio-Rad)	0.33		
1M Tris-HCl pH 6.8	0.25		
10% (w/v) SDS	0.02		
10% (w/v) APS	0.02		
TEMED	0.002		

Membranes were incubated for 5 minutes with ECL Prime reagent and then transferred to a film cassette (Sigma).The following steps were carried out in a dark-room lit by a safety light (Safe Light filter No. 68, Kodak). Medical X-ray film (A Plus, Konica Minolta Medical, Tokyo, Japan) was exposed to the membrane in a film cassette for between 10 seconds and 5 minutes, depending on the strength of the signal. The film was developed in a CP1000 automatic film processor (Agfa, Mortsel, Belgium) using Agfa G153 developer (Agfa, Mortsel, Belgium) solution and Agfa G353 fixer solution (Agfa, Mortsel, Belgium).

Table 2.11 Dilutions of primary antibodies used for western blotting

Primary antibodies			
Name	**Species**	**Dilution**	**Supplier; Catalogue number**
anti-ATM	Rabbit	1/1,000	Millipore; # 07-1286
anti-ATM (N-terminus)	Mouse	1/1,000	Prof. Domenico Delia, Milan
anti-phospho-S1981 ATM	Mouse	1/500	Millipore; # MAB3806
anti-adducin α (H-100)	Rabbit	1/10,000 (1/1,000 murine extracts)	Santa Cruz; # sc-25731
anti-phospho-S726 adducin	Rabbit	1/10,000	Santa Cruz; # sc-16736
anti-phospho-S345 Chk1	Rabbit	1/750	Cell Signalling; # 2348
anti-phospho-S317 Chk1	Rabbit	1/750	Cell Signalling; # 2344
anti-Chk1 (clone DCS-310)	Mouse	1/1,000 (1/5,000 murine extracts)	Sigma; # C-9358
anti-phospho-T68 Chk2	Rabbit	1/500	Cell Signalling; # 2661
anti-GAPDH	Mouse	1/10,000	Abcam; # 9484
anti-GFP	Mouse	1/1,000	Roche; # 11 814 460 001
anti-phospho-S139 H2AX (clone JBW301)	Mouse	1/500	Millipore; # 05-636
anti-polη	Rabbit	1/1,000	Abcam; # ab17725
anti-phospho-S4/S8 RPA2	Rabbit	1/5,000	Bethyl labs; # A300-245A
anti-RPA2 (Ab-3)	Mouse	1/4,000 – 1/8,000	Oncogene; # NA19L
anti-RPA2 (Clone RBF-4E4)	Rat	1/100	Prof. HP Nasheuer (CCB, NHIG)

2.2.14.1 Quantification of western blot band intensities

Where the intensity of individual bands was measured western blot images were acquired using the LAS-3000 luminescence imager (Fujifilm). Band intensities were quantified using Multi Gauge V2.2 software. The intensity of each band was normalised by subtracting the average background intensity, measured from at least three sites per image.

Table 2.12 Dilutions of secondary HRP-conjugated antibodies used for western blotting

Secondary antibodies		
HRP-conjugated goat anti-mouse IgG	1/10,000-1/50,000	Jackson ImmunoResearch # 115-035-003
HRP-conjugated goat anti-rabbit IgG	1/10,000-1/50,000	Jackson ImmunoResearch # 111-035-003
HRP-conjugated donkey anti-rat IgG	1/10,000-1/50,000	Jackson ImmunoResearch # 712-035-153

2.2.15 Preparation of protein lysates for Kinetworks™ phospho-site screen (KPSS 1.3)

NHEM were seeded at 4.5 x 10^5 cells per 60 mm tissue culture dish. At least four dishes per condition were seeded per experiment. 50% of the medium was changed 48 hr following seeding. 72 hrs post-seeding NHEM were mock-treated or exposed to 75kJ/m^2 UVA-irradiation (as outlined in Section 2.2.5). For these experiments PBS without $CaCl_2$ was utilised during UVA-irradiation. For the Kinexus assay lysates from four independent experiments were pooled to achieve sufficient quantity of protein: 500 µg of protein per sample. Protein lysates were prepared 3 hr post-UVA treatment. All steps of the following procedure were carried out on ice. Media was removed from the dishes using a vacuum pump and cells were washed in 2 ml of ice-cold PBS. Cells were scraped in Kinexus lysis buffer (2 mM EGTA, 5 mM EDTA, 1% (v/v) Triton X-100, 20 mM MOPS pH 7.0) with added phosphatase inhibitors, protease inhibitors and reducing agents, see

Table 2.13 and transferred to a 1.5 ml Eppendorf tube. Lysates were sonicated on ice, three times for 10 sec at 20% amplitude using a Digital Sonifier® cell disrupter (Branson Ultrasonics Corporation, USA), with 20 sec intervals between each pulse. Samples were then centrifuged at 14,000 rpm for 30 min at 4°C. The resulting supernatant containing soluble proteins was transferred to a new pre-labelled 1.5 ml Eppendorf tube. The protein concentration in each sample was determined using the DC assay, as outlined in Section 2.2.12. Lysates were stored at -80°C until sufficient protein (500 µg per sample) was collected. Protein lysates from four independent experiments were defrosted on ice, pooled and concentrated by centrifuging at 4°C for 10-20 min at 10,000 rpm in a Millipore Biomax centrifugal filter with a 5 kDa cut-off (catalogue no. UFV5BCC25; Millipore, MA, USA). Protein concentration was determined using the DC assay, and was adjusted to a final concentration of exactly 1 mg/ml and the volume exactly 0.5 ml, in a 3:1 ratio with Kinexus lysis buffer (50% (v/v) glycerol, 125 mM Tris-HCl, pH 6.8, 4% (w/v) SDS, 0.08% (w/v) bromophenol blue, 5% (v./v) β-mercaptoethanol). Lysates were denatured by incubating at 100°C for 4 minutes. Denatured lysates were shipped on dry-ice to Kinexus Bioinformatics Corporation, Vancouver, Canada for analysis using the Kinetworks™ phospho-site broad coverage pathway screen (KPSS 1.3).

The following steps were carried out by Kinexus Corp. Proteins were separated by SDS-PAGE and probed with a cocktail of phospho-antibodies, specific for the proteins in the KPSS 1.3 assay, using a specialised 20-lane multi-immunoblotting apparatus. Antibody binding was visualised using a chemoluminescence system. The intensity of each band was quantified, normalised between blots and expressed in counts per minute (CPM). The resulting multi-immunoblot images and MS Excel spread sheets with band intensity data was supplied by Kinexus Corp.

Table 2.13 Phosphatase inhibitors, protease inhibitors and reducing agents added to Kinexus lysis buffer

	Name	Stock concentration	Final concentration
Phosphatase inhibitors	Sodium fluoride (NaF)	500mM	30mM
	β-glycerophosphate	500mM	60mM
	Sodium orthovanadate (Na_3VO_4)	100mM	1mM
Protease inhibitors	Pepstatin	1.5mM	5µM
	Leupeptin	2mM	10µM
	Phenylmethylsulfonyl fluoride (PMSF)	100mM	1mM
Reducing reagent	Dithiothreitol (DTT)	1M	1mM

2.2.16 Fluorescence microscopy

2.2.16.1 Coverslip preparation

Square (22 x 22 mm) or round (diameter 13 mm) glass coverslips (thickness no. 1.5; VWR) were cleaned and sterilised prior to use. Coverslips were immersed in concentrated HCl and incubated overnight in a Class I fume hood. Following 5 washes in ddH_2O, coverslips were boiled in ddH_2O for 15 min. Coverslips were allowed to cool and were washed a further 5 times in ddH_2O, followed by 4 washes in 100% (v/v) ethanol. Coverslips were then placed individually on tissue paper in a Class II laminar flow hood and dried overnight under UV light. Coverslips were kept sterile by storing in sealed 100 mm sterile tissue culture dishes.

2.2.16.2 Collagen I coating of glass coverslips

To enhance the adhesiveness of melanocyte cells to the surface, glass coverslips were coated with collagen prior to use. Bovine collagen I (BD; Cat # 354231) was diluted 1/60 in 0.01 M filter-sterilised HCl. Round

coverslips were placed in 4-well dishes and square coverslips placed in 35 mm dishes, and covered in 250 µl or 1 ml of collagen solution, respectively. Coverslips were incubated for 1 hr at room temperature in a laminar flow hood. Excess collagen solution was removed and coverslips were washed once in double the volume of PBS. Coverslips were allowed to dry at room temperature in the laminar flow hood for 30 min with the lids of the dishes removed. Coverslips were used immediately.

2.2.16.3 Sample preparation and fixation

Cells were seeded onto the coverslips, pre-coated with collagen where indicated, as outlined for individual experiments. Cells were incubated for at least 36 hr before treatment. At indicated times post-treatment, media was removed and cells were washed gently in pre-warmed PBS. Cells were fixed in 4% paraformaldehyde (PFA), diluted from a 16% (v/v) stock solution (Electron Microscopy Sciences) in PBS, at room temperature for 30 min in the case of the melanocytes or 10 min for all other cells. Cells were washed twice for 5 min in PBS and then either stored in PBS at 4°C or processed immediately. All experiments involving fluorescence detection of GFP-tagged proteins were processed and imaged within 48 hr, due to the quenching of GFP fluorescence observed when samples were incubated for extended periods.

2.2.16.4 Fluorescence analysis of polη-GFP

Cells expressing GFP-tagged proteins were stored in light-proof boxes at all times to avoid excessive quenching of the GFP fluorescence. Cells were permeabilised by incubating in PBS containing 0.1% (w/v) Triton X-100 twice for 5 min, at room temperature. Cells were incubated with DAPI (25 ng/ml) diluted in PBS for 10 min at room temperature to stain DNA. Cells were then washed in PBS, followed by a wash in ddH_2O. Coverslips were air dried before mounting on SuperFrost glass slides (Fisher) in 5 µl of SlowFade (Invitrogen). The edges of the coverslip were sealed with nail varnish. Slides were either imaged immediately or stored at 4°C if required.

2.2.16.5 Immunostaining

Following fixation, cells were permeabilised by incubating twice for 5 min at room temperature in a solution of PBS containing 0.1% Triton X-100 (PBS-TX; 1 ml per 35 mm dish or 500 µl per well of a 4-well plate). Non-specific sites were blocked by incubating in blocking solution [either PBS-TX containing 1% BSA, or PBS-TX containing 1% BSA and 10% normal goat serum (NGS)] for 30 min at room temperature with gentle rocking. Coverslips were placed on parafilm in a light-proof box and incubated with primary antibodies, diluted in blocking solution (30 µl per round coverslip or 100 µl per square coverslips), for 1 hr at room temperature or 37ºC (Table 2.14). To prevent coverslips drying out when incubated at 37ºC, damp tissue paper was placed around the edges of the box surrounding the coverslips. Following incubation with appropriate primary antibody, coverslips were transferred to culture dishes and washed four times at room temperature for 5 min in PBS-TX, with gentle rocking. Samples were returned to the light-proof box for incubation with the appropriate fluorescently-conjugated secondary antibody diluted in blocking solution, for 1 hr at room temperature or 37ºC. Coverslips were then washed four times at room temperature for 5 min in PBS-TX, with gentle rocking. Following a quick wash in PBS and ddH_2O, coverslips were air dried and mounted in SlowFade containing DAPI.

2.2.16.6 Fluorescence analysis of EdU incorporation, using click chemistry

Cells were mock-treated or exposed to UVA-irradiation and incubated with EdU (10 µM) for 30 min prior to fixation, at the indicated times post-treatment as outlined in Section 2.2.16.3. Where indicated, cells were first labelled with primary and secondary antibodies as outlined in Section 2.2.16.5. Incorporated EdU was labelled with an Alexa Fluor® 495-conjugated azide using the Click-iT™ kit (Invitrogen) as per manufacturer's instructions. Briefly, excess secondary antibody was removed and coverslips were washed three times for 5 min in PBS-TX. The Click-iT™ reaction buffer was prepared as outlined in the kit instruction manual by the sequential addition of the reagents (1X Click-iT reaction buffer, component E ($CuSO_4$), Alexa Fluor® 495-conjugated azide and 1X Click-iT reaction

buffer additive); the reaction mix was vortexed after the addition of each reagent. Following two washed in PBS containing 3% BSA, coverslips were transferred to parafilm in a light proof-box and were incubated with Click-iT reaction buffer for 30 min at room temperature. Cells were washed twice for 5 min in PBS-3% BSA followed by three washes in PBS-TX, one wash in PBS and one wash in ddH_2O. Coverslips were air dried and mounted in SlowFade containing DAPI.

2.2.16.7 Fluorescence microscopy data analysis

Fluorescence microscopy images were captured using a DeltaVision core system (Applied Precision), controlling an interline charge-coupled device camera (CoolSnap HQ2; Roper), mounted on an inverted microscope (IX-71; Olympus). Images were captured using the 60X objective, at 2 x 2 binning and 0.2 µm z sections. For EdU intensity analysis, at least 100 cells per sample were scored; each cell was manually classed as EdU positive or negative. The EdU signal intensity of each nucleus was measured, from deconvolved unscaled images, using ImagePro V6.3 software. Briefly, a mask was created in the DAPI channel to define the nucleus. The nuclear mask was applied to images in the TRITC channel, and the mean fluorescent intensity of the nuclear mask was obtained. The mean EdU intensity of each nucleus was then corrected by subtracting (i) the mean background fluorescence intensity outside the nucleus mask and (ii) the mean background intensity of the EdU negative nuclei. Data was processed and graphs prepared using Microsoft excel software.

Table 2.14 Dilutions and conditions of primary and secondary antibodies used for immunofluorescence

Primary antibodies					
Name	**Species**	**Dilution**	**Supplier; Cat #**	**Blocking solution (+/- NGS)**	**Antibody incubation temperature**
anti-ATM	Rabbit	1/2,000	Millipore; # 07-1286	+	37°C
anti-Chk1	Mouse	1/1,000	Sigma; # C-9358	-	37°C
anti-GFP	Mouse	1/1,000	Roche; # 11814460001	-	RT
anti-phospho-ATM-S1981	Mouse	1/500	Millipore; # MAB3806	+	37°C
anti-TRP1	Mouse	1/1,000	Santa Cruz; # sc-58438	-	RT
anti-γH2AX	Mouse	1/5,000	Millipore; # 05-636	+	37°C

Fluorescently-conjugated secondary antibodies		
Name	**Dilution**	**Supplier; Cat #**
Alexa Fluor 488-conjugated goat anti-mouse IgG	1/1,000	Invitrogen; #A-11001
Alexa Fluor 488-conjugated goat anti-rabbit IgG	1/1,000	Invitrogen; #A-11008
Alexa Fluor 594-conjugated goat anti-mouse IgG	1/1,000	Invitrogen; #A-11005
Alexa Fluor 594-conjugated goat anti-mouse IgG	1/1,000	Invitrogen; #A-11012

2.2.17 DNA isolation

2.2.17.1 DNA isolation using GenElute™ DNA miniprep kit

At the times indicated for individual experiments, adherent cells were collected by trypsinisation. Cells were centrifuged at 1,200 rpm for 5

minutes at 4°C. The cells was resuspended in 1 ml of ice-cold PBS and transferred to a 1.5 ml Eppendorf tube. Cells were centrifuged at 14,000 rpm for 10 sec and washed once more in 1 ml of ice cold PBS. Cell pellets were stored at -20°C until the time of DNA extraction.

DNA extraction was performed utilising the GenElute™ Mammalian Genomic DNA Miniprep Kit (Sigma) according to the manufacturer's instructions. The following steps were carried out at room temperature unless otherwise stated. Cells were resuspended in 200 µl of resuspension solution. To isolate RNA-free DNA, 20 µl of RNase A was added to the cell suspension and incubated at room temperature for 2 mins. Cells were lysed by the addition of 20 µl of Proteinase K solution and 200 µl of Lysis Solution C, followed by incubation at 70°C for 10 minutes. During the incubation, the GenElute Miniprep Binding Column was prepared for DNA loading by washing with 500 µl of Column Preparation Solution, followed by centrifugation at 12,000 x g for 1 minute in an Eppendorf centrifuge. The flow-through was discarded. 200 µl of ethanol was added to the lysate and mixed by vortexing for 10 seconds, to achieve a homogenous mixture. The lysate was then transferred into the pre-prepared binding column and centrifuged at 6,600 x g for 1 minute. The flow-through was discarded and the binding column placed into a new 2 ml collection tube. DNA bound to the binding column was washed with 500 µl of wash solution, followed by centrifugation at 6,600 x g for 1 minute. The flow-through was discarded and the binding column placed into a new 2 ml collection tube. DNA was further washed with 200 µl of wash solution and centrifuged at 16,000 x g for 3 minutes. The flow through was discarded and the binding column placed into a new 2 ml collection tube. 200 µl of Elution Solution (10 mM Tris-HCl, 0.5 mM EDTA, pH 9.0) was added to the centre of the column and incubated at room temperature for 5 minutes. To elute the DNA, the samples were centrifuged at 6,660 x g for 5 minutes. Eluted DNA was stored at 4°C.

2.2.17.2 DNA concentration and quality analysis

The concentration and purity of DNA was determined using a NanoDrop-1000 spectrometer (NanoDrop Technologies Inc.), by measuring the

absorbance at 260 nm and 280 nm of the DNA in elution buffer. Pure DNA in elution buffer has an A_{260}:A_{280} ratio of 1.6 – 1.9.

2.2.18 Immuno-slot blotting

2.2.18.1 DNA preparation

DNA extracted as described in Section 2.2.17.1, was diluted in ddH_2O to a final concentration of 1.25 µg/µl. A 500 µl solution was prepared per sample. DNA was denatured by incubating at 100°C for 10 minutes using a heat block. Samples were cooled immediately by placing in an ice-bath for 5 minutes. Samples were centrifuged briefly in a PicoFuge, 100 µl of 1M ammonium acetate was added and each sample was mixed by pipetting.

2.2.18.2 Slot-blot

DNA was blotted onto Amersham Hybond N^+ nitrocellulose membrane (GE Healthcare) using a Minifold II Slot-Blot System (Schleicher and Schuell) attached to a Buchi-Vacuum pump V-700 (BUCHI Labortechnik, AG, Switzerland). Nitrocellulose membrane and two sheets of filter paper were cut to the exact size of the apparatus, and pre-soaked for 5 minutes in 1 M ammonium acetate solution before assembly of the slot-blot apparatus. Slot-blot wells to be utilised were washed with 200 µl of 1 M ammonium acetate. The vacuum was applied for 2 minutes to clear the wells. Only wells in the centre of the apparatus, nearest to the vacuum attachment site, were used to ensure consistency in DNA blotting, which could be affected by the varying strength of the vacuum across the apparatus. With the vacuum turned off, 120 µl of DNA solution, equivalent to 250 ng of DNA, was added to the wells. The vacuum was turned on for 2 minutes to fully clear the wells. With the vacuum turned off, 200 µl of 1 M ammonium acetate was added to each well. The vacuum was turned on for 2 minutes to fully clear the wells. The slot-blot apparatus was disassembled, the membrane was labelled and washed in 5 X SSC buffer (0.75 M NaCl, 75 mM sodium citrate, pH 7.0) for 5 minutes at room temperature, while rocking. The membrane was then placed on dry filter paper and incubated at 80°C for 40 minutes to fix the DNA to the membrane. Membranes were

either stored at 4°C in the dark overnight, or processed for immuno-blotting immediately.

2.2.18.3 Immuno-detection

The membrane was rehydrated by incubating in PBS for 5 minutes at room temperature. Non-specific binding sites were blocked by incubating the membrane in 20 ml of 5% blocking buffer (PBS, 0.2% (v/v) Tween®-20, 5 % (w/v) non-fat powdered milk) for 1 hr at room temperature, while rocking. Membranes were incubated with a 1/4,000 dilution of anti-thymine dimer antibody (Abcam; Catalogue no. ab10347) in 5% blocking solution for 4 hrs at room temperature while rocking. The anti-thymine dimer antibody recognises thymine-containing dimers in single-stranded DNA. Unbound primary antibody was removed by washing in 20 ml of PBS containing 0.2% (v/v) Tween-20, three times for 7 minutes at room temperature, while rocking. Antibody binding was detected by probing the membrane with a HRP-conjugated anti-mouse secondary antibody at 1/25,000 dilution in 3 % blocking solution for 1 hr at room temperature while rocking. Binding was visualised using the Amersham ECL Prime chemoluminescence reagent as outlined in Section 2.2.14. Images were acquired using the LAS-3000 Fujifilm imager.

2.2.18.4 Densitometry

The intensity of individual bands was measured using Multi Gauge V2.2 software. The intensity of each band was corrected by subtracting (i) the average background intensity, measured from at least three sites per image, and (ii) the intensity of the appropriate mock-treated control.

2.2.19 Melanin assay

The total melanin content of cells was measured using a spectrophotometric assay described in (Friedmann and Gilchrest, 1987; Smit et al., 2001). Synthetic melanin (Sigma; Cat no. M8631), dissolved in 1 M NaOH, at concentrations between 10-100 µg/ml, was used as a standard for the assay. Cell pellets were dissolved in 1 M NaOH, to a final concentration of 1 x 10^6 cells/ml. 200 µl of the cell suspension and the melanin standards were pipetted in duplicate on a 96-well plate. The absorbance at 475 nm was

measured on a Victor^2 1420 Multilabel Counter (Wallac, MA, USA). A standard curve was plotted using Microsoft Excel software. The concentration of melanin in each samples was determined using the formula $y = mx + c$, where y = absorbance, m = slope of the trend line, x = protein concentration (µg/µl) and c = the y-axis intercept of the trend line.

2.2.20 Data analysis and statistics

All results presented in the following sections are representative of at least three independent experiments, unless otherwise stated. Statistical tests were carried out using Microsoft Excel software, as outlined for individual experiments. Analysis of variance (ANOVA) was the primary statistical test used to test the null hypothesis that the data sets are equal. $P<0.05$ was designated as significant, representing a significant difference between the data sets analysed.

3 Results

The role of DNA polymerase eta in the response of human cells to long-wavelength UVA radiation

Sarah Conmy[1] and Michael P. Carty[1]

Manuscript in preparation for submission to *DNA Repair*

[1] DNA Damage Response laboratory, Centre for Chromosome Biology, School of Natural Sciences, National University of Ireland, Galway

Key words: UVA-radiation, DNA polymerase eta (polη), translesion synthesis (TLS), DNA damage response (DDR), Chk1, cell cycle

3.1 Introduction

Exposure to solar UV radiation is the major risk factor in the development of skin cancer, the most common cancer worldwide (IARC, 2010). Solar UV radiation is divided in to UVC (200-280 nm), UVB (280-315 nm) and UVA (315-400 nm). UV radiation reaching the earth's surface is composed of approximately 95% long-wavelength UVA radiation and 5% UVB radiation (Nunez et al., 1994), as UVC and UVB wavelengths less than 290 nm are blocked by the ozone layer (Freeman et al., 1989). Accumulating evidence indicates that exposure to UVA radiation is a significant risk factor for skin cancer, and UVA radiation was recently defined as a class I carcinogen by the International Association for Research on Cancer (IARC; El Ghissassi et al., 2009). UVA-exposure is specifically implicated as a risk factor in the development of melanoma, the most fatal form of skin cancer, which arises from the malignant transformation of melanocytes, the pigment producing skin cells located in the basal epidermis. UVA radiation penetrates deeper into the skin than UVB, making the melanocytes, a target cell for UVA exposure *in vivo* (Bruls et al., 1984; Meinhardt et al., 2008). Moreover, an increased risk of melanoma is associated with brief intense sun exposure and sunburn in childhood (Whiteman et al., 2001), and the use of UVA-emitting sunbeds (Lazovich et al., 2010).

The induction of pre-mutagenic DNA lesions by UVB radiation is considered an essential step in UV-induced skin carcinogenesis (Pfeifer and Besaratinia, 2012). Cyclobutane pyrimidine dimers (CPDs) and pyrimidine (4–6) pyrimidone photoproducts (6,4-PPs), the major UVB-induced DNA lesions, are formed by direct absorption of UV radiation by DNA bases. Since DNA absorbs maximally at approximately 300 nm, UVA is less efficiently absorbed than UVB (Freeman et al., 1989). However, it is now well established that UVA also induces CPDs, in cultured cells, whole human skin and plasmid DNA (Douki et al., 2003; Jiang et al., 2009; Mouret et al., 2006; Perdiz et al., 2000). Although induced approximately 10^3 times less efficiently per J/m^2 than UVB (Perdiz et al., 2000), CPDs are the most abundant UVA-induced lesion (Mouret et al., 2006). There is some

evidence that suggests that UVA also induces 6,4-PPs, albeit at much lower levels than UVA-induced CPDs (Cortat et al., 2013; Schuch et al., 2009). Along with DNA photolesions, UVA also induces oxidative stress, which can result in oxidative DNA damage, including formation of the 8-oxo-7,8-dihydro-2'-deoxyguanosine (8-oxo-G) lesion (Kielbassa et al., 1997). However, UVA-induced 8-oxo-G lesions are approximately three-fold less abundant than UVA-induced CPDs in CHO cells (Douki et al., 2003). Error-prone replication past unrepaired DNA photolesions can give rise to C-T and CC-TT transition mutations, considered UV signature mutations (Wikonkal and Brash, 1999). UV signature mutations are found in the *TP53* gene in >50% of non-melanoma skin cancers (Brash et al., 1991; Ziegler et al., 1993), and were recently identified in key melanoma genes, including *PREX1* and *RAC1* (Hodis et al., 2012; Krauthammer et al., 2012). UV signature mutations are not only induced by UVB, but are also the most common UVA-induced mutation in cultured human skin cells and whole mouse skin (Ikehata et al., 2008; Kappes et al., 2006).

To protect against the mutagenic effects of DNA lesions, cells activate the DNA damage response (DDR), a biochemical process that plays a critical role in the recognition and repair of DNA lesions, as well as the activation of cell cycle checkpoints, or the induction of cell death if the damage is too severe (Niida and Nakanishi, 2006; Zhou and Elledge, 2000). While the nucleotide excision repair (NER) pathway repairs UVC-induced DNA photolesions, some lesions can persist into S-phase, where they block progression of replicative polymerases. Translesion synthesis (TLS), an integral component of the DDR, allows cells to continue replication past replication-blocking DNA lesions in the template, through recruitment of specialised TLS polymerases. TLS polymerases are typically low fidelity polymerases in respect to undamaged DNA, but can carry out error-free replication past specific DNA lesions. DNA polymerase eta (polη) is a Y-family TLS polymerase which can carry out error-free replication past UVC-induced dithymidine dimers *in vitro*, preferentially inserting two adenines opposite a dithymidine dimer (Johnson et al., 1999b; Masutani et al., 1999a). The enlarged open active site of polη can accommodate the two

bases of a CPD, facilitating lesion bypass (Biertumpfel et al., 2010; Silverstein et al., 2010). Mutations in the *POLH* gene, which encodes polη, gives rise to xeroderma pigmentosum variant (XPV) (Johnson et al., 1999a; Masutani et al., 1999b), an inherited genetic disorder characterised by sun sensitivity and elevated levels of sunlight-induced skin cancer, including melanoma (Cleaver, 1972). XPV cells are differentiated from classic NER-deficient XP complementation groups, by mild UVC sensitivity, but hypersensitivity to UVC and caffeine (Arlett et al., 1975). At a molecular level, polη-deficient XPV cells are characterised by delayed replication and hypermutability following UVC exposure (Lehmann et al., 1975; Maher et al., 1976).

Following UVC-exposure, enhanced replication fork stalling results in increased DDR activation in polη-deficient cells, compared to polη-expressing cells (Cruet-Hennequart et al., 2006; Despras et al., 2010). Stalled replication forks result in activation of the S-phase replication checkpoint, mediated by the ataxia telangiectasia and Rad3-related (ATR) kinase and the checkpoint kinase, Chk1 (Bartek et al., 2004; Branzei and Foiani, 2010). ATR is activated in an ATR interacting protein (ATRIP)-dependent manner, by replication protein A (RPA)-coated single stranded DNA (ssDNA) (Zou and Elledge, 2003), formed as a result of helicase-mediated unwinding of DNA downstream of the stalled replication fork (Byun et al., 2005). RPA is a heterotrimeric ssDNA-binding protein. The N-terminal region of RPA2 is subject to phosphorylation in a cell cycle-dependent manner (Wold, 1997), and in response to DNA damage, including PIKK-mediated phosphorylation on S4/S8 (Cruet-Hennequart et al., 2006; Oakley and Patrick, 2010). Chk1 is a key ATR substrate, and is activated by ATR-mediated phosphorylation on S317 and S345 (Zhao and Piwnica-Worms, 2001). Activated Chk1 then phosphorylates a number of substrates, including the Cdc25 family of phosphatases, which inhibits cell cycle progression through S and G2/M in the presence of damage, by preventing cyclin-dependent kinase (CDK) dephosphorylation and activation (Chen et al., 2003; Xiao et al., 2003).

While it has recently been demonstrated that NER plays a role in the removal of UVA-induced DNA photolesions (Cortat et al., 2013), the role of TLS and polη in the response to UVA radiation is not well studied. Given the importance of polη in the bypass of CPDs, we have investigated whether polη plays a role in DNA replication following exposure of cells to UVA radiation, under conditions when CPDs are induced. Here we show for the first time that polη is involved in the recovery from UVA-induced inhibition of DNA replication, and is recruited to nuclear foci following UVA-irradiation. Furthermore, the ATR-Chk1 pathway is strongly activated in polη-deficient cells following UVA-exposure, and plays a key role in the survival of UVA-irradiated polη-deficient cells.

3.2 Results

3.2.1 Effect of polη expression on UVA-sensitivity

The expression of polη and XPA proteins in the fibroblast cell lines used in this study were analysed by western blotting (Figure 3.1A). Polη protein was not detected in extracts from XP30RO cells (Figure 3.1A, lane 2), consistent with the presence of a mutation in exon 2 of the *POLH* gene (Johnson et al., 1999a; Masutani et al., 1999b), but was detected in extracts from TR30-2 cells, which constitutively express polη from a *POLH* transgene (Figure 3.1A, lane 3). Consistent with a mutation in the *XPAC* gene (Satokata et al., 1992a), XPA protein was not detected in XP12RO cells (Figure 3.1A, lane 5), but was detected in XP12RO-C5 cells (Figure 3.1A, lane 6), which are derived from XP12RO and constitutively express XPA from an *XPAC* transgene (Köberle et al., 2006).

Consistent with previous reports that UVA induces CPDs in the DNA of irradiated cultured cells (Mouret et al., 2006; Perdiz et al., 2000), using immunoblotting and an anti-thymidine dimer antibody, CPDs were detected in genomic DNA isolated from XP30RO cells exposed to 100-300 kJ/m^2 UVA (Figure 3.1B). CPDs were also observed in XP30RO cells exposed to UVC doses as low as 0.5 J/m^2 (Figure 3.1B). The relative intensity of each band was analysed and, consistent with a report that UVC is approximately 10^5 times more efficient than UVA at inducing CPD per J/m^2 (Perdiz et al., 2000), the CPD signal intensity at 100 kJ/m^2 UVA was approximately equal to the intensity obtained following exposure of cells to 0.5-1 J/m^2 UVC irradiation (Figure 3.1B).

To investigate if polη expression affected the sensitivity of cells to long-wavelength UVA radiation, polη-deficient XP30RO and polη-expressing TR30-2, fibroblasts were exposed to increasing does of UVA radiation, up to 150 kJ/m^2 UVA, and cell survival was determined using the clonogenic colony-forming assay (Figure 3.1C). In parallel, the UVA-sensitivity of XPA-deficient (XP12RO), XPA-expressing (XP12RO-C5) and the normal transformed fibroblast (NFF) cell lines to UVA radiation was determined

(Figure 3.1C). There was no significant difference in the sensitivity of any of the cell lines examined following exposure of cells to up to 100 kJ/m^2 UVA radiation (Figure 3.1C). However, polη-deficient XP30RO cells were approximately two-fold more sensitive to 150 kJ/m^2 UVA, compared to polη-expressing TR30-2 cells (Figure 3.1C). While not statistically significant (p=0.06), the reduction in survival of polη-deficient cells to UVA radiation, indicates that polη may play a role in the response of cells to UVA radiation. XPA-deficient XP12RO cells were significantly more sensitive to 150 kJ/m^2 UVA than isogenic XPA-expressing XP12RO-C5 cell line (Figure 3.1C), consistent with a recent report that XPA-deficient XP12BE cells are more sensitive to UVA radiation than NER-proficient cells (Cortat et al., 2013).

To control for the phenotype observed following UVA-exposure (Figure 3.1C), the sensitivity of the cells to short-wavelength UVC radiation was assessed (Figure 3.1D). Polη-deficient XP30RO cells are mildly sensitive to UVC compared to pol-expressing TR30-2 cells, with an approximately two-fold decrease in XP30RO survival observed following exposure to 5 J/m^2 UVC radiation, compared to TR30-2 cells (Figure 3.1D), consistent with previous reports (Cruet-Hennequart et al., 2006; Stary et al., 2003; Yamada et al., 2000). XP12RO XPA-deficient cells were hypersensitive to UVC (Figure 3.1D), and consistent with previous reports, expression of XPA protein, as in XP12RO-C5 cells, rescued this UVC hypersensitivity (Figure 3.1D; Cleaver et al., 1995; Zeng et al., 1997).

While polη-deficient XPV cells are mildly sensitive to UVC radiation compared to NER-deficient XP cells (Figure 3.1D; Cleaver 1972), polη-deficient cells are hypersensitive to UVC radiation in the presence of caffeine (Figure 3.1F; Arlett et al., 1975; Cleaver et al., 1999; Cruet-Hennequart et al., 2006). To investigate the effect of caffeine on UVA survival, XP30RO and TR30-2 cells were mock-treated or exposed to UVA-irradiation and subsequently treated with 1 mM caffeine (Figure 3.1E). Caffeine significantly sensitised XP30RO polη-deficient cells to UVA radiation compared to polη-expressing TR30-2 cells (Figure 3.1E). Caffeine

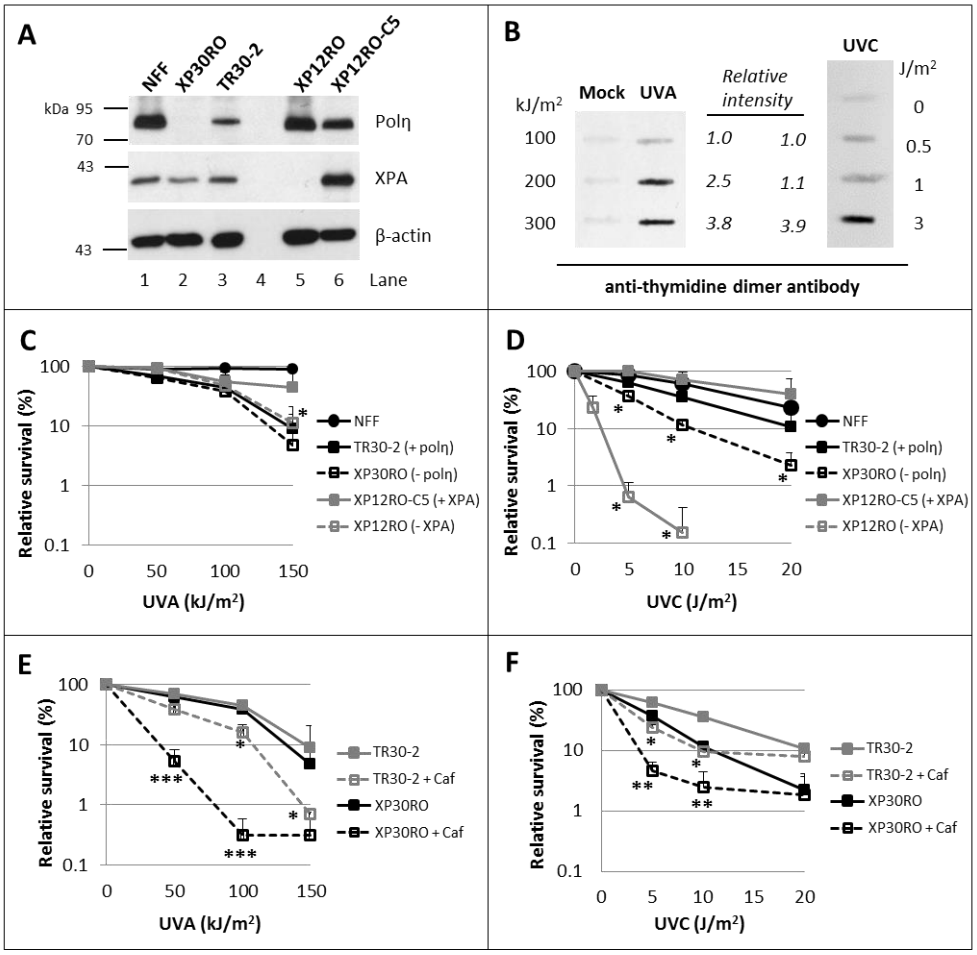

Figure 3.1 Effect of polη expression on the sensitivity of human cells to UVA radiation. (A) 20 µg of protein was separated by SDS-PAGE and the expression of polη and XPA proteins was analysed by western blotting. β-actin was used as a loading control. **(B)** DNA was extracted from mock-treated or UVC- or UVA-irradiated XP30RO cells immediately post-treatment. 250 ng of DNA was blotted onto nitrocellulose membrane and probed with an anti-thymidine dimer antibody. Bound antibody was detected with a HRP-conjugated anti-mouse IgG secondary antibody, and visualised using the ECL prime system. Relative band intensities were calculated as outlined in Section 2.2.18.4, and are presented relative to the intensity of the 100 kJ/m^2 UVA-treated sample. Blots are representative of results obtained from at least three independent experiments. **(C-F)** Cells were mock-treated or exposed to the indicated doses of UVA or UVC irradiation. Where indicated (D and F), 1 mM caffeine (Caf) was added to the culture medium immediately following irradiation. 24 hr following irradiation, cells were trypsinised, re-seeded at 1 x 10^5 cells per 60 mm Cell$^+$ dish and incubated for 9 days. Where indicated (D and F), 1 mM caffeine was added to the medium following re-seeding and remained for the duration of the assay. Cells were fixed and stained in dimethylene blue solution and the number of colonies was scored. The survival of the irradiated cells is expressed relative to the survival of the appropriate mock-treated control cells. The survival of irradiated and caffeine-treated cells is expressed relative to the survival of mock-treated and caffeine-treated control cells. Data represents the average of three independent experiments;

error bars represent one standard deviation. **(C-D)** * represents statistical difference between XP30RO and TR30-2 cells or XP12RO and XP12RO-C5 cells. **(E-F)** * represents statistical difference between UV-irradiated and UV-irradiated and caffeine-treated cells. * $p<0.05$, ** $p<0.01$ and *** $P<0.001$ as determined using one-way ANOVA.

reduced the survival of XP30RO polη-deficient cells by 12-fold following exposure to 50 kJ/m^2 UVA, whereas caffeine only reduced TR30-2 UVA survival by less than 2-fold at the same dose (Figure 3.1E).

As previously mentioned, polη-deficient XPV cells are hypersensitive to UVC radiation in the presence of caffeine. Consistent with previous reports (Arlett et al., 1975; Cleaver et al., 1999; Cruet-Hennequart et al., 2006), caffeine sensitised XP30RO to 5 J/m^2 UVC by 8-fold, while polη-expressing TR30-2 cell were only 2.5-fold more sensitive to 5 J/m^2 UVC-irradiation and caffeine (Figure 3.1F).

The role of polη in caffeine-induced UVA sensitivity was directly tested in TR30-9 cells (Figure 3.2B). TR30-9 cells express tetracycline-inducible polη (Figure 3.2A; Cruet-Hennequart et al., 2006); thus the effect of polη expression on cell survival can be directly tested in an isogenic cell line. Consistent with the effect of caffeine on UVA survival of XP30RO cells reflecting the polη-deficient status of the cells, polη-deficient TR30-9 cells were significantly more sensitive to UVA radiation in the presence of caffeine compared to polη-expressing TR30-9 cells (Figure 3.2B). Cell viability was measured 48 hr following UVA exposure using the trypan blue dye-exclusion assay, as untreated TR30-9 cells did not efficiently form colonies. The effect of caffeine on the UVC sensitivity of polη-expressing and polη-deficient TR30-9 cells was also examined (Figure 3.2C). Polη-deficient TR30-9 cells were mildly sensitive to UVC radiation compared to polη-expressing TR30-9 cells, but were hypersensitive to UVC and caffeine (Figure 3.2C), consistent with Figure 3.1F and Cruet-Hennequart et al., 2006.

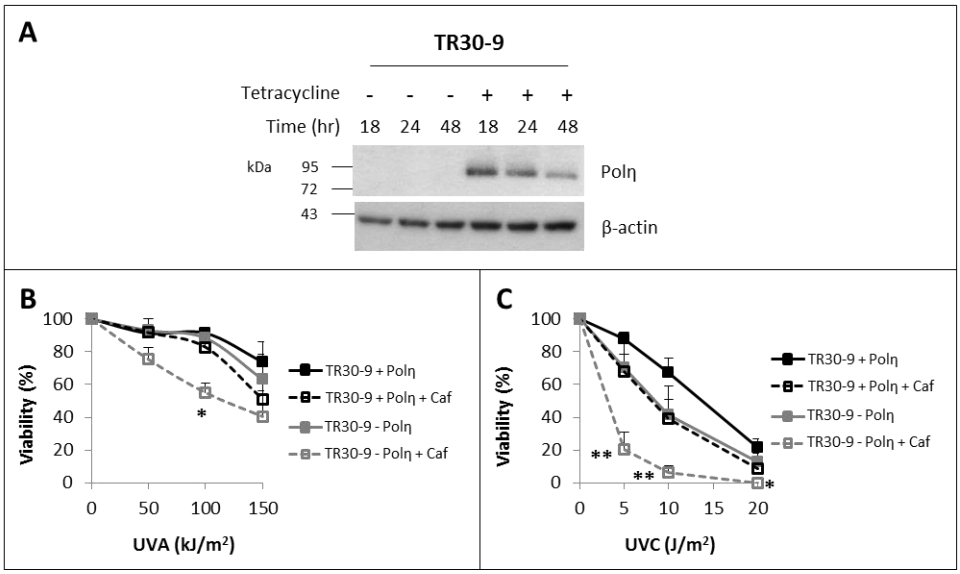

Figure 3.2 Effect of polη-expression on TR30-9 cell viability following UVA irradiation. (A) TR30-9 cells were treated with 0.1 µg/ml tetracycline or an equal volume of DMSO. Cells lysates were prepared at the indicated times following tetracycline addition. 20 µg of protein was separated by SDS-PAGE and polη expression was analysed by western blotting. β-actin was used as a loading control. **(B-C)** TR30-9 cells were treated with tetracycline, as outline in (A) for 18 hr prior to mock-treatment or exposure to the indicated doses of UV-irradiation. 1 mM caffeine was added to the medium immediately following UV-exposure and remained for the duration of the experiment. Cells were incubated for 48 hr and cell viability was assessed using the trypan blue dye-exclusion assay. The viability of UV-irradiated cells was expressed as a percentage of the viability of the appropriate mock-treated control cells. The viability of UV-irradiated and caffeine-treated cells was expressed as a percentage of the viability of the appropriate mock-treated and caffeine-treated control cells. Data represents the mean of three independent experiments; error bars represent one standard deviation. Asterisks indicate statistical difference between UV-irradiated and UV-irradiated and caffeine-treated cells. * $p<0.05$ and ** $p<0.01$ as determined using one-way ANOVA.

The effect of caffeine on the sensitivity of cells to UVA was independent of XPA protein, as no significant decrease in survival XP12RO or XP12RO-C5 cells was observed when cells were co-treated with UVA and caffeine, compared to UVA alone (Supplementary Figure 3.9), at doses where a significant decrease in cell survival was observed in polη-deficient cells (Figure 3.1E). Since caffeine acts as a PIK kinase inhibitor (Sarkaria et al., 1999), the effect of another PIK kinase inhibitor, wortmannin (Sarkaria et al., 1998), on the UVA sensitivity of polη-deficient XP30RO cells was also

analysed (Supplementary Figure 3.10). Wortmannin (10 μM) sensitised polη-deficient XP30RO cells to UVA irradiation to a similar extent as caffeine (Supplementary Figure 3.10); this supports the conclusion that polη-deficient cells are particularly dependent on PIKK-mediated signalling for survival following UVA radiation. Furthermore, reflecting a specific role for polη in the response to UVA radiation, rather than a generic response of polη-deficient cells to DNA damage, caffeine did not sensitise XP30RO cells to ionising radiation (Supplementary Figure 3.11).

3.2.2 Effect of polη-expression on DNA replication following UVA exposure

Polη plays a key role in the replication of UVC-damaged DNA (Cordonnier and Fuchs, 1999; Cruet-Hennequart et al., 2006; Lehmann et al., 1975). Here we investigated whether polη expression also modulates DNA replication following exposure to UVA-irradiation. XP30RO and TR30-2 cells were mock-treated or exposed to 100 kJ/m^2 UVA-radiation. One hour prior to harvesting, cells were incubated with the thymidine analogue BrdU, to label cells actively undergoing DNA replication, and analysed by flow cytometry. The level of BrdU incorporation immediately following UVA-irradiation was not determined, since BrdU is a type 1 photosensitiser (Sugiyama et al., 1990) which can cause damage to DNA if present during UVA irradiation (Cecchini et al., 2005; Manak et al., 1981). In fact, elevated levels of γH2AX, an established marker of DSBs (Redon et al., 2011; Rogakou et al., 1998a), were observed in XP30RO cells exposed to UVA radiation in the presence of BrdU (Supplementary Figure 3.12).

BrdU incorporation decreased rapidly following UVA irradiation in a polη-independent manner (Figure 3.3A and B). The percentage of BrdU-positive cells decreased from 38% in mock-treated cells, to 13% in UVA-irradiated XP30RO cells, and from 36% to 14% in TR30-2 cells, by one hour post-UVA (Figure 3.3B). This is consistent with previous reports of UVA-induced inhibition of DNA replication immediately following exposure, in normal human fibroblast cells (de Laat et al., 1996; Runger et al., 2012).

While the UVA-induced decrease in DNA replication was independent of polη-expression, the subsequent recovery from UVA-induced replication arrest was significantly delayed in polη-deficient XP30RO cells compared to polη-expressing TR30-2 cells (Figure 3.3A and B). The percentage of BrdU-positive TR30-2 cells increased to 26% three hours following UVA irradiation, while the only 16% of the UVA-irradiated XP30RO cells were BrdU-positive at this time (Figure 3.3B). This statistically significant difference in the percentage of BrdU-positive cells between UVA-irradiated XP30RO and TR30-2 cells was also evident six hours post-UVA (Figure 3.3B). In the absence of UVA-exposure, the percentage of BrdU-positive cells was similar in the two cell lines, over the time course analysed (Figure 3.3B). Ten hours following UVA exposure, the percentage of BrdU-positive cells in UVA-irradiated samples was similar to that of mock-treated samples in both cell lines (Figure 3.3B). Overall, this data indicates that polη modulates the recovery from UVA-induced inhibition of DNA replication.

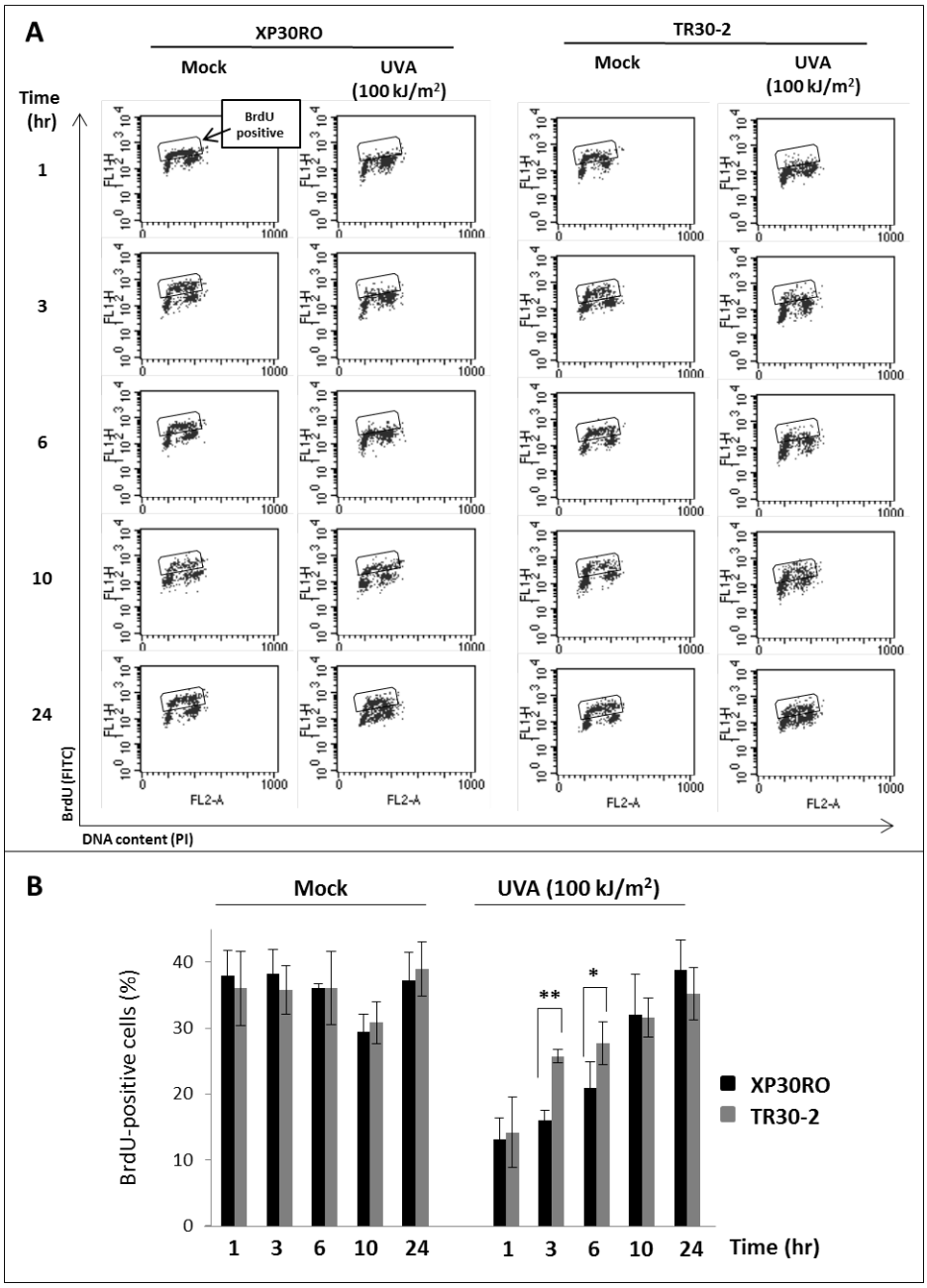

Figure 3.3 Effect of polη expression on DNA replication in UVA-irradiated cells. XP30RO and TR30-2 cells were mock-treated or exposed to 100 kJ/m^2 UVA-irradiation. Cells were incubated with BrdU (10 µM) for 1 hr prior to harvesting at the indicated times following UVA-exposure. Cells were fixed in 70 % ethanol. BrdU was labelled with a FITC-conjugated anti-BrdU antibody and DNA was stained with propidium iodide (PI). Samples were analysed using a FACS Calibur, and data was analysed using CellQuest™ software. **(A)** Dot plots are representative of four independent experiments. The BrdU-positive population is indicated by an arrow. **(B)** The percentage of BrdU-positive cells, calculated from the dot plots shown in (A). Data represents four independent experiments; error bars represent one standard deviation. * $p<0.05$, ** $p<0.01$ represents statistical difference between XP30RO and TR30-2 cells, as determined by one-way ANOVA.

3.2.3 Effect of polη-expression on UVA-induced DNA damage responses

Replication fork stalling at sites of DNA damage can activate an S-phase replication checkpoint (Bartek et al., 2004; Branzei and Foiani, 2010), which is mediated in part by ATR-mediated phosphorylation of the checkpoint protein Chk1 (see Section 3.1). The replication checkpoint is strongly activated in polη-deficient cells, following exposure to UVC radiation (Cruet-Hennequart et al., 2006; Despras et al., 2010). Since polη deficiency is associated with delayed recovery from UVA-induced inhibition of DNA replication (Figure 3.3), we analysed the relationship between replication inhibition and activation of the ATR-Chk1 pathway in polη-deficient XP30RO cells and polη-expressing TR30-2 cells.

The expression of polη was analysed following UVA exposure, polη protein was not detected in extracts from XP30RO cells (Figure 3.4; upper panels), consistent with Figure 3.1A. Polη was expressed in mock-treated TR30-2 cells throughout the time course analysed (Figure 3.4; upper panels). However, 24 and 48 hr following UVA exposure, the levels of polη protein were dramatically reduced in TR30-2 cells (Figure 3.4; lanes 23-24). A similar decrease in the level of polη-GFP fusion protein was observed following UVA-irradiation in TRG-16 cells (Supplementary Figure 3.13). This data suggests that UVA modulates the cellular levels of polη, and supports a role for polη in the response to UVA radiation. Polη levels were previously shown to be down-regulated following UVC radiation, in a proteasome-dependent manner (Cruet-Hennequart et al., 2006; Jung et al., 2012).

Chk1 phosphorylation on S317, analysed by western blotting using a phospho-specific antibody, was used as a marker of S-phase replication checkpoint activation (see Section 3.1). Phosphorylation of Chk1 on S317 was strongly increased in polη-deficient XP30RO cells immediately following UVA-irradiation, and was sustained up to 48 hr following UVA-irradiation (Figure 3.4). In polη-expressing TR30-2 cells, Chk1 is only weakly phosphorylated on S317 (Figure 3.4). UVA-irradiation or polη-

expression had no effect on the levels of total Chk1 (Figure 3.4). Overall this data shows that UVA-induced Chk1 phosphorylation on S317 is strongly enhanced in polη-deficient cells.

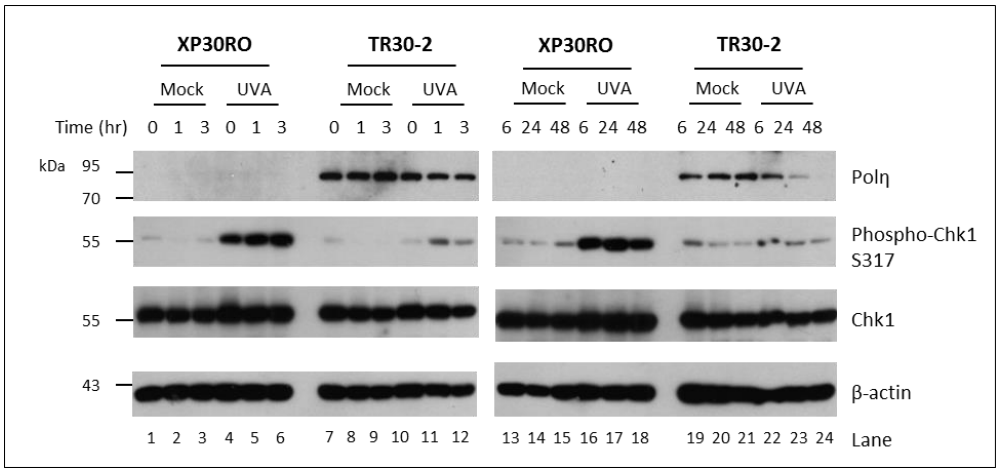

Figure 3.4 Effect of polη expression of UVA-induced phosphorylation of Chk1. XP30RO and TR30-2 cells were mock-treated or exposed to 100 kJ/m^2 UVA-irradiation. Cell lysates were prepared at the indicated times following irradiation. 20 µg of protein was separated by SDS-PAGE and the levels of the indicated proteins were analysed by western blotting. β-actin was used as a loading control.

3.2.4 Effect of caffeine on UVA-induced DNA damage response activation and cell cycle progression

Caffeine selectively sensitised polη-deficient cells to UVA radiation (Figure 3.1E and Figure 3.2B). At a molecular level it is proposed that the effect of caffeine on the UVC-sensitivity of polη-deficient cells, is due to caffeine-mediated inhibition of PIK kinases (Sarkaria et al., 1999), in particular ATR (Heffernan et al., 2009). Consistent with caffeine acting as an inhibitor of ATR under these conditions, caffeine reduced UVA-induced phosphorylation of Chk1 on S317, which was particularly evident in XP30RO cells (Figure 3.5A; lanes 4 vs. 3).

Since caffeine reduced UVA-induced Chk1 phosphorylation (Figure 3.5A), and Chk1 is a key regulator of cell cycle progression, the effect of caffeine on cell cycle distribution following UVA exposure, in XP30RO and TR30-2 cells was investigated (Figure 3.5B). Caffeine induced a significant increase

in the percentage of UVA-irradiated polη-deficient XP30RO cells with S-phase DNA content, 24 hr following treatment (Figure 3.5B; histograms). This suggests that caffeine modulates cell cycle checkpoint activation in polη-deficient cells. Moreover, the caffeine-induced S-phase accumulation of UVA-irradiated XP30RO cells, is associated with an approximately four-fold increase in the percentage of cells with inhibited replication, as defined as cells with S-phase DNA content, but reduced BrdU staining (Figure 3.5B; dot plots). Caffeine-induced effects on cell cycle distribution in UVA-irradiated TR30-2 cells were much less evident (Figure 3.5B), which may reflect the decreased dependence of polη-expressing cells on ATR-Chk1 signalling following exposure to UVA irradiation.

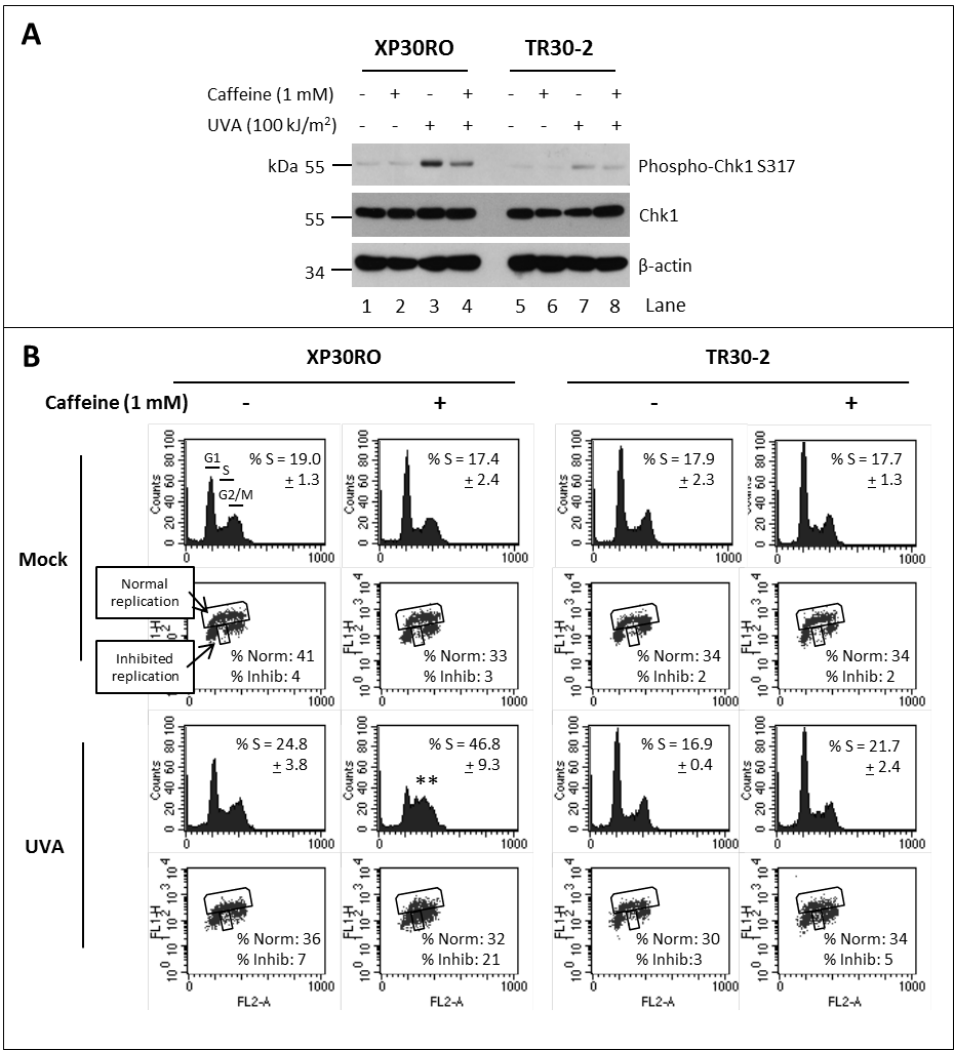

Figure 3.5 Effect of caffeine on cell cycle distribution in UVA exposed cells (A) XP30RO and TR30-2 cells were mock-treated or exposed to 100 kJ/m^2 UVA-irradiation. Where indicated, caffeine (1 mM) was added to the culture media immediately post-UVA and remained until the time of harvest. Cell extracts were prepared 3 hr post-UVA. 20 µg of protein was separated by SDS-PAGE. The levels of Chk1 and phospho-Chk1 S317 were analysed by western blotting. β-actin was used as a loading control. **(B)** XP30RO and TR30-2 cells were mock-treated or exposed to 100 kJ/m^2 UVA-irradiation. Where indicated, caffeine (1 mM) was added to the culture media immediately post-UVA and remained until the time of harvest. Cells were incubated with BrdU (10 µM) for 1 hr prior to fixation, in 70 % ethanol, at 24 hr post-UVA. BrdU was labelled with a FITC-conjugated anti-BrdU antibody, and DNA was stained with propidium iodide (PI). Cells were analysed using a FACS Calibur. Data was analysed using CellQuest software. Histogram plots showing cell cycle distribution are representative of three independent experiments. The average percentage of cells with S-phase DNA content, ± one standard deviation, is shown. ** $p<0.01$, represents statistically significant difference in the percentage of S-phase cells between XP30RO and TR30-2 cells, as determined using one-way ANOVA. Dot plots showing BrdU incorporation are derived from one experiment. Cells stained positive for BrdU were classed as undergoing

normal replication, and cells with S-phase DNA content with reduced BrdU incorporation were classed as undergoing inhibited replication, using the gates shown. The percentage of cells undergoing normal (norm) or inhibited (inhib) replication is shown.

Inhibited replication forks can generate stretches of ssDNA, which are unstable, and can lead to the formation of DNA strand breaks (Feng et al., 2011). Phosphorylation of the histone H2AX on S139 (γH2AX) and RPA2 on S4S8 are widely used markers of DSBs and replication stress-induced DNA strand breaks, respectively (Cruet-Hennequart et al., 2006; Liaw et al., 2011; Redon et al., 2011; Rogakou et al., 1998b). Caffeine increased the levels of UVA-induced γH2AX and phospho-RPA2-S4S8 (Figure 3.6A). This effect of caffeine on DNA strand breaks was elevated in polη-deficient XP30RO cell, compared to polη-expressing TR30-2 cells (Figure 3.6A; lane 4 vs. 8). Moreover, caffeine significantly reduced the percentage of viable XP30RO cells following UVA irradiation, compared to TR30-2 cells, as determined 48 hr following UVA irradiation using the trypan blue dye-exclusion assay (Figure 3.6B).

In summary, in polη-deficient cells caffeine reduced UVA-induced Chk1 phosphorylation (Figure 3.5A) and increased UVA-induced accumulation of cells in S phase (Figure 3.5B). This was associated with an increase in DNA replication inhibition (Figure 3.5B) and an increase in markers of DNA strand breaks (Figure 3.6A) and followed by loss of cell viability (Figure 3.6B). The data suggests that in the absence of polη a caffeine-sensitive pathway, possibly the ATR-Chk1 pathway, plays an important role in UVA survival.

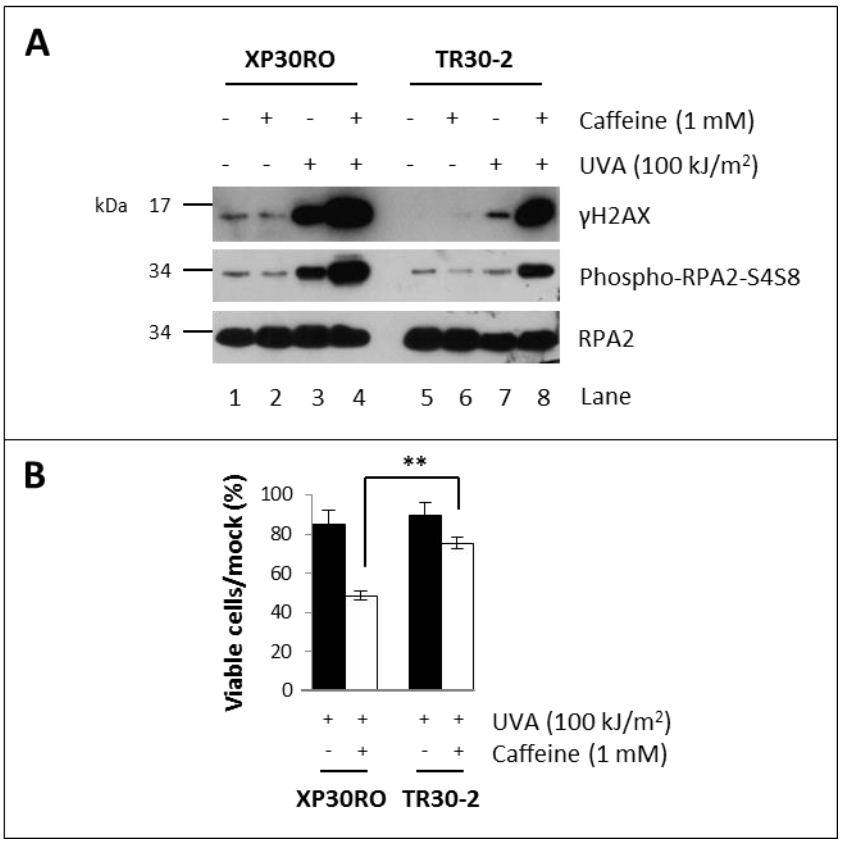

Figure 3.6 Effect of caffeine on UVA-induced DNA strand breaks. (A) XP30RO and TR30-2 cells were mock-treated or exposed to 100 kJ/m^2 UVA-irradiation. Where indicated, caffeine (1 mM) was added to the culture media immediately post-UVA, and remained until the time of harvest. Cell extracts were prepared 24 hr post-UVA. 20 µg of protein was separated by SDS-PAGE. The levels of phospho-RPA2-S4S8 and γH2AX were analysed by western blotting using phospho-specific antibodies. RPA2 was used as a loading control. **(B)** XP30RO and TR30-2 cells were mock-treated or UVA-irradiated and treated with caffeine as outlined in (A). 48 hr post-UVA cell viability was assessed using the trypan blue dye-exclusion assay. The viability of UVA-irradiated cells is expressed as a percentage of the viability of the appropriate mock-treated control cells. The viability of UVA-irradiated and caffeine-treated cells is expressed as a percentage of the viability of the appropriate mock-treated and caffeine-treated control cells. Data represents the mean of three independent experiments; error bars represent one standard deviation. * $p<0.01$ represents a significant difference between XP30RO and TR30-2 cells, as determined using one-way ANOVA.

3.2.5 Effect of UVA-irradiation on polη localisation

Polη re-localises to nuclear foci following exposure of cells to UVC-radiation and cisplatin (Albertella et al., 2005; Kannouche et al., 2001). If

polη plays a role in replication in UVA-irradiated cells, then polη should also be localised to nuclear foci following UVA-exposure. The effect of UVA radiation on polη localisation was investigated in TRG-16 cells, which express a tetracycline-inducible polη-GFP fusion protein (Figure 3.7A). Polη-GFP fusion protein has a predicted molecular weight of 105 kDa. Following incubation of TRG-16 cells with tetracycline for 24 hr, polη-GFP was detected by western blotting using an anti-polη antibody, as a band of approximately 105 kDa (Figure 3.7A; lane 2). As a control for polη expression, extracts from XP30RO and TR30-2 cells were analysed in parallel. As outlined in Figure 3.1A, XP30RO extracts did not contain polη, and TR30-2 cells expressed wild type polη, which has a molecular weight of 78 kDa (Figure 3.7; lanes 3 and 4, respectively).

During unperturbed conditions polη was distributed homogenously in the nucleus of the majority of cells (Figure 3.7B (i); Kannouche et al., 2001). In approximately 10% of mock-treated cells, polη-GFP foci were observed (Figure 3.7C and D), consistent with previous reports (Kannouche et al., 2001). For the purpose of the present analysis, cells with greater than eight polη-GFP foci per nucleus were scored as polη-GFP foci-positive. Following UVA-irradiation, polη-GFP rapidly re-localised to nuclear foci (Figure 3.7C). The peak of polη-GFP localisation to nuclear foci occurred 1 hour following UVA-irradiation, at this time approximately 30% of polη-GFP-expressing TRG-16 cells contained polη-GFP foci (Figure 3.7C). After the initial rapid recruitment of polη-GFP to nuclear foci following UVA-irradiation, the percentage of cells with polη-GFP foci decreased, such that 6 hr post-UVA the percentage of cells with polη-GFP foci had returned to mock-treated levels (Figure 3.7C).

As a positive control for polη-GFP recruitment to nuclear foci, tetracycline-induced TRG-16 cells were exposed to 20 J/m^2 UVC irradiation (Figure 3.7B (iv)). In contrast to UVA, the peak of polη-GFP localisation to nuclear foci occurred 4 hr following UVC exposure, with approximately 30% of polη-GFP positive TRG-16 cells containing polη-GFP foci at this time (Figure 3.7D). Further highlighting the differential response of cells to UVA

and UVC radiation, polη-GFP foci were still detected in approximately 30% of cells 6 hr following exposure to UVC radiation (Figure 3.7D). Four hours following UVC exposure, a small yet reproducible decrease in the percentage polη-GFP foci-positive TRG-16 cells was observed (Figure 3.7D), this may represent bi-phasic polη recruitment to foci following UVC exposure, but this was not investigated further here.

To confirm that UVA-induced polη-GFP foci result from tight association of polη with chromatin, cells were pre-extracted with 1% (v/v) Triton X-100 prior to fixation, as described in Kannouche et al. (2001). Triton X-100 pre-extraction strongly reduced the diffuse nuclear polη-GFP signal, while UVA-induced polη-GFP foci were still detectable by fluorescence microscopy (Figure 3.7B (iii)). UVC-induced polη-GFP foci were also detectable following Triton X-100 pre-extraction (Figure 3.7B (v)), consistent with a previous report (Kannouche et al., 2001).

To confirm that polη-GFP localisation to foci is a direct consequence of UVA exposure, and not due to any possible contaminating short-wavelength UV radiation, cells were exposed to UVA radiation through short-wavelength UV filters (Supplementary Figure 3.14). Localisation of polη-GFP to nuclear foci was significantly induced following exposure to UVA radiation through both filter 1 and filter 2, which block the transmission of UV wavelengths less than 315 and 350 nm, respectively (Supplementary Figure 3.14 and Figure 2.3). This strongly supports the conclusion that polη-GFP localisation to foci is a direct consequence of UVA exposure. For these experiments, cells were exposure to UVA through the filters for an identical duration; however, addition of filters reduced the UVA dose rate received by the cells (Table 2.8). Since the percentage of polη-GFP foci-positive cells reduced following the addition of short-wavelength UV filters (Supplementary Figure 3.14), this provides evidence that polη-GFP localisation to nuclear foci is a dose dependent event.

In summary, the data presented here provides evidence that polη-GFP is rapidly recruited to nuclear foci following UVA irradiation, and that the foci reflect chromatin-association of polη-GFP.

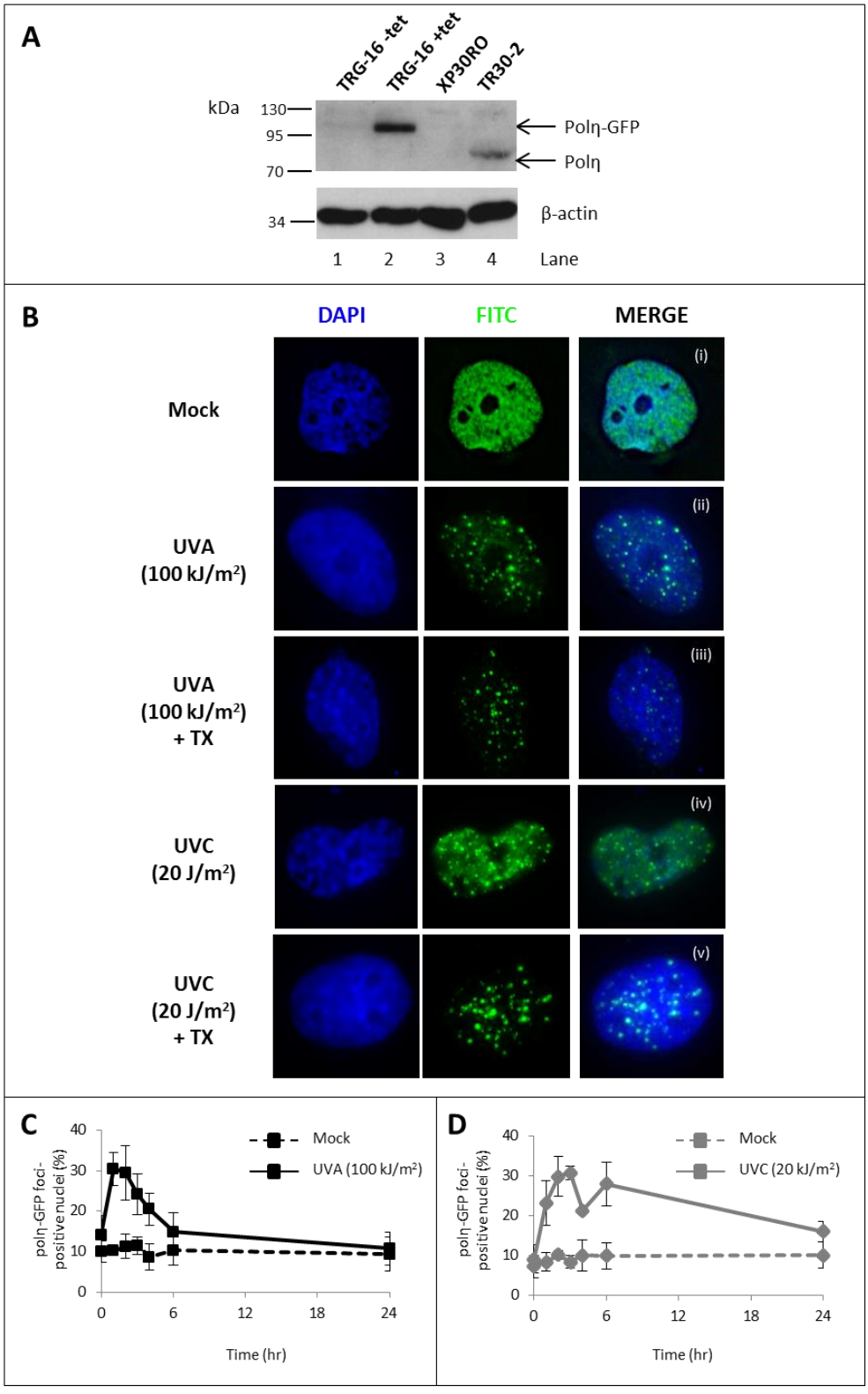

Figure 3.7 Effect of UVA-radiation on polη nuclear localisation. (A) TRG-16 cells were incubated, or not, with 0.1 µg/ml tetracycline for 24 hr and cell lysates were prepared. 20 µg of protein was separated by SDS-PAGE. The levels of polη and polη-GFP fusion protein were analysed by western blotting using an anti-polη antibody. Protein extracts from polη-deficient XP30RO and polη-expressing TR30-2 cells were used as controls.

β-actin was used as a loading control. **(B)** TRG-16 cells were cultured on glass coverslips and incubated with tetracycline as outlined in (A). Cells were mock-treated or exposed to either 100 kJ/m^2 UVA or 20 J/m^2 UVC radiation. 1 hr post-UVA (ii) or 3 hr post-UVC (iv), cells were fixed in 4 % PFA. DNA was stained with DAPI. Images were captured under 100X magnification using a DeltaVision fluorescence microscope. Where indicated (+TX), cells were pre-extracted with 1% (v/v) Triton X-100 for 10 min on ice prior to fixation. **(C)** TRG-16 cells were exposed to UVA-irradiation as outlined in (B). Cells were fixed at the indicated the times following UVA irradiation. Polη-GFP-expressing cells were visualised by fluorescence microscopy under 60X magnification. The percentage of polη-GFP expressing cells containing polη-GFP foci was scored. Cells with greater than eight polη-GFP foci were scored as polη-GFP foci-positive. At least 100 polη-GFP expressing cells were scored per condition. Data represents the average of three independent experiments; error bars represent one standard deviation. **(D)** The percentage of polη-GFP-expressing TRG-16 cells with polη-GFP foci at indicated times post-UVC (20 J/m^2) was determined as outlined in (C).

3.2.6 Correlation of UVA-induced polη-GFP foci with DNA replication

The timing of recovery from UVA-induced replication inhibition (Figure 3.3B), correlates with the timing of UVA-induced polη-GFP localisation to nuclear foci (Figure 3.7C). Furthermore, polη-deficient cells experience delayed recovery from UVA-induced replication inhibition (Figure 3.3B). Taken together, these results suggest that polη plays a role in DNA replication following UVA exposure.

To directly analyse whether formation of polη-GFP foci correlate with DNA replication on an individual cell basis, fluorescence microscopy was used (Figure 3.8). DNA replication was quantified in each cell by measuring the intensity of fluorescently-labelled EdU incorporated in DNA. In parallel, the distribution of polη-GFP in each cell was also analysed. Due to the presence of copper in the Click-iT™ EdU labelling kit, which is known to quench GFP fluorescence (Bálint et al., 2013), polη-GFP was labelled with an anti-GFP antibody and visualised using an Alexa Fluor® 488-conjugated secondary antibody. Under these conditions, the mean EdU intensity was approximately 3-fold lower in UVA-irradiated compared to mock-treated

TRG-16 cells (Figure 3.8B), consistent with UVA-induced replication inhibition (Figure 3.3). Moreover, the percentage of TRG-16 cells with polη-GFP foci was 2.7-fold increased in UVA-irradiated cells compared to mock-treated cells (Figure 3.8C), consistent with Figure 3.7C.

Polη-GFP foci were exclusively observed in cells stained positively for EdU (Figure 3.8C); this is consistent with a role for polη the replication of DNA. In addition, some polη-GFP foci were found to co-localise with EdU foci in UVA-irradiated cells, identified as yellow foci in merged images (Figure 3.8A (v); arrows). This is consistent with a previous report that polη foci co-localise with BrdU and PCNA following UVC-irradiation (Kannouche et al., 2001). Overall, this data provides direct evidence which supports the role of polη in the replication of UVA damaged DNA.

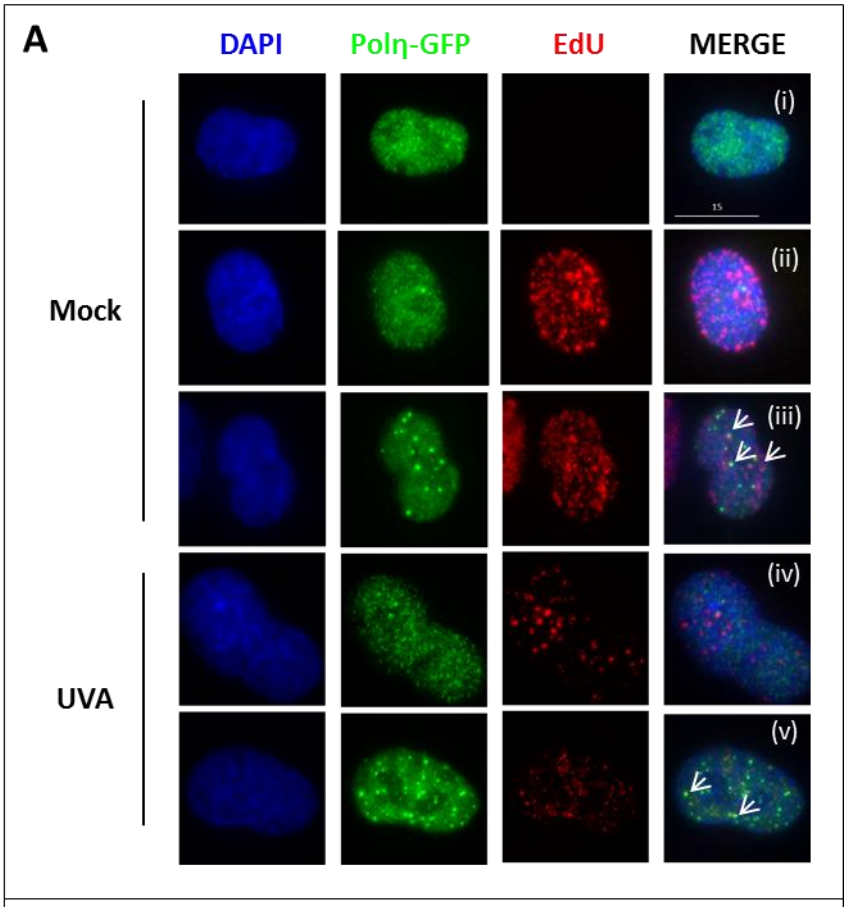

C

	Polη-GFP expressing cells (%)				
	EdU-negative		EdU-positive		
Polη-GFP distribution	Pan-nuclear	Foci	Pan-nuclear	Foci	n
Mock	41	0	42	17	322
UVA	40	0	14	46	278

Figure 3.8 Correlation of UVA-induced polη-GFP foci and DNA replication. TRG-16 cells grown on glass coverslips, incubated with tetracycline (0.1 µg/ml) for 24 hr to induce polη-GFP protein expression, and mock-treatment or exposed to 100 kJ/m^2 UVA. Cells were incubated with EdU (10µM) for 30 min prior to fixation in 4% PFA 1 hr post-UVA. Polη-GFP was visualised by staining with an anti-GFP antibody followed by

an Alexa Fluor® 488-conjugated secondary antibody. EdU was labelled using the Click-IT™ EdU Alexa Fluor® 594 imaging kit (Invitrogen). DNA was stained using DAPI. Cells were mounted in SlowFade and visualised using a DeltaVision fluorescence microscope. **(A)** Representative images of mock-treated or UVA-irradiated TRG-16 cells showing the observed staining patterns of polη-GFP: pan-nuclear staining (i and iv) or nuclear foci (ii, iii, and v). Images were captured under 60X magnification. **(B)** Images of polη-GFP-expressing cells were captured using the 60X objective. The EdU fluorescence intensity of each nucleus was quantified as outlined in Section 2.2.16.7. Box-and-whisker plot shows the distribution of EdU intensities for each sample. The middle of the boxes represents the median value of EdU intensity. The top (black) and bottom (grey) boxes represent the 75^{th} and 25^{th} percentile respectively. The ends of the whiskers represent the maximum and minimum EdU intensity values measured. **(C)** The EdU status of each cell was determined visually. The nuclear distribution of polη-GFP was classed as homogeneously distributed (pan-nuclear) or containing >8 polη-GFP foci (Foci). Quantification of cells in each condition is expressed as a percentage of the total number of polη-GFP expressing cells scored in each condition (n). Data is representative at least 130 cells per condition, derived from two independent experiments.

3.3 Discussion

Exposure to long-wavelength UVA radiation, which accounts for >95% of the solar UV radiation reaching the earths' surface, is a risk factor in the development of skin cancer. While it is now well established that UVA radiation induces DNA damage, in the form of CPDs (Mouret et al., 2006; Perdiz et al., 2000), and to a lesser extent 8-oxo-G and 6,4-PP lesions (Cortat et al., 2013; Kielbassa et al., 1997; Schuch et al., 2009), the cellular responses to UVA-induced DNA damage are not well characterised. Recently it was demonstrated that the nucleotide excision repair (NER) pathway plays a role in the removal of UVA-induced DNA photolesions (Cortat et al., 2013). Since CPDs are the most common UVA-induced DNA photoproduct (Mouret et al., 2006; Perdiz et al., 2000), and given the importance of polη in the bypass of CPDs, we investigated whether polη plays a role in DNA replication following exposure of cells to UVA radiation, under conditions where CPDs are induced.

To investigate whether polη plays a role in the response of cells to UVA radiation, the UVA sensitivity of polη-expressing and -deficient cell lines was determined. Polη-deficient XP30RO cells were more sensitive to UVA radiation than polη-expressing TR30-2 cells, particularly at higher UVA doses (Figure 3.1C; 150 kJ/m^2 UVA), suggesting polη plays a role in the response of cells to UVA. The effect of polη-expression on UVA sensitivity was directly investigated using TR30-9 cells, which express polη from a tetracycline-inducible promoter. As untreated TR30-9 cells did not efficiently form colonies under the conditions used here, cell viability was determined 48 hr following irradiation, using the trypan blue dye-exclusion assay. While the effect of polη expression on UVA sensitivity was less pronounced in TR30-9 cells this may reflect differences in the assays used to measure viability. It should also be noted that polη-deficient TR30-9 cells were slightly less sensitive to UVC radiation than parental XP30RO cells (Cruet-Hennequart et al., 2006). Similar to the TR30-9 cells, polη-expression had little effect on the viability of XP30RO and TR30-2 cells, measured 48 hr following UVA irradiation. These results suggest that short-

term cell viability following UVA exposure is polη-independent, but that polη-expression plays a role in determining the long-term clonogenic survival of cells following UVA irradiation.

It was of interest to investigate the survival of NER-deficient cells to UVA radiation, given the key role of NER in the repair of UV photolesions. Using XPA-deficient XP12RO cells and the isogenic XP12RO-C5 cells, which are derived from XP12RO and constitutively expresses XPA protein from an *XPAC* transgene, the role of XPA in UVA survival was analysed (Figure 3.1C). XPA-deficient cells were significantly more sensitive to UVA radiation than XPA-expressing cells (Figure 3.1C), consistent with a recent report (Cortat et al., 2013).

The mild reduction in UVA survival of polη-deficient compared to XPA-deficient cells, mirrors the phenotypes observed following exposure of cells UVC radiation (Figure 3.1D; Cleaver 1975), and is likely to reflect the relative contribution of TLS-dependent CPD bypass versus XPA-dependent CPD removal in determining cell survival. If the yield of UVA-induced CPDs is an important determinant of cell survival following UVA exposure, then, since 100 kJ/m^2 UVA and 1 J/m^2 UVC are broadly equivalent in terms of dimer inducing ability based on immunoblot results, the relative survival of polη-deficient cells would be expected to be approximately equal at these doses, which is the case observed here. Overall the data supports a role for DNA polη in the survival of UVA-irradiated cells.

The selective effect of caffeine on UVA sensitivity toward polη-deficient cells compared to polη-expressing cells supports the interpretation that polη plays a role in the response to UVA radiation. Caffeine significantly sensitised XP30RO polη-deficient cells to UVA, as determined by both clonogenic cell survival and cell viability 48 hr following UVA. Moreover, caffeine significantly sensitised polη-deficient TR30-9 cells to UVA compared to the isogenic polη-expressing TR30-9 cells. It is well documented that polη-deficient cells are hypersensitive to UVC radiation in the presence of caffeine (Arlett et al., 1975; Cleaver et al., 1999; Cruet-Hennequart et al., 2006) and (Figure 3.1D and Figure 3.2C). It is proposed

that caffeine acts as a PIK kinase inhibitor (Sarkaria et al., 1999) and abrogates UVC-induced S and G2/M checkpoints (Kaufmann et al., 2003). Since polη-deficient cells have increased UVC-induced PIKK-mediated DDR activation, compared to polη-expressing cells (Cruet-Hennequart et al., 2006; Despras et al., 2010), this could explain the decreased UVC survival of polη-deficient cells by caffeine. The role of caffeine as a PIKK inhibitor in the UVA response will be discussed in detail below.

Polη plays a key role in the replication of UVC-damaged DNA, and polη-deficient cells experience prolonged DNA replication inhibition following UVC exposure compared to polη-expressing cells (Cordonnier and Fuchs, 1999; Cruet-Hennequart et al., 2006; Lehmann et al., 1975). Here we investigated if polη is also involved in replication following exposure to UVA radiation. UVA induced a rapid decrease in DNA replication in both XP30RO and TR30-2 cells that was independent of polη-expression. Consistent with previous reports, UVA-induced inhibition of DNA synthesis was maximal immediately following UVA exposure (de Laat et al., 1996; Runger et al., 2012). Importantly, the timing of UVA-induced inhibition of DNA replication is different to the reported UVC-induced replication inhibition, which peaks later following UVC (Cruet-Hennequart et al., 2006). DNA replication inhibition recovered in both XP30RO and TR30-2 cells by 10 hr following UVA irradiation, consistent with previous reports of replication recovery within 2-7 hr following UVA-irradiation in human fibroblasts (de Laat et al., 1996; Runger et al., 2012). However, recovery from DNA replication inhibition after UVA irradiation was delayed in polη-deficient cells between three and six hours following UVA exposure. Furthermore, the timing of recovery from UVA-induced replication inhibition in polη-deficient cells corresponds with the time during which polη-GFP is localised to nuclear foci in TRG-16 cells. This supports the hypothesis that the delay in replication recovery in polη-deficient XP30RO cells is due, at least in part, to a defect in polη-mediated replication of UVA-damaged DNA.

Further supporting a role for polη in the response to UVA radiation, a significant reduction in the level of polη was observed in UVA irradiated TR30-2 and TRG-16 cells, 24 and 48 hr following treatment. Polη levels were previously reported to be reduced following exposure to UVC radiation (Cruet-Hennequart et al., 2006; Jung et al., 2012). Polη is monoubiquitinated in unperturbed cells, which prevents the interaction of polη with PCNA, and TLS activity (Bienko et al., 2010). Moreover, polη is polyubiquitinated in a Mdm2-dependent manner following UVC irradiation which targets polη for proteosomal degradation (Jung et al., 2012). Little is known about the mechanisms controlling polη removal from nuclear foci following TLS-mediated bypass of the replication blocking lesion. However it is reasonable to propose that ubiquitin-mediated proteosomal degradation could play a role in regulating this process. Further studies are required to elucidate the mechanisms regulating polη protein levels following UVA exposure.

Since UVA induced DNA replication inhibition, we investigated activation of the replication checkpoint in UVA-irradiated cells. The replication checkpoint, activated by RPA-coated ssDNA (Zou and Elledge, 2003), formed as a result of replication fork stalling, involves ATR-mediated Chk1 phosphorylation on S317 and S345 (Zhao and Piwnica-Worms, 2001). Chk1 phosphorylated on S317 was strongly elevated in polη-deficient XP30RO cells following UVA irradiation. However, the weak phosphorylation of Chk1 observed in TR30-2 cells, suggests that UVA-induced inhibition of replication was independent of Chk1 activation. In fact, it was previously reported that rapid UVA-induced inhibition of DNA replication is independent of the ATR-Chk1, ATM-Chk2 and p38α MAPK pathways in human fibroblasts (Girard et al., 2008). It was proposed that UVA-induced oxidative damage to proteins, rather than DNA damage, is responsible for the initial UVA-induced inhibition of replication (Girard et al., 2008), which may explain the fact that the initial UVA-induced inhibition of replication occurs to a similar level in XP30RO and TR30-2 cells. However further investigation into the mechanism of UVA-induced inhibition of DNA replication is required.

Consistent with delayed recovery of UVA-induced inhibition of replication in XP30RO cells, Chk1 is strongly phosphorylated in XP30RO cells following UVA exposure. However, strong Chk1 phosphorylation is sustained in XP30RO cells up to 48 hr following UVA irradiation, after recovery from the initial UVA-induced inhibition of DNA replication occurs. This suggests that Chk1 plays a role independent of checkpoint activation under these conditions. It was recently reported that Chk1 is essential for resumption of replication in UVC-irradiated polη-deficient cells, and that under these conditions Chk1 plays a role in maintaining stalled replication fork stability (Despras et al., 2010). If not stabilised, stalled replication forks can collapse and lead to the formation of DNA strand breaks (Feng et al., 2011). Replication arrest in XPV cells is associated with DSB formation, as indirectly analysed by γH2AX foci formation (Limoli et al., 2002). Caffeine treatment, which reduced UVA-induced Chk1 phosphorylation, also increased the levels of γH2AX and phospho-RPA2-S4S8, indirect markers of DNA strand breaks, in UVA irradiated polη-deficient XP30RO cells. It should be noted that following UVC irradiation γH2AX focal distribution is different to that observed following IR (Cleaver, 2011). UVC-induced γH2AX foci are reported to occur at sites of NER, as well as stalled replication forks, and pan-nuclear γH2AX staining is associated with apoptosis induction (Cleaver, 2011), so interpretation of UVA-induced γH2AX as a marker of replication-induced DSBs was made cautiously. However, the data provides indirect evidence that Chk1 could play a role in maintaining replication fork stability following UVA-irradiation in XP30RO cells. More specific Chk1 inhibitors, or siRNA-mediated Chk1 knockdown, are required to definitively characterise the role for Chk1 in the response of polη-deficient cells to UVA irradiation. A similar reduction in UVA viability, following treatment of polη-deficient cells with another PIKK inhibitor wortmannin supports the role of caffeine as a PIKK inhibitor. Further studies are required to define the mechanistic basis of the caffeine-mediated UVA sensitivity in polη-deficient cells.

As mentioned above, polη-GFP localised to nuclear foci following UVA exposure. Consistent with the UVA-dependence of polη-GFP localisation to nuclear foci, the timing of polη-GFP localisation to foci following UVA was different to the observed localisation following UVC, with focal localisation occurring earlier following UVA than after UVC. Moreover, our analysis of polη-GFP recruitment to nuclear foci following UVC radiation is consistent with a previous report (Kannouche et al., 2001). Furthermore, polη-GFP was recruited to nuclear foci when cells were exposed to UVA irradiation through short-wavelength UV filters, providing evidence that polη-GFP localisation to nuclear foci observed following UVA exposure is not due to contaminating short-wavelength UV radiation. UVA-induced polη-GFP localisation to foci was observed to occur exclusively in replicating cells, supporting a role for polη in replication of UVA damaged DNA. In mock-treated cells, the small proportion of polη-GFP foci-positive cells were also replicating cells, suggesting a role for polη in DNA replication during unperturbed conditions. Supporting this, polη has been shown to play a role in maintaining fragile site stability in unperturbed cells (Rey et al., 2009).

Based on the data presented here, we propose that polη plays a role in the replication of UVA-damaged DNA. This work provides the first direct evidence that polη is mobilised in response to UVA radiation. While it is reasonable to suggest that the role of polη in the response to UVA is to carry out replication past UVA-induced CPDs, polη has also been shown to play a role in replication past other DNA lesions, including the 8-oxo-G lesions and clusters of oxidative lesions (Haracska et al., 2000b; Zlatanou et al., 2011), which are also induced by UVA (Greinert et al., 2012; Kielbassa et al., 1997). The identification of a role for polη in the replication of UVA-damaged DNA highlights the possible contribution of polη to preventing UVA-induced skin carcinogenesis, particularly in XPV patients, defective in polη.

3.4 Supplementary information

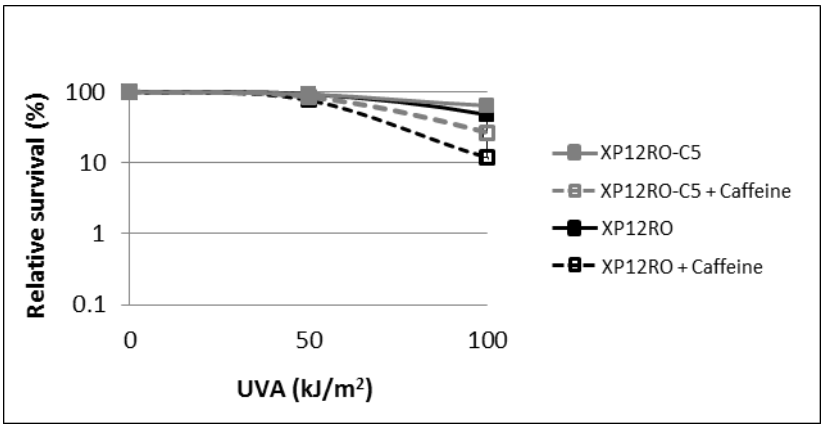

Supplementary Figure 3.9 Effect of caffeine on UVA survival of XPA-expressing and XPA-deficient cells. XP12RO and XP12RO-C5 cells were mock-treated or exposed to the indicated doses of UVA irradiation. Where indicated, 1 mM caffeine was added to the culture medium immediately following irradiation. 24 hr following irradiation, cells were trypsinised, re-seeded at 1 x 10^5 cells per 60 mm $Cell^+$ dish and incubated for 9 days. Where indicated, 1 mM caffeine was added to the medium following re-seeding and remained for the duration of the assay. Cells were fixed and stained in dimethylene blue solution and the number of colonies was scored. The survival of the irradiated cells is expressed as a percentage of the survival of the appropriate mock-treated control cells. The survival of irradiated and caffeine-treated cells is expressed as a percentage of the survival of mock-treated and caffeine-treated control cells. Data represents the average of three independent experiments; error bars represent one standard deviation. No statistical differences were found between UVA-irradiated and UVA-irradiated and caffeine-treated cells, as determined using one-way ANOVA.

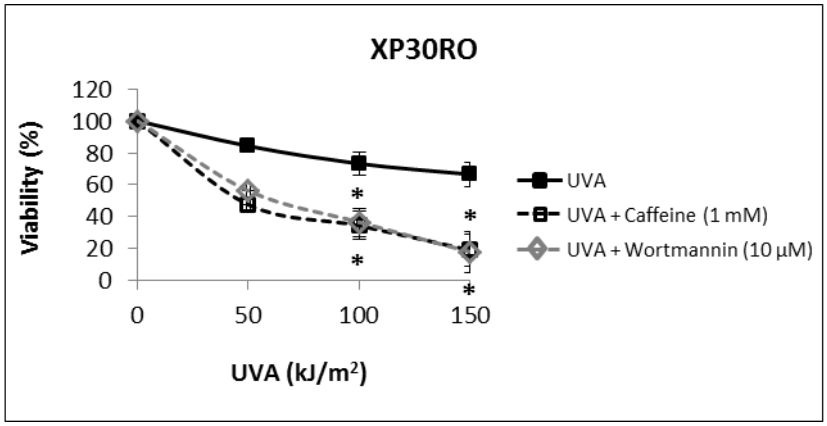

Supplementary Figure 3.10 Effect of wortmannin on UVA sensitivity of polη-deficient XP30RO cells. XP30RO cells were mock-treatment or exposed to the indicated doses of UVA-irradiation. 1 mM caffeine or 10 µM wortmannin was added to the medium immediately following UV-exposure and remained for the duration of the experiment. Cells were incubated for 48 hr and cell viability was assessed using the trypan blue dye-exclusion assay. The viability of UV-irradiated cells is expressed as a percentage of the viability of the appropriate mock-treated control cells. The viability of UV-irradiated and drug-treated cells is expressed as a percentage of the viability of the appropriate mock-treated and drug-treated control cells. Data represents the mean of three independent experiments; error bars represent one standard deviation. *$p<0.05$ represents statistical difference between UVA-irradiated and UVA-irradiated and drug-treated cells, as determined using one-way ANOVA.

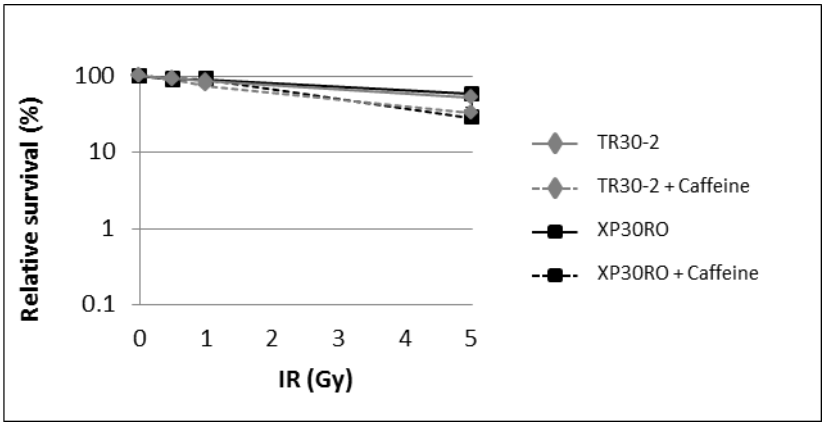

Supplementary Figure 3.11 Effect of polη-expression IR sensitivity. XP30RO and TR30-2 cells were mock-treated or exposed to the indicated doses of ionising radiation (IR). Where indicated, 1 mM caffeine was added to the culture medium immediately following irradiation. 24 hr following irradiation, cells were trypsinised, re-seeded at 1 x 10^5 cells per 60 mm $Cell^+$ dish and incubated for 9 days. Where indicated, 1 mM caffeine was added to the medium following re-seeding and remained for the duration of the assay. Cells were fixed and stained in dimethylene blue solution and the number of colonies was scored. The survival of the irradiated cells is expressed as a percentage of the survival of the appropriate mock-treated control cells. The survival of irradiated and caffeine-treated cells is expressed as a percentage of the survival of mock-treated and caffeine-treated control cells. Data represents the average of three independent experiments; error bars represent one standard deviation. No statistical differences were found between irradiated and irradiated and caffeine-treated cells, as determined using one-way ANOVA.

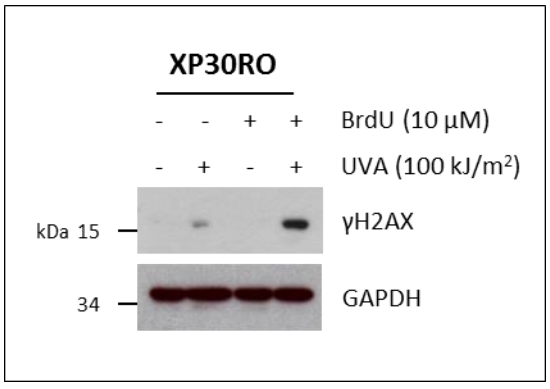

Supplementary Figure 3.12 Effect of BrdU on UVA-induced γH2AX. XP30RO were incubated, or not, with 10 µM BrdU for 1 hr prior to mock-treatment or exposure to 100 kJ/m^2 UVA radiation. Cell lysates were prepared immediately following irradiation. 20 µg of protein was separated by SDS-PAGE and the levels of γH2AX were analysed by western blotting. GAPDH was used as a loading control.

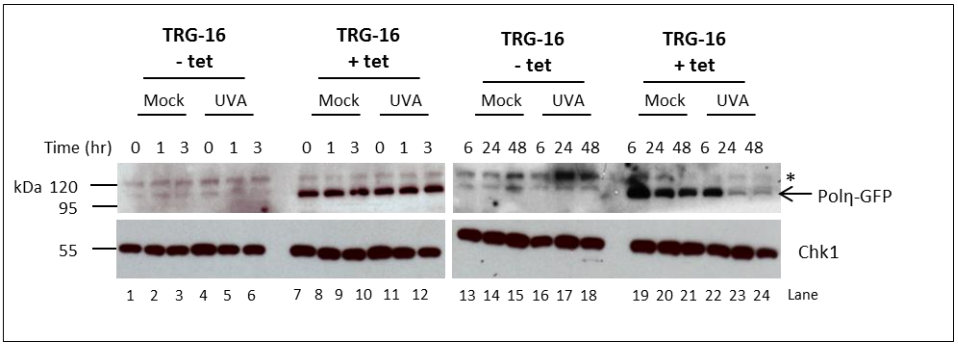

Supplementary Figure 3.13 Effect of UVA-radiation on polη-GFP expression in TRG-16 cells. TRG-16 cells were incubated, or not, with 0.1 µg/ml tetracycline (tet) or an equal volume of DMSO. Cells were mock-treated or exposed to 100 kJ/m^2 UVA radiation 24 hr following tet addition. Cells lysates were prepared at the indicated times following tetracycline addition. 20 µg of protein was separated by SDS-PAGE and polη expression was analysed by western blotting. Chk1 was used as a loading control. * non-specific band.

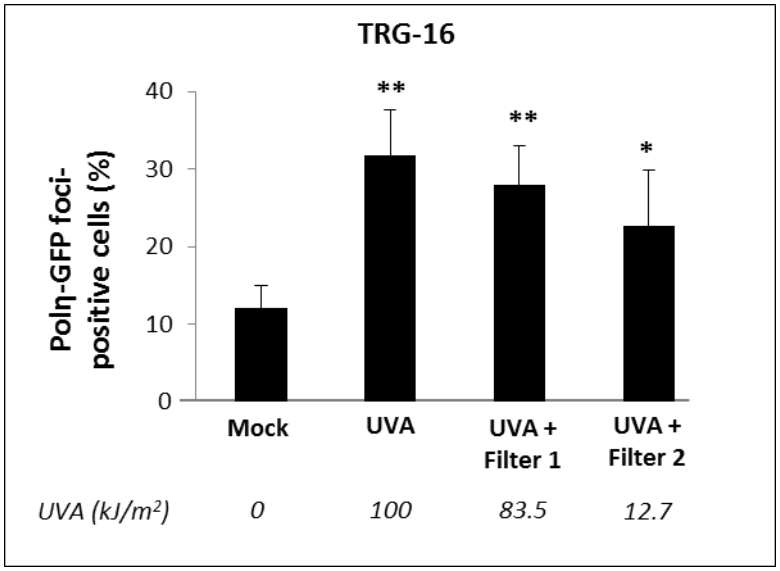

Supplementary Figure 3.14 Effect of short-wavelength UV filters on polη recruitment to nuclear foci following UVA irradiation. TRG-16 cells grown on glass coverslips, and incubated with 0.1 µg/ml tetracycline for 24 hr, to induce polη-GFP expression. Cells were mock-treatment or exposed UVA irradiation for an 80 min duration. Where indicated cells were exposed to UVA radiation through short-wavelength UV filters. Filter 1 blocks short-wavelength UV less than 315 nm, and filter 2 blocks the transmission of the majority of UV radiation less than 350 nm (Section 2.2.5). UV filters reduce the UV fluency reaching the cells (calculated in Table 2.8); the UVA dose received under each condition is shown in italics. 1 hr following UVA exposure cells were fixed in 4% PFA. DNA was stained with DAPI. Images were captured under 60X magnification using a DeltaVision fluorescence microscope. The percentage of polη-GFP expressing TRG-16 cells containing polη-GFP foci were scored. Cells with greater than eight polη-GFP foci were scored as polη-GFP foci-positive. At least 100 polη-GFP expressing cells were scored per condition. Data represents the average of three independent experiments; error bars represent one standard deviation. *$p<0.05$ and **$p<0.01$ represents statistical difference between mock-treated and UVA-irradiated cells, as determined using one-way ANOVA.

4 Results

The response of primary normal human epidermal melanocytes to long-wavelength UVA radiation

4.1 Characterisation of cultured primary normal human epidermal melanocytes (NHEM)

Primary neonatal normal human epidermal melanocytes (NHEM), isolated from a Caucasian male, were purchased from Lonza and routinely cultured in MGM-4 media (Lonza; Section 2.2.2.4).

4.1.1 Analysis of melanocyte-specific characteristics of NHEM

4.1.1.1 Analysis of TRP1 expression

The melanocytic-specificity of NHEM was characterised by Lonza (see Section 2.2.2.4). To independently characterise the melanocyte specificity of NHEM, the expression of the melanosome-specific protein tyrosinase-related protein 1 (TRP1) was analysed by western blotting and immunofluorescence (Yavuzer and Goding, 1994). TRP1 was detected by western blotting as a band of approximately 75 kDa in NHEM lysates, but was not detected in lysates from a normal fibroblast cell line (NFF; Figure 4.1A), consistent with the melanocytic lineage of NHEM.

The cellular localisation of TRP1 in NHEM was analysed by immunofluorescence using the same anti-TRP1 antibody and visualised using an Alexa Fluor® 594-conjugated secondary antibody. Anti-TRP1 stained melanosomes were observed as discrete organelles throughout the cell body of NHEM (Figure 4.1B (i-iii)). In the majority of NHEM, an accumulation of TRP1-stained melanosomes was observed at the extranuclear periphery (Figure 4.1B). This may represent the endoplasmic reticulum and/or Golgi apparatus, the sites of melanosome biogenesis (Dell'Angelica, 2003). Consistent with TRP1 being exclusively expressed in melanocytes (Yavuzer and Goding, 1994), immunofluorescence staining of TRP1 was not detected in the normal fibroblast cell line, NFF (Figure 4.1B (iv)).

Anti-TRP1 stained protrusions were observed extending from NHEM cell bodies, in particular in UVA-irradiated cells (Figure 4.1B (ii-iii)). While the UVA-dependence of this effect was not investigated further here, these protrusions were similar in appearance to melanosome-containing

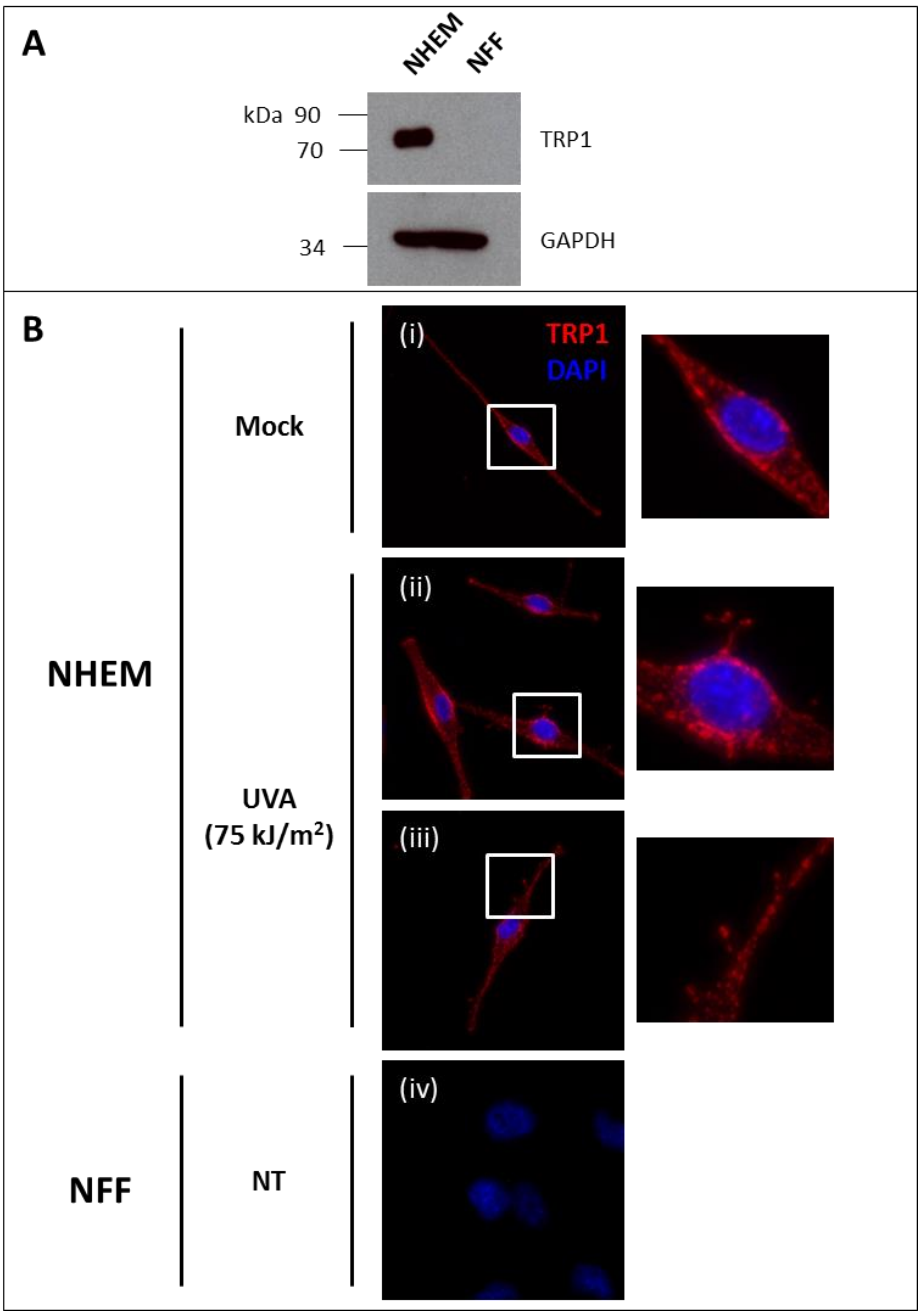

Figure 4.1 Analysis of TRP1 expression and localisation in NHEM. (A) Protein extracts (20 µg) from NHEM and NFF were separated by SDS-PAGE and analysed by western blotting for the expression of TRP1. GAPDH was used as a loading control. **(B)** NHEM were grown on collagen-coated coverslips, mock-treated or irradiated with 75 kJ/m^2 UVA and fixed in 4% PFA 6 hr post-irradiation **(i-iii)**. NFF were grown on glass coverslips. Cell were not treated (NT) and fixed in 4% PFA at 70% confluence **(iv)**. Immunofluorescence staining for TRP1 was performed as outlined in Section 2.2.16.5. Bound anti-TRP1 was detected using an Alexa Fluor® 594-conjugated secondary antibody. DNA was stained using DAPI. Images were captured at 60 X magnification using a Delta Vision fluorescence microscope. White boxes mark the area of the image shown at 3 times magnification on the right-hand side of the respective panels.

protrusions observed between melanocytes and keratinocytes in a melanocyte/keratinocyte co-culture system (Scott et al., 2002). These protrusions have been proposed to represent a mechanism of melanosome transfer between the two cell types (Scott et al., 2002).

4.1.1.2 Analysis of the melanin content

Melanin, the photoprotective pigment responsible for skin colour and tanning, is selectively synthesised in melanocytes (Abdel-Malek and Swope, 2011). The total melanin content of cultured NHEM was quantified using the spectrophotometric melanin assay as described in Section 2.2.19. This assay is based on the absorption of light by melanin at 475 nm, and does not differentiate between eumelanin and pheomelanin (Friedmann and Gilchrest, 1987; Smit et al., 2001). Using this assay the total melanin content of NHEM was determined to be 11.4 µg/10^6 cells (Figure 4.2B). This is similar to the total melanin content (9.8 µg/10^6 cells) previously reported in melanocytes from type I skin (Wenczl et al., 1998). The melanin content of the highly pigmented murine melanocyte cells (Section 2.2.1.2) was 10-fold higher than that of NHEM (Figure 4.2B). The non-pigmented fibroblast TR30-2 cell line also had a measurable absorbance at 475 nm, 2-fold lower than that of NHEM (Figure 4.2B). However the spectrophotometric assay used here does not control for the presence of other biomolecules which absorb at 475 nm.

A

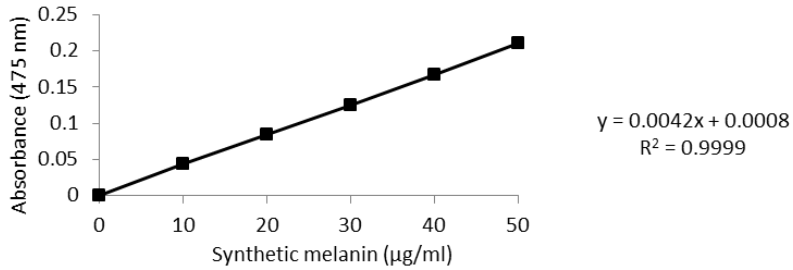

B

	Pigmentation	Absorbance (475 nm)	Melanin content (µg/10^6 cells)
NHEM	Light (Caucasian)	0.0487 ± 0.004	11.4 ± 1.1
Murine melanocyte	Dark	0.4690 ± 0.040	111.5 ± 9.6
TR30-2	Non-pigmented fibroblast	0.0242 ± 0.003	5.6 ± 0.7

Figure 4.2 Determination of the total melanin content of cells. (A) Standard curve of synthetic melanin absorbance at 475 nm. The equation of the linear trend line and R^2 statistic are shown. **(B)** The total melanin content of cells was measured as outlined in Section 2.2.19. Data represents the average of two experiments, ± one standard deviation.

4.1.2 Normal growth and cell cycle distribution

To determine the growth rate of NHEM, cells were seeded at a density of 8 x 10^4 cells per 35 mm dish. At 48 hr intervals, the cells were trypsinised, and the number of cells per dish were counted (Figure 4.3A). Following an initial lag phase of up to approximately 48 hr post-seeding, the doubling time of NHEM in culture was calculated to be approximately 96 hr (Figure 4.3A). This is similar to the doubling time of 4-5 days previously reported for cultured primary human melanocytes (Devi et al., 2009; Im et al., 1992).

To further characterise the normal growth of NHEM in culture, cell cycle distribution was analysed (Figure 4.3B). NHEM were cultured on 35 mm dishes and fixed in ethanol at 24 hr intervals. DNA was stained with PI, and the cell cycle distribution was analysed by flow cytometry (Figure 4.3B). 48 hr post-seeding the majority of NHEM (75%) were in G1 (Figure 4.3C). At 72 hr post-seeding the percentage of S phase cells increased by 14% compared to 48 hr (Figure 4.3C). This was coupled with a decreased in the percentage of cells in G1 (Figure 4.3C). By 96 and 120 hr post-seeding the percentage of S-phase cells was decreased to 8.9% and 6.4%, respectively

(Figure 4.3C). This was coupled with an increase in the percentage cells in G2/M-phase (Figure 4.3C). The cell cycle distribution at 144 hr is similar to that at 48 hr, with the majority of cells being in G1-phase (Figure 4.3C). This is consistent with the doubling time of approximately 96 hr calculated from the growth rate analysis (Figure 4.3A).

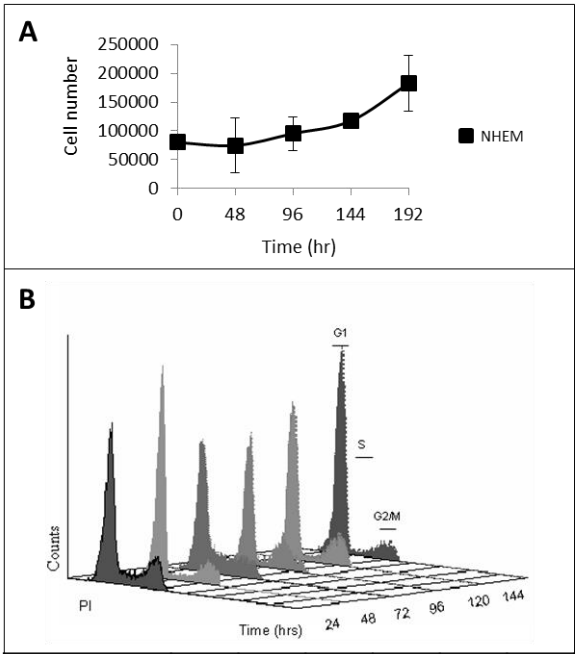

C	Time (hr)	24	48	72	96	120	144
% cells	G1	61.2	75.3	58.4	66.3	69.7	79.9
	S	23.1	11.8	25.6	8.9	6.4	8.0
	G2/M	15.6	12.8	15.9	24.7	23.9	11.9

Figure 4.3 Normal growth and cell cycle distribution of cultured NHEM. (A) NHEM were seeded at 8 x 10^4 cells per 35 mm dish. Fresh media was added every 48 hr. At 48 hr intervals cells were trypsinised and counted. The total number of cells per dish was calculated. Samples were analysed in duplicate. Data represents the mean of three independent experiments; error bars represent one standard deviation. **(B)** NHEM were cultured as outlined in (A), and fixed in 70% ethanol at 24 hr intervals. Cells were stained with PI and cell cycle distribution was analysed by flow cytometry. Representative graphs of PI staining versus cell counts are shown. **(C)** Quantitation of cell cycle distribution as shown in (B), presented in tabular form. Data is generated from one experiment.

4.1.3 Optimisation of UVA-irradiation conditions for NHEM

Calcium is reported to play an essential role in melanocyte homeostasis, including maintaining melanocyte morphology and attachment, as well as in

cellular signalling and melanogenesis (Carsberg et al., 1995; Cook et al., 2003; Tang et al., 1994; Wicks et al., 2011). UVA irradiation conditions were optimised by first testing the effect of calcium on the morphology of mock-treated and UVA-irradiated NHEM (Figure 4.4). UVA irradiation was carried out in PBS in the presence or absence of 50 µM $CaCl_2$, a concentration equal to that in the normal MGM-4 culture medium. Overall $CaCl_2$ addition protected against the morphological changes observed when cells were mock-treated in PBS alone (Figure 4.4). Based on this data all further UVA-irradiation experiments were carried out in PBS containing 50 µM $CaCl_2$.

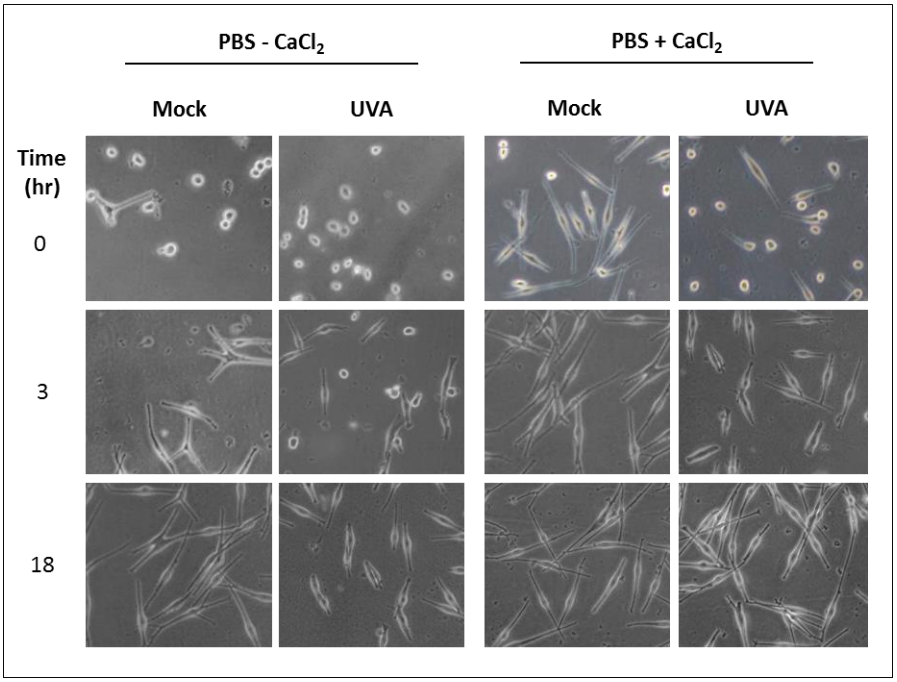

Figure 4.4 Effect of $CaCl_2$ on NHEM morphology following UVA exposure. NHEM were mock-treated or exposed to 75 kJ/m^2 UVA-irradiation in PBS or in PBS containing 50 µM $CaCl_2$. Phase contrast images of NHEM were taken at indicated times post-treatment under 60X magnification on an Olympus light microscope attached to an Olympus digital camera.

4.1.4 Sensitivity of NHEM to UVA-radiation

While the clonogenic cell survival assay is widely accepted as the standard method to measure cell survival and the ability of cells to divide following

exposure to a variety of toxic agents (Munshi et al., 2005), preliminary experiments in which NHEM were seeded at densities from 1 x 10^3 to 2.5 x 10^4 cells per 60 mm $Cell^+$-coated dishes (Sarstedt) and incubated for up to 21 days, revealed that following cell division, NHEM moved and spread apart, such that individual cells rather than colonies were present on the culture dishes. This spreading phenomenon by cultured primary human melanocytes was previously reported by Yohn et al. (1992). Thus, the clonogenic survival assay could not be utilised. Instead, the effect of UV-irradiation on NHEM viability, 48 hr following irradiation, was determined using the trypan blue dye-exclusion assay, as outlined in Section 2.2.9 (Figure 4.5). NHEM viability following UV-exposure was expressed as a percentage of the viable cells in the appropriate mock-treated controls (see Section 2.2.9.2). Overall, mock-treatment did not significantly affect cell viability. The average percentage of non-viable cells in mock-treated controls was 7.1% $\pm$ 4.1. For comparison, the viability of NHEM following UV-exposure was compared to that of TR30-2 cells, a SV40-transformed fibroblast cell line.

NHEM were relatively resistant to UVA radiation up to 75 kJ/m^2 UVA, where 97% of the cells remain viable (Figure 4.5A). At doses of 150 kJ/m^2 and 200 kJ/m^2 UVA, NHEM viability was reduced to 79% and 40%, respectively (Figure 4.5A). This is consistent with a previous report where the viability of primary human melanocytes was 80% following exposure to 150 kJ/m^2 UVA and 50% following exposure to 200 kJ/m^2 UVA (Yohn et al., 1992). No significant difference in cell viability was observed between NHEM and TR30-2 cells following exposure to UVA-radiation (Figure 4.5A). This is consistent with a previous report that the survival rate observed for primary human melanocytes and G361 melanoma cells was not significantly different following UVA-exposure (Kowalczuk et al., 2006).

The effect of UVB and UVC radiation on NHEM cell viability was also determined (Figure 4.5B and C). Overall, NHEM were found to be more resistant to UVB and UVC radiation than TR30-2 cells (Figure 4.5B and C). Following exposure to 50 J/m^2 UVB, NHEM viability was 97%, whereas

TR30-2 viability was <30% (Figure 4.5B). At UVB doses greater than 50 J/m^2, NHEM viability decreased in a dose-dependent manner, with 30% viable cells remaining following exposure to 200 J/m^2 UVB (Figure 4.5B).

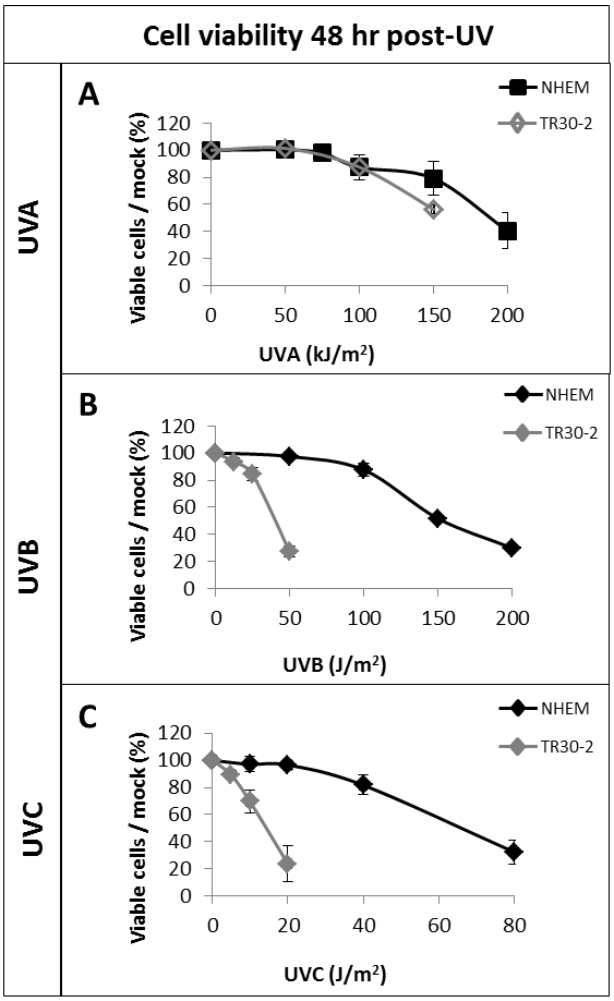

Figure 4.5 NHEM viability 48 hr following UV-irradiation. NHEM or TR30-2 cells were mock-treated or exposed to UVA **(A)**, UVB **(B)** or UVC **(C)** radiation. Cells were incubated for 48 hr and cell viability was assessed using the trypan blue dye-exclusion assay. Viable (transparent) and non-viable (blue) cells were scored; at least 100 cells were counted per condition. The percentage of viable cells in UV-irradiated samples was expressed as a percentage of the viable cells in the appropriate mock-treated control. Data represents the mean of at least three independent experiments; error bars represent one standard deviation.

Similarly, following exposure to 20 J/m^2 UVC, NHEM viability was 96%, whereas TR30-2 viability was only 20% at the same dose (Figure 4.5C). At UVC doses greater than 20 J/m^2, NHEM viability decreased in a dose-

dependent manner, with approximately 30% viability observed following exposure to 80 J/m^2 UVC (Figure 4.5). The relatively high resistance of NHEM to UVB and UVC compared to TR30-2 cells is consistent with a report that primary human melanocytes were more resistant to UVB and UVC irradiation than G361 melanoma cells (Kowalczuk et al., 2006).

4.1.5 Summary

Melanocytes are a specialised skin cell and are characterised by the ability to synthesise the photoprotective pigment melanin. Consistent with a melanocytic origin, NHEM expressed the melanosome specific protein TRP1 (Figure 4.1; Bhawan (1997)) and had a melanin content similar to that previously reported for Caucasian melanocytes (Figure 4.2; Wenczl et al. 1998).

The doubling time of NHEM in culture was approximately 96 hr, under the normal growth conditions used here (Figure 4.3A). From NHEM cell cycle distribution analysis, the highest proportion of cells in S phase was observed 72 hr following seeding on culture dishes (Figure 4.3C). Based on these observations, the experimental outline for treatment of NHEM was optimised as follows: following seeding, fresh media was added at 48 hr intervals. NHEM were treated with UVA-irradiation or other agents 72 hr post-seeding, where the highest proportion of S-phase cells was observed (Figure 4.3C). Based on morphological analysis (Figure 4.4), NHEM were mock-treated or exposed to UVA in PBS containing 50 µM $CaCl_2$, which protected mock-treated cells from morphological changes.

NHEM exhibited a dose-dependent decrease in viability following exposure to UVA radiation (Figure 4.5A). In the following experiments designed to characterise the molecular responses of NHEM to UVA radiation, most of the experiments were carried out at 75 kJ/m^2 UVA radiation where cell viability was 97% (Figure 4.5A). An important consideration when choosing the UVA dose at which to characterise NHEM responses was to choose a biologically relevant dose. 75 kJ/m^2 UVA-radiation is

approximately equivalent to 25 minutes of mid-day sun exposure in Paris (Kuluncsics et al., 1999).

4.2 Analysis of the effect of UVA radiation on cell cycle progression and DNA replication in NHEM

Exposure of cells to DNA damaging agents, such as UVC radiation, activates the DDR which can lead to cell cycle arrest (Cruet-Hennequart et al., 2006). Arrest of the cell cycle is proposed to allow time for the DNA repair machinery to repair damaged DNA (Elledge, 1996; Kaufmann and Paules, 1996). Since UVA irradiation induces DNA damage in the form of CPDs and 8-oxo-G (Cadet et al., 2009; Girard et al., 2011; Mouret et al., 2006; Perdiz et al., 2000), both of which have been identified in UVA-irradiated primary human melanocytes (Mouret et al., 2012), the effect of UVA-irradiation on NHEM cell cycle progression and DNA synthesis was investigated.

4.2.1 Analysis of the effect of UVA radiation in NHEM cell cycle distribution

NHEM cell cycle distribution was analysed as outlined in Section 2.2.10.2. Briefly, NHEM were mock-treated or exposed to 75 kJ/m^2 UVA-irradiation and fixed at the indicated times post-treatment. Cells were stained with PI and DNA content was analysed by flow cytometry. Overall, exposure to 75 kJ/m^2 UVA irradiation did not result in any significant difference in NHEM cell cycle distribution compared to mock-treated controls (Figure 4.6).

A time-dependent, but UVA-independent, decrease in the percentage of cells in S-phase was observed 24 hr post-treatment (Figure 4.6B, middle panel). 24 hr post-treatment corresponds to 96 hr post-seeding. Thus, the time-dependent decrease in S-phase population observed here (Figure 4.6B), is consistent with that observed 96 hr post-seeding when cell cycle progression was analysed under unperturbed conditions (Figure 4.3C).

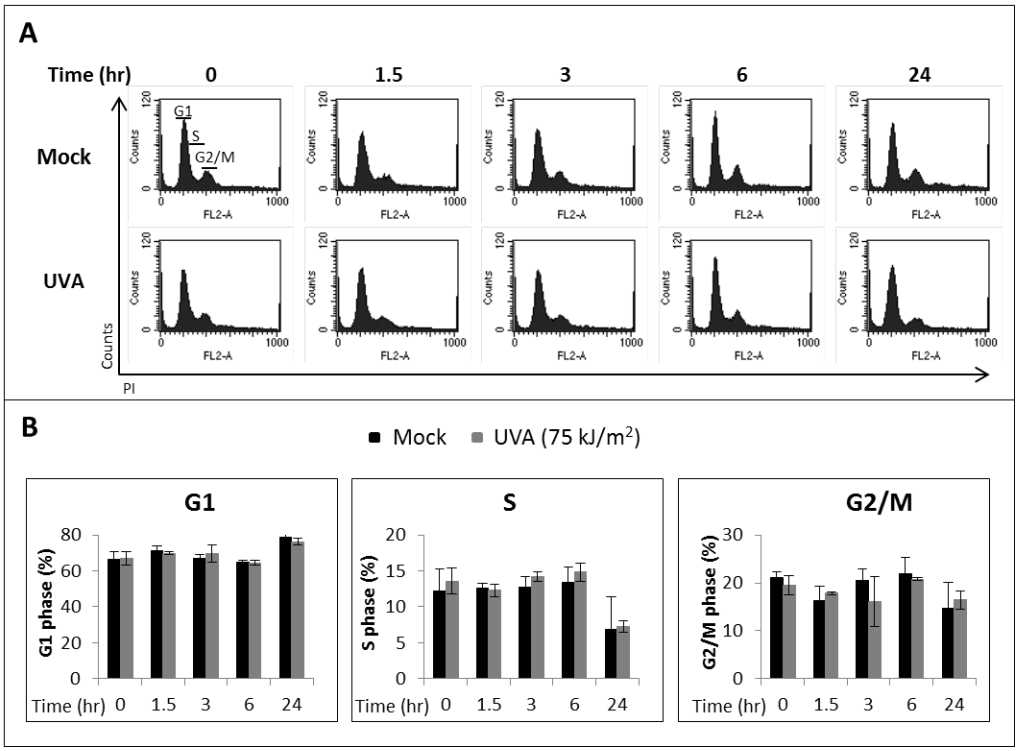

Figure 4.6 Effect of UVA radiation on NHEM cell cycle distribution. NHEM were mock-treated or exposed to 75 kJ/m^2 UVA-irradiation and fixed in 70% ethanol at the indicated times post-irradiation. Cellular DNA was stained with PI, samples were analysed using a FACS Calibur, and data was analysed using CellQuest software. **(A)** Representative histogram plots showing cell cycle distribution. **(B)** The percentage of cells in each cell cycle phase was calculated from the histograms in (A). Data represents the mean of at least four independent experiments; error bars represent one standard deviation.

4.2.2 Analysis of the effect of UVA radiation on DNA synthesis in NHEM

While cell cycle analysis using the PI staining method as described above (Section 4.2.1), provides information on the cell cycle phase distribution, it does not provide any information on the actual percentage of cells actively undergoing DNA synthesis. Here, the effect of UVA irradiation on DNA synthesis in NHEM was investigated using two independent techniques. Both approaches are based on the incorporation of nucleoside analogues that are subsequently detected using a fluorescent probe. Thus, the percentage of cells actively incorporating nucleoside analogues (ie. undergoing DNA replication) can be determined.

4.2.2.1 Effect of UVA radiation on BrdU incorporation

The effect of UVA radiation on BrdU incorporation was analysed by flow cytometry (Figure 4.7). NHEM were mock-treated or exposed to 75 kJ/m^2 UVA radiation. Cells were incubated with 10 µM BrdU for 1.5 hr, before fixing in 70% ethanol at the indicated times post-irradiation. BrdU incorporation was detected using a FITC-conjugated anti-BrdU antibody, DNA was stained with PI and cells were analysed by flow cytometry. BrdU positive cells were defined as having a FITC signal above a threshold value, set by staining cells that had not been incubated with BrdU with the FITC-conjugated anti-BrdU antibody (Figure 4.7A negative control). In the present experiments cells were not incubated with BrdU during the period of UVA-irradiation, since BrdU is a type I photosensitiser (Sugiyama et al., 1990) which when exposed to light, can lead to damage of both DNA and proteins (Cecchini et al., 2005; Manak et al., 1981).

Within 1.5 hr after UVA-irradiation, the percentage of BrdU-positive cells in UVA-irradiated NHEM was significantly lower than in the mock-treated controls, with a decrease from 19% to 12% observed (Figure 4.7B, *p=0.04). This is consistent with UVA-induced inhibition of DNA synthesis, as observed in XP30RO and TR30-2 cells (Figure 3.3), and previously in normal human fibroblasts (de Laat et al., 1996; Girard et al., 2008). Consistent with recovery from the initial UVA-induced inhibition of DNA synthesis, the percentage of BrdU-positive cells increased by 4% in UVA-irradiated samples, 3 hr post-irradiation (Figure 4.7B). No significant difference in the percentage of BrdU-positive cells between mock-treated and UVA-irradiated NHEM was observed 6 hr post-irradiation (Figure 4.7B). The percentage of BrdU-positive cells in the mock-treated samples did not change significantly over time up to 6 hr post-UV, with on average 18.5% $\pm$ 2.7 BrdU-positive cells detected (Figure 4.7B). Overall this data is consistent with a rapid and transient UVA-induced inhibition of DNA replication in NHEM.

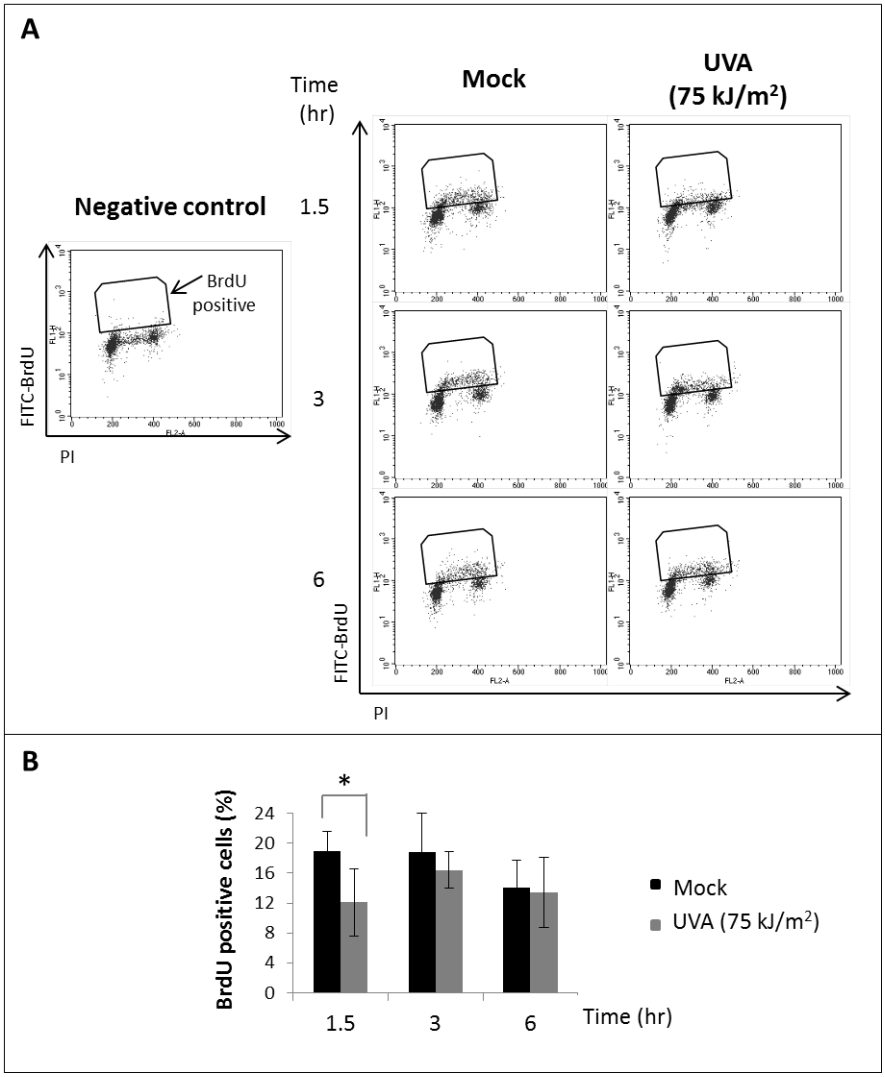

Figure 4.7 Effect of UVA radiation on BrdU incorporation in NHEM. NHEM were mock-treated or exposed to 75 kJ/m^2 UVA-irradiation. Cells were incubated with 10 µM BrdU for 1.5 hr prior to fixing in 70% ethanol at the indicated times post-irradiation. BrdU was labelled with a FITC-conjugated anti-BrdU antibody and DNA was stained with propidium iodide. Samples were analysed using a FACS Calibur, and data analysed using CellQuest software. **(A)** Dot plots are representative of four independent experiments. **(B)** The percentage of BrdU-positive cells as calculated from the dot plots shown in (A). Data represents the average of four independent experiments; error bars represent one standard deviation. * p=0.04, as determined using one-way ANOVA.

4.2.2.2 Effect of UVA radiation on EdU incorporation in NHEM

UVA irradiation induced rapid and transient inhibition of DNA synthesis in NHEM, as determined using the flow cytometry-based BrdU incorporation assay (Figure 4.7). While this assay is widely used in the field of cell cycle

analysis (Cruet-Hennequart et al., 2006; Girard et al., 2008; Runger et al., 2012), it is not without limitations, including the requirement for DNA denaturation, since the anti-BrdU antibody only recognises BrdU in single-stranded DNA. In the case of NHEM prolonged (1.5 hr) incubation with BrdU was required to generate sufficient signal for analysis (as determined from preliminary experiments), which limited the time points that could be examined. Thus, EdU incorporation was analysed by fluorescence microscopy, to independently confirm the effects of UVA radiation on DNA synthesis in NHEM (Figure 4.8).

The advantages of the EdU Click iT™ assay over the BrdU flow cytometry assay include: (i) the Click iT™ reaction used to label incorporated EdU does not require DNA denaturation, (ii) incubation of cells with EdU for 30 min is sufficient to detect incorporated EdU by this assay, thus providing a more concise snapshot of replication capacity, and (iii) the assay allows the quantification of EdU intensity in individual cells, thus providing information not only on the percentage of cells undergoing DNA synthesis but also the relative level of DNA synthesis in individual cells.

Analysis of EdU incorporation by fluorescence microscopy showed rapid UVA-induced inhibition of DNA synthesis in NHEM (Figure 4.8B). In the first 30 min after UVA exposure, the percentage of EdU-positive cells in NHEM was significantly lower than in mock-treated cells, with two-fold fewer EdU-positive cells in UVA-irradiated samples (Figure 4.8B). This is consistent with UVA-induced inhibition of DNA synthesis in NHEM observed in Figure 4.7. In the following 30 min, the percentage of EdU-positive cells in UVA-irradiated samples began to increase, but overall UVA-irradiated samples had fewer EdU-positive cells (Figure 4.8B). At 3 hr and 6 hr post-irradiation, there was no significant difference between the percentages of EdU-positive cells in mock-treated or UVA-irradiated samples (Figure 4.8B). This is consistent with flow cytometric data, showing that DNA replication had recovered to pre-irradiation levels by 3 hr post-UVA (Figure 4.7B).

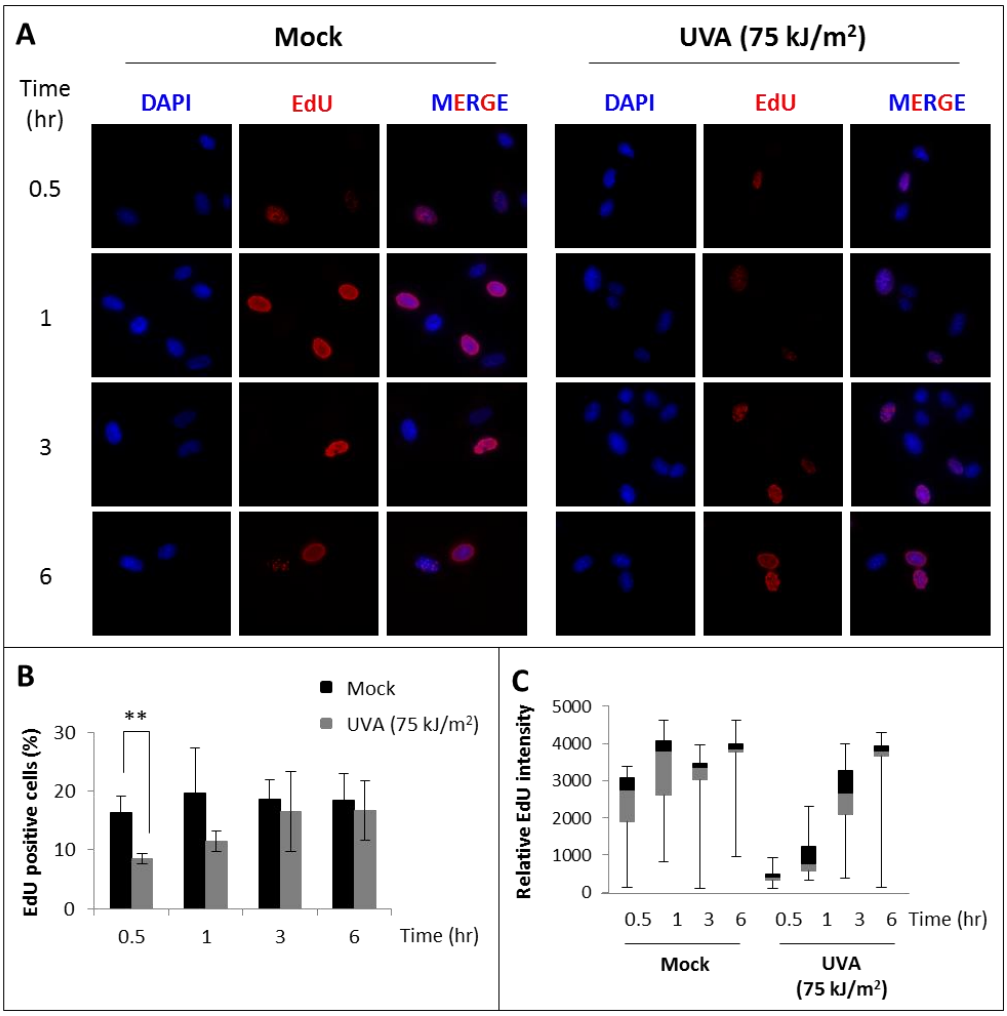

Figure 4.8 Effect of UVA in EdU incorporation in NHEM. NHEM were cultured on collagen-coated glass coverslips and mock-treated or exposed to 75 kJ/m^2 UVA-radiation. Cells were incubated with 10 µM EdU media for 30 min, prior to fixing in 4% PFA at the indicated times post-irradiation. EdU was stained using the EdU Alexa Fluor® 594 Click iT® kit (Invitrogen). DNA was stained using DAPI and cells were mounted in SlowFade. Images were captured using the 60X objective on a DeltaVision fluorescence microscope. **(A)** Representative images of mock-treated or UVA-irradiated NHEM showing EdU incorporation. Images were captured under 60X magnification. **(B)** The percentage of EdU positive cells was scored manually. At least 100 cells were counted per condition. Data is representative of three independent experiments; error bars represent one standard deviation. ** p=0.01, as determined using one-way ANOVA. **(C)** The EdU fluorescence intensity of each nucleus was quantified as outlined in Section 2.2.16.7. Box-and-whisker plot shows the distribution of the EdU intensities for each sample. The middle of the boxes represents the median EdU intensity value. The top (black) and bottom (grey) boxes represent the 75th and 25th percentile, respectively. The ends of the whiskers represent the maximum and minimum EdU intensity values. Data derived from two independent experiments. At least 100 cells were scored per condition per experiment.

Along with the observed decrease in the percentage of EdU-positive cells in the first 30 min following UVA exposure (Figure 4.8B), the mean EdU intensity of UVA-irradiated cells was 7-fold lower than that of mock-treated cells (Figure 4.8C). Consistent with recovery from UVA-induced inhibition of DNA synthesis, by 3 hr post-irradiation the mean EdU intensity of UVA-irradiated cells had returned to approximately the same levels as that of mock-treated control cells (Figure 4.8C).

4.2.3 Summary

Exposure of NHEM to 75 kJ/m^2 UVA-irradiation did not affect overall cell cycle distribution over a 24 hr period (Figure 4.6). This is consistent with a previous report that UVB, but not UVA, induced cell cycle arrest in primary human fibroblasts (Runger et al., 2012). However, exposure of NHEM to 75 kJ/m^2 UVA-irradiation induced a rapid but transient inhibition of DNA replication, determined by two independent approaches (Figure 4.7 and Figure 4.8). There was a significant reduction in the percentage of NHEM undergoing DNA replication up to 1.5 hr post-UVA, with recovery from UVA-induced inhibition of DNA synthesis observed by 3 hr post-UVA (Figure 4.7B and Figure 4.8B). The rapid transient inhibition of DNA synthesis by UVA-radiation is consistent with previous reports that UVA induces inhibition of DNA synthesis in primary human fibroblasts (de Laat et al., 1996; Runger et al., 2012) and transformed human fibroblasts (Girard et al., 2008).

4.3 Characterisation UVA-induced DNA damage responses in NHEM

The DNA damage response (DDR), mediated in part by the PIK kinases, ATR and ATM, is activated in cells in response to DNA damage, and mediates DNA repair, inhibition of cell cycle progression in the presence of damage or activates cell death when damage is too severe (see Section 1.7). It is now well established that UVA induces DNA damage, including CPD and 8-oxo-G lesions, in a number of cell types including primary human melanocytes (Girard et al., 2011; Mouret et al., 2006; Mouret et al., 2012; Perdiz et al., 2000) However, the effects of UVA radiation on DDR

activation in primary human melanocytes has not been systematically investigated to date. Thus, the activation of ATR- and ATM-mediated DDR pathways was analysed in primary normal human epidermal melanocytes.

4.3.1 UVA-induced phosphorylation of cell cycle checkpoint proteins

The effect of UVA radiation on two major DNA damage-activated PIK kinases, ATR and ATM, in NHEM was analysed by investigating the phosphorylation status of key substrates by western blotting, using phospho-specific antibodies (Figure 4.9).

Exposure of NHEM to 75 kJ/m^2 UVA induced rapid phosphorylation of Chk1 on S345 and S317, two ATR phosphorylation sites (Liu et al., 2000; Zhao and Piwnica-Worms, 2001). UVA-induced phosphorylation of Chk1 on both S345 and S317 were transient events, and the extent of phosphorylation reduced to background levels 3 hr and 6 hr following irradiation, respectively (Figure 4.9). The level of total Chk1 did not vary over the time course examined here (Figure 4.9). The rapid transient phosphorylation of Chk1 on S345 and S317 correlates with the strong inhibition of DNA synthesis observed in UVA-irradiated NHEM (Figure 4.7 and Figure 4.8).

Chk2 was phosphorylated on T68 following exposure of NHEM to 75 kJ/m^2 UVA (Figure 4.9). Phosphorylation of Chk2 on T68 is a well-established ATM substrate (Matsuoka et al., 2000a). Like Chk1 phosphorylation, UVA-induced Chk2 phosphorylation on T68 was a rapid event. However in contrast to Chk1 phosphorylation, Chk2 phosphorylation was sustained up to 6 hr post-UVA (Figure 4.9).

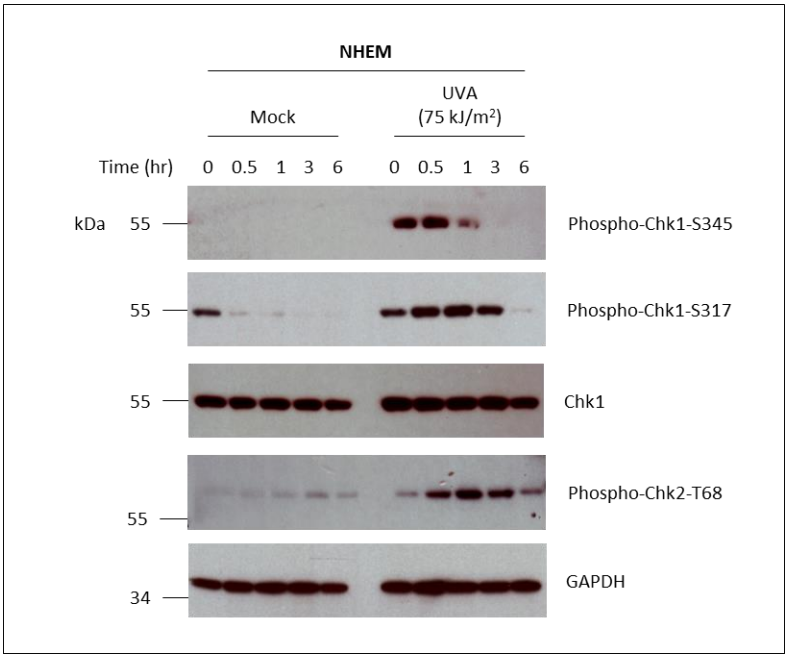

Figure 4.9 UVA-induced phosphorylation of checkpoint proteins in NHEM. NHEM were mock-treated or exposed to 75 kJ/m^2 UVA-radiation, and cell lysates were prepared at indicated times post-irradiation. 20 µg of protein was separated by SDS-PAGE. The phosphorylation status of Chk1 and Chk2 was analysed by western blotting using phospho-specific antibodies. The levels of total Chk1 were also analysed. GADPH was used as a loading control.

4.3.2 Characterisation of the role of Chk1 in the response of NHEM to UVA

Chk1 plays an important role in the DNA replication checkpoint (see Section 1.8.3.1 and Bartek et al., (2004), Branzei and Foiani, (2010)). Since UVA-induced Chk1 phosphorylation (Figure 4.9) correlates with UVA-induced inhibition of DNA synthesis (Figure 4.7 and Figure 4.8), the role of Chk1 in the response of NHEM to UVA radiation was further investigated.

To further analyse UVA-induced phosphorylation of Chk1, NHEM were exposed to increasing doses of UVA irradiation. Cell lysates were prepared 3 hr post-irradiation and the level of Chk1 phosphorylated on S317 was analysed by western blotting (Figure 4.10). These was a dose dependent increase in Chk1 phosphorylation on S317 following exposure to up to 150 kJ/m^2 UVA (Figure 4.10).

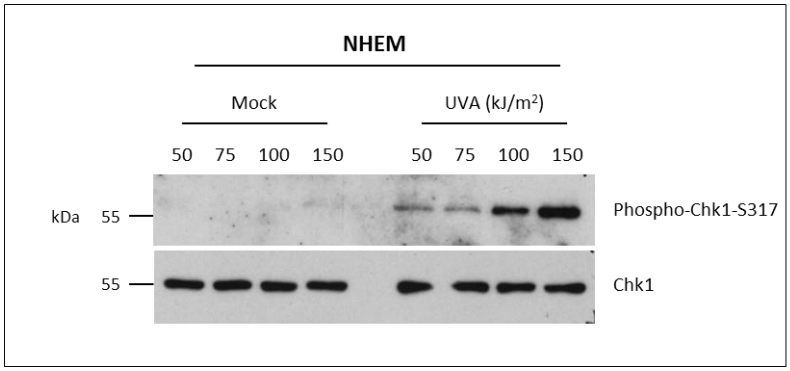

Figure 4.10 Dose-dependence of UVA-induced phosphorylation of Chk1. NHEM were mock-treated or exposed to 75 kJ/m^2 UVA-radiation, and cell lysates were prepared 3 hr post-irradiation. 20 µg of protein was separated by SDS-PAGE. The phosphorylation status of Chk1 on S317 was analysed by western blotting using a phospho-specific antibody. The levels of total Chk1 were also analysed.

Since UVA-induced rapid inhibition of DNA synthesis in NHEM, which is indicative of replication checkpoint activation, the role of Chk1 in UVA-induced inhibition of DNA replication was analysed. If Chk1 kinase plays a role in UVA-induced inhibition of DNA synthesis, then inhibition of Chk1 activity should affect this response. Chk1 kinase activity was inhibited using UCN-01 an established small molecule of Chk1 kinase (Busby et al., 2000; Graves et al., 2000). UCN-01 is widely used as a Chk1 inhibitor due to its 100-fold specificity for Chk1 over Chk2 (Busby et al., 2000), however, it should be noted that UCN-01 also inhibits PKC isoforms with an IC_{50} in the same nM range as Chk1 (Seynaeve et al., 1994). UVA-induced inhibition of DNA synthesis, as measured by a reduction in the percentage of BrdU-positive cells, was independent of UCN-01 treatment (Figure 4.11) This suggests that the observed initial UVA-induced inhibition of DNA synthesis was Chk1-independent. Consistent with this, siRNA-mediated Chk1 knockdown in transformed human fibroblasts did not prevent UVA-induced inhibition of DNA synthesis (Girard et al., 2008). DMSO-treated NHEM recovered from UVA-induced inhibition DNA synthesis by 6 hr post-irradiation as previously observed (Figure 4.7). However, UCN-01 treatment abrogated the recovery of BrdU incorporation in UVA-irradiated NHEM (Figure 4.11). This suggests that while Chk1 activity is not required

for the initial rapid inhibition of DNA synthesis after UVA, recovery of DNA replication following UVA-exposure is Chk1-dependent.

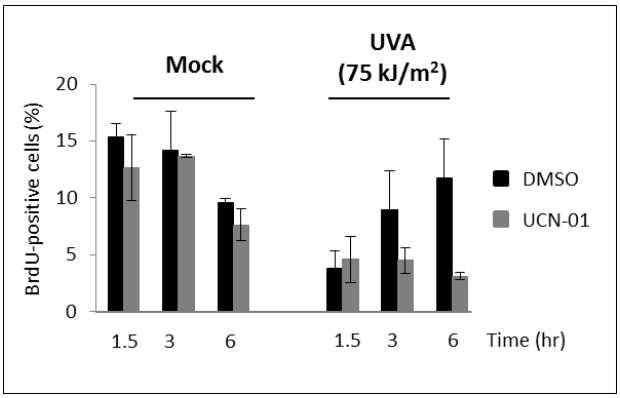

Figure 4.11 Effect of Chk1 kinase inhibition on UVA-induced decrease in DNA synthesis. NHEM were incubated with 100 nM UCN-01, or an equal volume of DMSO vehicle control, for 30 min prior to mock-treatment or exposure to 75 kJ/m^2 UVA radiation. Cells were incubated with 10 µM BrdU for 1.5 hr prior to fixing in 70% ethanol at the indicated times post-UVA. Incorporated BrdU was labelled with a FITC-conjugated anti-BrdU antibody and DNA was stained with propidium iodide. Samples were analysed using a FACS Calibur, and data analysed using CellQuest software. The percentage of BrdU-positive cells was quantified. Data represents the mean of two independent experiments; error bars represent one standard deviation.

Abrogation of DNA damage-induced checkpoint activation can result in cell death (Jackson et al., 2000; Ma et al., 2011). The effect of Chk1 inhibition on UVA viability of NHEM was analysed 48 hr following UVA irradiation using the trypan blue dye-exclusion assay (Figure 4.12). Two independent small molecule inhibitors of Chk1, UCN-01 and Chir-124, were utilised. Equimolar concentrations of UCN-01 and Chir-124 were previously shown to abrogate cell cycle checkpoints in response to topoisomerase poisons and enhance induced cell death in MDA breast cancer cells (Tse et al., 2007). Incubation of NHEM with 100 nM UCN-01 or 100 nM Chir-124 significantly reduced NHEM viability 48 hr following exposure to 75 kJ/m^2 UVA (Figure 4.12). UCN-01- or Chir-124-treatment alone did not have any significant effect on the viability of mock-treated cells (Figure 4.12). This

data suggests that Chk1 activity modulates NHEM survival following exposure to UVA irradiation.

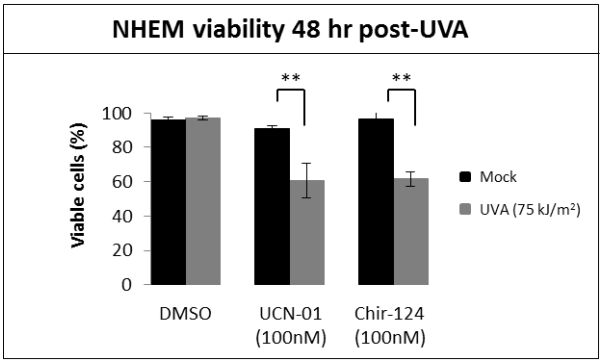

Figure 4.12 Effect of Chk1 kinase inhibition on the sensitivity of NHEM to UVA radiation. NHEM incubated with 100 nM UCN-01 or Chir-124 or an equal volume of DMSO vehicle control, for 30 min prior to irradiation. Cells were mock-treated or exposed to 75 kJ/m^2 UVA-irradiation. Media containing the drug was returned to cells immediately following irradiation and cells were incubated for 48 hr. Cell viability was determined using the trypan blue dye-exclusion assay. Viable (transparent) and non-viable (blue) cells were scored; at least 100 cells were counted per condition. The percentage viable cells was calculated as a percentage of the total cell count. Data represents the mean of four independent experiments for UCN-01 treated samples or two independent experiments for Chir-124 treated samples, error bars represent one standard deviation. ** $p<0.01$ as determined using one-way ANOVA.

4.3.3 Summary

The data presented here provides evidence that UVA induces activation of both the ATR-Chk1 and ATM-Chk2 pathways in NHEM (Figure 4.9). This is the first report of activation of these DDR pathways in primary human melanocytes following UVA-irradiation. The relationship between Chk1 activation and UVA-induced inhibition of DNA synthesis was investigated using small molecule inhibitors of Chk1. While Chk1 is not involved in the initial UVA-induced inhibition of DNA synthesis, Chk1 plays a role in the recovery from UVA induced inhibition of DNA synthesis. Furthermore, a role for Chk1 in modulating NHEM survival following exposure to UVA

was demonstrated. Overall, the data is consistent with an important role for Chk1 in the response of NHEM to UVA radiation.

4.4 Characterisation of the effect of Chk1 expression on the response of murine melanocytes to UVA radiation

In the previous section (Section 4.3.2) an important role for Chk1 in the response of NHEM to UVA-irradiation was identified. Manipulation of Chk1 activity using small molecule chemical inhibitors has the disadvantage of potential off-target effects (Seynaeve et al., 1994). Thus to independently assess the role of Chk1 in the response of melanocytes to UVA radiation, a murine melanocyte cell line, generated in the laboratory of Prof. D. Gillespie (Beatson Institute, Glasgow, UK), in which Chk1 expression can be abrogated in a 4-hydroxytamoxifen (4-OHT)-dependent manner, was utilised (see Section 2.2.1.2.2 and Figure 2.1). Murine melanocytes expressing or lacking Chk1 were then exposed to UVA radiation, and the effect of Chk1 status on cell viability, cell cycle distribution and apoptosis induction was determined.

4.4.1 Characterisation of 4-OHT-induced Chk1 knockdown in murine melanocytes

The efficiency of 4-OHT-mediated Chk1 knockdown in murine melanocytes was analysed by western blotting (Figure 4.13). Cells were treated with 1 mM 4-OHT, or an equal volume of ethanol vehicle control, at 24 hr intervals, as outlined in Figure 4.13A. Chk1 expression was analysed by western blotting, and the relative intensity of the Chk1 bands was calculated (Figure 4.13B). 48 hr following 4-OHT addition (T48), the level of Chk1 in the 4-OHT treated cells was 50% of that in the ethanol-treated control cells (Figure 4.13B; lane 5 vs 2). By T72, the level of Chk1 in the 4-OHT-treated cells was reduced to 10% of the level in the control cells (Figure 4.13B; lane 6 vs 3). Thus, efficient Chk1 knockdown could be achieved in the murine melanocytes by the addition of 4-OHT.

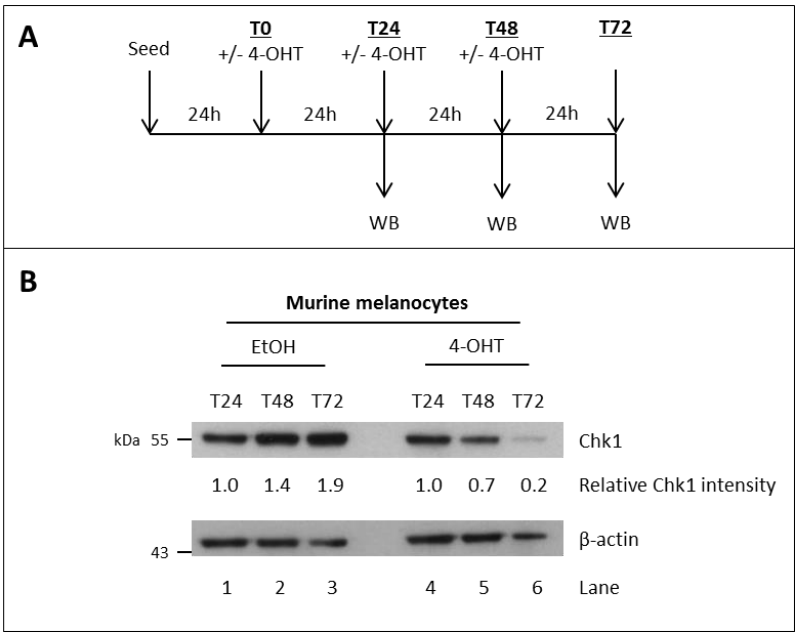

Figure 4.13 4-OHT induced Chk1 knockdown in murine melanocytes. (A) Experimental outline for optimisation of 4-OHT-mediated Chk1 knockdown in the murine melanocyte cell line. **(B)** Murine melanocytes were seeded at 3.5 x 10^6 cells per 60 mm dish. At 24 hr intervals, fresh media was added and cells were treated with 1mM 4-OHT, or an equal volume of ethanol, as vehicle control. Cell lysates were prepared at the indicated times. 20 µg of protein was separated by SDS-PAGE and Chk1 expression was analysed by western blotting. The relative intensity of Chk1 was determined. The intensity of each band was normalised to the intensity of the β-actin loading control. Relative band intensities are expressed as a proportion of the T24 ethanol-treated sample.

4.4.2 UVA-induced Chk1 phosphorylation in murine melanocytes

To determine if Chk1 is activated in murine melanocytes in response to UVA radiation, cells were mock-treated or exposed to 50 kJ/m^2 UVA irradiation and the phosphorylation status of Chk1 was analysed by western blotting using an antibody specific for Chk1 phosphorylated on S345, which is conserved between mouse and human (Figure 4.14). Chk1 phosphorylation on S345 was already detectable at the end of the irradiation period (Figure 4.14). By 3 hr post-UVA, phospho-Chk1-S345 levels had decreased to a level similar to mock-treated controls (Figure 4.14). The level of total Chk1 did not change significantly over time or with UVA exposure (Figure 4.14). Overall this data is consistent with data from NHEM (Figure

4.9), and shows that Chk1 phosphorylation occurs rapidly following UVA exposure, but the response is transient.

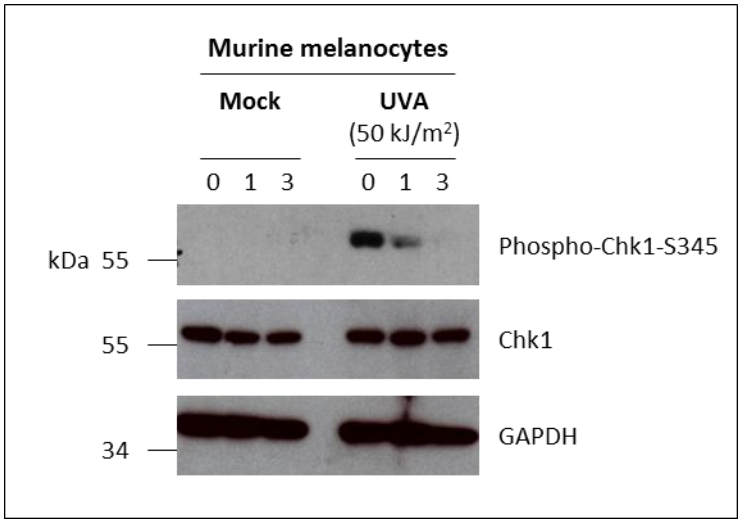

Figure 4.14 UVA-induced phosphorylation of Chk1 in murine melanocytes. Murine melanocytes were seeded at 3.5 x 10^6 cells per 60 mm dish and cultured for 48 hr, fresh media added at 24 hr intervals. Cells were mock-treated or exposed to 50 kJ/m^2 UVA-radiation. Cell lysates were prepared at the indicated times post-treatment. 20 µg of protein was separated by SDS-PAGE and the levels of phospho-S345 Chk1 and total Chk1 were analysed by western blotting. GAPDH was used as a loading control.

4.4.3 Effect of Chk1 expression on murine melanocyte cell cycle following UVA

Since UVA induces Chk1 phosphorylation in murine melanocytes (Figure 4.14), the effect of 4-OHT-mediated Chk1 knockdown on cell cycle distribution in UVA-irradiated murine melanocytes was investigated (Figure 4.15). Exposure to UVA doses up to 100 kJ/m^2 had little effect on cell cycle distribution in ethanol-treated murine melanocytes (Figure 4.15). However, in 4-OHT treated cells, exposure to 50 kJ/m^2 UVA resulted in an approximately 3-fold increase in the percentage of sub-G1 cells, coupled with a decrease in the proportion of cells in G2/M phase (Figure 4.15B). Furthermore, exposure of 4-OHT-treated murine melanocytes to 100 kJ/m^2 resulted in a significant alteration in cell cycle distribution compared to mock-treated cells (Figure 4.15B). Specifically there was a 3-fold decrease

in the percentage of G1 cells, coupled with an increase in the percentage of S and G2/M phase cells, and an increase in cells with > 4n DNA content (Figure 4.15B). This data suggests that Chk1 regulates murine melanocyte cell cycle progression following exposure to UVA irradiation.

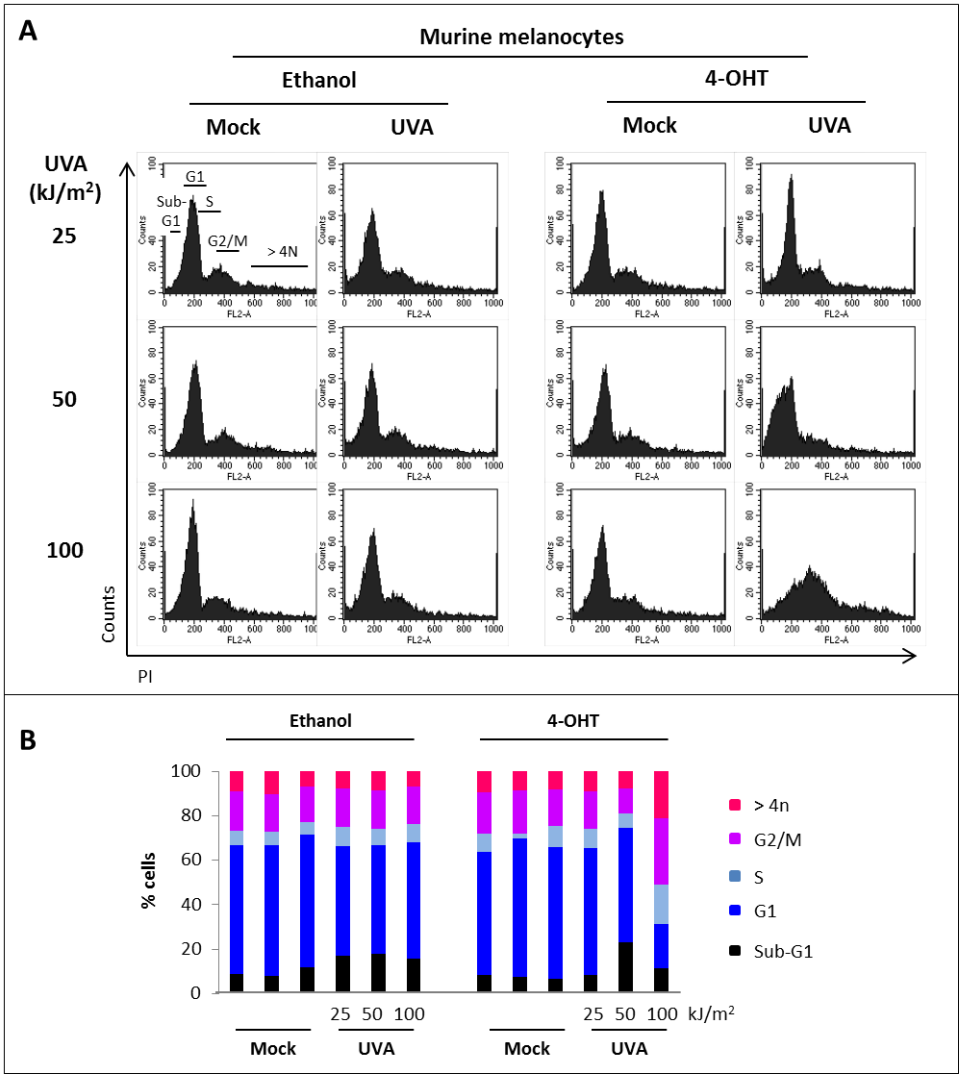

Figure 4.15 Effect of Chk1 expression on cell cycle progression in murine melanocyte following UVA exposure. Murine melanocytes were treated with 4-OHT (1 mM), or an equal volume of ethanol, at 24 hr intervals. 48 hr after the initial 4-OHT treatment, cells were mock-treated or exposed to the indicated doses of UVA irradiation. 24 hr post-irradiation cells were fixed in 70% ethanol. Cellular DNA was stained with PI, samples were analysed using a FACS Calibur, and data was analysed using CellQuest software. **(A)** Histogram plots showing cell cycle distribution are shown. **(B)** The percentage of cells in each cell cycle phase was calculated from the histograms in (A). Data is derived from one experiment.

4.4.4 Effect of Chk1 expression on survival of UVA irradiated murine melanocytes

Exposure of 4-OHT-treated murine melanocytes to UVA-irradiation lead to an increased in the percentage of sub-G1 cells (Figure 4.15B), indicative of cell death (Elmore, 2007). The effect of Chk1 expression on UVA survival of murine melanocytes was further analysed. In contrast to NHEM (Section 4.1.4), murine melanocytes efficiently formed colonies, with approximately 25% cloning efficiency observed from mock-treated cells (Table 4.1). However, following 4-OHT-mediated Chk1 knockdown, only about 2% of murine melanocytes form colonies (Table 4.1). The reduced cloning efficiency of Chk1-depleted murine melanocytes is consistent with Chk1 being essential for viability (Liu et al., 2000), and required for normal replication (Syljuåsen et al., 2005). Following exposure to 100 kJ/m^2 UVA-irradiation, the survival of Chk1-expressing murine melanocyte was approximately 34% of the mock-treated control cells (Table 4.1). This is approximately two-fold less than the UVA survival observed for normal transformed human fibroblasts (NFF; Figure 3.1C) and approximately equal to the UVA survival of XP30RO cells at this UVA dose (Figure 3.1C).

Table 4.1 Loss of Chk1 clonogenicity in Chk1-deficint murine melanocyte. Murine melanocytes were treated with 4-OHT, to induce Chk1 knockdown, or ethanol, vehicle control, at 24 hr intervals, up to 48 hr post-seeding. Cells were mock-treated or exposed to 100 kJ/m^2 UVA irradiation. Cells were incubated for 24 hr, and then trypsinised and re-seeded at a density of 1 x 10^3 cells per 60 mm Cell$^+$-coated dish. Cells were incubated for 9 days and colonies were then stained with coomassie blue and scored. Cloning efficiency is expressed as a percentage of the number of colonies counted relative to the number of cells seeded. Survival is expressed as a percentage of the colonies in UVA-irradiated relative to the appropriate mock-treated sample. Data represents the mean of two independent experiments, +/- one standard deviation.

	Murine melanocytes			
	Ethanol (+ Chk1)		**4-OHT (- Chk1)**	
	Mock	**UVA (100 kJ/m^2)**	**Mock**	**UVA (100 kJ/m^2)**
Cloning efficiency (%)	25.2 +/- 0.1	8.5 +/- 1.2	2.0 +/- 0.1	0
Survival (%)	100	33.9 +/- 4.6	100	0

As 4-OHT-treated murine melanocytes do not efficiently form colonies, the effect of Chk1 knockdown on UVA viability was assessed using PI-exclusion 48 hr following UVA-exposure (Figure 4.16). Due to the high pigmentation of the murine melanocyte cell line (Figure 4.2), the trypan blue dye-exclusion assay could not be utilised, as it was difficult to visually distinguish blue (non-viable) cells, among the black cell population. Thus, a flow cytometry-based PI-exclusion assay was utilised (see Section 2.2.10.1; Figure 4.16A). Murine melanocytes were treated as outlined in Figure 4.16A. Chk1 expression at the time of viability assessment (T96), was analysed by western blotting (Figure 4.16B). As outlined in Figure 4.13, 4-OHT-treatment reduced Chk1 levels; at T96 Chk1 expression in 4-OHT treated cells was below the detectable limits of the assay (Figure 4.16B).

In order to quantify cell viability using PI-exclusion assay, a threshold PI intensity value was set in the negative control, which contained cells that were not incubated with PI (Figure 4.16C, negative control). Cells with PI intensities below the threshold were defined as PI-negative and viable, while cells with intensities above the threshold were defined as PI-positive and non-viable (Figure 4.16C). Up to T96, 4-OHT treatment had no significant effect on the viability of murine melanocytes (Figure 4.16D). However, 4-OHT-treated murine melanocytes were significantly more sensitive to UVA-radiation at doses of 37.5 kJ/m^2 UVA and above (Figure 4.16D). Following exposure to 150 kJ/m^2 UVA the viability of 4-OHT-treated murine melanocytes was reduced by approximately 5-fold, compared to ethanol-treated cells (Figure 4.16D). This data is consistent with a role for Chk1 in the survival of murine melanocytes following UVA exposure. Overall, the sensitivity of murine melanocytes (ethanol-treated) 48 hr post-UVA is approximately equal to that observed for NHEM up to doses of 150 kJ/m^2 UVA (Figure 4.16D, Figure 4.5A).

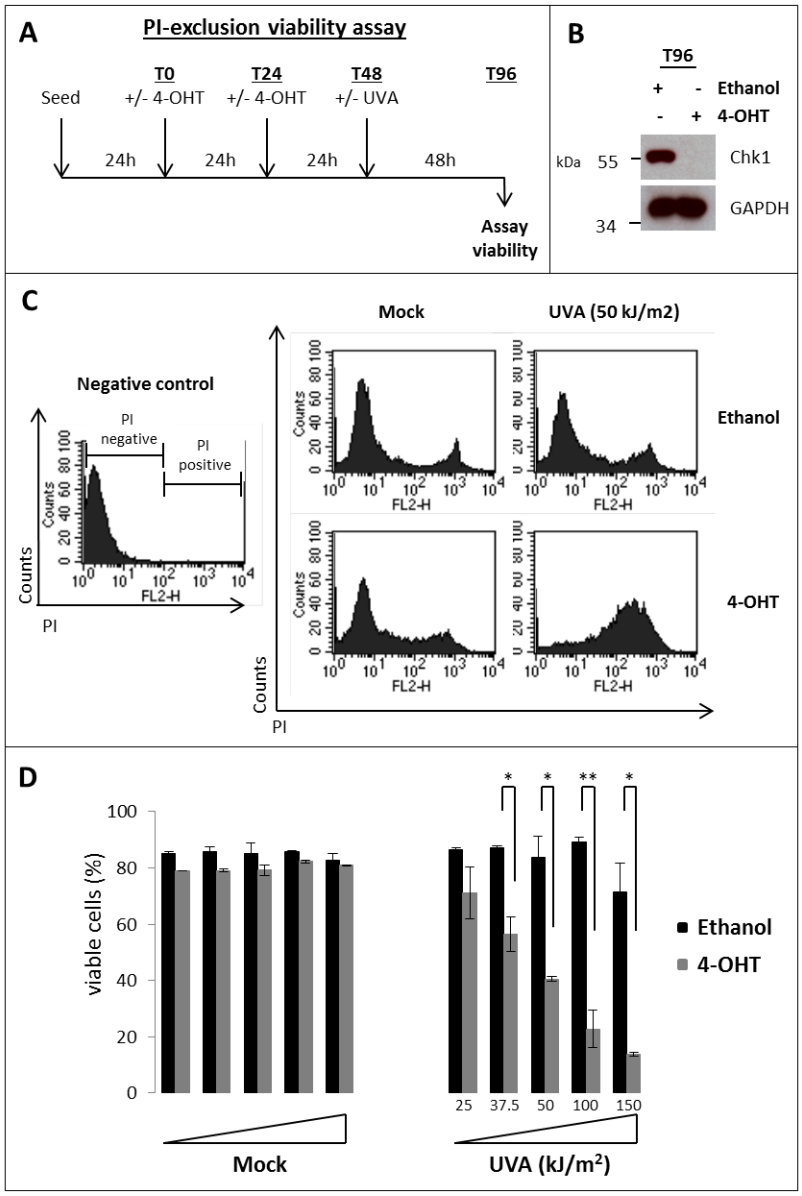

Figure 4.16 Effect of Chk1 expression in UVA-sensitivity of murine melanocytes. (A) Experimental outline. **(B)** Murine melanocytes were treated with 4-OHT (1 mM) or an equivalent volume of ethanol at 24 hr intervals as outlined in (A). Cell lysates were prepared at T96 and Chk1 was analysed using western blotting. GAPDH was used as a loading control. **(C)** Murine melanocytes were treated with 4-OHT, as outlined in (A). Cells were mock-treated or exposed to increasing doses of UVA radiation at T48. Cells were incubated for 48 hr post-UVA and cell viability was assessed using the flow cytometry-based PI-exclusion assay. Representative histograms showing PI intensity vs. cell number. The threshold intensity of PI-negative (viable) cells was set in the PI-negative control. Cells with a PI intensity above this threshold value were classed as PI-positive (non-viable). **(D)** The percentage of viable cells is expressed as a percentage of the total cell population analysed. Data represents the mean of three independent experiments; error bars represent one standard deviation. Statistical differences in viability between Chk1-expressing and Chk1-deficent cells are shown. * $p<0.05$ and ** $p<0.01$, as determined using one-way ANOVA.

To investigate the cell death pathway responsible for the reduction in viability observed following exposure of 4-OHT-treated murine melanocytes to UVA (Figure 4.16D), 4-OHT- or ethanol-treated cells were mock-treated or exposed to 37.5 kJ/m^2 UVA and cell lysates were analysed by western blotting for two well-established markers of apoptosis, the cleavage fragments of caspase-3 and Poly (ADP-ribose) polymerase (PARP) (Figure 4.17; Elmore (2007)).

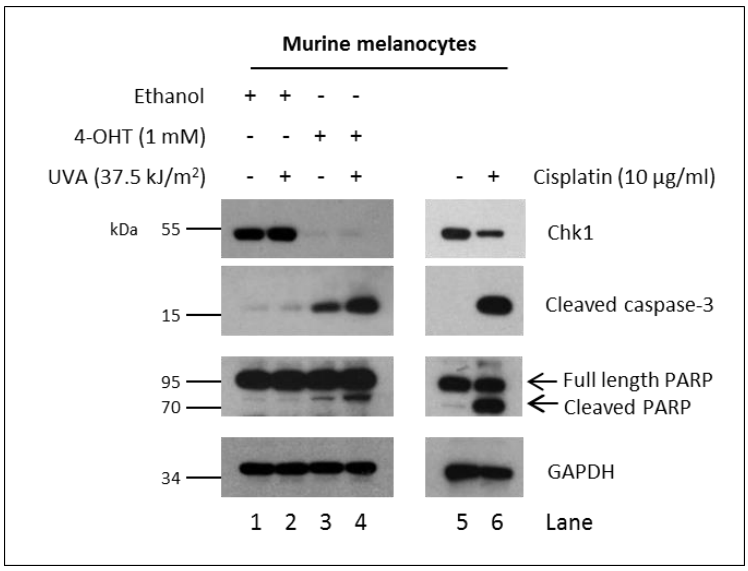

Figure 4.17 Effect of Chk1 down regulation on UVA-induced markers of apoptosis. Murine melanocytes were seeded at 3.5 x 10^6 cells per 60 mm dish and treated with 1 mM 4-OHT at 24 hr intervals to induce Chk1 down-regulation. Control cells were incubated with an equivalent volume of ethanol. Cells were mock-treated or exposed to 37.5 kJ/m^2 UVA irradiation, 72 hr post-seeding. 3 hr post-UVA cells, including floating cells, were harvested for western blotting. As a positive control for apoptosis, cells were also treated with 10 µg/ml cisplatin for 24 hr and the total cell population, including floating cells, was then harvested for western blotting. 20 µg of protein was separated by SDS-PAGE and analysed by western blotting. The 17 kDa cleavage fragment of caspase-3 was detected using an anti-cleaved caspase-3 antibody. Full length (116 kDa) PARP and the 89 kDa cleavage fragment were detected using an anti-PARP antibody. Chk1 levels were analysed using an anti-Chk1 antibody, and GAPDH was used as a loading control.

As a positive control for apoptosis induction, murine melanocytes were treated with 10 µg/ml cisplatin for 24 hr (Figure 4.17, lane 6). As previously observed (Figure 4.13B), 4-OHT-treatment reduced Chk1 expression in

murine melanocytes (Figure 4.17; upper panel; lanes 3 and 4). Exposure of 4-OHT-treated cells to 37.5 kJ/m^2 UVA-irradiation increased the levels of caspase-3 and PARP cleavage (Figure 4.17; lane 4), suggesting that in the absence of Chk1, UVA-induces apoptosis in murine melanocytes.

4.4.5 Summary

Consistent with observations in primary human melanocytes (Section 4.3.2), Chk1 is phosphorylated in murine melanocytes in response to UVA exposure (Figure 4.14). 4-OHT-mediated down-regulation of Chk1 in murine melanocytes, resulted in dysregulation of the cell cycle (Figure 4.15), a reduction in cell viability (Figure 4.16) and the induction of apoptotic markers (Figure 4.17), following exposure to UVA-radiation. This suggests that Chk1 plays an important role in modulating the response of murine melanocyte to UVA radiation. Thus, the murine melanocyte cell line, in which Chk1 expression can be conditionally down-regulated, represents a useful model in which to investigate the role of Chk1 in the response of melanocytes to UVA radiation.

4.5 Characterisation of ATM in UVA irradiated NHEM

Chk2 phosphorylation on T68 was observed in UVA-irradiated NHEM (Figure 4.6). Phosphorylation of Chk2 on T68 is a well-established ATM substrate site, readily induced in response to IR-induced DSBs (Matsuoka et al., 2000a). To investigate whether UVA radiation induces DSBs in NHEM, the induction of H2AX phosphorylation on S139 (γH2AX), a widely-used indirect marker of DSBs (Cleaver, 2011; Rogakou et al., 1999; Rogakou et al., 1998b), was investigated (Figure 4.18). As a positive control for DSB induction, NHEM were exposed to 10 Gy IR (Figure 4.18). IR-induced γH2AX was detected in discrete nuclear foci in the majority of NHEM immediately following IR exposure (Figure 4.18 A). γH2AX staining decreased over time, but staining was still detected in IR-irradiated NHEM at 6 hr post-IR (Figure 4.18 A). Consistent with the immunofluorescence data, γH2AX was detected by western blotting in extracts of IR-exposed NHEM (Figure 4.18B). In contrast, no significant induction of γH2AX was

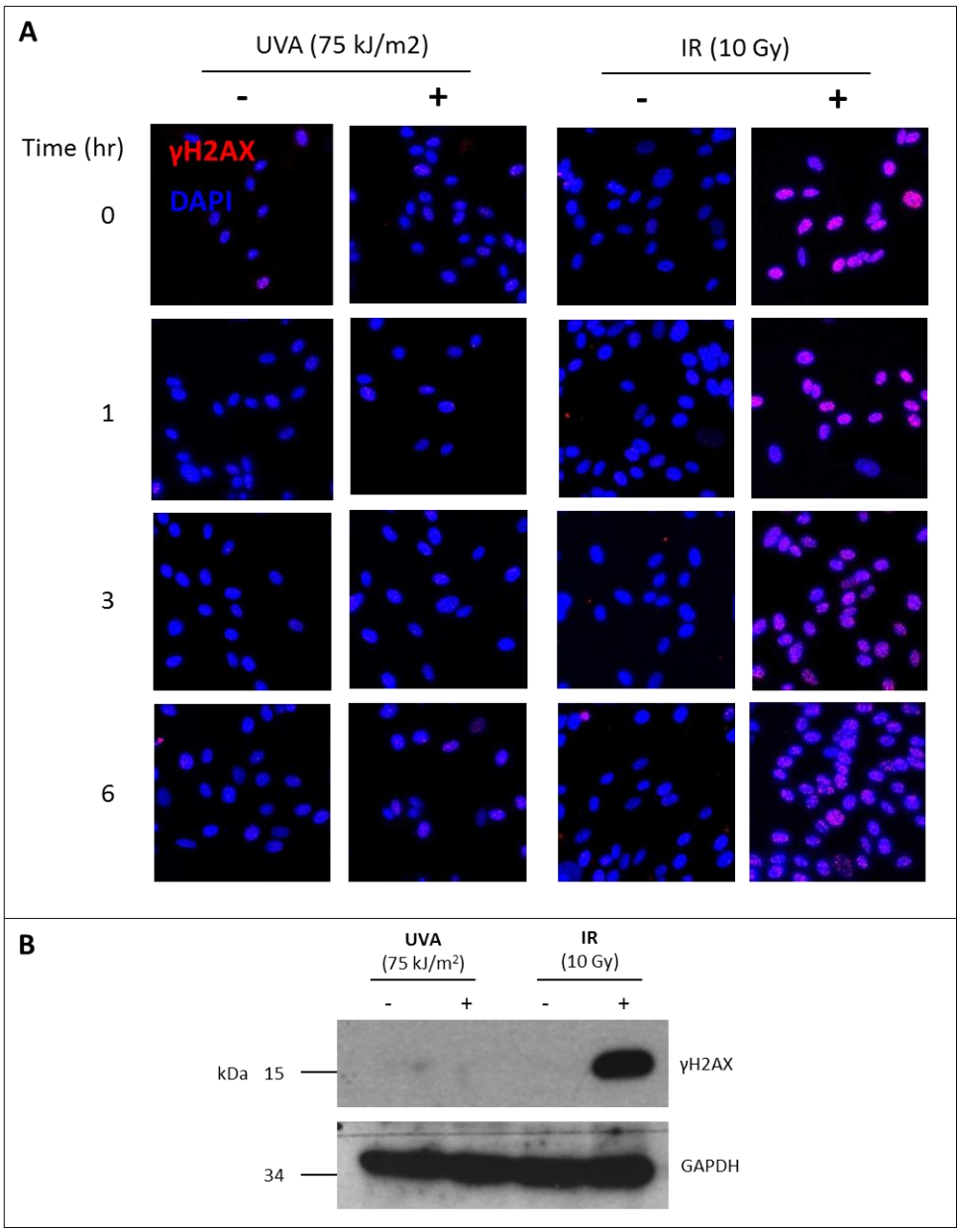

Figure 4.18 Effect of UVA exposure on γH2AX levels in NHEM (A) NHEM, cultured on collagen-coated glass coverslips, were mock-treated or exposed to 75 kJ/m^2 UVA-irradiation or to 10 Gy IR. Cells were fixed in 4% PFA, at the indicated times post-UVA or IR. Cells were incubated with an anti-γH2AX antibody, and bound antibody was detected using an Alexa Fluor® 594-conjugated secondary antibody. Cellular DNA was stained with DAPI. Cells were mounted in SlowFade and visualised using a DeltaVision fluorescence microscope. **(B)** NHEM were mock-treated or exposed to 75 kJ/m^2 UVA-irradiation or 10 Gy IR. Whole cell lysates were prepared 1 hr post-UVA or 30 min post-IR by scraping in RIPA lysis buffer and sonication was carried out, as outlined in Section 2.2.11. 20 µg of protein was separated by SDS-PAGE and γH2AX was analysed by western blotting. GAPDH was used as a loading control.

detected in UVA-exposed NHEM by immunofluorescence or western blotting over the time course examined (Figure 4.18A and B). This data is consistent with previous reports that UVA radiation does not induce significant DSBs in primary or transformed human fibroblasts (Girard et al., 2008; Rizzo et al., 2011).

Since phosphorylation of Chk2 on T68 is generally mediated by ATM, but UVA does not induce detectable DSBs (Figure 4.18), then the question arises as to what is the activating factor of ATM following UVA exposure of NHEM. As outlined in Section 1.7.3, ATM is activated in response to oxidative stress in a DSB-independent manner (Guo et al., 2010b). Using the DCF oxidative stress assay (outlined in Section 2.2.10.3), induction of oxidative stress following exposure to UVA radiation was assessed (Figure 4.19). DCF fluorescence intensity was increased in UVA-irradiated NHEM compared to mock-treated cells (Figure 4.19); supporting the conclusion that UVA induces oxidative stress in NHEM. This is consistent with UVA-induced oxidative stress in cultured human fibroblasts (Girard et al., 2008). As a control, NHEM were treated with *N*-acetyl-cysteine (NAC), a commonly used antioxidant (Girard et al., 2008). NAC reduced UVA-induced DCF fluorescent intensity to below the levels in mock-treated cells (Figure 4.19), consistent with the observed UVA-induced increase in DCF fluorescence intensity (Figure 4.19) resulting from oxidative stress. Induction of oxidative stress by UVA provides a possible mechanism for ATM activation in UVA-irradiated NHEM (Guo et al., 2010b), in the absence of detectable DSBs.

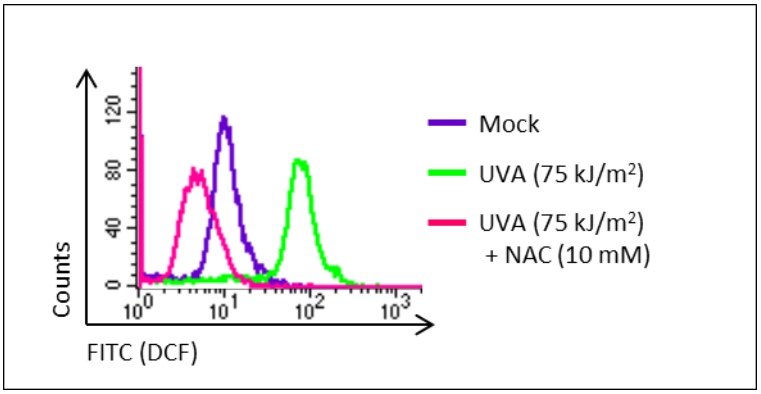

Figure 4.19 UVA radiation-induced ROS in NHEM. NHEM were incubated with 10 µM 2', 7'-dichlorofluroescein diacetate (DCFH-DA) for 30 min prior to mock-treatment or exposure to 75 kJ/m^2 UVA irradiation. Where indicated cells were also pre-incubated with 10 mM *N*-acetyl-cysteine (NAC). DCFH-DA and NAC were present in the PBS during irradiation. The previously removed media containing DCFH-DA and NAC was returned to the cells immediately post-UVA. Cells were incubated for 30 min before analysis using a FACS Calibur to determine the intensity of FITC (DCF) staining in each sample. Graph is representative of three independent experiments.

The expression of ATM protein in NHEM was analysed by western blotting (Figure 4.20A). Two bands of >250 kDa were detected using an anti-ATM antibody in NHEM extracts. These bands was not detected in extracts of GM05849 cells, an ATM-deficient fibroblast cell line, thus the bands were considered to represent ATM protein (Figure 4.20A). Melanocytes are a unique skin cell type, that develop in the neural crest and display morphological features typical of neuronal cells, including dendritic-like projections (see Section 1.5). While ATM is mainly localised in the nucleus of cycling cells, in neuronal cells, ATM is predominantly cytosolic (Barlow et al., 2000; Boehrs et al., 2007; Li et al., 2009). A proportion of ATM has also been found to localise to the cytosol in non-neuronal cells, where it interacts with peroxisomes, sites of oxidative metabolism (Watters et al., 1999). This suggests that different pools of ATM in various cellular locations could play diverse roles, independent of the DSB response. ATM was expressed in NHEM at a relatively high level compared to normal transformed fibroblasts (NFF), and comparable to the levels observed in the human neuronal-like neuroblastoma cell line, SH-SY5Y (Figure 4.20A).

However, when the cellular localisation of ATM in NHEM was analysed by immunofluorescence (Figure 4.20B). ATM was found to be localised predominantly in the nucleus of NHEM cells (Figure 4.20B). Consistent with a previous report (Boehrs et al., 2007), ATM was detected in the cytosol of SH-SY5Y cells (Figure 4.20B; lower panel). Moreover, no significant relocalisation of ATM was observed 1 hr following exposure of NHEM to 75 kJ/m^2 UVA (Figure 4.20C).

Phosphorylation of ATM on S1981 is a widely used marker of ATM activation, and is detected following treatment of cells with either IR or hydrogen peroxide, which induce DSBs and oxidative stress, respectively (Bakkenist and Kastan, 2003; Guo et al., 2010b). Phosphorylation of ATM on S1981 following exposure of NHEM to UVA and IR was investigated by immunofluorescence using an anti-phospho-ATM S1981 antibody (Figure 4.21A). While phospho-ATM S1981 was detected in discrete nuclear foci following exposure of NHEM to 10 Gy IR (Figure 4.21A (iv)), no significant induction of phospho-ATM S1981 was observed following exposure to 75 kJ/m^2 UVA (Figure 4.21A (ii)). The ATM-deficient fibroblast cell line, GM05849 (Murnane et al., 1985), was used as a negative control for antibody specificity (Figure 4.21A (v)). This data suggests that phosphorylation of ATM on S1981 is not induced in NHEM following UVA exposure, but can be induced following IR exposure. However, it cannot be ruled out that UVA-induced phosphorylation of ATM on S1981 occurs but is not detectable by the phospho-specific antibody under these conditions. For example, the presence of ATM binding partners, or other post-translational modifications on ATM could interfere with antibody binding to the anti-phospho-ATM S1981 epitope.

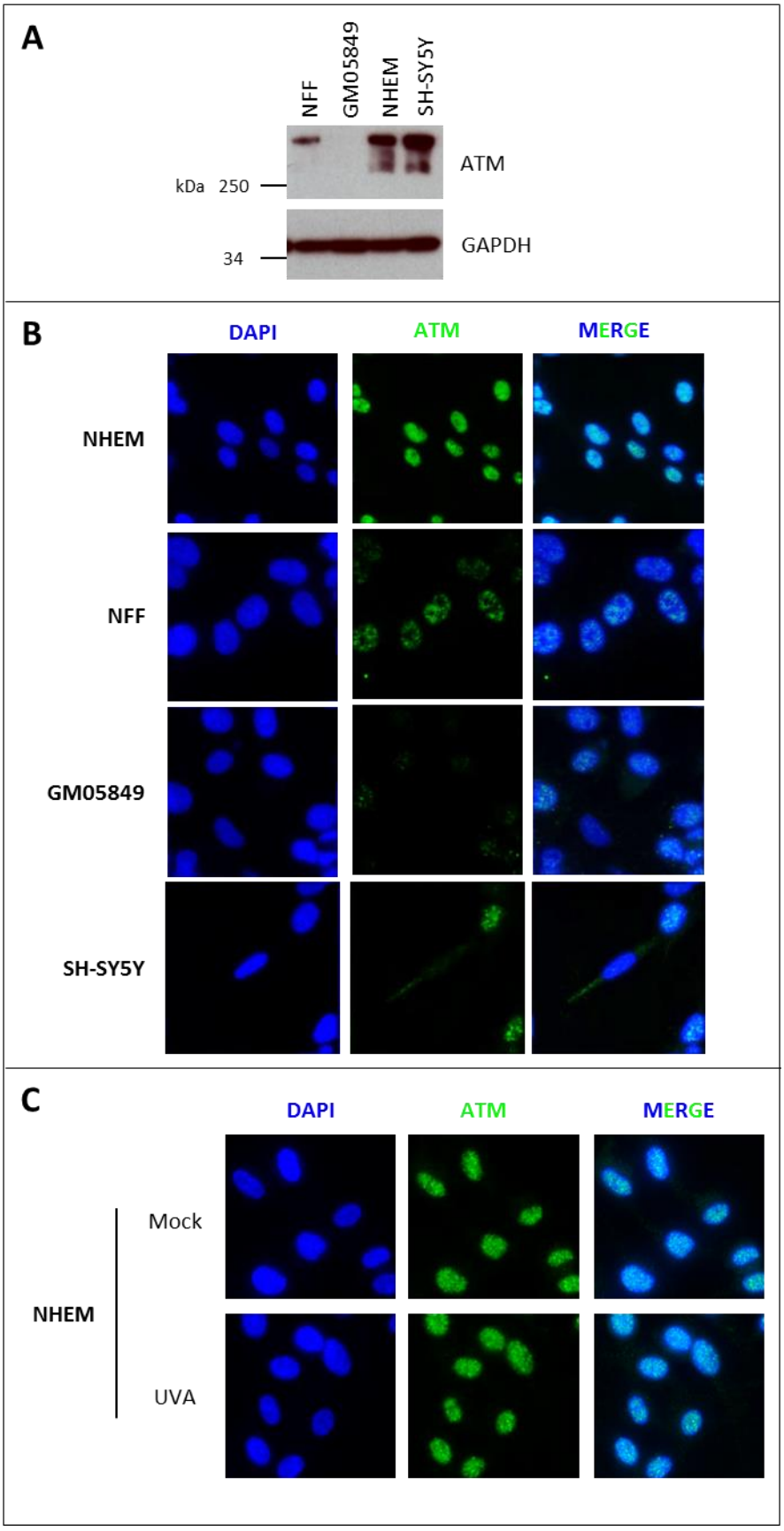
A
NFF
GM05849
NHEM
SH-SY5Y
kDa 250
ATM
34
GAPDH
B
DAPI
ATM
MERGE
NHEM
NFF
GM05849
SH-SY5Y
C
DAPI
ATM
MERGE
NHEM
Mock
UVA

Figure 4.20 (on previous page) Expression and cellular localisation of ATM in NHEM. (A) Cell lysates were prepared from cultures of NFF, GM05849, NHEM and SH-SY5Y cells, at approximately 70% confluence. 20 µg of protein from each cell lysate was separated by SDS-PAGE, and analysed by western blotting using anti-ATM (Millipore) and anti-GAPDH antibodies, respectively. **(B)** NHEM and SH-SY5Y cells were cultured on collagen-coated glass coverslips. NFF and GM05849 cells were cultured on glass coverslips. Cells were fixed in 4% PFA at 70% confluence. Cells were stained using an anti-ATM (Millipore) antibody and bound antibody was detected using an Alexa Fluor® 488-conjugated secondary antibody. DNA was stained using DAPI. Cells were mounted in SlowFade and visualised using a DeltaVision fluorescence microscope. **(C)** NHEM were cultured on collagen-coated glass coverslips and mock-treated or exposed to 75 kJ/m^2 UVA irradiation. Cells were fixed in 4% PFA, 1 hr post-UVA and processed for immunofluorescence analysis as outlined in (A).

Phosphorylation of ATM on S1981 was also analysed by western blotting (Figure 4.21B). Consistent with the above immunofluorescence data (Figure 4.21A), phospho-ATM S1981 was not detected in extracts of UVA-irradiated NHEM (Figure 4.21B, lane 2). As a positive control for ATM phosphorylation on S1981, XP30RO cells were exposed to 10 Gy IR. Phospho-ATM S1981 levels were increased in IR-exposed XP30RO cells, indicating that this form of ATM can be detected by western blotting under these conditions (Figure 4.21B; lane 4). Interestingly, the overall levels of ATM were increased in NHEM following UVA-irradiation (Figure 4.21B; lane 2 vs. 1), and in IR irradiated XP30RO cells (Figure 4.21B; right panel).

Furthermore, using the anti-ATM antibody, a slower mobility form of ATM was detected in extracts of UVA-irradiated NHEM (Figure 4.21B; * lane 2), and following IR-exposure of XP30RO (Figure 4.21B; * lane 4). The gel migration of slow mobility form of ATM protein (Figure 4.21B; *), corresponded to that observed for phospho-ATM S1981 detected in XP30RO cell extracts, by alignment of the molecular weight markers on the films (Figure 4.21B). This data suggests that ATM levels are modulated in NHEM in response to UVA irradiation, and that a modified slow mobility form of the protein is induced.

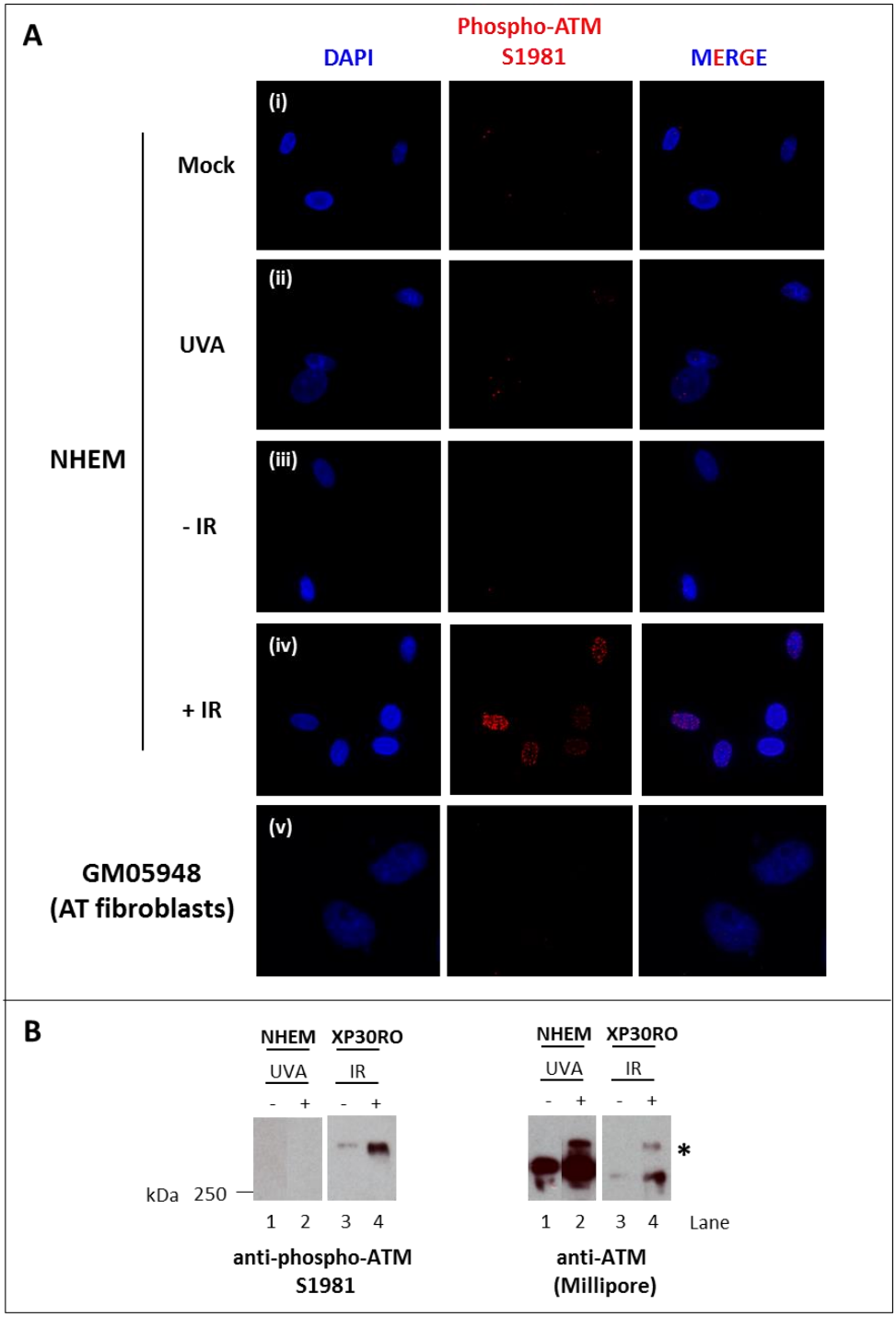

Figure 4.21 ATM phosphorylation on S1981 in NHEM. (A) (i-iv) NHEM cultured on collagen-coated glass coverslips were mock-treated or exposed to 75 kJ/m^2 UVA-irradiation or 10 Gy IR. Cells were fixed 1 hr post-UVA or 30 min post-IR in 4% PFA. **(v)** GM05849 (AT fibroblasts), cultured on glass coverslips, were fixed at 70% confluence in 4% PFA. Cells were incubated with an anti-phospho-ATM S1981 antibody and bound antibody was detected using an Alexa Fluor® 594-conjugated secondary antibody. Cellular DNA was stained with DAPI. Coverslips were mounted in SlowFade and visualised using a DeltaVision fluorescence microscope. **(B)** NHEM were mock-treated or exposed to 75 kJ/m^2 UVA-irradiation.

XP30RO cells were mock-treated or exposed to 10 Gy IR. Cell lysates were prepared 30 min post-irradiation. 20 µg of protein was separated on an 8% SDS-PAGE gel, and analysed by western blotting using an anti-phospho-ATM S1981 antibody. The membrane was then stripped and re-probed with an anti-ATM (Millipore) antibody. * marks the slow mobility band.

To further investigate the effect of UVA-irradiation on ATM in NHEM, ATM protein was analysed by western blotting using two independent anti-ATM antibodies (Figure 4.22): anti-ATM (N-terminal) (a generous gift from Dr. D. Delia, Istituto Nazionale Tumori, Milano, Italy), and a commercially available anti-ATM antibody (raised against the internal Abl-interacting domain of ATM; used in Figure 4.21B) purchased from Millipore. Consistent with Figure 4.21B, the UVA-induced increase in ATM protein level was detected using both anti-ATM antibodies (Figure 4.22).

Moreover, a UVA-induced slow mobility form of ATM was detected using both anti-ATM antibodies (Figure 4.22; *). While exposure to IR does not affect the levels of ATM protein in NHEM (Figure 4.22; lane 4), a slow mobility form of ATM was also detected in IR-exposed NHEM (Figure 4.22; lane 4; *). Interestingly, the slower mobility form of ATM was more readily detected by the N-terminal anti-ATM antibody (Figure 4.22; lanes 2 vs. 4), suggesting that the two slow mobility forms of ATM, induced following UVA or IR exposure, may represent two distinct modified forms of ATM. The nature of the post-translational modifications giving rise to the different mobility forms of ATM detectable by western blotting was not further analysed, but may reflect multiple post-translational modifications of ATM (Kinoshita et al., 2009). ATM can be modified by acetylation (Sun et al., 2005), and phosphorylation on other sites, including S367 and S1893 (Kozlov et al., 2006).

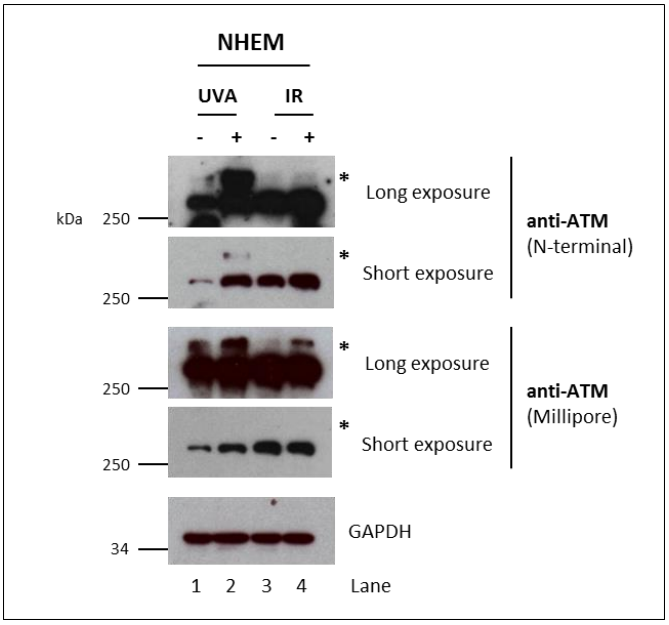

Figure 4.22 Effect of UVA irradiation on ATM levels in NHEM. NHEM were mock-treated or exposed to 75 kJ/m^2 UVA radiation or 10 Gy IR. Cell lysates were prepared 1 hr post-UVA or 30 min post IR. 20 µg of protein was separated on 8% SDS-PAGE gels and western blotting using two different anti-ATM antibodies was used to analyse the effects of UVA and IR on ATM levels. Duplicate samples were loaded onto a 12% gel, and probed with anti-GAPDH as a loading control. * marks the slow mobility form of ATM.

The data presented above provides evidence that ATM protein is modified in NHEM following exposure to UVA-irradiation. To investigate the role of ATM in the response of NHEM to UVA radiation, the effect of ATM kinase inhibition, using the specific small molecule inhibitor KU-60019 (Golding et al., 2009), on cell viability was analysed (Figure 4.23). KU-60019 significantly reduced the viability of UVA-irradiated NHEM by approximately 20% compared to mock-treated control cells 48 hr following irradiation (Figure 4.23). This suggests that ATM may play a role in mediating NHEM survival following UVA irradiation.

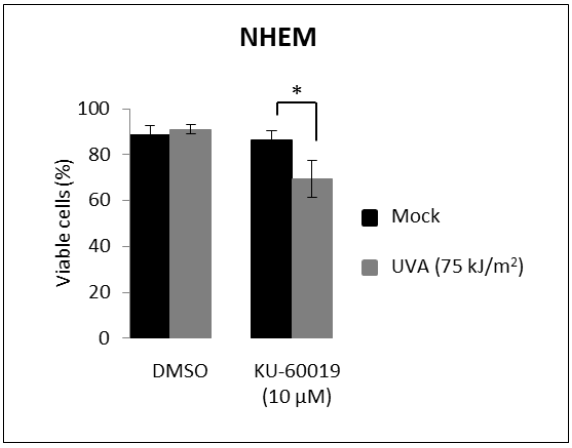

Figure 4.23 Effect of ATM inhibition on NHEM viability following UVA exposure. NHEM were incubated with 10 μM KU-60019 or an equal volume of DMSO, for 30 min prior to mock-treatment or exposure to 75 kJ/m^2 UVA-irradiation. The previously removed media containing drugs was returned to the cells immediately post-UVA and remained for the duration of the experiment. Cell viability was assessed by flow cytometry 48 hr post-UVA using the PI exclusion assay. The percentage viable cells are expressed as a percentage of the total cell population analysed. Data represents the mean of three independent experiments; error bars represent one standard deviation. * $p<0.05$, as determined using one-way ANOVA.

4.5.1 Summary

The effect of UVA-irradiation on ATM in NHEM was investigated. Overall, NHEM express relatively high levels of ATM compared to normal transformed human fibroblasts (NFF; Figure 4.20). While DSB-induced ATM activation is well established, UVA does not induce significant γH2AX (Figure 4.18), indicating that DSBs are not induced by UVA in NHEM. ATM can also be activated in response to oxidative stress, independent of DSB's. UVA induced oxidative stress in NHEM, as determined using the DCF oxidative stress assay (Figure 4.19), suggesting that oxidative stress may contribute to ATM activation in UVA-irradiated NHEM. Phosphorylation of ATM on S1981, a widely-used as a marker of ATM activation, was not detected in UVA-irradiated NHEM under the conditions used here (Figure 4.21). However, ATM levels were elevated in UVA-irradiated NHEM compared to mock-treated control cells (Figure 4.22). Moreover, a slow-mobility form of ATM was detected in UVA-irradiated NHEM, suggesting ATM is modified in the response to UVA in

NHEM. Moreover, KU-60019, a small molecule inhibitor of ATM kinase activity, reduced NHEM viability following UVA exposure, further evidence that ATM is involved in the response of NHEM to UVA radiation.

4.6 Proteomics screen for UVA-induced alterations in protein phosphorylation

In the previous sections (Sections 4.3-4.5), activation of PIKK-mediated DDR signalling in UVA-irradiated NHEM was characterised. To investigate the effect of UVA-irradiation on global cellular signalling in NHEM, a Kinetworks™ phospho-site broad coverage pathway screen (KPSS 1.3; Kinexus Corp., Canada) was utilised. Using this approach, it was possible to analyse the effect of UVA exposure on the phosphorylation status of 36 phospho-epitopes, on 35 different proteins, in parallel. The phospho-sites examined in the screen represent proteins involved in diverse cellular signalling pathways, including cell survival, proliferation, apoptosis, transcription and cytoskeletal dynamics. This approach has been used in a number of published studies, including comparison of differential cisplatin-induced phosphorylation events between apoptotic and non-apoptotic human cells (O'Meara et al., 2010), and to identify nocodozole-induced phosphorylations in HeLa cells (Shi et al., 2006).

NHEM cell lysates were prepared 3 hours following mock-treatment or exposure to 75 kJ/m^2 UVA, using the conditions recommended by Kinexus (Section 2.2.15). Treatment conditions were selected based on observations that a number of DDR proteins were rapidly phosphorylated in NHEM exposed to 75 kJ/m^2 UVA (Figure 4.9). Lysates from four independent experiments were pooled to generate 500 µg of protein per sample, as required for the assay. Lysates were shipped to Kinexus Corporation (Vancouver, Canada), where proteins from each sample were separated on a single SDS-PAGE gel and subsequently immunoblotted with a cocktail of phospho-specific antibodies (Figure 4.24). Phospho-proteins were identified based on gel mobility using custom-designed software (Kinexus Corporation). Band intensities were measured and normalised between individual blots. The percentage change in band intensity between mock-

treated and UVA-irradiated NHEM cell lysates, for each phospho-site detected, is presented in Table 4.2. Percentage changes in band intensities greater than 20% were considered meaningful.

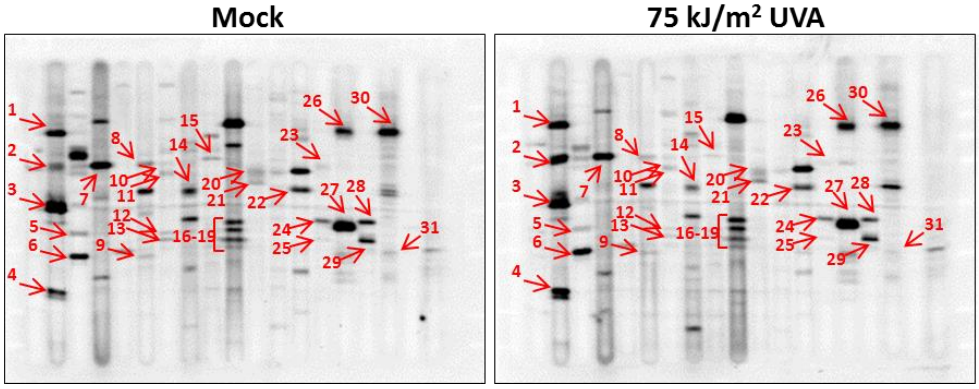

Figure 4.24 Analysis of UVA-induced changes in the phosphorylation status of signalling proteins in NHEM using Kinexus phospho-site screen. NHEM were mock-treated or exposed to 75 kJ/m^2 UVA-irradiation. Cell lysates were prepared 3 hr post-irradiation, using conditions recommended by Kinexus (Section 2.2.15). Lysates from four independent experiments were combined to generate 500 µg of protein per sample, as required for the assay. Denatured lysates were shipped to Kinexus Corporation (Canada) for analysis using the Kinetworks™ phospho-site broad coverage pathway screen (KPSS 1.3). The resulting immunoblots are shown. Arrows point to bands identified by western-blotting, while numbers correspond to the phospho-proteins listed in Table 4.3.

Of the 36 phospho-epitopes analysed using the Kinetworks™ screen, 11 phospho-epitopes were not detected in either mock-treated or UVA-irradiated NHEM (Table 4.2, ND). In some cases where more than one phospho-site on a particular protein was investigated, not all phospho-sites were detected, for example phosphorylation of PKBα/AKT on S473 was detected but phosphorylation of T308 was not (Table 4.2). In some cases multiple forms of a protein having different gel mobilities were detected by a single antibody, as in the case of phospho-Raf-S259 for which two bands were detected (Table 4.2 and Figure 4.24; bands 20-21). Post-translational modification of proteins, including phosphorylation, can result in slower mobility on SDS-PAGE gels. Many proteins are modified on numerous sites, and various combinations of modifications can therefore generate multiple forms of the protein having different gel mobilities. The basis of

these changes in gel mobility was not further investigated in the present study.

Table 4.2 List of phospho-sites analysed using the Kinetworks™ screen (KPSS 1.3). Band numbers correspond to bands numbered in Figure 4.24. ND=signal not detectable in NHEM extracts under these conditions.

Kinetworks™ screen (KPSS 1.3)			
Band No.	**Protein name (Abbreviation)**	**Epitope**	**Band intensity UVA/mock (%)**
1	α-adducin	S726	52
2	γ-adducin	S693	243
3	Src proto-oncogene encoded protein kinase (Src)	Y530	-17
4	Cyclin-dependent protein serine kinase 1/2 (CDK1/2)	Y15	89
5	MAPK/ERK protein serine kinase 1/2 (MEK 1/2)	S218+S222	-24
6	B23 (nucleophosmin, numatrin, nucleolar protein NO38)	S4	28
7	Protein-serine kinase C α (PKCα)	S657	-11
8	Protein-serine kinase C α/β2 (PKCα/β2)	T638/T641	-33
9	MAPK/ERK protein serine kinase 3/6 (MEK 3/6)	S218/S207	-1
10	Ribosomal protein serine S6 kinase β1 (S6Kβ1)	T412	-17
11	Ribosomal protein serine S6 kinase β1 (S6Kβ1)	T412	-10
12	Extracellular regulated protein serine kinase 1 (ERK1/p44 MAPK)	T202+Y204	-52
13	Extracellular regulated protein serine kinase 2 (ERK2/p42 MAPK)	T185+Y187	-56
14	SMA- and mothers against decapentaplegic homologs 1/5/8 (Smad1/5/8)	S463+S465/ S463+S465/ S465+S467	-35
15	Signal transducer and activator of transcription 3 (STAT3)	S727	-60
16	Jun proto-oncogene-encoded AP1 transcription factor (Jun)	S73	31
17	Jun proto-oncogene-encoded AP1 transcription factor (Jun)	S73	-31
18	Jun proto-oncogene-encoded AP1 transcription factor (Jun)	S73	16
19	Jun proto-oncogene-encoded AP1 transcription factor (Jun)	S73	39
20	Raf1 proto-oncogene-encoded protein serine kinase (Raf1)	S259	-16
21	Raf1 proto-oncogene-encoded protein serine kinase (Raf1)	S259	40
22	Protein-serine kinase B α (PKBα/AKT1)	S473	-16

23	Mitogen and stress-activated protein serine kinase 1 (Msk1)	S376	-30
24	Glycogen synthase-serine kinase 3 α (GSK3α)	S21	-27
25	Glycogen synthase-serine kinase 3 β (GSK3β)	S9	-11
26	Retinoblastoma-associated protein 1 (Rb)	S780	-15
27	cAMP response element binding protein 1 (CREB1)	S133	3
28	Glycogen synthase-serine kinase 3 α (GSK3α)	Y279	-27
29	Glycogen synthase-serine kinase 3 β (GSK3β)	Y216	-6
30	Retinoblastoma-associated protein 1 (Rb)	S807+S811	7
31	Mitogen-activated protein-serine kinase p38α p38α (MAPK)	T180+Y182	-51
ND	Double-stranded RNA-dependent protein-serine kinase (PKR1)	T451	
ND	Jun N-terminus protein-serine kinase (JNK)	T183+Y185	
ND	N-methyl-D-aspartate (NDMA) glutamate receptor 1 subunit zeta (NR1)	S896	
ND	Protein-serine kinase B α (PKBα/AKT1)	T308	
ND	Protein-serine kinase C δ (PKCδ)	T507	
ND	Protein-serine kinase C ε (PKCε)	S729	
ND	Ribosomal S6 protein-serine kinase 1/3 (RSK1/3)	T359+S363/ T356+S360	
ND	Signal transducer and activator of transcription 1 α (STAT1α)	Y701	
ND	Signal transducer and activator of transcription 1 β (STAT1β)	Y701	
ND	Signal transducer and activator of transcription 5A (STAT5A)	Y694	
ND	Src proto-oncogene encoded protein kinase (Src)	Y419	

4.6.1 UVA-induced alterations in cellular signalling pathways in NHEM

Using the approach outlined above, a number of cellular signalling pathways were found to be differentially regulated in UVA-irradiated NHEM, including the CDK-mediated cell cycle pathway, the mitogen-activated Raf-MEK-ERK pathway and the membrane skeletal-associated PKC-adducin pathway (Figure 4.29). It should be noted that this data is derived from a single Kinexus screening experiment; however, the data

represents four independent UVA-irradiation experiments that were combined to generate protein for the Kinexus screen.

4.6.1.1 UVA-induced alterations in cell cycle-related proteins

Phosphorylation of CDK1/2 on Y15 was increased by 89% in UVA irradiated NHEM compared to mock-treated control cells (Figure 4.25A). CDK activity regulates cell cycle progression (Section 1.8). Phosphorylation of CDK1 on Y15 by Wee1 kinase inhibits CDK1 activity and prevents mitotic entry (Parker and Piwnica-Worms, 1992). Moreover Wee1 activity is activated by Chk1-mediated phosphorylation (O'Connell et al., 1997), consistent with the observed Chk1 phosphorylation in UVA-irradiated NHEM (Figure 4.9). Furthermore, phosphorylation of Rb on S807 was reduced by 15% in UVA irradiated NHEM compared to mock-treated control cells (Figure 4.25A). Hyper-phosphorylation of Rb, including CDK-mediated S807 phosphorylation, promotes the G1 to S-phase cell cycle transition, by releasing E2F transcription factor, sequestered inactive by hypophosphorylated Rb (Harbour et al., 1999). Both the increase in inhibitory phosphorylation of CDK1/2 on Y15 and decrease in Rb phosphorylation on S807 are consistent with UVA-induced inhibition of cell cycle progression in NHEM.

4.6.1.2 UVA-induced alterations in Raf-MEK-ERK pathway

The phosphorylation status of a number of members of the Raf-MEK-ERK pathway was found to be modulated by UVA exposure in NHEM (Figure 4.25C). The Raf-MEK-ERK pathway is of particular interest in the context of melanocytes as activating mutations in B-Raf are found in >60% of melanomas (Davies et al., 2002). Overall, following UVA-exposure the phosphorylation changes observed were consistent with down regulation of the pathway. As noted above, two mobility forms of Raf1 were detected using the anti-phospho-S259-Raf1 antibody (Figure 4.24; bands 20 and 21). Phosphorylation of S259 inhibits Raf1 kinase activity (Zimmermann and Moelling, 1999). The slow mobility form of phospho-Raf1-S259 (Figure 4.25C; band 20) was reduced by 16% and the faster mobility form (Figure 4.25C; band 21) was increased by 40% in UVA-irradiated NHEM. By

combining the intensities of phospho-Raf1-S259 bands overall UVA-induced an increase in the inhibitory phosphorylation of Raf1 on S259 in NHEM. During mitogen-activated signalling Raf1 phosphorylates and activates downstream kinases MEK1 and MEK2 (Kyriakis et al., 1992). Consistent with UVA-induced inhibition of Raf1, overall MEK1 phosphorylation on S217 and MEK2 phosphorylation on S221 was decreased by 24% in UVA irradiated NHEM (Figure 4.25; band 5). MEK1/2 mediate signal transduction through phosphorylation and activation of ERK1 and ERK2 kinases (Boulton et al., 1991). Consistent with UVA-induced inhibition of the Raf-MEK-ERK pathway in NHEM, activating phosphorylation of ERK1 on T202+Y204 was reduced by 52% and phosphorylation of ERK2 on T185+Y187 was reduced by 56% in UVA-irradiated NHEM compared to mock-treated controls (Figure 4.25C). While further mechanistic studies are required to uncover the link between Raf1 phosphorylation and MEK/ERK signalling in UVA-irradiated NHEM, the present data provides initial evidence that UVA modulates this pathway in NHEM.

4.6.1.3 UVA-induced alterations in the PKC-adducin membrane skeleton-associated pathway

UVA exposure resulted in a 243% increase in phosphorylation of the cytoskeleton protein γ-adducin on S693 and a 52% increase in α-adducin phosphorylation on S726 in NHEM (Figure 4.25B). Adducin heterodimers cap the fast-growing ends of F-actin filaments and promote spectrin-actin binding at the plasma membrane (Matsuoka et al., 2000b). PKC-mediated phosphorylation of α-adducin on S726 inhibits adducin function (Matsuoka et al., 1998), and is associated with increased migration of MDCK cells (Chen et al., 2007). UVA-induced α-adducin phosphorylation on S726 in NHEM is characterised in detail below (Section 4.7). Phosphorylation of PKCα/β2 on T638/T641, which inhibits PKC kinase activity (Parekh et al., 2000), was reduced by 33% in UVA-irradiated NHEM (Figure 4.25B). Moreover, phosphorylation of PKCα on S657 (Figure 4.25B), another inactivating phosphorylation (Parekh et al., 2000), was also slightly (11%)

reduced in UVA-irradiated NHEM. Collectively this data suggests that UVA-modulates PKC activity in NHEM.

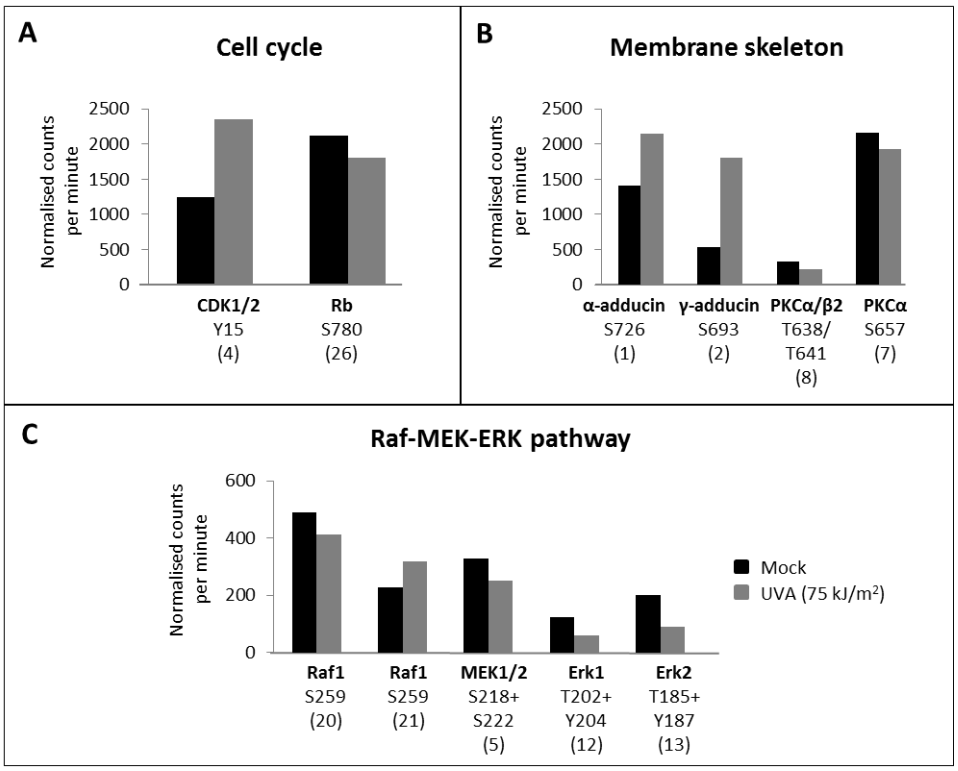

Figure 4.25 UVA-induced alterations in NHEM cellular signalling pathways. NHEM were mock-treated or exposed to 75 kJ/m^2 UVA-irradiation and cell lysates were prepared 3 hr post-UVA. Protein phosphorylation was analysed using the Kinetworks™ KPSS 1.3 screen as outlined in Section 2.2.15. Quantification of selected band intensities of phosphoproteins involved in **(A)** cell cycle, **(B)** membrane skeleton, and **(C)** Raf-MEK-ERK signalling pathways are shown. Numbers in brackets refer to the band numbers in Figure 4.24 and Table 4.2.

4.6.2 Summary

The results of the Kinetworks™ multi-immunoblot screen, provide evidence that UVA radiation can modulate diverse signalling pathways in NHEM, including pathways involved in cell cycle regulation, cell proliferation and survival, and membrane skeleton-dynamics (Figure 4.25). Since the results are based on a single screening experiment, further validation of the observations is required to determine if the observations are true and reproducible.

UVA-induced negative regulation of cell cycle progression in NHEM is supported by the changes in CDK1/2 and Rb phosphorylation, identified in the screen (Figure 4.25B). This is consistent with the observation that UVA induced phosphorylation of the checkpoint kinases Chk1 and Chk2 (Figure 4.9), which can inhibit cell cycle progression following DNA damage (Section 1.8). Moreover, changes in the phosphorylation status of key components of the Raf-MEK-ERK pathway in UVA-irradiated NHEM (Figure 4.25C), which regulates cell proliferation and survival, suggests multiple signalling pathways mediate the response of NHEM to UVA exposure. Furthermore, a striking increase in the phosphorylation of the membrane skeleton proteins, α-adducin and γ-adducin, was observed in UVA-irradiated NHEM (Figure 4.25B). Overall the data derived from the Kinetworks screen highlights the diverse signalling pathways modulated in UVA-irradiated NHEM.

4.7 Characterisation of UVA-induced phosphorylation of α-adducin

Phosphorylation of the cytoskeletal proteins α- and γ-adducin on S726 and S693, respectively, was significantly increased in the Kinetworks™ multi-immunoblot screen (Figure 4.24; lanes 1 and 2). It was of interest to further investigate this UVA-induced effect, in particular since S726 on α-adducin was recently identified as a potential substrate of the checkpoint kinase Chk1 (Blasius et al., 2011), which is strongly activated in UVA-irradiated NHEM (Figure 4.6).

The adducin family of cytoskeletal proteins is composed of three members: α-, β- and γ-adducin. Adducin family members share a conserved structure; composed of an amino terminal head domain, a central neck domain and carboxyl tail domain (Matsuoka et al., 2000b). Adducin heterodimers, composed of α-β or α-γ dimers, function to cap the fast-growing ends of F-actin filaments and promote spectrin-actin binding at the plasma membrane (Matsuoka et al., 2000b). Within the tail domain is a 22-residue myristoylated alanine-rich C kinase substrate (MARCKS)-like domain, which contains multiple phosphorylation sites. PKC-mediated phosphorylation of α-adducin on S726, within the MARCKS-like domain,

inhibits adducin function (Matsuoka et al., 1998), and is associated with increased migration of MDCK cells (Chen et al., 2007).

4.7.1 Characterisation of UVA-induced phosphorylation of α-adducin on S726

To independently validate the UVA-induced increase in α-adducin phosphorylation on S726 observed in the Kinetworks™ screen (Figure 4.24), the effect of UVA-irradiation on phosphorylation of α-adducin on S726 in NHEM was analysed by western blotting using a phospho-specific antibody (Figure 4.26). UVA-exposure induced rapid phosphorylation of α-adducin on S726, detectable immediately following irradiation (Figure 4.26; lane 6). UVA-induced phosphorylation of α-adducin on S726 peaked between 1 and 3 hr following exposure of cells to 75 kJ/m^2 UVA (Figure 4.26; lanes 7 and 8). At later time's post-UVA, the levels of phosphorylation decreased to a level comparable to that of mock-treated cells (Figure 4.26). This data supports the novel observation identified in the Kinetworks™ screen, that exposure to long-wavelength UVA radiation induces phosphorylation of α-adducin on S726 in NHEM.

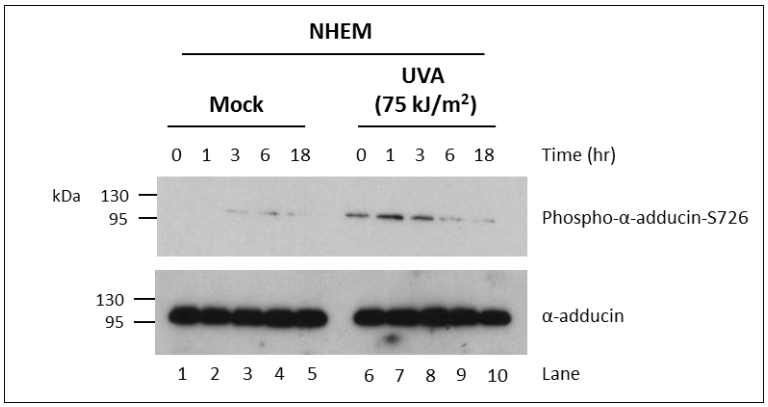

Figure 4.26 Effect of UVA on α-adducin phosphorylation in NHEM. NHEM were mock-treated or exposed to 75 kJ/m^2 UVA and cell lysates were prepared at indicated times post-irradiation. 20 µg of protein was separated by SDS-PAGE and the levels of phospho-α-adducin-S726 and total α-adducin were analysed by western blotting. Blot is representative of at least three independent experiments.

4.7.2 Characterisation of the Chk1-dependence of UVA-induced α-adducin phosphorylation on S726

UVA induces phosphorylation of α-adducin on S726 in NHEM (Figure 4.26). Phosphorylation of α-adducin on S726 was previously identified as a novel potential Chk1 substrate in a chemical genetics screen carried out in HeLa cells (Blasius et al., 2011). Since Chk1 is strongly phosphorylated in NHEM following UVA exposure (Figure 4.9), the Chk1-dependence of UVA-induced α-adducin phosphorylation on S726 was investigated. If Chk1 kinase is responsible for UVA-induced phosphorylation of α-adducin on S726, then inhibition of Chk1 kinase should abrogate UVA-induced α-adducin phosphorylation. To test this hypothesis, NHEM were incubated with two separate small molecule inhibitors of Chk1: UCN-01, see Section 4.3.2 (Busby et al., 2000; Graves et al., 2000), and Chir-124 (Tse et al., 2007), and then exposed to UVA irradiation. Phospho-α-adducin S726 was analysed by western blotting using a phospho-specific antibody (Figure 4.27).

Incubation with UCN-01 reduced UVA-induced phosphorylation of α-adducin on S726 by approximately 7.5-fold compared to DMSO-treated controls (Figure 4.27A; lane 2 versus 4), suggesting that UVA-induced phosphorylation of α-adducin on S726 is dependent on a UCN-01-inhibitable kinase. UVA-induced phosphorylation of Chk1 on S317 was still detected under these conditions (Figure 4.27A; lane 2), consistent with previously observed UVA-induced phosphorylation of Chk1 on NHEM (Figure 4.9). Chk1 phosphorylation on S317 was increased in UCN-01 treated cells (Figure 4.27A; lanes 3 and 4). This is consistent with a previous report that Chk1 inhibition, using small molecule inhibitors, results in increased Chk1 phosphorylation on S317 and S345 (Leung-Pineda et al., 2006). Chk1 kinase activity is required for PP2A-mediated dephosphorylation of Chk1, required to keep basal levels of Chk1 activity low under unperturbed conditions (Leung-Pineda et al., 2006).

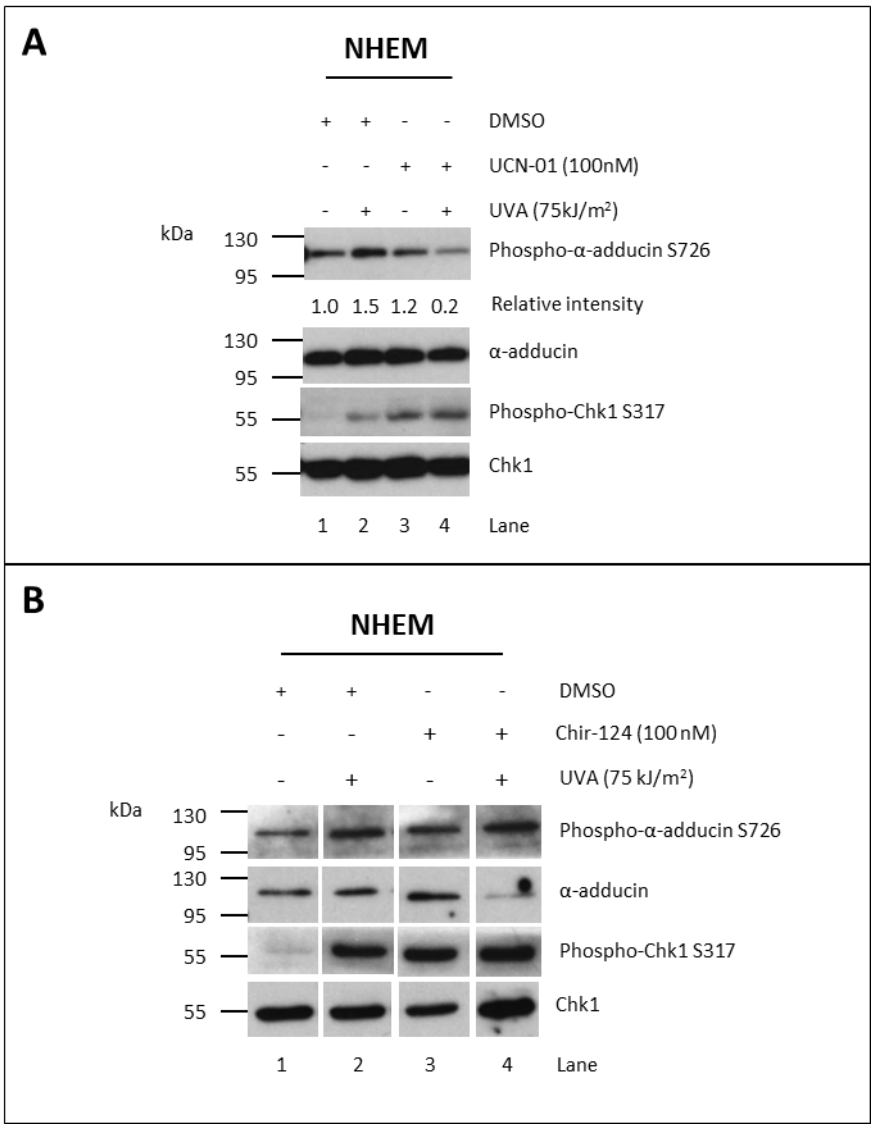

Figure 4.27 Effect of Chk1 inhibition on UVA-induced phosphorylation of α-adducin on S726 in NHEM. (A) NHEM were pre-incubated with 100 nM UCN-01 or an equal volume of DMSO, for 30 min prior to mock-treatment or exposure to 75 kJ/m^2 UVA-irradiation. The previously removed media containing drugs was returned to the cells immediately post-UVA, and remained for the duration of the experiment. Cell lysates were prepared 1 hr post-UVA. 20 µg of protein was separated by SDS-PAGE. Phosphorylation of α-adducin on S726 and phosphorylation of Chk1 on S317 was analysed by western blotting using phospho-specific antibodies. Total α-adducin and total Chk1 levels were also analysed. The relative P-α-adducin-S726 band intensities were quantified using Multi Gauge software, normalised to total α-adducin levels and the mean intensity of three independent experiments is expressed as a fraction of mock-treated and DMSO treated samples (lane 1). **(B)** NHEM were pre-incubated with 100 nM Chir-124 or an equal volume of DMSO for 30 min and treated as outlined in (A). All samples were run on one gel, exposed for identical time periods and cropped for presentation purposes. Blots are representative of at least three independent experiments.

Incubation of NHEM with 100 nM Chir-124, followed by exposure to 75 kJ/m^2 UVA-radiation, did not reduce the level of UVA-induced phospho-α-adducin-S726 compared to UVA-irradiation alone (Figure 4.27B; lane 4 vs. 2). The level of Chk1 phosphorylation on S317 was increased in Chir-124-treated samples, even in the absence of UVA exposure (Figure 4.27B; lane 3). Providing indirect evidence supporting Chk1 inhibition by Chir-124, on the basis of the negative feedback loop outlined above (Leung-Pineda et al., 2006). This data indicates that a kinase targeted by UCN-01, other than Chk1, is responsible for UVA-induced phosphorylation of Chk1. However, the levels of total α-adducin were reduced in Chir-124-treated cells following UVA-irradiation (Figure 4.27B; lane 4), suggesting that inhibition of Chk1, using Chir-124, can modulate the levels of α-adducin protein.

To independently investigate the Chk1-dependence of UVA-induced α-adducin phosphorylation on S726, Chk1 was down-regulated in murine melanocytes by the addition of 4-OHT (Figure 4.13). Cells were then exposed to 25 kJ/m^2, a dose at which >75% of Chk1-depleted cells were viable (Figure 4.16B). Phospho-α-adducin-S726 was analysed by western blotting using the same anti-phospho-α-adducin S726 antibody which recognises the conserved C-terminal phosphorylated site in both human and mouse α-adducin (Figure 4.28A). However, UVA-irradiation did not induce phosphorylation of α-adducin on S726 in murine melanocytes, but in fact reduced the levels of α-adducin on S726 compared to mock-treated control cells (Figure 4.28A; lanes 2 and 4 vs. 1 and 3). Similarly, UVA-irradiation did not induce phosphorylation of α-adducin on S726 in normal transformed fibroblasts (NFF; Figure 4.28B), suggesting that UVA-induced phosphorylation of α-adducin on S726 may be cell type-specific. However, consistent with the effect of Chir-124 on total α-adducin levels in UVA-irradiated NHEM (Figure 4.27B; lane 4), total α-adducin levels were also reduced in Chk1-depleted murine melanocytes following UVA exposure (Figure 4.28A; lane 4). Whether Chk1 inhibition or depletion directly modulates the levels of α-adducin following UVA-exposure remains undetermined. It was reported that α-adducin was cleaved by caspase-3 during cisplatin-induced apoptosis in renal epithelial cells (van de Water et

al., 2000). Since Chir-124-treatment of NHEM, and Chk1-depletion in murine melanocytes, resulted in decreased viability following UVA exposure (Figure 4.12 and Figure 4.16), this may account for the reduced α-adducin levels observed under these conditions. However, the role of caspase-3-mediated cleavage of α-adducin was not analysed here.

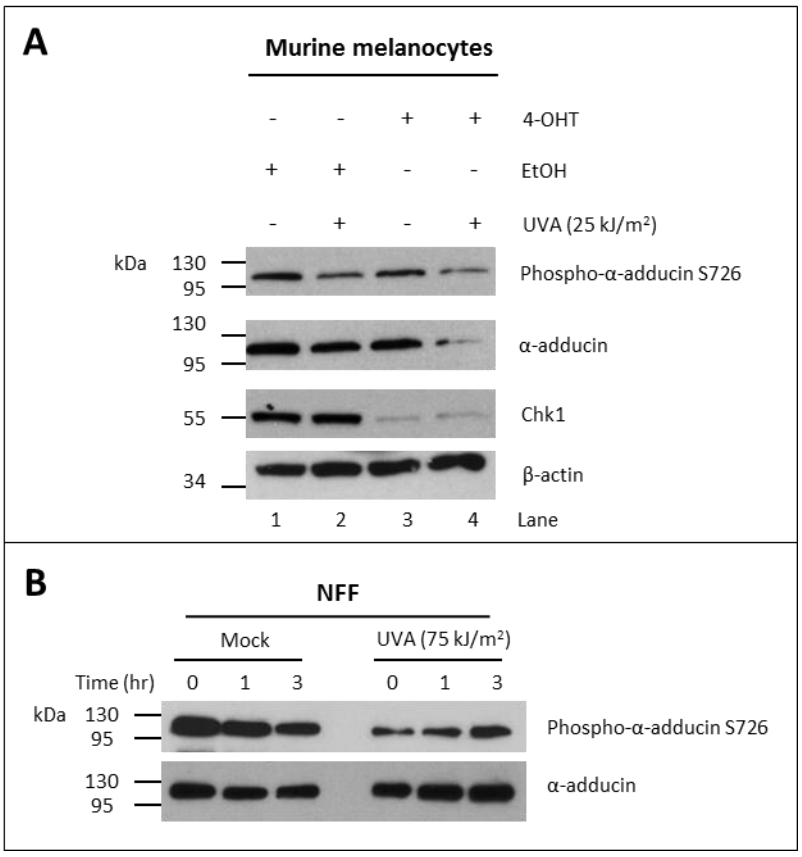

Figure 4.28 Effect of Chk1 down-regulation on α-adducin phosphorylation. (A) Murine melanocytes were treated with 1 µM 4-OHT, or an equal volume of ethanol, at 24 hr intervals. 48 hr after the initial 4-OHT treatment, cells were mock-treated or exposed to 25 kJ/m^2 UVA-irradiation. Cell lysates were prepared 2 hr post-UVA. 30 µg of protein was separated by SDS-PAGE, and analysed by western blotting for the expression of phospho-α-adducin-S726, total α-adducin and Chk1. β-actin was used as a loading control. Blot is representative of at least three independent experiments. **(B)** Normal transformed human fibroblasts (NFF) were mock-treated or exposed to 75 kJ/m^2 UVA. Cell lysates were prepared at the indicated times post-irradiation. 20 µg of protein was separated by SDS-PAGE and analysed by western blotting for phospho-α-adducin-S726 and total α-adducin.

The data outlined above suggests that a UCN-01-inhibitable kinase, other than Chk1, is responsible for UVA-induced phosphorylation of α-adducin on S726 in NHEM (Figure 4.27). Since S726 of α-adducin is a known PKCδ substrate (Chen, Hsieh et al. 2007), the role of PKCδ in UVA-induced phosphorylation of α-adducin on S726 in NHEM was examined using rottlerin, a specific small molecule inhibitor of PKCδ (Gschwendt et al., 1994). Incubation of NHEM with 10 µM rottlerin did not reduce UVA-induced phospho-α-adducin-S726 (Figure 4.29A; lane 6 vs. 2), but rather increased the levels of phospho-α-adducin-S726 in both mock-treated and UVA-irradiated cells (Figure 4.29A; lanes 5 and 6). Consistent with Figure 4.27A, UCN-01 reduced UVA-induced phosphorylation of α-adducin on S716 in NHEM under these conditions (Figure 4.29A; lane 4 vs 2).

PKCδ-mediated phosphorylation of α-adducin on S726 was elevated in Masin-Darby Canine Kidney (MDCK) cells in response to treatment with phorbol 12-myristate 13-acetate (PMA; Chen et al., 2007). To investigate the role of PKCδ in PMA-induced phosphorylation of α-adducin on S726 in NHEM, cells were treated with 100 nM PMA in the presence or absence of rottlerin, and phospho-α-adducin-S726 was analysed by western blotting (Figure 4.29B). PMA treatment induced phospho-α-adducin-S726 in NHEM (Figure 4.29B; lane 2). However, incubation with rottlerin had little effect on PMA-induced phospho-α-adducin-S726 in NHEM (Figure 4.29B; lane 6 vs 2), and overall rottlerin treatment increased the basal levels of phospho-α-adducin S726 (Figure 4.29B; lanes 5 and 6). UCN-01 treatment reduced PMA-induced phospho-α-adducin-S726 in NHEM (Figure 4.29B; lane 4 vs 2). Interestingly, UCN-01 can inhibit certain PKC isoforms, including PKC α, β and γ, in *in* vitro kinase assays, with an IC_{50} value of approximately 30 nM (Seynaeve, Kazanietz et al. 1994), in the same range as UCN-01 inhibition of Chk1, which has an IC_{50} of 11nM in *in vitro* kinase assays (Busby et al., 2000).

The effect of another PKC inhibitor, Gö-6983, on UVA-induced phospho-α-adducin-S726 in NHEM was analysed (Figure 4.29C). Gö-6983 is a pan-PKC inhibitor, inhibiting the classical PKC isoforms α, β and γ, as well as PKCδ, in the low nM range in *in vitro* kinase assays (Gschwendt et al.,

1996). Incubation with 10µM Gö-6983 reduced UVA-induced phospho-α-adducin-S726 in NHEM (Figure 4.29C; lane 4 vs. 2). Overall, this data, along with the observation that UCN-01-treatment reduced the levels of α-adducin S726 phosphorylation, supports the conclusion that kinases targeted by both UCN-01 and Gö 6983, possibly a PKC isoform, but not Chk1, is responsible for phosphorylation of α-adducin on S726 following exposure of NHEM to UVA irradiation.

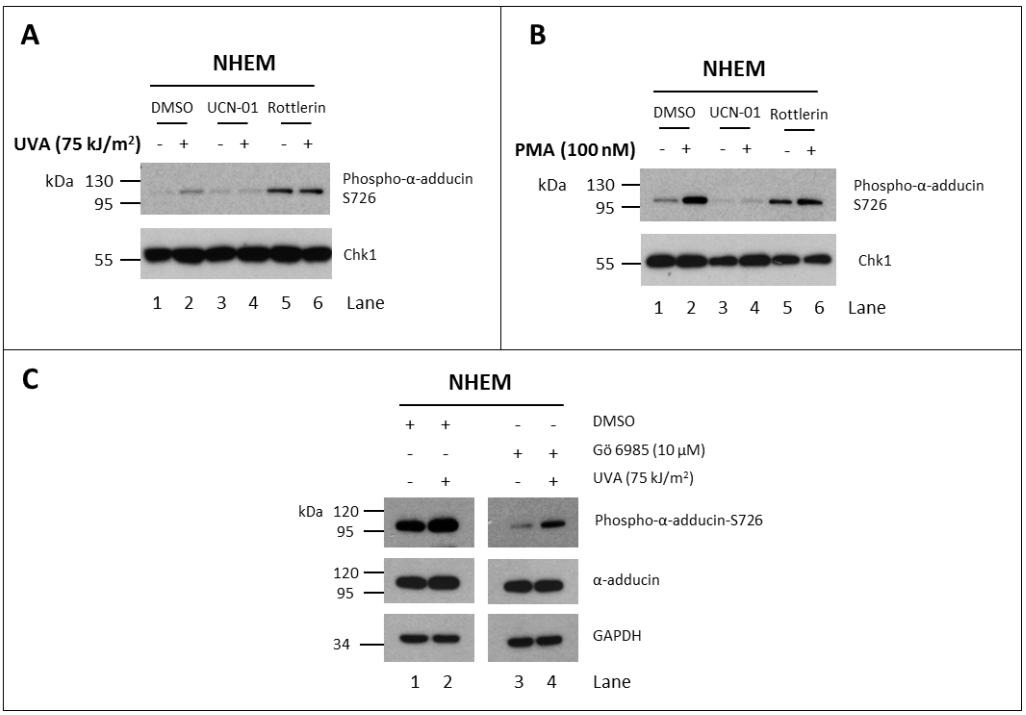

Figure 4.29 Effect of PKC inhibitors on UVA-induced phosphorylation of α-adducin on S726 in NHEM. (A) NHEM were pre-treated with 100 nM UCN-01, 10 µM Rottlerin or an equal volume of DMSO, for 30 min prior to mock-treatment or exposure to 75 kJ/m^2 UVA-irradiation. The previously removed media containing drugs was returned to the cells immediately post-UVA and remained for the duration of the experiment. Cell lysates were prepared 1 hr post-UVA. **(B)** NHEM were pre-treated with 100 nM UCN-01 or 10 µM Rottlerin for 30 min prior to treatment with 100 nM PMA or an equal volume of DMSO. Cell lysates were prepared 15 min following the addition of PMA. **(C)** NHEM were pre-treated with 10 µM Gö 6983 or an equal volume of DMSO, for 30 min prior to mock-treatment or exposure to 75 kJ/m^2 UVA-irradiation. Previously removed media containing drugs was returned to the cells immediately post-UVA and remained for the duration of the experiment. Cell lysates were prepared 1 hr post-UVA. **(A-C)** 20 µg of protein was separated by SDS-PAGE and the levels of indicated proteins were analysed by western blotting using specific antibodies. **(C)** Samples were run on one gel, and exposed for identical time periods; blots were cropped for presentation purposes.

4.7.3 Summary

The novel observation identified in the Kinetworks™ screen, that phosphorylation of α-adducin on S726 was significantly increased in UVA-irradiated NHEM, was validated using western blotting (Figure 4.26). Moreover, this UVA-induced phosphorylation event may be specific to primary human melanocytes, as phospho-α-adducin-S726 was not induced by UVA in murine melanocytes or human normal transformed fibroblasts (NFF) cells (Figure 4.28). However, further investigation of this event in other cell types is required.

While a recent chemical genetics screen identified S726 of α-adducin as a potential novel Chk1 substrate (Blasius et al., 2011), the evidence provided above suggests that Chk1 is not the kinase directly responsible for UVA-induced phosphorylation of α-adducin on S726 in NHEM (Figure 4.27). Instead, a kinase targeted by both UCN-01 and Gö-6983, likely a PKC isoform, may be the kinase responsible for UVA-induced phosphorylation of α-adducin on S726 in NHEM (Figure 4.27A and Figure 4.29C). Abrogation of Chk1 in NHEM and murine melanocytes, using either the Chk1 inhibitor Chir-124, or 4-OHT-mediated Chk1 knockdown, respectively, reduced the levels of total α-adducin in UVA-irradiated cells (Figure 4.27B and Figure 4.28A), suggesting Chk1 may modulate α-adducin levels. However, this may be an indirect effect, due to loss of cell viability under these conditions which may result in caspase-3-mediated α-adducin cleavage and degradation, further investigation into this effect are required.

Overall, the data provides evidence that exposure of primary human melanocytes to long-wavelength UVA radiation induces phosphorylation of the cytoskeletal protein α-adducin on S726. However further mechanistic studies are required to elucidate the relationship between α-adducin, PKC and Chk1 in the response of NHEM to UVA radiation.

4.8 Discussion

Despite the increasing evidence that exposure to UVA radiation is a risk factor in the development of melanoma (Mitchell, 2012; Moan et al., 1999; Wang et al., 2001), the cellular responses to UVA-induced DNA damage in primary human melanocytes are not well characterised on a molecular level. Melanoma arises from the malignant transformation of melanocytes, specialised pigment-producing cells located in the basal epidermis of the skin. Long-wavelength UVA radiation can penetrate deep into the basal layers of the epidermis meaning melanocytes are a target cell for UVA exposure *in vivo* (Bruls et al., 1984; Meinhardt et al., 2008). UVA radiation-induced DNA damage, including CPDs and 8-oxo-G lesions, has been detected in UVA-exposed human melanocytes, both in culture and in the skin (Mouret et al., 2006; Mouret et al., 2012). In the present study the effects of UVA radiation on cell viability, cell cycle progression and DNA damage response activation were assessed in cultured primary normal human epidermal melanocytes.

There was a dose-dependent decrease in NHEM cell viability following exposure to UVA radiation as determined using the trypan blue dye-exclusion assay 48 hr after irradiation. At a dose of 150 kJ/m^2 UVA viability was reduced to 79%, consistent with a previous report where approximately 80% viability was observed 24 hr following exposure of primary human melanocytes to 150 kJ/m^2 UVA (Yohn et al., 1992). The effect of UVA on the viability of NHEM was compared to that of TR30-2 cells, a SV40-transformed human fibroblast cell line. No significant difference in viability was observed between NHEM and TR30-2 cells following UVA-radiation. A previous report observed no significant difference in UVA survival between primary human melanocytes and G361 melanoma cells (Kowalczuk et al., 2006). It has been reported that primary human melanocytes are more resistant to UVA radiation than normal keratinocytes (de Leeuw et al., 1994; Larsson et al., 2005; Mouret et al., 2012).

In contrast to the response to UVA, NHEM were more resistant to short wavelength UVB- and UVC-irradiation compared to the TR30-2 fibroblast cell line. It is proposed that UVB- and UVC-induced cell death results as a consequence of cells attempting to replicate DNA in the presence of UV-induced DNA damage, resulting in replication fork collapse and DSB formation, leading to cell death (Kaufmann, 2010). The molecular basis of the differential sensitivity of primary melanocytes and transformed fibroblasts to different wavelengths of UV radiation was not further investigated in this present study. However a number of factors could contribute to the relative resistance of NHEM to UVB and UVC radiation. Since the melanin content of human skin inversely correlated with the amount of UV induced DNA photolesions (Tadokoro et al., 2003), the melanin content of NHEM could result in less UVB- and UVC-induced DNA damage than in TR30-2 cells, which may account for the increased resistance of NHEM to UVB- and UVC- irradiation. However, it was recently reported that UVB-induces similar levels of CPDs in cultured primary melanocyte and keratinocytes (Mouret et al., 2012). The different distributions of melanin in cultured melanocytes and whole human skin was proposed to account for the differential protective effects of melanin against UV-induced DNA damage, observed in the two experimental systems (Mouret et al., 2012). In cultured melanocytes melanin is located within melanosomes in the cytosol affording little protection to melanocyte DNA, while in the skin melanin is also located in supranuclear caps in keratinocytes protecting the DNA (Kobayashi et al., 1998b). Since S-phase arrest is a common consequence of UVC- and UVB-radiation (Kowalczuk et al., 2006), the high percentage of TR30-2 cells in S-phase, approximately 35% (Figure 3.3), compared to only approximately 15% of NHEM may contribute to the increased resistance of NHEM to UVC- and UVB-irradiations. Reports regarding the relative sensitivity of human melanocytes and keratinocytes to short-wavelength UV radiation are conflicting, one report showed melanocytes to be greatly sensitised to UVB compared to keratinocytes (Mouret et al., 2012), while other reports have shown little difference in the UVB survival of melanocyte and keratinocytes (de Leeuw et al., 1994; Larsson et al., 2005)

Based on the viability studies, UVA-induced DNA damage responses in NHEM were characterised at 75 kJ/m^2 UVA, following which, viability was 97% 48 hr after exposure. This dose is biologically relevant and is approximately equivalent to 25 minutes of mid-day sun exposure in Paris (Kuluncsics et al., 1999).

While exposure of NHEM to 75 kJ/m^2 UVA-exposure did not affect overall NHEM cell cycle distribution, over the time course analysed, UVA induced a rapid but transient inhibition of DNA synthesis. A rapid decrease in DNA synthesis has been previously observed in UVA-irradiated primary human fibroblasts (de Laat et al., 1996; Runger et al., 2012), but has not been reported in primary melanocytes. A previous report showed that exposure of primary human melanocyte to UVA radiation induced prolonged G1/G0 arrest (Kowalczuk et al., 2006). However, this effect was obtained using much higher doses of UVA (400-1,000 kJ/m^2) than were used in this study. In Kowalczuk et al., (2006), the survival of primary human melanocyte exposed to 800 kJ/m^2 was reported to be approximately 40% (Kowalczuk et al., 2006), whereas in this study NHEM viability was reported to be approximately 40% following exposure to 200 kJ/m^2 UVA. It has been reported that the survival of HaCaT keratinocytes following UVA exposure decreases with decreasing dose rate (Shorrocks et al., 2007). The dose rate of the UVA source used in this study is approximately 30-times less than that used in Kowalczuk et al., (2006), this could explain the reduced survival of melanocytes used in this study. The effect of higher doses of UVA radiation on NHEM cell cycle distribution was not investigated here. The lack of a detectable effect of UVA on NHEM overall cell cycle distribution, in this study, is likely due to the transient nature of the observed DNA replication arrest. In primary human fibroblasts it has been reported that at equitoxic doses, of 200 kJ/m^2 UVA and 200 J/m^2 UVB, UVA is less efficient at inducing cell cycle arrest than UVB, possibly due to reduced UVA-induced p53 phosphorylation (Runger et al., 2012). This reduced cell cycle arrest following UVA has been proposed to explain why at equitoxic does UVA is 3.5-fold more mutagenic than UVB, even though

at the same dose UVA-induced 10^3 times less CPDs than UVB on a per joule basis (Perdiz et al., 2000; Runger et al., 2012).

Consistent with UVA-induced inhibition of DNA synthesis, exposure of NHEM to UVA induced a rapid and transient phosphorylation of Chk1 on S345 and S317. DNA damage-induced Chk1 activation normally results in phosphorylation of the Cdc25 family of phosphatases, which inhibits cell cycle progression by preventing CDK activation (Section 1.8). Furthermore, Chk1 slows the rate of replication fork progression and inhibits the firing of new origins in response to DNA damage (Section 1.8.3.1 and Section **Error! Reference source not found.**). While the observed rapid transient VA-induced phosphorylation of Chk1 correlated with the UVA-induced inhibition of DNA synthesis in NHEM, it was found that inhibition of Chk1, using UCN-01, did not abrogate UVA-induced inhibition of DNA synthesis. Thus Chk1 is not responsible for the initial UVA-induced inhibition of DNA synthesis in NHEM. This conclusion was also reached by Girard et al., (2008), where siRNA-mediated Chk1 knockdown in human transformed fibroblast cell lines did not abrogate UVA-induced inhibition of DNA synthesis. Furthermore, UVA-induced inhibition of DNA synthesis was independent of ATM, ATR and p38α in human fibroblasts (Girard et al., 2008). However, incubation with the antioxidant NAC resulted in partial rescue of UVA-induced inhibition of DNA synthesis (Girard et al., 2008), supporting a role for oxidative stress in UVA-induced inhibition of replication in human fibroblasts. ROS-mediated damage to proteins, rather than DNA, was proposed to be responsible for the UVA-induced inhibition of DNA synthesis, but direct experimental evidence for this is currently lacking (Girard et al., 2008).

A role for CPDs in rapid UVA-induced replication inhibition has been argued against, in particular since UVB, which induces approximately 10^3 times more CPDs per J/m^2 than UVA (Perdiz et al., 2000), does not result in rapid and transient inhibition of DNA synthesis, but instead induces a delayed and sustained inhibition of DNA synthesis and accumulation of cells in S-phase (de Laat et al., 1996; Runger et al., 2012). UVA also

induces single stranded breaks (SSBs) in DNA (Douki et al., 2003). The rapid induction and fast repair of these lesions have implicated SSBs as a causative factor in UVA-induced inhibition of DNA synthesis. UVA-induced SSBs are repaired rapidly in human fibroblasts with 90% removal 15 min post-exposure to UVA (Roza et al., 1985), which could account for the transient UVA-induced DNA synthesis arrest observed. However, SSB induction was not directly analysed in NHEM, and the proximal inducer of the observed rapid UVA-induced decrease in DNA synthesis in NHEM remains to be determined.

DNA synthesis recovered in NHEM to the level in untreated cells by 3 hr post-irradiation. Treatment with the Chk1 inhibitor UCN-01 delayed this recovery of DNA replication following UVA exposure. Mechanistically, it has been proposed that Chk1 stabilises stalled replication forks, for example following UVC irradiation in polη-deficient fibroblasts (Despras et al., 2010). Inhibition of Chk1 could therefore impair recovery from replication inhibition by leading to fork collapse. Furthermore, Chk1 may have a role in NHEM survival following UVA exposure, as treatment with two separate Chk1 inhibitors, UCN-01 and Chir-124, significantly reduced cell viability 48 hr following UVA exposure.

To directly investigate the role of Chk1 in the response of melanocytes to UVA exposure, a murine melanocyte cell line in which Chk1 expression can be conditionally down-regulated by the addition of 4-OHT, was utilised. Chk1-depleted murine melanocytes were significantly more sensitive to UVA radiation than Chk1-expressing cells. Moreover, the decrease in viability of Chk1-deficient cells following exposure to UVA radiation was accompanied by an increase in caspase-3 and PARP cleavage, providing evidence that apoptosis is induced in murine melanocytes under these conditions (Elmore, 2007; Los et al., 2002; Nicholson et al., 1995). Moreover, following exposure to 100 kJ/m^2 UVA Chk1-depleted murine melanocytes showed significant alterations in cell cycle distribution, including a reduction in the percentage of G1 cells, and an increase in cells in the S and G2/M phases, and in the number of cells with >4n DNA

content. The data obtained using the murine melanocyte cell line supports an important role for Chk1 in regulating cell cycle progression following UVA exposure.

The importance of the replication stress response in UVA-irradiated primary melanocytes is highlighted by the fact that a recently identified protein in the replication stress response, F-box DNA helicase 1 (FBH1), was found to be down-regulated in melanomas (Jeong et al., 2013a). Of a panel of 19 melanoma cell lines, 55% were found to have deletions in the *FBH1* gene, and FBH1 protein levels were found to be low in four out of nine melanoma cell lines tested (Jeong et al., 2013a). FBH1 is a member of the UvrD family of DNA helicase, which is required for the generation of DSBs at arrested replication forks in response to UVC and HU (Jeong et al., 2013b). DSB formation promotes apoptosis and elimination of excessively damaged cells (Jeong et al., 2013b). By acting to prevent the survival of UV-damaged cells, FBH1 plays an anti-carcinogenic role. Down-regulation of FBH1 in SK-MEL2 melanoma cells was associated with decreased DDR activation in response to HU-treatment, including decreased phospho-p53-S15, γH2AX and phospho-RPA2-S4S8 (Jeong et al., 2013a). Interestingly FBH1 depletion did not abrogate Chk1 phosphorylation on S317 in response to HU or UVC in U2OS cells. Furthermore FBH1-depleted cells were less sensitive to UVC irradiation (Jeong et al., 2013b). Down regulation of FBH1 in melanoma is proposed to promote melanoma survival in the presence of chronic replication stress, such as that induced by UV exposure. It would be of interest to investigate the expression of FBH1 in primary human melanocytes, specifically in response to UVA irradiation, and to determine the effect of siRNA mediated FBH1-down regulation on NHEM survival post-UVA.

UVA-irradiation also induced phosphorylation of Chk2 on T68, known to be phosphorylated by ATM in response to IR-induced DSBs (Matsuoka et al., 2000a). Since ATM is primarily activated in response to DSBs, effect of UVA radiation on the induction of γH2AX, a widely-used indirect marker of DSBs, was investigated (Cleaver, 2011; Rogakou et al., 1999; Rogakou et

al., 1998b). However, significant UVA-induced γH2AX was not detected in NHEM. This is consistent with a number of reports where DSBs were not detected in UVA-irradiated primary and transformed human fibroblasts, using γH2AX or the neutral comet assay to detect DSBs (Girard et al., 2008; Rizzo et al., 2011). ATM can also be activated by ROS, in a DSB-independent manner (Guo et al., 2010b). UVA exposure induced oxidative stress in NHEM, as determined using the DCF oxidative stress assay. While phosphorylation of ATM on S1981 is widely-used readout of ATM kinase activation (Bakkenist and Kastan, 2003; Guo et al., 2010b), no significant induction of phospho-ATM-S1981 was detectible in UVA-irradiated NHEM using either western blotting or immunofluorescence. UVA-induced activation of ATM kinase activity cannot be ruled out since it is reported that phosphorylation on S1981 is dispensable for ATM kinase activity *in vitro* (Lee and Paull, 2005). Moreover, phosphorylation of the murine equivalent of S1981, S1897, is dispensable for murine ATM activation (Pellegrini et al., 2006). It is also possible that a combination of UVA-induced ATM modifications could interfere with antibody binding to the S1981 epitope, since ATM can also be modified by phosphorylation on S376 and S1893 and acetylation on K3016 (Kozlov et al., 2006; Sun et al., 2007). In a recent study of UVA-irradiated primary human fibroblasts phosphorylation of ATM on S1981 was detected in a portion of cells by immunofluorescence (Runger et al., 2012). The authors suggest that in contrast to IR-induced ATM phosphorylation which is observed in all IR-exposed cells, UVA-induced ATM phosphorylation may occur in a cell cycle phase dependent manner (Runger et al., 2012).

ATM protein levels were observed to be increased in UVA-irradiated cells compared to mock-treated NHEM. Moreover, a slow-mobility form of ATM was detected in extracts from UVA-exposed NHEM. This may represent a post-translationally modified form of the protein. The preferential detection of UVA-modified ATM by an N-terminal anti-ATM antibody supports the conclusion that ATM is differentially modified in response to UVA and IR in NHEM. Further studies, for example using mass spectrometry, are

required to identify the sites that are modified on the slow-mobility form of ATM detectable in UVA-irradiated NHEM.

The rapid increase in ATM levels in UVA-irradiated NHEM, observed 1 hr following irradiation, suggests that a transcription-independent mechanism regulates ATM levels in NHEM. A PIKK interacting protein, Tel2, has been shown to regulate ATM levels in MEFs (Takai et al., 2007). Although the exact mechanism of action of Tel2 in regulating ATM levels has not been elucidated, the authors suggest interaction of ATM with Tel2 could prevent proteasome-mediated ATM degradation (Takai et al., 2007). It would therefore be of interest to investigate Tel2 levels, and the interaction of Tel2 with ATM following UVA exposure in NHEM. It has also been reported that the 5'untranslated regions (UTR) of ATM mRNA is subject to extensive alternative splicing which could contribute to the rapid modulation of ATM protein levels in response to stimuli (Savitsky et al., 1997).

Evidence is accumulating that DNA damage-independent ATM functions during the oxidative stress response are important in regulating cell survival and proliferation (Ito et al., 2004; Kim and Wong, 2009; Okuno et al., 2012). This is highlighted by progressive neuronal degradation observed in ATM-deficient individuals, in particular the Purkinje cells, which are known to be susceptible to high levels of oxidative stress (Kastan and Lim, 2000; Shiloh and Ziv, 2013). Moreover, the function of ATM in promoting the anti-oxidant defence is associated with ATM-mediated production of the anti-oxidant co-factor nicotinamide adenine dinucleotide phosphate (NAPDH) and the synthesis of nucleotides (Cosentino et al., 2011), which may be required for DNA repair or the recovery from UVA-induced inhibition of DNA synthesis. Overall the data suggests that primary human melanocytes express a relatively high level of ATM, and that both the levels and post-translational modification status of ATM is modulated in response to UVA-irradiation. Treatment of NHEM with KU-60019, a specific ATM inhibitor (Golding et al., 2009), significantly reduced cell viability, further supporting a role for ATM in the response of NHEM to UVA radiation.

The data presented above provides evidence that UVA-exposure activates PIKK-mediated DDR signalling pathways in NHEM, including phosphorylation of the key PIKK-substrates Chk1 and Chk2. The effect of UVA radiation on the phosphorylation status of proteins involved in other signalling pathways, including pathways regulating cell cycle progression, cell survival and proliferation, and cytoskeleton dynamics, were analysed a Kinexus phospho-site screen (Section 4.6). It should be noted that the results discussed below are derived from a single Kinexus screening experiment; which represents four independent UVA-irradiation experiments as cell lysates were pooled to generate sufficient protein for the Kinexus screen. Further experiments are required to validate the Kinexus screen results.

In the Kinexus screen the inhibitory phosphorylation of CDK1/2 on Y15 (Parker and Piwnica-Worms, 1992) was found be increased in UVA-irradiated NHEM. Activated CDK1/2 promotes cell cycle progression (see Section 1.8), while wee1-mediated phosphorylation of CDK1 on Y15 inactivates CDK1s activity, thus preventing cell cycle progression (Parker and Piwnica-Worms, 1992). It would be of interest to further investigate CDK regulation in response to UVA radiation, particularly as significant UVA-induced cell cycle arrest was not observed in NHEM under these conditions. Inhibitory phosphorylation of CDK may represent a rapid and transient event in the cellular response of NHEM to UVA radiation, similar to that observed for UVA-induced Chk1 and Chk2 phosphorylation. Interestingly, a number of studies have shown that both CDK1 and CDK2 are overexpressed in melanomas, especially in advanced metastatic melanoma, which may contribute to melanoma cell survival and proliferation (Abdullah et al., 2011; Jaeger et al., 2007; Tang et al., 1999).

The Kinexus phospho-site screen also revealed alterations in the mitogen-activated Raf-MEK-ERK signalling pathway in UVA-irradiated NHEM. UVA-induced regulation of this signalling pathway is of particular interest since activating mutations in *BRAF* are found in more than 60% of melanomas (Davies et al., 2002). Furthermore, in those melanomas carrying wild-type *BRAF*, alterations in other components of the MAPK kinase pathway have been reported, including the presence of activating mutations

in *NRAS*, and down-regulation of Raf-1 kinase inhibitory protein (RKIP) (Alsina et al., 2003; Schuierer et al., 2004). The results of the screen indicate that overall UVA down-regulates the Raf-MEK-ERK signalling pathway. Activation of the Raf-MEK-ERK pathway is generally considered to promote cell survival and proliferation, although opposing outcomes, including a role in cell cycle inhibition, have also been described (McCubrey et al., 2007). Thus, it would be important to investigate the functional consequence of the UVA-induced changes in the phosphorylation status of Raf-MEK-ERK pathway proteins in primary human melanocytes.

The Kinexus phospho-site screen also identified a 2-fold increase in phosphorylation of the cytoskeletal protein α-adducin on S726 in UVA-irradiated NHEM. UVA-induced phosphorylation of α-adducin on S726 in NHEM was independently validated by western blotting using a phospho-specific antibody. Validation of UVA-induced α-adducin phosphorylation may suggest that the changes in phosphorylation identified using the Kinexus screen represent true UVA-induced phosphorylation events.

S726 of α-adducin was recently identified in a chemical genetics screen as a novel potential Chk1 substrate (Blasius et al., 2011). Since Chk1 is strongly phosphorylated in UVA-irradiated NHEM, the Chk1 dependence of UVA-induced α-adducin phosphorylation on S726 was investigated, using small molecule inhibitors of Chk1. UCN-01 is a widely-used as a Chk1 inhibitor as it shows 100-fold specificity for Chk1 over Chk2, based on IC_{50} values from *in vitro* kinase assays (Busby et al., 2000). While UCN-01 inhibited UVA-induced phosphorylation of α-adducin on S726, Chir-124 another Chk1 inhibitor (Tse et al., 2007), did not affect UVA-induced phosphorylation of α-adducin, suggesting that a UCN-01-targeted kinase, other than Chk1, is responsible for UVA-induced phosphorylation of α-adducin on S726 in NHEM. S726 of α-adducin is also known to be phosphorylated by PKCδ in response to PMA treatment in Madin-Darby canine kidney (MDCK) cells (Chen et al., 2007). While a PKCδ-specific inhibitor, rottlerin (Gschwendt et al., 1994), did not reduce UVA-induced phospho-α-adducin-S726, another PKC inhibitor Gö-6983 (Gschwendt et al., 1996), which inhibits PKCα, β, γ, δ and ζ in the low nM range, reduced

UVA-induced phospho-α-adducin-S726. Interestingly some studies have shown that PKCδ levels are reduced in cultured primary human melanocytes (Oka et al., 1995; Selzer et al., 2002). Moreover, UCN-01 has been reported to inhibit PKC isoforms α, β, and γ with IC_{50} values similar to Chk1, in *in vitro* kinase assays (Seynaeve et al., 1994). Consistent with our observation that UCN-01 specifically reduces phospho-α-adducin-S726 in NHEM, a phase I trial of UCN-01 for the treatment of refractory neoplasms reported a reduction in phospho-α-adducin-S726 in the plasma of individuals treated with UCN-01 (Sausville et al., 2001). Further investigation is required to identify the exact kinase responsible for UVA-induced phospho-α-adducin-S726 in NHEM.

It was observed that incubation of NHEM with Chir-124 or Chk1-depletion in the murine melanocytes resulted in a reduction of α-adducin protein following UVA irradiation. Whether this effect is a direct effect of Chk1 inhibition or deletion remains to be deciphered. However, α-adducin can be cleaved by caspase-3 during cisplatin-induced apoptosis in renal epithelial cells (van de Water et al., 2000). Thus the reduced viability under these conditions may account for the reduction of α-adducin levels. Phosphorylation of α-adducin on S726 was found to precede caspase-3 mediated cleavage, it was not reported if phospho-α-adducin on S726 was required for caspase-3 mediated cleavage (van de Water et al., 2000), however if this is the case it may explain why a reduction in α-adducin levels were not observed following UCN-01 treatment, where NHEM cell viability was by the same percentage as with Chir-124 treatment.

Although not directly investigated here, it would be of interest to investigate the functional consequences of UVA-induced phospho-α-adducin-S726 in NHEM. Phosphorylation of α-adducin on S726 reduced adducin function in capping the fast growing ends of F-actin and recruiting spectrin (Matsuoka et al., 1998). Moreover, phosphorylation of α-adducin on S726 in MDCK cells promotes cell mobility (Chen et al., 2007). It was previously reported that UVA irradiation of murine melanoma cells enhanced metastasis, which correlated with UVA-induced changes in cell adhesion molecules (Pastila et al., 2011; Pastila and Leszczynski, 2005). It would be of interest to

investigate the role of UVA-induced phosphorylation of α-adducin with regards to its effect on NHEM cell mobility. As mentioned above, phosphorylation of α-adducin on S726 was also identified as an early event in cisplatin-induced apoptosis (van de Water et al., 2000). However, since NHEM retained 97% viability following exposure to 75 kJ/m^2 UVA, adducin phosphorylation may not be involved in apoptosis under these conditions.

Overall the data presented here provides novel insights into the cellular signalling pathways modulated in primary human melanocytes following exposure to long-wavelength UVA radiation.

5 General discussion

5.1 General discussion

Exposure to solar UV radiation, which is composed of approximately 95% UVA radiation and 5% UVB radiation, is the major risk factor in the development of skin cancer (de Gruijl, 1999; Runger, 2007). The molecular mechanisms linking exposure to short-wavelength UVB radiation with skin carcinogenesis are relatively well defined (see Section 1.2), and are mediated through the induction of pre-mutagenic DNA photolesions, including CPDs and 6,4-PPs. While UVA-irradiation also induces CPDs, albeit 10^3 times less efficiently than UVB, on a per joule basis (Mouret et al., 2006; Perdiz et al., 2000), the contribution of UVA exposure to skin carcinogenesis has only recently been elucidated (see Section 1.4).

Understanding the molecular events that mediate the response of cells to UVA radiation could provide novel insights into how UVA exposure leads to skin cancer. Here we provide evidence, for the first time, that DNA polymerase η (polη) plays a role in the replication of UVA-damaged DNA in human cells (Chapter 3). Since polη carries out error-free replication past dithymidine CPDs *in vitro* and *in vivo* (Johnson et al., 1999b; Masutani et al., 1999a; Masutani et al., 2000), this may indicate that polη contributes to the prevention of UVA-induced skin carcinogenesis, by reducing the mutagenic consequences of replication of DNA containing UVA-induced dithymidine CPDs, the most common UVA-induced DNA lesions (Mouret et al., 2006). A role for polη in the bypass of UVA-induced CPDs may be of particular importance since it is reported that UVA-induced CPDs persist for longer than UVB-induced CPDs in human skin (Mouret et al., 2006). Thus the likelihood that the replication machinery will encounter a CPD that requires polη for bypass may be higher following UVA exposure. However, further studies are required to identify the UVA-induced lesion(s) that are bypassed by polη. Moreover, although not directly investigated here, polη may play an important role in the bypass of UVA-induced CPDs in melanocytes, since melanocytes were reported to be defective in the repair of UVA-induced DNA photolesions (Wang et al., 2010). As noted above,

this could increase the likelihood that a replication fork will encounter a CPD in the template.

Our novel observation that polη is involved in the replication of UVA-damaged DNA, as well as the recent report that repair of UVA-induced DNA damage requires XPA, a key protein in the nucleotide excision repair pathway (Cortat et al., 2013), highlights the possible contribution of UVA-induced DNA damage to skin carcinogenesis. This is particularly important in XPV individuals lacking polη and in XP individuals with defects in NER. Although not investigated here, replication of UVA-damaged DNA in XPV cells by other more error-prone TLS polymerases, including polι (Tissier et al., 2000), could contribute to skin carcinogenesis. Together this data highlights the importance of UVA-protection in the prevention of skin cancer, which is particularly important in XPV and XP individuals who lack key components of the normal UVA response.

While exposure to UVA radiation is a risk factor in the development of melanoma (Section 1.6.1), the molecular mechanisms linking UVA exposure and melanoma development remain unclear. It is important to characterise the cellular pathways that mediate the initial response of primary melanocytes to UVA radiation, as this could provide insight into how changes in these pathways could contribute to UVA-induced melanoma.

Here we provide evidence that the normal response of primary human melanocytes to UVA radiation involves PIKK-mediated DNA damage response (DDR) signalling, involving activation of both ATR-Chk1 and ATM-Chk2 pathways. DDR signalling plays an important role in protecting genomic integrity (see Section 1.7), thus these pathways may normally play a role in protecting the melanocyte genome from the deleterious effects of UVA exposure. While this present study focused on characterising UVA-induced DNA damage response signalling pathways, the response of melanocytes to UVA radiation is more complex. We provide evidence that multiple cellular signalling pathways, including the mitogen-activated Raf-MEK-ERK pathway and the cytoskeleton-associated PKC-adducin pathway,

are differentially regulated in primary melanocytes following UVA irradiation, however functional analysis of the roles of these pathways in the response of primary melanocytes to UVA exposure requires further study. Moreover, although not studied here, melanocytes also respond to UVA irradiation by stimulating melanogenesis, and the tanning response (Wicks et al., 2011).

While the evidence supporting a link between UVA exposure and melanoma development is outlined in Section 1.6.1, a number of issues complicate the association between UV-exposure and melanoma development. These include the fact that melanoma frequently occurs on non-sun exposed areas of the body (Whiteman and Green, 2011), and that the oncogenic drivers of melanoma, including *BRAF*, do not normally harbour UV signature mutations (Davies et al., 2002). It has also been proposed that melanin itself contributes to melanoma development through an oxidative stress-dependent pathway (Wittgen and van Kempen, 2007). Recently a UV-independent pathway to melanoma, specifically associated with elevated levels of pheomelanin was described, in a transgenic mouse strain that mimics the human red hair/light skin phenotype (Mitra et al., 2012). In this study, introduction of the melanoma-associated activating $BRAF^{V600E}$ mutation, in the absence of other genetic alterations or UV-exposure, was sufficient to promote melanoma development in this mouse strain (Mitra et al., 2012). A role for pheomelanin in melanoma development is supported by the fact that fair-skinned individuals have an elevated risk of melanoma development compared to dark-skinned individuals, where the primary pigment is eumelanin (Neugut et al., 1994).

Given the biologically and genetically distinct types of melanoma which can arise, the cell of origin of melanoma remains unclear (Whiteman et al., 2011). As well as the epidermis, melanocytes are found at other anatomical locations, including the hair follicle, eye, brain and heart. Hair follicle melanocytes are responsible for hair colour, and this melanocyte population is maintained by the melanocyte stem cells (MSCs) located in the hair bulge (Kauser et al., 2011). MSCs also function to repopulate the epidermis following UVB irradiation (Chou et al., 2013). Interestingly MSCs were

shown to migrate to the epidermis in an undifferentiated state following UVB (Chou et al., 2013). MSCs in the epidermis represent another melanocyte population which are potentially exposed to solar UV radiation. Given the requirement for B-Raf signalling for MSC entry into the cell cycle (Valluet et al., 2012), and the fact that B-Raf signalling is commonly activated in melanomas (Davies et al., 2002), MSCs could be implicated in melanoma development. Thus it would be of interest to investigate the response of MSCs to solar UV-radiation; in particular the effect of solar UV radiation on MSC survival and differentiation would be informative.

5.2 Summary

Accumulating evidence indicates that exposure to long-wavelength UVA radiation, which accounts for >95% of solar UV radiation reaching the earth's surface, is a significant risk factor for the development of skin cancer, particularly melanoma (Mitchell, 2012; Runger, 2007). In line with this, UVA radiation was defined as a class I carcinogen by the IARC (El Ghissassi et al., 2009). It is now well established that UVA radiation induces DNA damage, with CPDs being to most common UVA-induced DNA lesion (Mouret et al., 2006; Mouret et al., 2012; Perdiz et al., 2000). Here we provide evidence that DNA polymerase eta (polη), a specialised TLS polymerase which carries out error-free replication past dithymidine dimers *in vitro* (Johnson et al., 1999b; Masutani et al., 1999a), plays a role in the replication of UVA damaged DNA in human cells. We show that polη is mobilised to discrete nuclear foci following UVA exposure, and that these foci occur exclusively in cells undergoing DNA replication. Furthermore, we provide evidence that polη-deficient cells rely on a caffeine-sensitive, ATR-Chk1-mediated, pathway for survival following UVA irradiation. Overall, the data provides evidence that UVA-induced DNA damage tolerance is mediated, at least in part, by polη. The identification of a role for polη in the replication of UVA-damaged DNA highlights the possible contribution of polη to preventing UVA-induced skin carcinogenesis, which is of particular relevance to XPV individuals lacking polη.

Exposure to UVA radiation is a risk factor in the development of melanoma (Mitchell and Fernandez, 2012; Moan et al., 1999; Wang et al., 2001). However, the molecular mechanisms linking UVA exposure and melanoma remain unclear. While melanocytes represent a target cell for UVA exposure *in vivo*, as UVA can penetrate deeply into the basal layers of the epidermis where the melanocytes are located (Bruls et al., 1984), and UVA induces DNA damage in UVA-exposed melanocytes (Mouret et al., 2012), the effect of UVA irradiation on DNA damage response signalling in primary human melanocytes is not well studied. It is important to characterise the cellular pathways that mediate the normal response of primary melanocytes to UVA

radiation, as this could provide insight into how changes in these pathways could contribute to UVA-induced melanoma. Here we provide evidence that UVA induces a PIKK-mediated DNA damage response in primary normal human epidermal melanocytes (NHEM), involving both the ATR-Chk1 and the ATM-Chk2 pathways. Moreover, an important role for Chk1 in the response to UVA-irradiation in primary human melanocytes was identified, particularly in the recovery from UVA-induced inhibition of DNA synthesis. Using a phospho-proteomic screen, UVA-induced changes were identified in the phosphorylation status of proteins involved in a number of signalling pathways, including the CDK cell cycle pathway, the mitogen activated Raf-MEK-ERK pathway and the cytoskeleton-associated PKC-adducin pathway.

Collectively, the results presented here provide information, at a molecular level, on the early responses of human skin cells to long-wavelength UVA radiation. In particular we identify for the first time a role for polη in the replication of UVA-damaged DNA in human fibroblasts. Furthermore, we provide novel insights into the cellular signalling pathways activated in primary human melanocytes following exposure to UVA radiation.

5.3 Future directions

The present study identified a novel role for polη in replication of UVA-damaged DNA. Since polη is known to bypass dithymidine CPDs *in vitro* and *in vivo* (Johnson et al., 1999b; Masutani et al., 1999a; Masutani et al., 2000), and CPDs are the most common UVA-induced DNA lesion (Mouret et al., 2006), we propose that polη is involved in the bypass of UVA-induced CPDs. However, this hypothesis was not directly tested here. Since polη is also involved in the bypass of other DNA lesions, including 8-oxo-G (Haracska et al., 2000b; Zlatanou et al., 2011), it would be of interest to directly identify the major UVA-induced DNA lesion(s) bypassed by pol. Immunofluorescence investigation of the recruitment of polη to sites of UVA-induced DNA lesions in individual cells, using commercially available antibodies specifically recognising either CPD and 8-oxo-G lesions (Mitchell and Brooks, 2010) could be informative.

The mechanisms regulating polη localisation to nuclear foci following UVA exposure were not analysed here. Monoubiquitination of PCNA is considered a key regulator of polη recruitment to nuclear foci following UVC radiation, since polη specifically interacts with monoubiquitinated PCNA (Kannouche et al., 2004). It would be of interest to analyse the effect of UVA radiation on PCNA monoubiquitination. More recently, other key regulators of polη recruitment to foci following UVC irradiation have been identified, including Nbs1 (Yanagihara et al., 2011), FANCD2 (Fu et al., 2013), and BRCA1 (Tian et al., 2013). Polη protein was observed to be reduced at later times following UVA exposure (Figure 3.4). Polη levels were previously shown to be down-regulated following UVC radiation, in a proteasome-dependent manner (Cruet-Hennequart et al., 2006; Jung et al., 2012). The effect of proteasome inhibition, for example using MG-132, on polη levels following UVA exposure would be informative as to whether the UVA-mediated polη turnover is proteasome-dependent.

Polη-deficient cells were not greatly sensitised to UVA radiation compared to polη-expressing cells at the doses used in this study. However, the evidence provided suggests that polη plays an important role in the

replication of UVA-damaged DNA. This leads to the question of the mechanism of UVA-induced DNA damage tolerance in polη-deficient cells. It is suggested that in the absence of polη, other error-prone polymerases, including polι, could contribute to bypass of DNA photolesions (Tissier et al., 2000). siRNA-mediated knockdown of other TLS polymerases in polη-deficient XP30RO cells, and analysis of cell survival would address whether these other polymerases are involved in the response to UVA irradiation.

Another important question not addressed here is whether polη plays a role in the response of biologically-relevant cell types, including primary melanocytes, to UVA radiation. Expression of GFP-tagged polη in NHEM and analysis of nuclear localisation following UVA exposure would address whether polη is localised to foci in melanocytes following UVA exposure. Furthermore, it would be of interest to analyse the effects of polη knockdown, using shRNA, in primary melanocytes, including the effect on UVA survival in the presence of caffeine, which is indicative of a polη-dependent process. It should be noted that genetic variations in the *POLH* gene, are associated with increased melanoma risk (Di Lucca et al., 2009), suggesting polη may play a role in the normal function of primary melanocytes.

It would be of interest to further validate the results of the Kinexus screen, especially the UVA-induced effects on Raf-MEK-ERK signalling pathway, since this pathway if so frequently deregulated in melanoma (Davies et al., 2002). Analysis of the functional consequences of UVA-induced phosphorylation of Raf-MEK-ERK signalling proteins, using small molecule inhibitors of the kinases or phosphatases involved in regulation of UVA-induced phosphorylation events, on the cellular outcomes to UVA exposure, including cell viability would be informative.

As mentioned above, functional characterisation of UVA-induced phosphorylation of α-adducin on S726 would be of interest. Phosphorylation of α-adducin on S726 reduced adducin function in capping the fast growing ends of F-actin and recruiting spectrin (Matsuoka et al., 1998), and in MDCK cells promoted cell motility (Chen et al., 2007). It was previously

reported that UVA irradiation of murine melanoma cells enhanced metastasis, and correlated with UVA-induced changes in cell adhesion molecules (Pastila et al., 2011; Pastila and Leszczynski, 2005). It would be interesting to investigate the role of UVA-induced phosphorylation of α-adducin on S726 in the context of NHEM cell motility, especially due to the highly metastatic nature of melanomas.

The primary normal human epidermal melanocyte (NHEM) cell system utilised in this study represents an important model in which to study the normal cellular responses of a biologically relevant cell type to UVA irradiation. As mentioned above, investigation of the response of melanocyte stem cells (MSCs) to UVA radiation would also be of interest. It was recently shown that IR-induced DNA damage resulted in premature differentiation of MSCs (Inomata et al., 2009), and that ATM played an important role in the process. Differentiation and survival of damaged MSCs could have implications in melanoma development. Since we provide evidence that ATM is modulated in the response of NHEM to UVA irradiation, the functional consequence of ATM knockdown on NHEM cell viability would be of interest.

In this study the effect of UVA radiation on NHEM was investigated by exposing NHEM to UVA radiation from a broadband UVA source through the plastic lids of the tissue culture dishes. The purpose of the plastic lid was to act as a short-wavelength UV filter, however this significantly decreased the UVA irradiance reaching the cells and resulted in increased exposure times (Table 2.8). It would be of interest to investigate if the effects of UVA radiation observed in this study, such as the induction of Chk1 phosphorylation, were observed when cells were exposed to UVA radiation with the lids removed, which would significantly reduce the exposure time. Moreover, to further investigate the wavelength-dependence on UVA-induced changes in NHEM cell signalling, exposure of NHEM to narrowband UVA sources would be informative.

While characterisation of the response of primary melanocytes to specific defined wavelengths of UV radiation is required to decipher the contribution

of the particular UV wavelengths to skin carcinogenesis, in reality cells are exposed to a combination of UVA and UVB radiation. Thus characterisation of the response of primary melanocytes to a combination of UVA and UVB, as well as exposure to UVA and UVB wavelengths individually, would allow an even more biologically-relevant response to be characterised.

6 Bibliography

Abdel-Malek, Z., and V. Swope. 2011. Epidermal Melanocytes: Regulation of Their Survival, Proliferation, and Function in Human Skin. *In* Melanoma Development. A. Bosserhoff, editor. Springer Vienna. 7-33.

Abdullah, C., X. Wang, and D. Becker. 2011. Expression analysis and molecular targeting of cyclin-dependent kinases in advanced melanoma. *Cell Cycle*. 10:977-988.

Aberdam, E., C. Bertolotto, E.V. Sviderskaya, V. de Thillot, T.J. Hemesath, D.E. Fisher, D.C. Bennett, J.-P. Ortonne, and R. Ballotti. 1998. Involvement of Microphthalmia in the Inhibition of Melanocyte Lineage Differentiation and of Melanogenesis by Agouti Signal Protein. *J. Biol. Chem.* 273:19560-19565.

Abraham, R.T. 2001. Cell cycle checkpoint signaling through the ATM and ATR kinases. *Genes Dev.* 15:2177-2196.

Agar, N., and A.R. Young. 2005. Melanogenesis: a photoprotective response to DNA damage? *Mutat. Res.* 571:121-132.

Albertella, M.R., C.M. Green, A.R. Lehmann, and M.J. O'Connor. 2005. A Role for Polymerase η in the Cellular Tolerance to Cisplatin-Induced Damage. *Cancer Res.* 65:9799-9806.

Ali, A., J. Zhang, S. Bao, I. Liu, D. Otterness, N.M. Dean, R.T. Abraham, and X.-F. Wang. 2004. Requirement of protein phosphatase 5 in DNA-damage-induced ATM activation. *Genes Dev.* 18:249-254.

Alsina, J., D.H. Gorsk, F.J. Germino, W. Shih, S.-E. Lu, Z.-G. Zhang, J.-M. Yang, W.N. Hait, and J.S. Goydos. 2003. Detection of Mutations in the Mitogen-Activated Protein Kinase Pathway in Human Melanoma. *Clin. Cancer Res.* 9:6419-6425.

Arellano, M., and S. Moreno. 1997. Regulation of CDK/cyclin complexes during the cell cycle. *Int. J. Biochem. Cell Biol.* 29:559-573.

Arlett, C.F., S.A. Harcourt, and B.C. Broughton. 1975. The influence of caffeine on cell survival in excision-proficient and excision-deficient xeroderma pigmentosum and normal human cell strains following ultraviolet-light irradiation. *Mutat. Res.* 33:341-346.

Ascierto, P., J. Kirkwood, J.-J. Grob, E. Simeone, A. Grimaldi, M. Maio, G. Palmieri, A. Testori, F. Marincola, and N. Mozzillo. 2012. The role of BRAF V600 mutation in melanoma. *J. Transl. Med.* 10:85-93.

Bakkenist, C.J., and M.B. Kastan. 2003. DNA damage activates ATM through intermolecular autophosphorylation and dimer dissociation. *Nature*. 421:499-506.

Bálint, E.-É., J. Petres, M. Szabó, C.-K. Orbán, L. Szilágyi, and B. Ábrahám. 2013. Fluorescence of a Histidine-Modified Enhanced Green Fluorescent Protein (EGFP) Effectively Quenched by Copper(II) Ions. *J Fluoresc*. 23:273-281.

Bansbach, C.E., R. Bétous, C.A. Lovejoy, G.G. Glick, and D. Cortez. 2009. The annealing helicase SMARCAL1 maintains genome integrity at stalled replication forks. *Genes Dev.* 23:2405-2414.

Bao, S., Q. Wu, R.E. McLendon, Y. Hao, Q. Shi, A.B. Hjelmeland, M.W. Dewhirst, D.D. Bigner, and J.N. Rich. 2006. Glioma stem cells promote radioresistance by preferential activation of the DNA damage response. *Nature*. 444:756-760.

Barlow, C., C. Ribaut-Barassin, T.A. Zwingman, A.J. Pope, K.D. Brown, J.W. Owens, D. Larson, E.A. Harrington, A.-M. Haeberle, J. Mariani, M. Eckhaus, K. Herrup, Y. Bailly, and A. Wynshaw-Boris. 2000. ATM is a cytoplasmic protein in mouse brain required to prevent lysosomal accumulation. *Proc. Natl. Acad. Sci.* 97:871-876.

Bartek, J., J. Bartkova, and J. Lukas. 2007. DNA damage signalling guards against activated oncogenes and tumour progression. *Oncogene*. 26:7773-7779.

Bartek, J., J. Falck, and J. Lukas. 2001. Chk2 kinase-a busy messenger. *Nat. Rev. Mol. Cell Biol.* 2:877-886.

Bartek, J., C. Lukas, and J. Lukas. 2004. Checking on DNA damage in S phase. *Nat. Rev. Mol. Cell Biol.* 5:792-804.

Bartek, J., and J. Lukas. 2001. Mammalian G1- and S-phase checkpoints in response to DNA damage. *Curr. Opin. Cell Biol.* 13:738-747.

Bartek, J., and J. Lukas. 2007. DNA damage checkpoints: from initiation to recovery or adaptation. *Curr. Opin. Cell Biol.* 19:238-245.

Bartkova, J., Z. Horejsi, K. Koed, A. Kramer, F. Tort, K. Zieger, P. Guldberg, M. Sehested, J.M. Nesland, C. Lukas, T. Orntoft, J. Lukas, and J. Bartek. 2005. DNA damage response as a candidate anti-cancer barrier in early human tumorigenesis. *Nature*. 434:864-870.

Bartkova, J., N. Rezaei, M. Liontos, P. Karakaidos, D. Kletsas, N. Issaeva, L.-V.F. Vassiliou, E. Kolettas, K. Niforou, V.C. Zoumpourlis, M. Takaoka, H. Nakagawa, F. Tort, K. Fugger, F. Johansson, M. Sehested, C.L. Andersen, L. Dyrskjot, T. Orntoft, J. Lukas, C. Kittas, T. Helleday, T.D. Halazonetis, J. Bartek, and V.G. Gorgoulis. 2006. Oncogene-induced senescence is part of the tumorigenesis barrier imposed by DNA damage checkpoints. *Nature*. 444:633-637.

Bassett, E., N.M. King, M.F. Bryant, S. Hector, L. Pendyala, S.G. Chaney, and M. Cordeiro-Stone. 2004. The Role of DNA Polymerase η in Translesion Synthesis Past Platinum–DNA Adducts in Human Fibroblasts. *Cancer Res.* 64:6469-6475.

Bell, D., J. Varley, T. Szydlo, D. Kang, D. Wahrer, K. Shannon, M. Lubratovich, S. Verselis, K. Isselbacher, J. Fraumeni, J. Birch, F. Li, J. Garber, and D. Haber. 1999. Heterozygous germ line hCHK2 mutations in Li-Fraumeni syndrome. *Science*. 286:2528-2531.

Bentley, N.J., D.A. Holtzman, G. Flaggs, K.S. Keegan, A. DeMaggio, J.C. Ford, M. Hoekstra, and A.M. Carr. 1996. The Schizosaccharomyces pombe rad3 checkpoint gene. *EMBO J.* 15:6641-6651.

Berger, M.F., E. Hodis, T.P. Heffernan, Y.L. Deribe, M.S. Lawrence, A. Protopopov, E. Ivanova, I.R. Watson, E. Nickerson, P. Ghosh, H. Zhang, R. Zeid, X. Ren, K. Cibulskis, A.Y. Sivachenko, N. Wagle, A. Sucker, C. Sougnez, R. Onofrio, L. Ambrogio, D. Auclair, T. Fennell, S.L. Carter, Y. Drier, P. Stojanov, M.A. Singer, D. Voet, R. Jing, G. Saksena, J. Barretina, A.H. Ramos, T.J. Pugh, N. Stransky, M. Parkin, W. Winckler, S. Mahan, K. Ardlie, J. Baldwin, J. Wargo, D. Schadendorf, M. Meyerson, S.B. Gabriel, T.R. Golub, S.N. Wagner, E.S. Lander, G. Getz, L. Chin, and L.A. Garraway. 2012. Melanoma genome sequencing reveals frequent PREX2 mutations. *Nature*. 485:502-506.

Bhatia, S., S.S. Tykodi, and J.A. Thompson. 2009. Treatment of Metastatic Melanoma: An Overview. *Oncology*. 23:488-496.

Bhawan, J. 1997. Mel-5: a novel antibody for differential diagnosis of epidermal pigmented lesions of the skin in paraffin-embedded sections. *Melanoma Res.* 7:43-48.

Bienko, M., C.M. Green, S. Sabbioneda, N. Crosetto, I. Matic, R.G. Hibbert, T. Begovic, A. Niimi, M. Mann, A.R. Lehmann, and I. Dikic. 2010. Regulation of Translesion Synthesis DNA Polymerase eta by Monoubiquitination. *Mol. Cell*. 37:396-407.

Biertumpfel, C., Y. Zhao, Y. Kondo, S. Ramon-Maiques, M. Gregory, J.Y. Lee, C. Masutani, A.R. Lehmann, F. Hanaoka, and W. Yang. 2010. Structure and mechanism of human DNA polymerase. *Nature*. 465:1044-1048.

Blasius, M., J. Forment, N. Thakkar, S. Wagner, C. Choudhary, and S. Jackson. 2011. A phospho-proteomic screen identifies substrates of the checkpoint kinase Chk1. *Genome Biology*. 12:R78.

Boehrs, J.K., J. He, M.-J. Halaby, and D.-Q. Yang. 2007. Constitutive expression and cytoplasmic compartmentalization of ATM protein in differentiated human neuron-like SH-SY5Y cells. *J. Neurochem.* 100:337-345.

Boudsocq, F., R.J. Kokoska, B.S. Plosky, A. Vaisman, H. Ling, T.A. Kunkel, W. Yang, and R. Woodgate. 2004. Investigating the Role of the Little Finger Domain of Y-family DNA Polymerases in Low Fidelity Synthesis and Translesion Replication. *J. Biol. Chem.* 279:32932-32940.

Boulton, S., A. Anderson, H. Swalwell, J.R. Henderson, P. Manning, and M.A. Birch-Machin. 2011. Implications of using the fluorescent probes, dihydrorhodamine 123 and 2′,7′-dichlorodihydrofluorescein diacetate, for the detection of UVA-induced reactive oxygen species. *Free Radic. Res.* 45:115-122.

Boulton, S.J. 2010. DNA repair: Decision at the break point. *Nature*. 465:301-302.

Boulton, T.G., S.H. Nye, D.J. Robbins, N.Y. Ip, E. Radzlejewska, S.D. Morgenbesser, R.A. DePinho, N. Panayotatos, M.H. Cobb, and G.D. Yancopoulos. 1991. ERKs: A family of protein-serine/threonine kinases that are activated and tyrosine phosphorylated in response to insulin and NGF. *Cell*. 65:663-675.

Branzei, D., and M. Foiani. 2010. Maintaining genome stability at the replication fork. *Nat. Rev. Mol. Cell Biol.* 11:208-219.

Brash, D.E., J.A. Rudolph, J.A. Simon, A. Lin, G.J. McKenna, H.P. Baden, A.J. Halperin, and J. Ponten. 1991. A role for sunlight in skin cancer: UV-induced p53 mutations in squamous cell carcinoma. *Proc. Natl. Acad. Sci. U. S. A.* 88:10124-10128.

Brown, E.J., and D. Baltimore. 2000. ATR disruption leads to chromosomal fragmentation and early embryonic lethality. *Genes Dev.* 14:397-402.

Bruls, W.A.G., H. Slaper, J.C. Van Der Leun, and L. Berrens. 1984. Transmission of human epidermis and stratum corneum as a function of the thickness in the ultraviolet and visable wavelengths *Photochem. Photobiol.* 40:485-494.

Bunz, F., A. Dutriaux, C. Lengauer, T. Waldman, S. Zhou, J. Brown, J. Sedivy, K. Kinzler, and B. Vogelstein. 1998. Requirement for p53 and p21 to sustain G2 arrest after DNA damage. *Science*. 282:1497-1501.

Burma, S., B. Chen, M. Murphy, A. Kurimasa, and D. Chen. 2001. ATM phosphorylates histone H2AX in response to DNA double-strand breaks. *J. Biol. Chem.* 276:42462 - 42467.

Burrell, R.A., S.E. McClelland, D. Endesfelder, P. Groth, M.-C. Weller, N. Shaikh, E. Domingo, N. Kanu, S.M. Dewhurst, E. Gronroos, S.K. Chew, A.J. Rowan, A. Schenk, M. Sheffer, M. Howell, M. Kschischo, A. Behrens, T. Helleday, J. Bartek, I.P. Tomlinson, and C. Swanton. 2013. Replication stress links structural and numerical cancer chromosomal instability. *Nature*. 494:492-496.

Busby, E.C., D.F. Leistritz, R.T. Abraham, L.M. Karnitz, and J.N. Sarkaria. 2000. The Radiosensitizing Agent 7-Hydroxystaurosporine (UCN-01) Inhibits the DNA Damage Checkpoint Kinase hChk1. *Cancer Res.* 60:2108-2112.

Byun, T.S., M. Pacek, M.-C. Yee, J.C. Walter, and K.A. Cimprich. 2005. Functional uncoupling of MCM helicase and DNA polymerase activities activates the ATR-dependent checkpoint. *Genes Dev.* 19:1040-1052.

Cadet, J., T. Douki, J.-L. Ravanat, and P. Di Mascio. 2009. Sensitized formation of oxidatively generated damage to cellular DNA by UVA radiation. *Photochem. Photobiol. Sci.* 8:903-911.

Cahill, D.P., K.W. Kinzler, B. Vogelstein, and C. Lengauer. 1999. Genetic instability and darwinian selection in tumours. *Trends Cell Biol.* 9:M57-M60.

Carsberg, C.J., K.T. Jones, G.R. Sharpe, and P.S. Friedmann. 1995. Intracellular calcium modulates the responses of human melanocytes to melanogenic stimuli. *J. Dermatol. Sci.* 9:157-164.

Cayrol, C., M. Knibiehler, and B. Ducommun. 1998. p21 binding to PCNA causes G1 and G2 cell cycle arrest in p53-deficient cells. *Oncogene*. 16:311-320.

Cecchini, S., C. Masson, C. La Madeleine, M.A. Huels, L. Sanche, J.R. Wagner, and D.J. Hunting. 2005. Interstrand Cross-Link Induction by UV Radiation in Bromodeoxyuridine-Substituted DNA: Dependence on DNA Conformation. *Biochemistry*. 44:16957-16966.

Centore, Richard C., Stephanie A. Yazinski, A. Tse, and L. Zou. 2012. Spartan/C1orf124, a Reader of PCNA Ubiquitylation and a Regulator of UV-Induced DNA Damage Response. *Mol. Cell*. 46:625-635.

Chakraborty, A., A. Slominski, G. Ermak, J. Hwang, and J. Pawelek. 1995. Ultraviolet B and Melanocyte-Stimulating Hormone (MSH) Stimulate mRNA Production for alpha-MSH Receptors and Proopiomelanocortin-Derived Peptides in Mouse Melanoma Cells and Transformed Keratinocytes. *J. Invest. Dermatol.* 105:655-659.

Chen, C.-L., Y.-T. Hsieh, and H.-C. Chen. 2007. Phosphorylation of adducin by protein kinase Cδ promotes cell motility. *J. Cell Sci.* 120:1157-1167.

Chen, M.-S., C.E. Ryan, and H. Piwnica-Worms. 2003. Chk1 Kinase Negatively Regulates Mitotic Function of Cdc25A Phosphatase through 14-3-3 Binding. *Mol. Cell. Biol.* 23:7488-7497.

Chen, P., C. Luo, Y. Deng, K. Ryan, J. Register, S. Margosiak, A. Tempczyk-Russell, B. Nguyen, P. Myers, K. Lundgren, C.-C. Kan, and P.M. O'Connor. 2000. Implications for Chk1 Regulation: The 1.7 Å Crystal Structure of Human Cell Cycle Checkpoint Kinase Chk1. *Cell*. 100:681-692.

Chen, Y.-w., J.E. Cleaver, F. Hanaoka, C.-f. Chang, and K.-m. Chou. 2006. A Novel Role of DNA Polymerase η in Modulating Cellular Sensitivity to Chemotherapeutic Agents. *Mol. Cancer Res.* 4:257-265.

Chen, Y., and Y. Sanchez. 2004. Chk1 in the DNA damage response: conserved roles from yeasts to mammals. *DNA Repair*. 3:1025-1032.

Cheng, K.C., D.S. Cahill, H. Kasai, S. Nishimura, and L.A. Loeb. 1992. 8-Hydroxyguanine, an abundant form of oxidative DNA damage, causes G----T and A----C substitutions. *J. Biol. Chem.* 267:166-172.

Chini, C.C.S., and J. Chen. 2003. Human Claspin Is Required for Replication Checkpoint Control. *J. Biol. Chem.* 278:30057-30062.

Chou, W.C., M. Takeo, P. Rabbani, H. Hu, W. Lee, Y.R. Chung, J. Carucci, P. Overbeek, and M. Ito. 2013. Direct migration of follicular melanocyte stem cells to the epidermis after wounding or UVB irradiation is dependent on Mc1r signaling. *Nat. Med.* 19:924-929.

Ciccia, A., A.L. Bredemeyer, M.E. Sowa, M.-E. Terret, P.V. Jallepalli, J.W. Harper, and S.J. Elledge. 2009. The SIOD disorder protein SMARCAL1 is an RPA-interacting protein involved in replication fork restart. *Genes Dev.*

Ciccia, A., Amitabh V. Nimonkar, Y. Hu, I. Hajdu, Yathish J. Achar, L. Izhar, Sarah A. Petit, B. Adamson, John C. Yoon, Stephen C. Kowalczykowski, David M. Livingston, L. Haracska, and Stephen J. Elledge. 2012. Polyubiquitinated PCNA Recruits the ZRANB3 Translocase to Maintain Genomic Integrity after Replication Stress. *Mol. Cell*. 47:396-409.

CIE Standard. 1998. Erythema reference action spectrum and standard erythema dose. *CIE S 007/E-1998.* Commission Internationale de l'EEclairage, Vienna.

Cimprich, K.A., and D. Cortez. 2008. ATR: an essential regulator of genome integrity. *Nat. Rev. Mol. Cell Biol.* 9:616-627.

Cimprich, K.A., T.B. Shin, C.T. Keith, and S.L. Schreiber. 1996. cDNA cloning and gene mapping of a candidate human cell cycle checkpoint protein. *Proc. Natl. Acad. Sci.* 93:2850-2855.

Cleaver, J.E. 1972. Xeroderma pigmentosum: variants with normal DNA repair and normal sensitivity to ultraviolet light *J. Invest. Dermatol.* 58:124-128.

Cleaver, J.E. 2011. γH2Ax: Biomarker of Damage or Functional Participant in DNA Repair "All that Glitters Is not Gold!". *Photochem. Photobiol.* 87:1230-1239.

Cleaver, J.E., V. Afzal, L. Feeney, M. McDowell, W. Sadinski, J.P.G. Volpe, D.B. Busch, D.M. Coleman, D.W. Ziffer, Y. Yu, H. Nagasawa, and J.B. Little. 1999. Increased Ultraviolet Sensitivity

and Chromosomal Instability Related to P53 Function in the Xeroderma Pigmentosum Variant. *Cancer Res.* 59:1102-1108.

Cleaver, J.E., and D. Bootsma. 1975. Xeroderma pigmentosum: Biochemical and Genetic characteristics *Annu. Rev. Genet.* 9:19-38.

Cook, A.L., P.D. Donatien, A.G. Smith, M. Murphy, M.K. Jones, M. Herlyn, D.C. Bennett, J.H. Leonard, and R.A. Sturm. 2003. Human Melanoblasts in Culture: Expression of BRN2 and Synergistic Regulation by Fibroblast Growth Factor-2, Stem Cell Factor, and Endothelin-3. *J. Invest. Dermatol.* 121:1150-1159.

Cordonnier, A.M., and R.P.P. Fuchs. 1999. Replication of damaged DNA: molecular defect in Xeroderma pigmentosum variant cells. *Mutat. Res.* 435:111-119.

Cortat, B., C.C.M. Garcia, A. Quinet, A.P. Schuch, K.M. de Lima-Bessa, and C.F.M. Menck. 2013. The relative roles of DNA damage induced by UVA irradiation in human cells. *Photochem. Photobiol. Sci.*

Cortez, D., S. Guntuku, J. Qin, and S.J. Elledge. 2001. ATR and ATRIP: Partners in Checkpoint Signaling. *Science*. 294:1713-1716.

Cosentino, C., D. Grieco, and V. Costanzo. 2011. ATM activates the pentose phosphate pathway promoting anti-oxidant defence and DNA repair. *EMBO J.* 30:546-555.

Costanzo, V., K. Robertson, C.Y. Ying, E. Kim, E. Avvedimento, M. Gottesman, D. Grieco, and J. Gautier. 2000. Reconstitution of an ATM-Dependent Checkpoint that Inhibits Chromosomal DNA Replication following DNA Damage. *Mol. Cell*. 6:649-659.

Costin, G.-E., and V.J. Hearing. 2007. Human skin pigmentation: melanocytes modulate skin color in response to stress. *FASEB J.* 21:976-994.

Courdavault, S., C. Baudouin, M. Charveron, A. Favier, J. Cadet, and T. Douki. 2004. Larger yield of cyclobutane dimers than 8-oxo-7,8-dihydroguanine in the DNA of UVA-irradiated human skin cells. *Mutat. Res.* 556:135-142.

Crombie, I. 1979. Racial differences in melanoma incidence. *Br. J. Cancer*. 40:185-193.

Cruet-Hennequart, S., S. Coyne, M.T. Glynn, G.G. Oakley, and M.P. Carty. 2006. UV-induced RPA phosphorylation is increased in the absence of DNA polymerase η and requires DNA-PK. *DNA Repair*. 5:491-504.

Cruet-Hennequart, S., K. Gallagher, A.M. Sokol, S. Villalan, A.M. Prendergast, and M.P. Carty. 2010. DNA polymerase eta, a key protein in translesion synthesis in human cells. *Subcell. Biochem.* 50:189-209.

Cruet-Hennequart, S., M.T. Glynn, L.S. Murillo, S. Coyne, and M.P. Carty. 2008. Enhanced DNA-PK-mediated RPA2 hyperphosphorylation in DNA polymerase eta-deficient human cells treated with cisplatin and oxaliplatin. *DNA Repair (Amst)*. 7:582-596.

D'Errico, M., A. Calcagnile, F. Canzona, B. Didona, P. Posteraro, R. Cavalieri, R. Corona, I. Vorechovsky, T. Nardo, M. Stefanini, and E. Dogliotti. 2000. UV mutation signature in tumor suppressor genes

involved in skin carcinogenesis in xeroderma pigmentosum patients. *Oncogene*. 19:463-367.

Davies, A.A., D. Huttner, Y. Daigaku, S. Chen, and H.D. Ulrich. 2008. Activation of Ubiquitin-Dependent DNA Damage Bypass Is Mediated by Replication Protein A. *Mol. Cell*. 29:625-636.

Davies, H., G.R. Bignell, C. Cox, P. Stephens, S. Edkins, S. Clegg, J. Teague, H. Woffendin, M.J. Garnett, W. Bottomley, N. Davis, E. Dicks, R. Ewing, Y. Floyd, K. Gray, S. Hall, R. Hawes, J. Hughes, V. Kosmidou, A. Menzies, C. Mould, A. Parker, C. Stevens, S. Watt, S. Hooper, R. Wilson, H. Jayatilake, B.A. Gusterson, C. Cooper, J. Shipley, D. Hargrave, K. Pritchard-Jones, N. Maitland, G. Chenevix-Trench, G.J. Riggins, D.D. Bigner, G. Palmieri, A. Cossu, A. Flanagan, A. Nicholson, J.W.C. Ho, S.Y. Leung, S.T. Yuen, B.L. Weber, H.F. Seigler, T.L. Darrow, H. Paterson, R. Marais, C.J. Marshall, R. Wooster, M.R. Stratton, and P.A. Futreal. 2002. Mutations of the BRAF gene in human cancer. *Nature*. 417:949-954.

Davis, E.J., C. Lachaud, P. Appleton, T.J. Macartney, I. Näthke, and J. Rouse. 2012. DVC1 (C1orf124) recruits the p97 protein segregase to sites of DNA damage. *Nat Struct Mol Biol*. 19:1093-1100.

Day, T.A., K. Palle, L.R. Barkley, N. Kakusho, Y. Zou, S. Tateishi, A. Verreault, H. Masai, and C. Vaziri. 2010. Phosphorylated Rad18 directs DNA Polymerase η to sites of stalled replication. *J. Cell. Biol.* 191:953-966.

De Fabo, E.C., F.P. Noonan, T. Fears, and G. Merlino. 2004. Ultraviolet B but not Ultraviolet A Radiation Initiates Melanoma. *Cancer Res.* 64:6372-6376.

de Gruijl, F.R. 1999. Skin cancer and solar UV radiation. *Eur. J. Cancer*. 35:2003-2009.

de Gruijl, F.R., H.J.C.M. Sterenborg, P.D. Forbes, R.E. Davies, C. Cole, G. Kelfkens, H. van Weelden, H. Slaper, and J.C. van der Leun. 1993. Wavelength Dependence of Skin Cancer Induction by Ultraviolet Irradiation of Albino Hairless Mice. *Cancer Res.* 53:53-60.

de Gruijl, F.R., H.J. van Kranen, and L.H.F. Mullenders. 2001. UV-induced DNA damage, repair, mutations and oncogenic pathways in skin cancer. *J. Photochem. Photobiol. B.* 63:19-27.

de Laat, A., J.C. van der Leun, and F.R. de Gruijl. 1997. Carcinogenesis induced by UVA (365-nm) radiation: the dose-time dependence of tumor formation in hairless mice. *Carcinogenesis*. 18:1013-1020.

de Laat, A., M. van Tilburg, J.C. van der Leun, W.A. van Vloten, and F.R. de Gruijl. 1996. Cell Cycle Kinetics Following UVA Irradiation in Comparison to UVB and UVC Irradiation. *Photochem. Photobiol.* 63:492-497.

de Leeuw, S., S. Janssen, J. Simons, P. Lohman, B. Vermeer, and A. Schothorst. 1994. The UV action spectra for the clone-forming ability of cultured human melanocytes and keratinocytes. *Photochem Photobiol.* 59:430-436.

Dell'Angelica, E.C. 2003. Melanosome biogenesis: shedding light on the origin of an obscure organelle. *Trends Cell Biol.* 13:503-506.

Despras, E., F. Daboussi, O. Hyrien, K. Marheineke, and P.L. Kannouche. 2010. ATR/Chk1 pathway is essential for resumption of DNA

synthesis and cell survival in UV-irradiated XP variant cells. *Hum. Mol. Genet.* 19:1690-1671.

Devi, S., R. Kedlaya, N. Maddodi, K.M.R. Bhat, C.S. Weber, H. Valdivia, and V. Setaluri. 2009. Calcium homeostasis in human melanocytes: role of transient receptor potential melastatin 1 (TRPM1) and its regulation by ultraviolet light. *Am. J. Physiol.* 297:C679-C687.

Di Lucca, J., M. Guedj, J.-J. Lacapère, M.C. Fargnoli, A. Bourillon, P. Dieudé, N. Dupin, P. Wolkenstein, P. Aegerter, P. Saiag, V. Descamps, C. Lebbe, N. Basset-Seguin, K. Peris, B. Grandchamp, and N. Soufir. 2009. Variants of the xeroderma pigmentosum variant gene (POLH) are associated with melanoma risk. *Eur. J. Cancer*. 45:3228-3236.

Di Micco, R., M. Fumagalli, A. Cicalese, S. Piccinin, P. Gasparini, C. Luise, C. Schurra, M. Garre, P. Giovanni Nuciforo, A. Bensimon, R. Maestro, P. Giuseppe Pelicci, and F. d'Adda di Fagagna. 2006. Oncogene-induced senescence is a DNA damage response triggered by DNA hyper-replication. *Nature*. 444:638-642.

Diffey, B.L. 2002. Sources and measurement of ultraviolet radiation. *Methods*. 28:4-13.

DiGiovanna, J.J., and K.H. Kraemer. 2012. Shining a Light on Xeroderma Pigmentosum. *J. Invest. Dermatol.* 132:785-796.

Ding, Q., Y.V.R. Reddy, W. Wang, T. Woods, P. Douglas, D.A. Ramsden, S.P. Lees-Miller, and K. Meek. 2003. Autophosphorylation of the Catalytic Subunit of the DNA-Dependent Protein Kinase Is Required for Efficient End Processing during DNA Double-Strand Break Repair. *Mol. Cell. Biol.* 23:5836-5848.

DiPaola, R.S. 2002. To Arrest or Not To G2-M Cell-Cycle Arrest : Commentary re: A. K. Tyagi et al., Silibinin Strongly Synergizes Human Prostate Carcinoma DU145 Cells to Doxorubicin-induced Growth Inhibition, G2-M Arrest, and Apoptosis. Clin. Cancer Res., 8: 3512–3519, 2002. *Clin. Cancer Res.* 8:3311-3314.

Douki, T., and J. Cadet. 2001. Individual Determination of the Yield of the Main UV-Induced Dimeric Pyrimidine Photoproducts in DNA Suggests a High Mutagenicity of CC Photolesions. *Biochemistry*. 40:2495-2501.

Douki, T., M. Court, S. Sauvaigo, F. Odin, and J. Cadet. 2000. Formation of the Main UV-induced Thymine Dimeric Lesions within Isolated and Cellular DNA as Measured by High Performance Liquid Chromatography-Tandem Mass Spectrometry. *J. Biol. Chem.* 275:11678-11685.

Douki, T., A. Reynaud-Angelin, J. Cadet, and E. Sage. 2003. Bipyrimidine Photoproducts Rather than Oxidative Lesions Are the Main Type of DNA Damage Involved in the Genotoxic Effect of Solar UVA Radiation *Biochemistry*. 42:9221-9226.

Drobetsky, E.A., J. Turcotte, and A. Châteauneuf. 1995. A role for ultraviolet A in solar mutagenesis. *Proc. Natl. Acad. Sci.* 92:2350-2354.

Dumstorf, C.A., A.B. Clark, Q. Lin, G.E. Kissling, T. Yuan, R. Kucherlapati, W.G. McGregor, and T.A. Kunkel. 2006. Participation of mouse DNA polymerase ι in strand-biased mutagenic bypass of

UV photoproducts and suppression of skin cancer. *Proc. Natl. Acad. Sci.* 103:18083-18088.

Eckert, R.L., J.F. Crish, and N.A. Robinson. 1997. The epidermal keratinocyte as a model for the study of gene regulation and cell differentiation. *Physiol. Rev.* 77:397-424.

El Ghissassi, F., R. Baan, K. Straif, Y. Grosse, B. Secretan, V. Bouvard, L. Benbrahim-Tallaa, N. Guha, C. Freeman, L. Galichet, and V. Cogliano. 2009. A review of human carcinogens-Part D: radiation. *Lancet Oncol.* 10:751-752.

Elledge, S.J. 1996. Cell Cycle Checkpoints: Preventing an Identity Crisis. *Science*. 274:1664-1672.

Eller, M.S., K. Ostrom, and B.A. Gilchrest. 1996. DNA damage enhances melanogenesis. *Proc. Natl. Acad. Sci.* 93:1087-1092.

Elmore, S. 2007. Apoptosis: A Review of Programmed Cell Death. *Toxicol. Pathol.* 35:495-516.

Falck, J., N. Mailand, R.G. Syljuasen, J. Bartek, and J. Lukas. 2001. The ATM-Chk2-Cdc25A checkpoint pathway guards against radioresistant DNA synthesis. *Nature*. 410:842-847.

Feng, W., S.C. Di Rienzi, M.K. Raghuraman, and B.J. Brewer. 2011. Replication Stress-Induced Chromosome Breakage Is Correlated with Replication Fork Progression and Is Preceded by Single-Stranded DNA Formation. *G3: Genes, Genomes, Genetics*. 1:327-335.

Fernandez, A.A., L. Paniker, R. Garcia, and D.L. Mitchell. 2012. Recent advances in sunlight-induced carcinogenesis using the Xiphophorus melanoma model. *Comp. Biochem. Physiol. C*. 155:64-70.

Fitzpatrick, T., and A. Breathnach. 1963. The epidermal melanin unit system *Dermatol Wochenschr.* 147:481-489.

Fitzpatrick, T.B. 1988. THe validity and practicality of sun-reactive skin types i through vi. *Arch. Dermatol.* 124:869-871.

Freeman, S.E., H. Hacham, R.W. Gange, D.J. Maytum, J.C. Sutherland, and B.M. Sutherland. 1989. Wavelength dependence of pyrimidine dimer formation in DNA of human skin irradiated in situ with ultraviolet light. *Proc. Natl. Acad. Sci.* 86:5605-5609.

Friedmann, P., and B. Gilchrest. 1987. Ultraviolet radiation directly induces pigment production by cultured human melanocytes. *J. Cell. Physiol.* 133:88-94.

Frosina, G., P. Fortini, O. Rossi, F. Carrozzino, G. Raspaglio, L.S. Cox, D.P. Lane, A. Abbondandolo, and E. Dogliotti. 1996. Two Pathways for Base Excision Repair in Mammalian Cells. *J. Biol. Chem.* 271:9573-9578.

Fu, D., F.D. Dudimah, J. Zhang, A. Pickering, J. Paneerselvam, M. Palrasu, H. Wang, and P. Fei. 2013. Recruitment of DNA polymerase eta by FANCD2 in the early response to DNA damage. *Cell Cycle*. 12:803-809.

Galluzzi, L., L. Senovilla, I. Vitale, J. Michels, I. Martins, O. Kepp, M. Castedo, and G. Kroemer. 2012. Molecular mechanisms of cisplatin resistance. *Oncogene*. 31:1869-1883.

Garbe, C., and T. Eigentler. 2007. Diagnosis and treatment of cutaneous melanoma: state of the art 2006. *Melanoma Res.* 17:117-127.

Gatei, M., S.P. Scott, I. Filippovitch, N. Soronika, M.F. Lavin, B. Weber, and K.K. Khanna. 2000. Role for ATM in DNA Damage-induced Phosphorylation of BRCA1. *Cancer Res.* 60:3299-3304.

Gatei, M., K. Sloper, C. Sörensen, R. Syljuäsen, J. Falck, K. Hobson, K. Savage, J. Lukas, B.-B. Zhou, J. Bartek, and K.K. Khanna. 2003. Ataxia-telangiectasia-mutated (ATM) and NBS1-dependent Phosphorylation of Chk1 on Ser-317 in Response to Ionizing Radiation. *J. Biol. Chem.* 278:14806-14811.

Gehen, S.C., R.J. Staversky, R.A. Bambara, P.C. Keng, and M.A. O'Reilly. 2008. hSMG-1 and ATM sequentially and independently regulate the G1 checkpoint during oxidative stress. *Oncogene*. 27:4065-4074.

Ghosal, G., and J. Chen. 2013. DNA damage tolerance: a double-edged sword guarding the genome. *Trans. Cancer Res.* 2:107-129.

Gilchrest, B.A., H.-Y. Park, M.S. Eller, and M. Yaar. 1996. Mechanisms of Ultraviolet Light-Induced Pigmentation. *Photochem. Photobiol.* 63:1-10.

Girard, P.-M., M. Pozzebon, F. Delacôte, T. Douki, V. Smirnova, and E. Sage. 2008. Inhibition of S-phase progression triggered by UVA-induced ROS does not require a functional DNA damage checkpoint response in mammalian cells. *DNA Repair*. 7:1500-1516.

Girard, P.M., S. Francesconi, M. Pozzebon, D. Graindorge, P. Rochette, R. Drouin, and E. Sage. 2011. UVA-induced damage to DNA and proteins: direct versus indirect photochemical processes. *Journal of Physics: Conference Series*. 261:012002.

Godar, D.E., R.J. Landry, and A.D. Lucas. 2009. Increased UVA exposures and decreased cutaneous Vitamin D3 levels may be responsible for the increasing incidence of melanoma. *Med. Hypotheses*. 72:434-443.

Göhler, T., S. Sabbioneda, C.M. Green, and A.R. Lehmann. 2011. ATR-mediated phosphorylation of DNA polymerase η is needed for efficient recovery from UV damage. *J. Cell. Biol.* 192:219-227.

Golding, S.E., E. Rosenberg, N. Valerie, I. Hussaini, M. Frigerio, X.F. Cockcroft, W.Y. Chong, M. Hummersone, L. Rigoreau, K.A. Menear, M.J. O'Connor, L.F. Povirk, T. van Meter, and K. Valerie. 2009. Improved ATM kinase inhibitor KU-60019 radiosensitizes glioma cells, compromises insulin, AKT and ERK prosurvival signaling, and inhibits migration and invasion. *Mol. Cancer Ther.* 8:2894-2902.

Goodarzi, A.A., J.C. Jonnalagadda, P. Douglas, D. Young, R. Ye, G.B.G. Moorhead, S.P. Lees-Miller, and K.K. Khanna. 2004. Autophosphorylation of ataxia-telangiectasia mutated is regulated by protein phosphatase 2A. *EMBO J.* 23:4451-4461.

Gorgoulis, V.G., L.-V.F. Vassiliou, P. Karakaidos, P. Zacharatos, A. Kotsinas, T. Liloglou, M. Venere, R.A. DiTullio, N.G. Kastrinakis, B. Levy, D. Kletsas, A. Yoneta, M. Herlyn, C. Kittas, and T.D. Halazonetis. 2005. Activation of the DNA damage checkpoint and genomic instability in human precancerous lesions. *Nature*. 434:907-913.

Gottlieb, T.M., and S.P. Jackson. 1993. The DNA-dependent protein kinase: Requirement for DNA ends and association with Ku antigen. *Cell*. 72:131-142.

Graves, P.R., L. Yu, J.K. Schwarz, J. Gales, E.A. Sausville, P.M. O'Connor, and H. Piwnica-Worms. 2000. The Chk1 Protein Kinase and the Cdc25C Regulatory Pathways Are Targets of the Anticancer Agent UCN-01. *J. Biol. Chem.* 275:5600-5605.

Greinert, R., B. Volkmer, S. Henning, E.W. Breitbart, K.O. Greulich, M.C. Cardoso, and A. Rapp. 2012. UVA-induced DNA double-strand breaks result from the repair of clustered oxidative DNA damages. *Nucleic Acids Res.*

Gschwendt, M., S. Dieterich, J. Rennecke, W. Kittstein, H.-J. Mueller, and F.-J. Johannes. 1996. Inhibition of protein kinase C μ by various inhibitors. Inhibition from protein kinase c isoenzymes. *FEBS Lett.* 392:77-80.

Gschwendt, M., H.J. Muller, K. Kielbassa, R. Zang, W. Kittstein, G. Rincke, and F. Marks. 1994. Rottlerin, a Novel Protein Kinase Inhibitor. *Biochem. Biophys. Res. Commun.* 199:93-98.

Guo, Z., R. Deshpande, and T.T. Paull. 2010a. ATM activation in the presence of oxidative stress *Cell Cycle*. 9:4805-4811.

Guo, Z., S. Kozlov, M.F. Lavin, M.D. Person, and T.T. Paull. 2010b. ATM Activation by Oxidative Stress. *Science*. 330:517-521.

Gupta, A., G.G. Sharma, C.S.H. Young, M. Agarwal, E.R. Smith, T.T. Paull, J.C. Lucchesi, K.K. Khanna, T. Ludwig, and T.K. Pandita. 2005. Involvement of Human MOF in ATM Function. *Mol. Cell. Biol.* 25:5292-5305.

Halaban, R., S.H. Pomerantz, S. Marshall, D.T. Lambert, and A.B. Lerner. 1983. Regulation of tyrosinase in human melanocytes grown in culture. *J. Cell. Biol.* 97:480-488.

Hanahan, D., and R.A. Weinberg. 2000. The Hallmarks of Cancer. *Cell*. 100:57-70.

Hanahan, D., and Robert A. Weinberg. 2011. Hallmarks of Cancer: The Next Generation. *Cell*. 144:646-674.

Haracska, L., S. Prakash, and L. Prakash. 2000a. Replication pastO 6-Methylguanine by Yeast and Human DNA Polymerase η. *Mol. Cell. Biol.* 20:8001-8007.

Haracska, L., S.-L. Yu, R.E. Johnson, L. Prakash, and S. Prakash. 2000b. Efficient and accurate replication in the presence of 7,8-dihydro-8-oxoguanine by DNA polymerase [eta]. *Nat. Genet.* 25:458-461.

Harbour, J.W., R.X. Luo, A.D. Santi, A.A. Postigo, and D.C. Dean. 1999. Cdk Phosphorylation Triggers Sequential Intramolecular Interactions that Progressively Block Rb Functions as Cells Move through G1. *Cell*. 98:859-869.

Hartwell, L., and T. Weinert. 1989. Checkpoints: controls that ensure the order of cell cycle events. *Science*. 246:629-634.

He, Y.Y., J. Pi, J.L. Huang, B.A. Diwan, M.P. Waalkes, and C.F. Chignell. 2006. Chronic UVA irradiation of human HaCaT keratinocytes induces malignant transformation associated with acquired apoptotic resistance. *Oncogene*. 25:3680-3688.

Heffernan, T.P., M. Kawasumi, A. Blasina, K. Anderes, A.H. Conney, and P. Nghiem. 2009. ATR-Chk1 Pathway Inhibition Promotes Apoptosis after UV Treatment in Primary Human Keratinocytes: Potential Basis for the UV Protective Effects of Caffeine. *J. Invest. Dermatol.* 129:1805-1815.

Hendel, A., P.H.L. Krijger, N. Diamant, Z. Goren, P. Langerak, J. Kim, T. Reißner, K.-y. Lee, N.E. Geacintov, T. Carell, K. Myung, S. Tateishi, A. D'Andrea, H. Jacobs, and Z. Livneh. 2011. PCNA Ubiquitination Is Important, But Not Essential for Translesion DNA Synthesis in Mammalian Cells. *PLoS Genet*. 7:e1002262.

Henner, W.D., L.O. Rodriguez, S.M. Hecht, and W.A. Haseltine. 1983. gamma Ray induced deoxyribonucleic acid strand breaks. 3' Glycolate termini. *J. Biol. Chem.* 258:711-713.

Héry, C., L. Tryggvadóttir, T. Sigurdsson, E. Ólafsdóttir, B. Sigurgeirsson, J.G. Jonasson, J.H. Olafsson, M. Boniol, G.B. Byrnes, J.-F. Doré, and P. Autier. 2010. A Melanoma Epidemic in Iceland: Possible Influence of Sunbed Use. *Am. J. Epidemiol.* 172:762-767.

Hodis, E., Ian R. Watson, Gregory V. Kryukov, Stefan T. Arold, M. Imielinski, J.-P. Theurillat, E. Nickerson, D. Auclair, L. Li, C. Place, D. DiCara, Alex H. Ramos, Michael S. Lawrence, K. Cibulskis, A. Sivachenko, D. Voet, G. Saksena, N. Stransky, Robert C. Onofrio, W. Winckler, K. Ardlie, N. Wagle, J. Wargo, K. Chong, Donald L. Morton, K. Stemke-Hale, G. Chen, M. Noble, M. Meyerson, John E. Ladbury, Michael A. Davies, Jeffrey E. Gershenwald, Stephan N. Wagner, Dave S.B. Hoon, D. Schadendorf, Eric S. Lander, Stacey B. Gabriel, G. Getz, Levi A. Garraway, and L. Chin. 2012. A Landscape of Driver Mutations in Melanoma. *Cell*. 150:251-263.

Hoeijmakers, J.H.J. 2001. Genome maintenance mechanisms for preventing cancer. *Nature*. 411:366-374.

Huang, T.T., S.M.B. Nijman, K.D. Mirchandani, P.J. Galardy, M.A. Cohn, W. Haas, S.P. Gygi, H.L. Ploegh, R. Bernards, and A.D. D'Andrea. 2006. Regulation of monoubiquitinated PCNA by DUB autocleavage. *Nat Cell Biol*. 8:341-347.

Huen, M.S.Y., and J. Chen. 2008. The DNA damage response pathways: at the crossroad of protein modifications. *Cell Res.* 18:8-16.

IARC. 2005. Exposure to artificial UV radiation and skin cancer. *Views and expert opinions of an IARC Working Group on Risk of Skin Cancer and Exposure to Artificial Ultraviolet Light that met in Lyon, France,*.

IARC. 2010. GLOBOCAN 2008.

Ikehata, H., K. Kawai, J.-i. Komura, K. Sakatsume, L. Wang, M. Imai, S. Higashi, O. Nikaido, K. Yamamoto, K. Hieda, M. Watanabe, H. Kasai, and T. Ono. 2008. UVA1 Genotoxicity Is Mediated Not by Oxidative Damage but by Cyclobutane Pyrimidine Dimers in Normal Mouse Skin. *J. Invest. Dermatol.* 128:2289-2296.

Im, S., S.K. Hann, Y.K. Park, and H.I. Kim. 1992. Culture of melanocytes obtained from normal and vitiligo subjects. *Yonsei Med. J.* 33:344-350.

Ito, K., A. Hirao, F. Arai, S. Matsuoka, K. Takubo, I. Hamaguchi, K. Nomiyama, K. Hosokawa, K. Sakurada, N. Nakagata, Y. Ikeda,

T.W. Mak, and T. Suda. 2004. Regulation of oxidative stress by ATM is required for self-renewal of haematopoietic stem cells. *Nature*. 431:997-1002.

Jablonski, N.G., and G. Chaplin. 2000. The evolution of human skin coloration. *J. Hum. Evol.* 39:57-106.

Jackson, J.R., A. Gilmartin, C. Imburgia, J.D. Winkler, L.A. Marshall, and A. Roshak. 2000. An Indolocarbazole Inhibitor of Human Checkpoint Kinase (Chk1) Abrogates Cell Cycle Arrest Caused by DNA Damage. *Cancer Res.* 60:566-572.

Jackson, S.P. 2002. Sensing and repairing DNA double-strand breaks. *Carcinogenesis*. 23:687-696.

Jaeger, J., D. Koczan, H.-J. Thiesen, S.M. Ibrahim, G. Gross, R. Spang, and M. Kunz. 2007. Gene Expression Signatures for Tumor Progression, Tumor Subtype, and Tumor Thickness in Laser-Microdissected Melanoma Tissues. *Clin. Cancer Res.* 13:806-815.

Jeong, Y.-T., L. Cermak, M.V. Guijarro, E. Hernando, and M. Pagano. 2013a. FBH1 protects melanocytes from transformation and is deregulated in melanomas. *Cell Cycle*. 12:1128-1132.

Jeong, Y.-T., M. Rossi, L. Cermak, A. Saraf, L. Florens, M.P. Washburn, P. Sung, C.L. Schildkraut, and M. Pagano. 2013b. FBH1 promotes DNA double-strand breakage and apoptosis in response to DNA replication stress. *J. Cell. Biol.* 200:141-149.

Jiang, Y., M. Rabbi, M. Kim, C. Ke, W. Lee, R.L. Clark, P.A. Mieczkowski, and P.E. Marszalek. 2009. UVA Generates Pyrimidine Dimers in DNA Directly. *Biophys. J.* 96:1151-1158.

Johnson, R.E., L. Haracska, S. Prakash, and L. Prakash. 2001. Role of DNA Polymerase η in the Bypass of a (6-4) TT Photoproduct. *Mol. Cell. Biol.* 21:3558-3563.

Johnson, R.E., C.M. Kondratick, S. Prakash, and L. Prakash. 1999a. hRAD30 Mutations in the Variant Form of Xeroderma Pigmentosum. *Science*. 285:263-265.

Johnson, R.E., S. Prakash, and L. Prakash. 1999b. Efficient Bypass of a Thymine-Thymine Dimer by Yeast DNA Polymerase, Poleta. *Science*. 283:1001-1004.

Jung, Y.-S., Y. Qian, and X. Chen. 2012. DNA polymerase eta is targeted by Mdm2 for polyubiquitination and proteasomal degradation in response to ultraviolet irradiation. *DNA Repair*. 11:177-184.

Kannouche, P., B.C. Broughton, M. Volker, F. Hanaoka, L.H.F. Mullenders, and A.R. Lehmann. 2001. Domain structure, localization, and function of DNA polymerase η, defective in xeroderma pigmentosum variant cells. *Genes Dev.* 15:158-172.

Kannouche, P., A.R. Fernandez de Henestrosa, B. Coull, A.E. Vidal, C. Gray, D. Zicha, R. Woodgate, and A.R. Lehmann. 2003. Localization of DNA polymerases eta and iota to the replication machinery is tightly co-ordinated in human cells. *EMBO J.* 22:1223-1233.

Kannouche, P.L., J. Wing, and A.R. Lehmann. 2004. Interaction of Human DNA Polymerase eta with Monoubiquitinated PCNA: A Possible Mechanism for the Polymerase Switch in Response to DNA Damage. *Mol. Cell*. 14:491-500.

Kappes, U.P., D. Luo, M. Potter, K. Schulmeister, and T.M. Runger. 2006. Short- and Long-Wave UV Light (UVB and UVA) Induce Similar Mutations in Human Skin Cells. *J. Invest. Dermatol.* 126:667-675.

Kappes, U.P., and T.M. Runger. 2005. No Major Role for 7,8-Dihydro-8-oxoguanine in Ultraviolet Light-Induced Mutagenesis. *Radiat. Res.* 164:440-445.

Karpenshif, Y., and K.A. Bernstein. 2012. From yeast to mammals: Recent advances in genetic control of homologous recombination. *DNA Repair*. 11:781-788.

Kastan, M.B., and D.-s. Lim. 2000. The many substrates and functions of ATM. *Nat. Rev. Mol. Cell Biol.* 1:179-186.

Kato, R., and H. Ogawa. 1994. An essential gene, ESR1, is required for mitotic growth, DNA repair and meiotic recombination Saccharomyces cerevisiae. *Nucleic Acids Res.* 22:3104-3112.

Kaufmann, W.K. 2010. The human intra-S checkpoint response to UVC-induced DNA damage. *Carcinogenesis*. 31:751-765.

Kaufmann, W.K., T.P. Heffernan, L.M. Beaulieu, S. Doherty, A.R. Frank, Y. Zhou, M.F. Bryant, T. Zhou, D.D. Luche, N. Nikolaishvili-Feinberg, D.A. Simpson, and M. Cordeiro-Stone. 2003. Caffeine and human DNA metabolism: the magic and the mystery. *Mutat. Res.* 532:85-102.

Kaufmann, W.K., and R.S. Paules. 1996. DNA damage and cell cycle checkpoints. *FASEB J.* 10:238-247.

Kauser, S., G.E. Westgate, M.R. Green, and D.J. Tobin. 2011. Human Hair Follicle and Epidermal Melanocytes Exhibit Striking Differences in Their Aging Profile which Involves Catalase. *J. Invest. Dermatol.* 131:979-982.

Kawamoto, T., K. Araki, E. Sonoda, Y.M. Yamashita, K. Harada, K. Kikuchi, C. Masutani, F. Hanaoka, K. Nozaki, N. Hashimoto, and S. Takeda. 2005a. Dual Roles for DNA Polymerase · in Homologous DNA Recombination and Translesion DNA Synthesis. *Mol. Cell*. 20:793-799.

Kawamoto, T., K. Araki, E. Sonoda, Y.M. Yamashita, K. Harada, K. Kikuchi, C. Masutani, F. Hanaoka, K. Nozaki, N. Hashimoto, and S. Takeda. 2005b. Dual Roles for DNA Polymerase η in Homologous DNA Recombination and Translesion DNA Synthesis. *Mol. Cell*. 20:793-799.

Kelfkens, G., F.R. de Gruijl, and J.C. van der Leun. 1991. Tumorigenesis by short-wave ultraviolet A: papillomas versus squamous cell carcinomas. *Carcinogenesis*. 12:1377-1382.

Kemp, M.G., Z. Akan, S. Yilmaz, M. Grillo, S.L. Smith-Roe, T.-H. Kang, M. Cordeiro-Stone, W.K. Kaufmann, R.T. Abraham, A. Sancar, and K. Ünsal-Kaçmaz. 2010. Tipin-Replication Protein A Interaction Mediates Chk1 Phosphorylation by ATR in Response to Genotoxic Stress. *J. Biol. Chem.* 285:16562-16571.

Kielbassa, C., L. Roza, and B. Epe. 1997. Wavelength dependence of oxidative DNA damage induced by UV and visible light. *Carcinogenesis*. 18:811-816.

Kim, J., and P.K.Y. Wong. 2009. Loss of ATM Impairs Proliferation of Neural Stem Cells Through Oxidative Stress-Mediated p38 MAPK Signaling. *Stem Cells*. 27:1987-1998.

Kinoshita, E., E. Kinoshita-Kikuta, H. Ujihara, and T. Koike. 2009. Mobility shift detection of phosphorylation on large proteins using a Phos-tag SDS-PAGE gel strengthened with agarose. *Proteomics*. 9:4098-4101.

Kirouac, K.N., and H. Ling. 2011. Unique active site promotes error-free replication opposite an 8-oxo-guanine lesion by human DNA polymerase iota. *Proc. Natl. Acad. Sci.* 108:3210-3215.

Klungland, A., and S. Bjelland. 2007. Oxidative damage to purines in DNA: Role of mammalian Ogg1. *DNA Repair*. 6:481-488.

Kobayashi, J., H. Tauchi, S. Sakamoto, A. Nakamura, K.-i. Morishima, S. Matsuura, T. Kobayashi, K. Tamai, K. Tanimoto, and K. Komatsu. 2002. NBS1 Localizes to gamma-H2AX Foci through Interaction with the FHA/BRCT Domain. *Curr. Biol.* 12:1846-1851.

Kobayashi, N., T. Muramatsu, Y. Yamashina, T. Shirai, T. Ohnishi, and T. Mori. 1998a. Melanin reduces ultraviolet-induced DNA damage formation and killing rate in cultured human melanoma cells. *J. Invest. Dermatol.* 101:685-689.

Kobayashi, N., A. Nakagawa, T. Muramatsu, Y. Yamashina, T. Shirai, M.W. Hashimoto, Y. Ishigaki, T. Ohnishi, and T. Mori. 1998b. Supranuclear Melanin Caps Reduce Ultraviolet Induced DNA Photoproducts in Human Epidermis. *J. Invest. Dermatol.* 110:806-810.

Köberle, B., V. Roginskaya, and R.D. Wood. 2006. XPA protein as a limiting factor for nucleotide excision repair and UV sensitivity in human cells. *DNA Repair*. 5:641-648.

Kowalczuk, C.I., M.C. Priestner, A.J. Pearson, R.D. Saunders, and S.D. Bouffler. 2006. Wavelength dependence of cellular responses in human melanocytes and melanoma cells following exposure to ultraviolet radiation. *Int. J. Radiat. Biol.* 82:781-792.

Kozlov, S.V., M.E. Graham, C. Peng, P. Chen, P.J. Robinson, and M.F. Lavin. 2006. Involvement of novel autophosphorylation sites in ATM activation. *EMBO J.* 25:3504-3514.

Kozmin, S., G. Slezak, A. Reynaud-Angelin, C. Elie, Y. de Rycke, S. Boiteux, and E. Sage. 2005. UVA radiation is highly mutagenic in cells that are unable to repair 7,8-dihydro-8-oxoguanine in Saccharomyces cerevisiae. *Proc. Natl. Acad. Sci. U. S. A.* 102:13538-13543.

Kraemer, K.H., M.M. Lee, and J. Scotto. 1987. Xeroderma pigmentosum: Cutaneous, ocular, and neurologic abnormalities in 830 published cases. *Arch. Dermatol.* 123:241-250.

Krauthammer, M., Y. Kong, B.H. Ha, P. Evans, A. Bacchiocchi, J.P. McCusker, E. Cheng, M.J. Davis, G. Goh, M. Choi, S. Ariyan, D. Narayan, K. Dutton-Regester, A. Capatana, E.C. Holman, M. Bosenberg, M. Sznol, H.M. Kluger, D.E. Brash, D.F. Stern, M.A. Materin, R.S. Lo, S. Mane, S. Ma, K.K. Kidd, N.K. Hayward, R.P. Lifton, J. Schlessinger, T.J. Boggon, and R. Halaban. 2012. Exome

sequencing identifies recurrent somatic RAC1 mutations in melanoma. *Nat. Genet.* 44:1006-1014.

Kudchadkar, R.R., K.S.M. Smalley, L.F. Glass, J.S. Trimble, and V.K. Sondak. 2013. Targeted therapy in melanoma. *Clin. Dermatol.* 31:200-208.

Kuluncsics, Z., D. Perdiz, E. Brulay, B. Muel, and E. Sage. 1999. Wavelength dependence of ultraviolet-induced DNA damage distribution: Involvement of direct or indirect mechanisms and possible artefacts. *J. Photochem. Photobiol. B*. 49:71-80.

Kumagai, A., J. Lee, H.Y. Yoo, and W.G. Dunphy. 2006. TopBP1 Activates the ATR-ATRIP Complex. *Cell*. 124:943-955.

Kurimasa, A., S. Kumano, N.V. Boubnov, M.D. Story, C.-S. Tung, S.R. Peterson, and D.J. Chen. 1999. Requirement for the Kinase Activity of Human DNA-Dependent Protein Kinase Catalytic Subunit in DNA Strand Break Rejoining. *Mol. Cell. Biol.* 19:3877-3884.

Kyriakis, J.M., H. App, X.-f. Zhang, P. Banerjee, D.L. Brautigan, U.R. Rapp, and J. Avruch. 1992. Raf-1 activates MAP kinase-kinase. *Nature*. 358:417-421.

Laine, J.-P., and J.-M. Egly. 2006. Initiation of DNA repair mediated by a stalled RNA polymerase IIO. *EMBO J.* 25:387-397.

Lara-Gonzalez, P., Frederick G. Westhorpe, and Stephen S. Taylor. 2012. The Spindle Assembly Checkpoint. *Curr. Biol.* 22:R966-R980.

Larsson, P., E. Andersson, U. Johansson, K. Ollinger, and I. Rosdahl. 2005. Ultraviolet A and B affect human melanocytes and keratinocytes differently. A study of oxidative alterations and apoptosis. *Exp. Dermatol.* 14:117-123.

Lavin, M.F. 2008. Ataxia-telangiectasia: from a rare disorder to a paradigm for cell signalling and cancer. *Nat. Rev. Mol. Cell Biol.* 9:759-769.

Lazovich, D., R.I. Vogel, M. Berwick, M.A. Weinstock, K.E. Anderson, and E.M. Warshaw. 2010. Indoor Tanning and Risk of Melanoma: A Case-Control Study in a Highly Exposed Population. *Cancer Epidemol. Biomarkers Prev.* 19:1557-1568.

Lee, C., F. Collichio, D. Ollila, and S. Moschos. 2013. Historical review of melanoma treatment and outcomes. *Clin. Dermatol.* 31:141-147.

Lee, J.-S., K.M. Collins, A.L. Brown, C.-H. Lee, and J.H. Chung. 2000. hCds1-mediated phosphorylation of BRCA1 regulates the DNA damage response. *Nature*. 404:201-204.

Lee, J., and T. Paull. 2005. ATM activation by DNA double-strand breaks through the Mre11-Rad50-Nbs1 complex. *Science*. 308:551-554.

Lee, T.H., J.M. Park, S.H. Leem, and T.H. Kang. 2012. Coordinated regulation of XPA stability by ATR and HERC2 during nucleotide excision repair. *Oncogene*.

Lehmann, A.R., S. Kirk-Bell, C.F. Arlett, M.C. Paterson, P.H. Lohman, E.A. de Weerd-Kastelein, and D. Bootsma. 1975. Xeroderma pigmentosum cells with normal levels of excision repair have a defect in DNA synthesis after UV-irradiation. *Proc. Natl. Acad. Sci. U. S. A.* 72:219-223.

Lehmann, A.R., A. Niimi, T. Ogi, S. Brown, S. Sabbioneda, J.F. Wing, P.L. Kannouche, and C.M. Green. 2007. Translesion synthesis: Y-family polymerases and the polymerase switch. *DNA Repair*. 6:891-899.

Lempiainen, H., and T.D. Halazonetis. 2009. Emerging common themes in regulation of PIKKs and PI3Ks. *EMBO J.* 28:3067-3073.

Lengauer, C., K.W. Kinzler, and B. Vogelstein. 1998. Genetic instabilities in human cancers. *Nature*. 396:643-649.

Leung-Pineda, V., C.E. Ryan, and H. Piwnica-Worms. 2006. Phosphorylation of Chk1 by ATR Is Antagonized by a Chk1-Regulated Protein Phosphatase 2A Circuit. *Mol. Cell. Biol.* 26:7529-7538.

Levine, A.J., J. Momand, and C.A. Finlay. 1991. The p53 tumour suppressor gene. *Nature*. 351:453-456.

Li, J., Y.R. Han, M.R. Plummer, and K. Herrup. 2009. Cytoplasmic ATM in Neurons Modulates Synaptic Function. *Curr. Biol.* 19:2091-2096.

Liaw, H., D. Lee, and K. Myung. 2011. DNA-PK-Dependent RPA2 Hyperphosphorylation Facilitates DNA Repair and Suppresses Sister Chromatid Exchange. *PLoS ONE*. 6:e21424.

Lim, D.-S., S.-T. Kim, B. Xu, R.S. Maser, J. Lin, J.H.J. Petrini, and M.B. Kastan. 2000. ATM phosphorylates p95/nbs1 in an S-phase checkpoint pathway. *Nature*. 404:613-617.

Limoli, C.L., E. Giedzinski, W.M. Bonner, and J.E. Cleaver. 2002. UV-induced replication arrest in the xeroderma pigmentosum variant leads to DNA double-strand breaks, γ-H2AX formation, and Mre11 relocalization. *Proc. Natl. Acad. Sci.* 99:233-238.

Lin, J.Y., and D.E. Fisher. 2007. Melanocyte biology and skin pigmentation. *Nature*. 445:843-850.

Lin, Q., A.B. Clark, S.D. McCulloch, T. Yuan, R.T. Bronson, T.A. Kunkel, and R. Kucherlapati. 2006. Increased Susceptibility to UV-Induced Skin Carcinogenesis in Polymerase η–deficient Mice. *Cancer Res.* 66:87-94.

Liu, J., T. Doty, B. Gibson, and W.-D. Heyer. 2010. Human BRCA2 protein promotes RAD51 filament formation on RPA-covered single-stranded DNA. *Nat Struct Mol Biol*. 17:1260-1262.

Liu, Q., S. Guntuku, X.-S. Cui, S. Matsuoka, D. Cortez, K. Tamai, G. Luo, S. Carattini-Rivera, F. DeMayo, A. Bradley, L.A. Donehower, and S.J. Elledge. 2000. Chk1 is an essential kinase that is regulated by Atr and required for the G2/M DNA damage checkpoint. *Genes Dev.* 14:1448-1459.

Liu, S., S. Bekker-Jensen, N. Mailand, C. Lukas, J. Bartek, and J. Lukas. 2006. Claspin Operates Downstream of TopBP1 To Direct ATR Signaling towards Chk1 Activation. *Mol. Cell. Biol.* 26:6056-6064.

Loeb, L.A. 1991. Mutator Phenotype May Be Required for Multistage Carcinogenesis. *Cancer Res.* 51:3075-3079.

Loeb, L.A., C.F. Springgate, and N. Battula. 1974. Errors in DNA Replication as a Basis of Malignant Changes. *Cancer Res.* 34:2311-2321.

Lookingbill, D.P., G.L. Lookingbill, and B. Leppard. 1995. Actinic damage and skin cancer in albinos in northern Tanzania: Findings in 164 patients enrolled in an outreach skin care program. *J. Am. Acad. Dermatol.* 32:653-658.

Lopes, M., M. Foiani, and J.M. Sogo. 2006. Multiple Mechanisms Control Chromosome Integrity after Replication Fork Uncoupling and Restart at Irreparable UV Lesions. *Mol. Cell*. 21:15-27.

Los, M., M. Mozoluk, D. Ferrari, A. Stepczynska, C. Stroh, A. Renz, Z. Herceg, Z.-Q. Wang, and K. Schulze-Osthoff. 2002. Activation and Caspase-mediated Inhibition of PARP: A Molecular Switch between Fibroblast Necrosis and Apoptosis in Death Receptor Signaling. *Mol. Biol. Cell*. 13:978-988.

Lowry, O.H., N.J. Rosebrough, A.L. Farr, and R.J. Randall. 1951. Protein measurement with the folin phenol reagent *J. Biol. Chem.* 193:265-275.

Lubin, D., and E.H. Jensen. 1995. Effects of clouds and stratospheric ozone depletion on ultraviolet radiation trends. *Nature*. 377:710-713.

Lucas, R., T. McMichael, W. Smith, and B. Armstrong. 2006. Solar ultraviolet radiation : global burden of disease from solar ultraviolet radiation. *World Health Organization, Public Health and the Environment, Geneva*.

Ma, C.X., J.W. Janetka, and H. Piwnica-Worms. 2011. Death by releasing the breaks: CHK1 inhibitors as cancer therapeutics. *Trends in Mol. Med.* 17:88-96.

MacDougall, C.A., T.S. Byun, C. Van, M.-c. Yee, and K.A. Cimprich. 2007. The structural determinants of checkpoint activation. *Genes Dev.* 21:898-903.

Macleod, K.F., N. Sherry, G. Hannon, D. Beach, T. Tokino, K. Kinzler, B. Vogelstein, and T. Jacks. 1995. p53-dependent and independent expression of p21 during cell growth, differentiation, and DNA damage. *Genes Dev.* 9:935-944.

Maher, V.M., L.M. Ouellette, R.D. Curren, and J.J. McCormick. 1976. Frequency of ultraviolet light-induced mutations is higher in xeroderma pigmentosum variant cells than in normal human cells. *Nature*. 261:593-595.

Mailand, N., J. Falck, C. Lukas, Sylju, aring, R.G. sen, M. Welcker, J. Bartek, and J. Lukas. 2000. Rapid Destruction of Human Cdc25A in Response to DNA Damage. *Science*. 288:1425-1429.

Maloisel, L., F. Fabre, and S. Gangloff. 2008. DNA Polymerase δ Is Preferentially Recruited during Homologous Recombination To Promote Heteroduplex DNA Extension. *Mol. Cell. Biol.* 28:1373-1382.

Mamely, I., M.A.T.M. van Vugt, V.A.J. Smits, J.I. Semple, B. Lemmens, A. Perrakis, R.H. Medema, and R. Freire. 2006. Polo-like Kinase-1 Controls Proteasome-Dependent Degradation of Claspin during Checkpoint Recovery. *Curr. Biol.* 16:1950-1955.

Manak, M.M., L. Aurelian, and P.O. Ts'o. 1981. Focus formation and neoplastic transformation by herpes simplex virus type 2 inactivated intracellularly by 5-bromo-2'-deoxyuridine and near UV light. *J. Virol.* 40:289-300.

Masutani, C., M. Araki, A. Yamada, R. Kusumoto, T. Nogimori, T. Maekawa, S. Iwai, and F. Hanaoka. 1999a. Xeroderma pigmentosum variant (XP-V) correcting protein from HeLa cells has a thymine dimer bypass DNA polymerase activity. *EMBO J.* 18:3491-3501.

Masutani, C., R. Kusumoto, S. Iwai, and F. Hanaoka. 2000. Mechanisms of accurate translesion synthesis by human DNA polymerase [eta]. *EMBO J.* 19:3100-3109.

Masutani, C., R. Kusumoto, A. Yamada, N. Dohmae, M. Yokoi, M. Yuasa, M. Araki, S. Iwai, K. Takio, and F. Hanaoka. 1999b. The XPV (xeroderma pigmentosum variant) gene encodes human DNA polymerase eta. *Nature*. 399:700-704.

Matsumoto, Y., and K. Kim. 1995. Excision of deoxyribose phosphate residues by DNA polymerase beta during DNA repair. *Science*. 269:699-702.

Matsuoka, S., B.A. Ballif, A. Smogorzewska, E.R. McDonald, K.E. Hurov, J. Luo, C.E. Bakalarski, Z. Zhao, N. Solimini, Y. Lerenthal, Y. Shiloh, S.P. Gygi, and S.J. Elledge. 2007. ATM and ATR Substrate Analysis Reveals Extensive Protein Networks Responsive to DNA Damage. *Science*. 316:1160-1166.

Matsuoka, S., G. Rotman, A. Ogawa, Y. Shiloh, K. Tamai, and S.J. Elledge. 2000a. Ataxia telangiectasia-mutated phosphorylates Chk2 in vivo and in vitro. *Proc. Natl. Acad. Sci.* 97:10389-10394.

Matsuoka, Y., X. Li, and V. Bennett. 1998. Adducin Is an In Vivo Substrate for Protein Kinase C: Phosphorylation in the MARCKS-related Domain Inhibits Activity in Promoting Spectrin–Actin Complexes and Occurs in Many Cells, Including Dendritic Spines of Neurons. *J. Cell. Biol.* 142:485-497.

Matsuoka, Y., X. Li, and V. Bennett. 2000b. Adducin: structure, function and regulation. *Cell. Mol. Life Sci.* 57:884-895.

Maya, R., M. Balass, S.-T. Kim, D. Shkedy, J.-F. Martinez Leal, O. Shifman, M. Moas, T. Buschmann, Z.e. Ronai, Y. Shiloh, M.B. Kastan, E. Katzir, and M. Oren. 2001. ATM-dependent phosphorylation of Mdm2 on serine 395: role in p53 activation by DNA damage. *Genes and Dev.* 15:1067-1077.

Mbeunkui, F., and D. Johann, Jr. 2009. Cancer and the tumor microenvironment: a review of an essential relationship. *Cancer Chemother. Pharmacol.* 63:571-582.

McCubrey, J.A., L.S. Steelman, W.H. Chappell, S.L. Abrams, E.W.T. Wong, F. Chang, B. Lehmann, D.M. Terrian, M. Milella, A. Tafuri, F. Stivala, M. Libra, J. Basecke, C. Evangelisti, A.M. Martelli, and R.A. Franklin. 2007. Roles of the Raf/MEK/ERK pathway in cell growth, malignant transformation and drug resistance. *Biochimica et Biophysica Acta (BBA) - Molecular Cell Research*. 1773:1263-1284.

McCulloch, S.D., R.J. Kokoska, P. Garg, P.M. Burgers, and T.A. Kunkel. 2009. The efficiency and fidelity of 8-oxo-guanine bypass by DNA polymerases delta and eta. *Nucleic Acids Res.* 37:2830-2840.

McCulloch, S.D., and T.A. Kunkel. 2008. The fidelity of DNA synthesis by eukaryotic replicative and translesion synthesis polymerases. *Cell Res.* 18:148-161.

McGregor, W.G., R.H. Chen, L. Lukash, V.M. Maher, and J.J. McCormick. 1991. Cell cycle-dependent strand bias for UV-induced mutations in the transcribed strand of excision repair-proficient human fibroblasts but not in repair-deficient cells. *Mol. Cell. Biol.* 11:1927-1934.

McMahon, S.B., H.A. Van Buskirk, K.A. Dugan, T.D. Copeland, and M.D. Cole. 1998. The Novel ATM-Related Protein TRRAP Is an Essential Cofactor for the c-Myc and E2F Oncoproteins. *Cell*. 94:363-374.

McMahon, S.B., M.A. Wood, and M.D. Cole. 2000. The Essential Cofactor TRRAP Recruits the Histone Acetyltransferase hGCN5 to c-Myc. *Mol. Cell. Biol.* 20:556-562.

McMillan, T.J., E. Leatherman, A. Ridley, J. Shorrocks, S.E. Tobi, and J.R. Whiteside. 2008. Cellular effects of long wavelength UV light (UVA) in mammalian cells. *J. Pharm. Pharmacol.* 60:969-976.

Meinhardt, M., R. Krebs, A. Anders, U. Heinrich, and H. Tronnier. 2008. Wavelength-dependent penetration depths of ultraviolet radiation in human skin. *J. Biomed. Optics*. 13:044030.

Menter, J., I. Willis, M. Townsel, G. Williamson, and C. Moore. 1991. Melanin is a Double-Edged Sword. *In* Photobiology. E. Riklis, editor. Springer US. 873-886.

Merwald, H., G. Klosner, C. Kokesch, M. Der-Petrossian, H. Hönigsmann, and F. Trautinger. 2005. UVA-induced oxidative damage and cytotoxicity depend on the mode of exposure. *J. Photochem. Photobiol. B.* 79:197-207.

Mills, K.D., D.O. Ferguson, and F.W. Alt. 2003. The role of DNA breaks in genomic instability and tumorigenesis. *Immunol. Rev.* 194:77-95.

Mirzoeva, O.K., and J.H.J. Petrini. 2001. DNA Damage-Dependent Nuclear Dynamics of the Mre11 Complex. *Mol. Cell. Biol.* 21:281-288.

Mitchell, D. 2012. Melanoma back in the UVA spotlight. *Pigment Cell Melanoma Res.* 25:540-541.

Mitchell, D., and B. Brooks. 2010. Antibodies and DNA Photoproducts: Applications, Milestones and Reference Guide. *Photochem. Photobiol.* 86:2-17.

Mitchell, D., and A. Fernandez. 2012. The photobiology of melanocytes modulates the impact of UVA on sunlight-induced melanoma. *Photochem. Photobiol. Sci.* 11:69-73.

Mitchell, D.L., A.A. Fernandez, R.S. Nairn, R. Garcia, L. Paniker, D. Trono, H.D. Thames, and I. Gimenez-Conti. 2010. Ultraviolet A does not induce melanomas in a Xiphophorus hybrid fish model. *Proc. Natl. Acad. Sci.* 107:9329-9334.

Mitra, D., X. Luo, A. Morgan, J. Wang, M.P. Hoang, J. Lo, C.R. Guerrero, J.K. Lennerz, M.C. Mihm, J.A. Wargo, K.C. Robinson, S.P. Devi, J.C. Vanover, J.A. D'Orazio, M. McMahon, M.W. Bosenberg, K.M. Haigis, D.A. Haber, Y. Wang, and D.E. Fisher. 2012. An ultraviolet-radiation-independent pathway to melanoma carcinogenesis in the red hair/fair skin background. *Nature*. 491:449-453.

Moan, J., A. Dahlback, and R.B. Setlow. 1999. Epidemiological Support for an Hypothesis for Melanoma Induction Indicating a Role for UVA Radiation. *Photochem. Photobiol.* 70:243-247.

Mouret, S., C. Baudouin, M. Charveron, A. Favier, J. Cadet, and T. Douki. 2006. Cyclobutane Pyrimidine Dimers Are Predominant DNA Lesions in Whole Human Skin Exposed to UVA Radiation. *Proc. Natl. Acad. Sci. U. S. A.* 103:13765-13770.

Mouret, S., A. Forestier, and T. Douki. 2012. The specificity of UVA-induced DNA damage in human melanocytes. *Photochem. Photobiol. Sci.* 11:155-162.

Mouret, S., C. Philippe, J. Gracia-Chantegrel, A. Banyasz, S. Karpati, D. Markovitsi, and T. Douki. 2010. UVA-induced cyclobutane pyrimidine dimers in DNA: a direct photochemical mechanism? *Org. Biomol. Chem.* 8:1706-1711.

Munshi, A., M. Hobbs, and R. Meyn. 2005. Clonogenic Cell Survival Assay. *In* Chemosensitivity. Vol. 110. R. Blumenthal, editor. Humana Press. 21-28.

Murnane, J.P., L.F. Fuller, and R.B. Painter. 1985. Establishment and characterization of a permanent pSV ori−-transformed ataxia-telangiectasia cell line. *Exp. Cell Res.* 158:119-126.

Nakajima, S., L. Lan, S.-i. Kanno, N. Usami, K. Kobayashi, M. Mori, T. Shiomi, and A. Yasui. 2006. Replication-dependent and -independent Responses of RAD18 to DNA Damage in Human Cells. *J. Biol. Chem.* 281:34687-34695.

NCRI. 2013a. Cancer in Ireland 2013: Annual report of the National Cancer Registry.

NCRI. 2013b. Cancer Trends No 20. Non-melanoma skin cancer.

Neal, J.A., V. Dang, P. Douglas, M.S. Wold, S.P. Lees-Miller, and K. Meek. 2011. Inhibition of Homologous Recombination by DNA-Dependent Protein Kinase Requires Kinase Activity, Is Titratable, and Is Modulated by Autophosphorylation. *Mol. Cell. Biol.* 31:1719-1733.

Nelson, J.R., C.W. Lawrence, and D.C. Hinkle. 1996. Deoxycytidyl transferase activity of yeast REV1 protein. *Nature*. 382:729-731.

Neugut, A.I., S. Kizelnik-Freilich, and C. Ackerman. 1994. Black-white differences in risk for cutaneous, ocular, and visceral melanomas. *Am. J. Public Health*. 84:1828-1829.

Nicholson, D.W., A. Ali, N.A. Thornberry, J.P. Vaillancourt, C.K. Ding, M. Gallant, Y. Gareau, P.R. Griffin, M. Labelle, Y.A. Lazebnik, N.A. Munday, S.M. Raju, M.E. Smulson, T.-T. Yamin, V.L. Yu, and D.K. Miller. 1995. Identification and inhibition of the ICE/CED-3 protease necessary for mammalian apoptosis. *Nature*. 376:37-43.

Niida, H., Y. Katsuno, B. Banerjee, M.P. Hande, and M. Nakanishi. 2007. Specific Role of Chk1 Phosphorylations in Cell Survival and Checkpoint Activation. *Mol. Cell. Biol.* 27:2572-2581.

Niida, H., and M. Nakanishi. 2006. DNA damage checkpoints in mammals. *Mutagenesis*. 21:3-9.

Nishioka, E., Y. Funasaka, H. Kondoh, A. Chakraborty, Y. Mishima, and M. Ichihashi. 1999. Expression of tyrosinase, TRP-1 and TRP-2 in ultraviolet-irradiated human melanomas and melanocytes: TRP-2 protects melanoma cells from ultraviolet B induced apoptosis. *Melanoma Res.* 9:433-443.

Noonan, F.P., J.A. Recio, H. Takayama, P. Duray, M.R. Anver, W.L. Rush, E.C. De Fabo, and G. Merlino. 2001. Neonatal sunburn and melanoma in mice. *Nature*. 413:271-272.

Noonan, F.P., M.R. Zaidi, A. Wolnicka-Glubisz, M.R. Anver, J. Bahn, A. Wielgus, J. Cadet, T. Douki, S. Mouret, M.A. Tucker, A. Popratiloff,

G. Merlino, and E.C. De Fabo. 2012. Melanoma induction by ultraviolet A but not ultraviolet B radiation requires melanin pigment. *Nat. Commun.* 3:884.

Nouspikel, T. 2009. DNA Repair in Mammalian Cells : Nucleotide excision repair: variations on versatility. *Cell. Mol. Life Sci.* 66:994-1009.

Nunez, M., B. Forgan, and C. Roy. 1994. Estimating ultraviolet radiation at the earth's surface. *Int. J. Biometeorol.* 38:5-17.

O'Connell, M.J., J.M. Raleigh, H.M. Verkade, and P. Nurse. 1997. Chk1 is a wee1 kinase in the G2 DNA damage checkpoint inhibiting cdc2 by Y15 phosphorylation. *EMBO J.* 16:545-554.

O'Driscoll, M., V.L. Ruiz-Perez, C.G. Woods, P.A. Jeggo, and J.A. Goodship. 2003. A splicing mutation affecting expression of ataxia-telangiectasia and Rad3-related protein (ATR) results in Seckel syndrome. *Nat. Genet.* 33:497-501.

O'Meara, E., S. Cruet-Hennequart, and M.P. Carty. 2010. Analysis of Protein Phosphorylation in Cisplatin-Treated Human Cells Following Annexin V-based Separation and Multi-Antibody Screening. *Cancer Genomics - Proteomics*. 7:279-286.

Oakley, G.G., and S.M. Patrick. 2010. Replication protein A: directing traffic at the intersection of replication and repair. *Front. Biosci.* 15:883-900.

Oe, T., N. Nakajo, Y. Katsuragi, K. Okazaki, and N. Sagata. 2001. Cytoplasmic Occurrence of the Chk1/Cdc25 Pathway and Regulation of Chk1 in Xenopus Oocytes. *Dev. Biol.* 229:250-261.

Ogi, T., Y. Shinkai, K. Tanaka, and H. Ohmori. 2002. Polκ protects mammalian cells against the lethal and mutagenic effects of benzo[a]pyrene. *Proc. Natl. Acad. Sci.* 99:15548-15553.

Oka, M., K. Ogita, H. Ando, U. Kikkawa, and M. Ichishashi. 1995. Differential Down-Regulation of Protein Kinase C Subspecies in Normal Hunam Melanocyte: Possible Involvement of the zeta sub-species in growth regulation. *J. Invest. Dermatol.* 105:567-571.

Okuno, Y., A. Nakamura-Ishizu, K. Otsu, T. Suda, and Y. Kubota. 2012. Pathological neoangiogenesis depends on oxidative stress regulation by ATM. *Nat. Med.* 18:1208-1216.

Pabla, N., K. Bhatt, and Z. Dong. 2012. Checkpoint kinase 1 (Chk1)-short is a splice variant and endogenous inhibitor of Chk1 that regulates cell cycle and DNA damage checkpoints. *Proc. Natl. Acad. Sci.* 109:197-202.

Painter, R.B. 1981. Radioresistant DNA synthesis: an intrinsic feature of ataxia telangiectasia. *Mutat. Res.* 84:183-190.

Panka, D.J., M.B. Atkins, and J.W. Mier. 2006. Targeting the Mitogen-Activated Protein Kinase Pathway in the Treatment of Malignant Melanoma. *Clin. Cancer Res.* 12:2371s-2375s.

Parekh, D.B., W. Ziegler, and P.J. Parker. 2000. Multiple pathways control protein kinase C phosphorylation. *EMBO J.* 19:496-503.

Park, H.Y., V. Russakovsky, S. Ohno, and B.A. Gilchrest. 1993. The beta isoform of protein kinase C stimulates human melanogenesis by activating tyrosinase in pigment cells. *J. Biol. Chem.* 268:11742-11749.

Parker, L., and H. Piwnica-Worms. 1992. Inactivation of the p34cdc2-cyclin B complex by the human WEE1 tyrosine kinase. *Science*. 257:1955-1957.

Pastila, R., S. Heinavaara, L. Ylianttila, and D. Leszczynski. 2011. In vivo UVA irradiation of mouse is more efficient in promoting pulmonary melanoma metastasis than in vitro. *Cancer Cell International*. 11:16.

Pastila, R., and D. Leszczynski. 2005. Ultraviolet A exposure alters adhesive properties of mouse melanoma cells. *Photodermatol. Photoimmunol. Photomed.* 21:234-241.

Pellegrini, M., A. Celeste, S. Difilippantonio, R. Guo, W. Wang, L. Feigenbaum, and A. Nussenzweig. 2006. Autophosphorylation at serine 1987 is dispensable for murine Atm activation in vivo. *Nature*. 443:222-225.

Peng, C.-Y., P.R. Graves, R.S. Thoma, Z. Wu, A.S. Shaw, and H. Piwnica-Worms. 1997. Mitotic and G2 Checkpoint Control: Regulation of 14-3-3 Protein Binding by Phosphorylation of Cdc25C on Serine-216. *Science*. 277:1501-1505.

Perdiz, D., P. Grof, M. Mezzina, O. Nikaido, E. Moustacchi, and E. Sage. 2000. Distribution and Repair of Bipyrimidine Photoproducts in Solar UV-irradiated Mammalian Cells. *J. Biol. Chem.* 275:26732-26742.

Peschiaroli, A., N.V. Dorrello, D. Guardavaccaro, M. Venere, T. Halazonetis, N.E. Sherman, and M. Pagano. 2006. SCF²TrCP-Mediated Degradation of Claspin Regulates Recovery from the DNA Replication Checkpoint Response. *Mol. Cell*. 23:319-329.

Petermann, E., and K.W. Caldecott. 2006. Evidence That the ATR/Chk1 Pathway Maintains Normal Replication Fork Progression during Unperturbed S Phase. *Cell Cycle*. 5:2203-2209.

Petermann, E., and T. Helleday. 2010. Pathways of mammalian replication fork restart. *Nat. Rev. Mol. Cell Biol.* 11:683-687.

Pfeifer, G.P., and A. Besaratinia. 2012. UV wavelength-dependent DNA damage and human non-melanoma and melanoma skin cancer. *Photochem. Photobiol. Sci.* 11:90-97.

Piette, J., M. Paule, M. Louis, and J. Decuyper. 1986. Damages induced in nucleci acids by photosensitization *Photochem. Photobiol.* 44:793-802.

Plettenberg, A., Ballaun, C., Pammer, J., Mildner, M., Strunk, D., Weininger, W. and Tschachler, E. 1995. Human Melanocytes and Melanoma Cells Constitutively Express the BcI-2 Proto-Oncogene in Situ and in Cell Culture. *Am. J. Pathol.* 146:651-659.

Povlsen, L.K., P. Beli, S.A. Wagner, S.L. Poulsen, K.B. Sylvestersen, J.W. Poulsen, M.L. Nielsen, S. Bekker-Jensen, N. Mailand, and C. Choudhary. 2012. Systems-wide analysis of ubiquitylation dynamics reveals a key role for PAF15 ubiquitylation in DNA-damage bypass. *Nat Cell Biol*. 14:1089-1098.

Puc, J., M. Keniry, H.S. Li, T.K. Pandita, A.D. Choudhury, L. Memeo, M. Mansukhani, V.V.V.S. Murty, Z. Gaciong, S.E.M. Meek, H. Piwnica-Worms, H. Hibshoosh, and R. Parsons. 2005. Lack of PTEN sequesters CHK1 and initiates genetic instability. *Cancer Cell*. 7:193-204.

Rebel, H., N. Kram, A. Westerman, S. Banus, H.J. van Kranen, and F.R. de Gruijl. 2005. Relationship between UV-induced mutant p53 patches and skin tumours, analysed by mutation spectra and by induction kinetics in various DNA-repair-deficient mice. *Carcinogenesis*. 26:2123-2130.

Redon, C.E., A.J. Nakamura, O.A. Martin, P.R. Parekh, U.S. Weyemi, and W.M. Bonner. 2011. Recent developments in the use of γ-H2AX as a quantitative DNA double-strand break biomarker. *Aging (Milano).* 3:168-172.

Rey, L., J.M. Sidorova, N. Puget, F. Boudsocq, D.S.F. Biard, R.J. Monnat, C. Cazaux, and J.-S. Hoffmann. 2009. Human DNA Polymerase η Is Required for Common Fragile Site Stability during Unperturbed DNA Replication. *Mol. Cell. Biol.* 29:3344-3354.

Rizzo, J.L., J. Dunn, A. Rees, and T.M. Runger. 2011. No Formation of DNA Double-Strand Breaks and No Activation of Recombination Repair with UVA. *J. Invest. Dermatol.* 131:1139-1148.

Robert, C., B. Muel, A. Benoit, L. Dubertret, A. Sarasin, and A. Stary. 1996. Cell Survival and Shuttle Vector Mutagenesis Induced by Ultraviolet A and Ultraviolet B Radiation in a Human Cell Line. *J. Invest. Dermatol.* 106:721-728.

Robertson, A.B., A. Klungland, T. Rognes, and I. Leiros. 2009. DNA Repair in Mammalian Cells: Base excision reapir: the long and short of it. *Cell. Mol. Life Sci.* 66:981-993.

Robinson, E.S., J.R.H. Hill, M.L. Kripke, and R.B. Setlow. 2000. The Monodelphis Melanoma Model: Initial Report on Large Ultraviolet A Exposures of Suckling Young. *Photochem. Photobiol.* 71:743-746.

Rochette, P.J., J.P. Therrien, R. Drouin, D. Perdiz, N. Bastien, E.A. Drobetsky, and E. Sage. 2003. UVA-induced cyclobutane pyrimidine dimers form predominantly at thymine–thymine dipyrimidines and correlate with the mutation spectrum in rodent cells. *Nucleic Acids Res.* 31:2786-2794.

Rogakou, E., D. Pilch, A. Orr, U. Ivanova, and W. Bonner. 1998a. DNA double-stranded breaks induce histone H2AX phophorylation on serine 139. *J. Biol. Chem.* 273:5858 - 5868.

Rogakou, E.P., C. Boon, C. Redon, and W.M. Bonner. 1999. Megabase Chromatin Domains Involved in DNA Double-Strand Breaks in Vivo. *The Journal of Cell Biology*. 146:905-916.

Rogakou, E.P., D.R. Pilch, A.H. Orr, V.S. Ivanova, and W.M. Bonner. 1998b. DNA Double-stranded Breaks Induce Histone H2AX Phosphorylation on Serine 139. *J. Biol. Chem.* 273:5858-5868.

Rothkamm, K., I. Krüger, L.H. Thompson, and M. Löbrich. 2003. Pathways of DNA Double-Strand Break Repair during the Mammalian Cell Cycle. *Mol. Cell. Biol.* 23:5706-5715.

Routaboul, C., A. Denis, and A. Vinche. 1999. Immediate pigment darkening: description, kinetic and biological function. *Eur. J. Dermatol.* 9:95-99.

Roza, L., G.P. van der Schans, and P.H.M. Lohman. 1985. The induction and repair of DNA damage and its influence on cell death in primary

human fibroblasts exposed to UVA or UVC irradiation. *Mutat. Res.* 146:89-98.

Runger, T.M. 2007. How Different Wavelengths of the Ultraviolet Spectrum Contribute to Skin Carcinogenesis: The Role of Cellular Damage Responses. *J. Invest. Dermatol.* 127:2103-2105.

Runger, T.M., B. Farahvash, Z. Hatvani, and A. Rees. 2012. Comparison of DNA damage responses following equimutagenic doses of UVA and UVB: A less effective cell cycle arrest with UVA may render UVA-induced pyrimidine dimers more mutagenic than UVB-induced ones. *Photochem. Photobiol. Sci.* 11:207-215.

Runger, T.M., and U.P. Kappes. 2008. Mechanisms of mutation formation with long-wave ultraviolet light (UVA). *In* Photodermatol. Photoimmunol. Photomed. Vol. 24. Wiley-Blackwell. 2-10.

Ryan, K.M., A.C. Phillips, and K.H. Vousden. 2001. Regulation and function of the p53 tumor suppressor protein. *Curr. Opin. Cell Biol.* 13:332-337.

Sage, E., B. Lamolet, E. Brulay, E. Moustacchi, A. Chteauneuf, and E.A. Drobetsky. 1996. Mutagenic Specificity of Solar UV Light in Nucleotide Excision Repair-Deficient Rodent Cells. *Proc. Natl. Acad. Sci. U. S. A.* 93:176-180.

Sale, J.E., A.R. Lehmann, and R. Woodgate. 2012. Y-family DNA polymerases and their role in tolerance of cellular DNA damage. *Nat. Rev. Mol. Cell Biol.* 13:141-152.

Sarkaria, J.N., E.C. Busby, R.S. Tibbetts, P. Roos, Y. Taya, L.M. Karnitz, and R.T. Abraham. 1999. Inhibition of ATM and ATR Kinase Activities by the Radiosensitizing Agent, Caffeine. *Cancer Res.* 59:4375-4382.

Sarkaria, J.N., R.S. Tibbetts, E.C. Busby, A.P. Kennedy, D.E. Hill, and R.T. Abraham. 1998. Inhibition of Phosphoinositide 3-Kinase Related Kinases by the Radiosensitizing Agent Wortmannin. *Cancer Res.* 58:4375-4382.

Satokata, I., K. Tanaka, N. Miura, M. Narita, T. Mimaki, Y. Satoh, S. Kondo, and Y. Okada. 1992a. Three nonsense mutations responsible for group A xeroderma pigmentosum. *Mutat. Res.* 273:193-202.

Satokata, I., K. Tanaka, S. Yuba, and Y. Okada. 1992b. Identification of splicing mutations of the last nucleotide exons, a nonsense mutation, and a missense mutation of the XPAC gene as a cause of group A xeroderma pigmentosum. *Mutat. Res.* 273:203-212.

Sausville, E.A., S.G. Arbuck, R. Messmann, D. Headlee, K.S. Bauer, R.M. Lush, A. Murgo, W.D. Figg, T. Lahusen, S. Jaken, X.-x. Jing, M. Roberge, E. Fuse, T. Kuwabara, and A.M. Senderowicz. 2001. Phase I Trial of 72-Hour Continuous Infusion UCN-01 in Patients With Refractory Neoplasms. *J. Clin. Oncol.* 19:2319-2333.

Savitsky, K., A. Bar-Shira, S. Gilad, G. Rotman, Y. Ziv, L. Vanagaite, D. Tagle, S. Smith, T. Uziel, S. Sfez, and e. al. 1995a. A single ataxia telangiectasia gene with a product similar to PI-3 kinase. *Science*. 268:1749-1753.

Savitsky, K., S. Sfez, D.A. Tagle, Y. Ziv, A. Sartiel, F.S. Collins, Y. Shiloh, and G. Rotman. 1995b. The complete sequence of the coding region

of the ATM gene reveals similarity to cell cycle regulators in different species. *Hum. Mol. Genet.* 4:2025-2032.

Savitsky, K., T. Uziel, S. Gilad, A. Sartiel, Y. Shiloh, G. Rotman, M. Platzer, A. Rosenthal, and O. Elroy-Stein. 1997. Ataxia-telangiectasia: structural diversity of untranslated sequences suggests complex post-transcriptional regulation of ATM gene expression. *Nucleic Acids Res.* 25:1678-1684.

Schuch, A.P., R. da Silva Galhardo, K.M. de Lima-Bessa, N.J. Schuch, and C.F.M. Menck. 2009. Development of a DNA-dosimeter system for monitoring the effects of solar-ultraviolet radiation. *Photochem. Photobiol. Sci.* 8:111-120.

Schuierer, M.M., F. Bataille, S. Hagan, W. Kolch, and A.-K. Bosserhoff. 2004. Reduction in Raf Kinase Inhibitor Protein Expression Is Associated with Increased Ras-Extracellular Signal-Regulated Kinase Signaling in Melanoma Cell Lines. *Cancer Res.* 64:5186-5192.

Scott, G., S. Leopardi, S. Printup, and B.C. Madden. 2002. Filopodia are conduits for melanosome transfer to keratinocytes. *J. Cell Sci.* 115:1441-1451.

Selzer, E., I. Okamoto, T. Lucas, R. Kodym, H. Pehamberger, and B. Jansen. 2002. Protein kinase C isoforms in normal and transformed cells of the melanocytic lineage. *Melanoma Res.* 12:201-209.

Setlow, R.B., E. Grist, K. Thompson, and A.D. Woodhead. 1993. Wavelengths Effective in Induction of Malignant Melanoma. *Proc. Natl. Acad. Sci. U. S. A.* 90:6666-6670.

Seynaeve, C.M., M.G. Kazanietz, P.M. Blumberg, E.A. Sausville, and P.J. Worland. 1994. Differential inhibition of protein kinase C isozymes by UCN-01, a staurosporine analogue. *Mol. Pharmacol.* 45:1207-1214.

Shachar, S., O. Ziv, S. Avkin, S. Adar, J. Wittschieben, T. Reiszner, S. Chaney, E.C. Friedberg, Z. Wang, T. Carell, N. Geacintov, and Z. Livneh. 2009. Two-polymerase mechanisms dictate error-free and error-prone translesion DNA synthesis in mammals. *EMBO J.* 28:383-393.

Shell, S.M., Z. Li, N. Shkriabai, M. Kvaratskhelia, C. Brosey, M.A. Serrano, W.J. Chazin, P.R. Musich, and Y. Zou. 2009. Checkpoint Kinase ATR Promotes Nucleotide Excision Repair of UV-induced DNA Damage via Physical Interaction with Xeroderma Pigmentosum Group A. *J. Biol. Chem.* 284:24213-24222.

Shi, X., H. Zhang, H. Paddon, G. Lee, X. Cao, and S. Pelech. 2006. Phosphorylation of STAT3 Serine-727 by Cyclin-Dependent Kinase 1 Is Critical for Nocodazole-Induced Mitotic Arrest. *Biochemistry*. 45:5857-5867.

Shieh, S.-Y., J. Ahn, K. Tamai, Y. Taya, and C. Prives. 2000. The human homologs of checkpoint kinases Chk1 and Cds1 (Chk2) phosphorylate p53 at multiple DNA damage-inducible sites. *Genes Dev.* 14:289-300.

Shiloh, Y., and Y. Ziv. 2013. The ATM protein kinase: regulating the cellular response to genotoxic stress, and more. *Nat. Rev. Mol. Cell Biol.* 14:197-210.

Shivji, M.K.K., and A.R. Venkitaraman. 2004. DNA recombination, chromosomal stability and carcinogenesis: insights into the role of BRCA2. *DNA Repair*. 3:835-843.

Shorrocks, J., N.D. Paul, and T.J. McMillan. 2007. The Dose Rate of UVA Treatment Influences the Cellular Response of HaCaT Keratinocytes. *J. Invest. Dermatol.* 128:685-693.

Silverstein, T.D., R.E. Johnson, R. Jain, L. Prakash, S. Prakash, and A.K. Aggarwal. 2010. Structural basis for the suppression of skin cancers by DNA polymerase. *Nature*. 465:1039-1043.

Smit, N.P.M., A.A. Vink, R.M. Kolb, M.-J.S.T. Steenwinkel, P.T.M. van den Berg, F. van Nieuwpoort, L. Roza, and S. Pavel. 2001. Melanin Offers Protection Against Induction of Cyclobutane Pyrimidine Dimers and 6–4 Photoproducts by UVB in Cultured Human Melanocytes. *Photochem. Photobiol.* 74:424-430.

Smits, V.A.J., P.M. Reaper, and S.P. Jackson. 2006. Rapid PIKK-Dependent Release of Chk1 from Chromatin Promotes the DNA-Damage Checkpoint Response. *Curr. Biol.* 16:150-159.

Sorensen, C.S., L.T. Hansen, J. Dziegielewski, R.G. Syljuasen, C. Lundin, J. Bartek, and T. Helleday. 2005. The cell-cycle checkpoint kinase Chk1 is required for mammalian homologous recombination repair. *Nat Cell Biol*. 7:195-201.

Sørensen, C.S., R.G. Syljuåsen, J. Falck, T. Schroeder, L. Rönnstrand, K.K. Khanna, B.-B. Zhou, J. Bartek, and J. Lukas. 2003. Chk1 regulates the S phase checkpoint by coupling the physiological turnover and ionizing radiation-induced accelerated proteolysis of Cdc25A. *Cancer Cell*. 3:247-258.

Sosman, J.A., K.B. Kim, L. Schuchter, R. Gonzalez, A.C. Pavlick, J.S. Weber, G.A. McArthur, T.E. Hutson, S.J. Moschos, K.T. Flaherty, P. Hersey, R. Kefford, D. Lawrence, I. Puzanov, K.D. Lewis, R.K. Amaravadi, B. Chmielowski, H.J. Lawrence, Y. Shyr, F. Ye, J. Li, K.B. Nolop, R.J. Lee, A.K. Joe, and A. Ribas. 2012. Survival in BRAF V600–Mutant Advanced Melanoma Treated with Vemurafenib. *N. Engl. J. Med.* 366:707-714.

Speroni, J., M.B. Federico, S.F. Mansilla, G. Soria, and V. Gottifredi. 2012. Kinase-independent function of checkpoint kinase 1 (Chk1) in the replication of damaged DNA. *Proc. Natl. Acad. Sci.* 109:7344-7349.

Spycher, C., E.S. Miller, K. Townsend, L. Pavic, N.A. Morrice, P. Janscak, G.S. Stewart, and M. Stucki. 2008. Constitutive phosphorylation of MDC1 physically links the MRE11–RAD50–NBS1 complex to damaged chromatin. *J. Cell. Biol.* 181:227-240.

Stary, A., P. Kannouche, A.R. Lehmann, and A. Sarasin. 2003. Role of DNA Polymerase eta in the UV Mutation Spectrum in Human Cells. *J. Biol. Chem.* 278:18767-18775.

Stelter, P., and H.D. Ulrich. 2003. Control of spontaneous and damage-induced mutagenesis by SUMO and ubiquitin conjugation. *Nature*. 425:188-191.

Stewart, G.S., B. Wang, C.R. Bignell, A.M.R. Taylor, and S.J. Elledge. 2003. MDC1 is a mediator of the mammalian DNA damage checkpoint. *Nature*. 421:961-966.

Stiff, T., M. O'Driscoll, N. Rief, K. Iwabuchi, M. Löbrich, and P.A. Jeggo. 2004. ATM and DNA-PK Function Redundantly to Phosphorylate H2AX after Exposure to Ionizing Radiation. *Cancer Res.* 64:2390-2396.

Stokes, M.P., J. Rush, J. MacNeill, J.M. Ren, K. Sprott, J. Nardone, V. Yang, S.A. Beausoleil, S.P. Gygi, M. Livingstone, H. Zhang, R.D. Polakiewicz, and M.J. Comb. 2007. Profiling of UV-induced ATM/ATR signaling pathways. *Proc. Natl. Acad. Sci.* 104:19855-19860.

Sugasawa, K., J.M.Y. Ng, C. Masutani, S. Iwai, P.J. van der Spek, A.P.M. Eker, F. Hanaoka, D. Bootsma, and J.H.J. Hoeijmakers. 1998. Xeroderma Pigmentosum Group C Protein Complex Is the Initiator of Global Genome Nucleotide Excision Repair. *Mol. Cell*. 2:223-232.

Sugiyama, H., Y. Tsutsumi, and I. Saito. 1990. Highly sequence-selective photoreaction of 5-bromouracil-containing deoxyhexanucleotides. *J. Am. Chem. Soc.* 112:6720-6721.

Sugiyama, T., and S.C. Kowalczykowski. 2002. Rad52 Protein Associates with Replication Protein A (RPA)-Single-stranded DNA to Accelerate Rad51-mediated Displacement of RPA and Presynaptic Complex Formation. *J. Biol. Chem.* 277:31663-31672.

Sun, Y., X. Jiang, S. Chen, N. Fernandes, and B.D. Price. 2005. A role for the Tip60 histone acetyltransferase in the acetylation and activation of ATM. *Proc. Natl. Acad. Sci. U. S. A.* 102:13182-13187.

Sun, Y., Y. Xu, K. Roy, and B.D. Price. 2007. DNA Damage-Induced Acetylation of Lysine 3016 of ATM Activates ATM Kinase Activity. *Mol. Cell. Biol.* 27:8502-8509.

Syljuåsen, R.G., C.S. Sørensen, L.T. Hansen, K. Fugger, C. Lundin, F. Johansson, T. Helleday, M. Sehested, J. Lukas, and J. Bartek. 2005. Inhibition of Human Chk1 Causes Increased Initiation of DNA Replication, Phosphorylation of ATR Targets, and DNA Breakage. *Mol. Cell. Biol.* 25:3553-3562.

Symington, L.S., and J. Gautier. 2011. Double-Strand Break End Resection and Repair Pathway Choice. *Annu. Rev. Genet.* 45:247-271.

Szabó, G. 1954. The Number of Melanocytes in Human Epidermis. *Br med. J.* 1:1016-1017.

Tadokoro, T., N. Kobayashi, B.Z. Zmudzka, S. Ito, K. Wakamatsu, Y. Yamaguchi, K.S. Korossy, S.A. Miller, J.Z. Beer, and V.J. Hearing. 2003. UV-induced DNA damage and melanin content in human skin differing in racial/ethnic origin. *FASEB J.* 17:1177-1179.

Takai, H., K. Naka, Y. Okada, M. Watanabe, N. Harada, S.i. Saito, C.W. Anderson, E. Appella, M. Nakanishi, H. Suzuki, K. Nagashima, H. Sawa, K. Ikeda, and N. Motoyama. 2002. Chk2-deficient mice exhibit radioresistance and defective p53-mediated transcription. *EMBO J.* 21:5195-5205.

Takai, H., R.C. Wang, K.K. Takai, H. Yang, and T. de Lange. 2007. Tel2 Regulates the Stability of PI3K-Related Protein Kinases. *Cell*. 131:1248-1259.

Takanashi, T., Y. Ogura, H. Taguchi, M. Hashizoe, and Y. Honda. 1997. Fluorophotometric quantitation of oxidative stress in the retina in vivo. *Invest. Ophthalmol. Vis. Sci.* 38:2721-2728.

Takeuchi, S., W. Zhang, K. Wakamatsu, S. Ito, V.J. Hearing, K.H. Kraemer, and D.E. Brash. 2004. Melanin acts as a potent UVB photosensitizer to cause an atypical mode of cell death in murine skin. *Proc. Natl. Acad. Sci. U. S. A.* 101:15076-15081.

Tanaka, A., S. Weinel, N. Nagy, M. O'Driscoll, Joey E. Lai-Cheong, Carol L. Kulp-Shorten, A. Knable, G. Carpenter, Sheila A. Fisher, M. Hiragun, Y. Yanase, M. Hide, J. Callen, and John A. McGrath. 2012. Germline Mutation in ATR in Autosomal- Dominant Oropharyngeal Cancer Syndrome. *Am. J. Hum. Genet.* 90:511-517.

Tang, A., M.S. Eller, M. Hara, M. Yaar, S. Hirohashi, and B.A. Gilchrest. 1994. E-cadherin is the major mediator of human melanocyte adhesion to keratinocytes in vitro. *J. Cell Sci.* 107:983-992.

Tang, L., G. Li, V. Tron, M. Trotter, and V. Ho. 1999. Expression of cell cycle regulators in human cutaneous malignant melanoma. *Melanoma Res.* 9:148-154.

Tapia-Alveal, C., T. Calonge, and M. O'Connell. 2009. Regulation of Chk1. *Cell Division*. 4:8.

Taylor, A., P. Byrd, C. McConville, and S. Thacker. 1994. Genetic and cellular features of ataxia telangiectasia. *Int. J. Radiat. Biol.* 65:65-70.

Tho, L., S. Libertini, R. Rampling, O. Sansom, and D.A.F. Gillespie. 2012. Chk1 is essential for chemical carcinogen-induced mouse skin tumorigenesis. *Oncogene*. 31:1366-1375.

Thomas, N.E., M. Berwick, and M. Cordeiro-Stone. 2006. Could BRAF Mutations in Melanocytic Lesions Arise from DNA Damage Induced by Ultraviolet Radiation? *J. Invest. Dermatol.* 126:1693-1696.

Tian, F., S. Sharma, J. Zou, S.-Y. Lin, B. Wang, K. Rezvani, H. Wang, J.D. Parvin, T. Ludwig, C.E. Canman, and D. Zhang. 2013. BRCA1 promotes the ubiquitination of PCNA and recruitment of translesion polymerases in response to replication blockade. *Proc. Natl. Acad. Sci.* 110:13558-13563.

Tibbetts, R.S., K.M. Brumbaugh, J.M. Williams, J.N. Sarkaria, W.A. Cliby, S.-Y. Shieh, Y. Taya, C. Prives, and R.T. Abraham. 1999. A role for ATR in the DNA damage-induced phosphorylation of p53. *Genes Dev.* 13:152-157.

Tibbetts, R.S., D. Cortez, K.M. Brumbaugh, R. Scully, D. Livingston, S.J. Elledge, and R.T. Abraham. 2000. Functional interactions between BRCA1 and the checkpoint kinase ATR during genotoxic stress. *Genes Dev.* 14:2989-3002.

Tissier, A., E.G. Frank, J.P. McDonald, S. Iwai, F. Hanaoka, and R. Woodgate. 2000. Misinsertion and bypass of thymine-thymine dimers by human DNA polymerase iota. *EMBO J.* 19:5259-5266.

Tornaletti, S., and G.P. Pfeifer. 1996. UV damage and repair mechanisms in mammalian cells. *Bioessays*. 18:221-228.

Trenz, K., A. Errico, and V. Costanzo. 2008. Plx1 is required for chromosomal DNA replication under stressful conditions. *EMBO J.* 27:876-885.

Tse, A.N., K.G. Rendahl, T. Sheikh, H. Cheema, K. Aardalen, M. Embry, S. Ma, E.J. Moler, Z.J. Ni, D.E. Lopes de Menezes, B. Hibner, T.G. Gesner, and G.K. Schwartz. 2007. CHIR-124, a Novel Potent Inhibitor of Chk1, Potentiates the Cytotoxicity of Topoisomerase I Poisons In vitro and In vivo. *Clin. Cancer Res.* 13:591-602.

Tung, B.S., W.G. McGregor, Y.-C. Wang, V.M. Maher, and J.J. McCormick. 1996. Comparison of the rate of excision of major UV photoproducts in the strands of the human HPRT gene of normal and xeroderma pigmentosum variant cells. *Mutat. Res.* 362:65-74.

Tyrrell, R.M. 1973. Induction of pyrimidine dimers in bacterial DNA by 365 nm radiation *Photochem. Photobiol.* 17:69-73.

Ulrich, H.D., and S. Jentsch. 2000. Two RING finger proteins mediate cooperation between ubiquitin-conjugating enzymes in DNA repair. *EMBO J.* 19:3388-3397.

Uziel, T., Y. Lerenthal, L. Moyal, Y. Andegeko, L. Mittelman, and Y. Shiloh. 2003. Requirement of the MRN complex for ATM activation by DNA damage. *EMBO J.* 22:5612-5621.

Valluet, A., S. Druillennec, C. Barbotin, C. Dorard, Anne H. Monsoro-Burq, M. Larcher, C. Pouponnot, M. Baccarini, L. Larue, and A. Eychène. 2012. B-Raf and C-Raf Are Required for Melanocyte Stem Cell Self-Maintenance. *Cell Reports*. 2:774-780.

van de Water, B., I.B. Tijdens, A. Verbrugge, M. Huigsloot, A.A. Dihal, J.L. Stevens, S. Jaken, and G.J. Mulder. 2000. Cleavage of the Actin-capping Protein α-Adducin at Asp-Asp-Ser-Asp633-Ala by Caspase-3 Is Preceded by Its Phosphorylation on Serine 726 in Cisplatin-induced Apoptosis of Renal Epithelial Cells. *J. Biol. Chem.* 275:25805-25813.

Veierød, M.B., E. Weiderpass, M. Thörn, J. Hansson, E. Lund, B. Armstrong, and H.-O. Adami. 2003. A Prospective Study of Pigmentation, Sun Exposure, and Risk of Cutaneous Malignant Melanoma in Women. *J. Natl. Cancer Inst.* 95:1530-1538.

Vermeulen, K., D.R. Van Bockstaele, and Z.N. Berneman. 2003. The cell cycle: a review of regulation, deregulation and therapeutic targets in cancer. *Cell Prolif.* 36:131-149.

Vilar, E., and S.B. Gruber. 2010. Microsatellite instability in colorectal cancer-the stable evidence. *Nat Rev Clin Oncol*. 7:153-162.

Vo, A.T., F. Zhu, X. Wu, F. Yuan, Y. Gao, L. Gu, G.-M. Li, T.-H. Lee, and C. Her. 2005. hMRE11 deficiency leads to microsatellite instability and defective DNA mismatch repair. *EMBO Rep*. 6:438-444.

Volpe, J.P.G., and J.E. Cleaver. 1995. Xeroderma pigmentosum variant cells are resistant to immortalization. *Mutat. Res.* 337:111-117.

Wade Harper, J., G.R. Adami, N. Wei, K. Keyomarsi, and S.J. Elledge. 1993. The p21 Cdk-interacting protein Cip1 is a potent inhibitor of G1 cyclin-dependent kinases. *Cell*. 75:805-816.

Walker, M., E.J. Black, V. Oehler, D.A. Gillespie, and M.T. Scott. 2009. Chk1 C-terminal regulatory phosphorylation mediates checkpoint

activation by de-repression of Chk1 catalytic activity. *Oncogene*. 28:2314-2323.

Wang, C., and S.P. Lees-Miller. 2013. Detection and Repair of Ionizing Radiation-Induced DNA Double Strand Breaks: New Developments in Nonhomologous End Joining. *Int. J. Radiat. Oncol. Biol. Phys.* 86:440-449.

Wang, H.-T., B. Choi, and M.-s. Tang. 2010. Melanocytes are deficient in repair of oxidative DNA damage and UV-induced photoproducts. *Proc. Natl. Acad. Sci.* 107:12180-12185.

Wang, J., X. Han, and Y. Zhang. 2012. Autoregulatory Mechanisms of Phosphorylation of Checkpoint Kinase 1. *Cancer Res.* 72:3786-3794.

Wang, S.Q., R. Setlow, M. Berwick, D. Polsky, A.A. Marghoob, A.W. Kopf, and R.S. Bart. 2001. Ultraviolet A and melanoma: A review. *J. Am. Acad. Dermatol.* 44:837-846.

Wang, X., R.D. Kennedy, K. Ray, P. Stuckert, T. Ellenberger, and A.D. D'Andrea. 2007a. Chk1-Mediated Phosphorylation of FANCE Is Required for the Fanconi Anemia/BRCA Pathway. *Mol. Cell. Biol.* 27:3098-3108.

Wang, X., L. Zou, T. Lu, S. Bao, K.E. Hurov, W.N. Hittelman, S.J. Elledge, and L. Li. 2006. Rad17 Phosphorylation Is Required for Claspin Recruitment and Chk1 Activation in Response to Replication Stress. *Mol. Cell*. 23:331-341.

Wang, Y., R. Woodgate, T.P. McManus, S. Mead, J.J. McCormick, and V.M. Maher. 2007b. Evidence that in Xeroderma Pigmentosum Variant Cells, which Lack DNA Polymerase η, DNA Polymerase ι Causes the Very High Frequency and Unique Spectrum of UV-Induced Mutations. *Cancer Res.* 67:3018-3026.

Ward, I.M., and J. Chen. 2001. Histone H2AX Is Phosphorylated in an ATR-dependent Manner in Response to Replicational Stress. *J. Biol. Chem.* 276:47759-47762.

Ward, I.M., K. Minn, K.G. Jorda, and J. Chen. 2003. Accumulation of Checkpoint Protein 53BP1 at DNA Breaks Involves Its Binding to Phosphorylated Histone H2AX. *J. Biol. Chem.* 278:19579-19582.

Watanabe, K., S. Tateishi, M. Kawasuji, T. Tsurimoto, H. Inoue, and M. Yamaizumi. 2004a. Rad18 guides pol eta to replication stalling sites through physical interaction and PCNA monoubiquitination. *EMBO J.* 23:3886-3896.

Watanabe, N., H. Arai, Y. Nishihara, M. Taniguchi, N. Watanabe, T. Hunter, and H. Osada. 2004b. M-phase kinases induce phospho-dependent ubiquitination of somatic Wee1 by SCFβ-TrCP. *Proc. Natl. Acad. Sci. U. S. A.* 101:4419-4424.

Waters , L.S., B.K. Minesinger, M.E. Wiltrout, S. D'Souza, R.V. Woodruff, and G.C. Walker. 2009. Eukaryotic Translesion Polymerases and Their Roles and Regulation in DNA Damage Tolerance. *Microbiol. Mol. Biol. Rev.* 73:134-154.

Watt, A.A.R., J.P. Bothma, and P. Meredith. 2009. The supramolecular structure of melanin. *Soft Matter*. 5:3754-3760.

Watters, D., P. Kedar, K. Spring, J. Bjorkman, P. Chen, M. Gatei, G. Birrell, B. Garrone, P. Srinivasa, D.I. Crane, and M.F. Lavin. 1999.

Localization of a Portion of Extranuclear ATM to Peroxisomes. *J. Biol. Chem.* 274:34277-34282.

Wenczl, E., G.P. Van der Schans, L. Roza, R.M. Kolb, A.J. Timmerman, N.P. Smit, S. Pavel, and A.A. Schothorst. 1998. (Pheo)melanin photosensitizes UVA-induced DNA damage in cultured human melanocytes. *J. Invest. Dermatol.* 111:678-682.

Whiteman, D., and A. Green. 2011. Epidemiology of Malignant Melanoma. *In* Skin Cancer - A World-Wide Perspective. R. Dummer, M.R. Pittelkow, K. Iwatsuki, A. Green, and N.M. Elwan, editors. Springer Berlin Heidelberg. 13-26.

Whiteman, D., C. Whiteman, and A. Green. 2001. Childhood sun exposure as a risk factor for melanoma: a systematic review of epidemiologic studies. *Cancer Causes Control*. 12:69-82.

Whiteman, D.C., W.J. Pavan, and B.C. Bastian. 2011. The melanomas: a synthesis of epidemiological, clinical, histopathological, genetic, and biological aspects, supporting distinct subtypes, causal pathways, and cells of origin. *Pigment Cell Melanoma Res.* 24:879-897.

Wicks, Nadine L., Jason W. Chan, Julia A. Najera, Jonathan M. Ciriello, and E. Oancea. 2011. UVA Phototransduction Drives Early Melanin Synthesis in Human Melanocytes. *Curr. Biol.* 21:1906-1911.

Wikonkal, N., and D. Brash. 1999. Ultraviolet radiation induced signature mutations in photocarcinogenesis. *J. Investig. Dermatol. Symp. Proc.* 4:6-10.

Wittgen, H.G.M., and L.C.L.T. van Kempen. 2007. Reactive oxygen species in melanoma and its therapeutic implications. *Melanoma Res.* 17:400-409

Wold, M.S. 1997. Replication Protein A:A Heterotrimeric, Single-Stranded DNA-Binding Protein Required for Eukaryotic DNA Metabolism. *Annu. Rev. Biochem.* 66:61-92.

Wondrak, G.T., M.K. Jacobson, and E.L. Jacobson. 2006. Endogenous UVA-photosensitizers: mediators of skin photodamage and novel targets for skin photoprotection. *Photochem. Photobiol. Sci.* 5:215-237.

Wright, J.A., K.S. Keegan, D.R. Herendeen, N.J. Bentley, A.M. Carr, M.F. Hoekstra, and P. Concannon. 1998. Protein kinase mutants of human ATR increase sensitivity to UV and ionizing radiation and abrogate cell cycle checkpoint control. *Proc. Natl. Acad. Sci.* 95:7445-7450.

Wu, X., S.M. Shell, Y. Liu, and Y. Zou. 2006. ATR-dependent checkpoint modulates XPA nuclear import in response to UV irradiation. *Oncogene*. 26:757-764.

Xiao, Z., Z. Chen, A.H. Gunasekera, T.J. Sowin, S.H. Rosenberg, S. Fesik, and H. Zhang. 2003. Chk1 Mediates S and G2 Arrests through Cdc25A Degradation in Response to DNA-damaging Agents. *J. Biol. Chem.* 278:21767-21773.

Xu, N., S. Libertini, Y. Zhang, and D.A. Gillespie. 2011. Cdk phosphorylation of Chk1 regulates efficient Chk1 activation and multiple checkpoint proficiency. *Biochem. Biophys. Res. Commun.* 413:465-470.

Yajima, H., K.-J. Lee, S. Zhang, J. Kobayashi, and B.P.C. Chen. 2009. DNA Double-Strand Break Formation upon UV-Induced

Replication Stress Activates ATM and DNA-PKcs Kinases. *J. Mol. Biol.* 385:800-810.

Yamada, A., C. Masutani, S. Iwai, and F. Hanaoka. 2000. Complementation of defective translesion synthesis and UV light sensitivity in xeroderma pigmentosum variant cells by human and mouse DNA polymerase η. *Nucleic Acids Res.* 28:2473-2480.

Yamashita, A., T. Ohnishi, I. Kashima, Y. Taya, and S. Ohno. 2001. Human SMG-1, a novel phosphatidylinositol 3-kinase-related protein kinase, associates with components of the mRNA surveillance complex and is involved in the regulation of nonsense-mediated mRNA decay. *Genes Dev.* 15:2215-2228.

Yanagihara, H., J. Kobayashi, S. Tateishi, A. Kato, S. Matsuura, H. Tauchi, K. Yamada, J. Takezawa, K. Sugasawa, C. Masutani, F. Hanaoka, Corry M. Weemaes, T. Mori, L. Zou, and K. Komatsu. 2011. NBS1 Recruits RAD18 via a RAD6-like Domain and Regulates Pol ·-Dependent Translesion DNA Synthesis. *Mol. Cell*. 43:788-797.

Yang, K., C.P. Weinacht, and Z. Zhuang. 2013. Regulatory Role of Ubiquitin in Eukaryotic DNA Translesion Synthesis. *Biochemistry*. 52:3217-3228.

Yang, X.H., B. Shiotani, M. Classon, and L. Zou. 2008. Chk1 and Claspin potentiate PCNA ubiquitination. *Genes Dev.* 22:1147-1152.

Yavuz, S., A.S. Yavuz, K.H. Kraemer, and P.E. Lipsky. 2002. The Role of Polymerase η in Somatic Hypermutation Determined by Analysis of Mutations in a Patient with Xeroderma Pigmentosum Variant. *J. Immunol.* 169:3825-3830.

Yavuzer, U., and C.R. Goding. 1994. Melanocyte-specific gene expression: role of repression and identification of a melanocyte-specific factor, MSF. *Mol. Cell. Biol.* 14:3494-3503.

Yohn, J.J., M.B. Lyons, and D.A. Norris. 1992. Cultured Human Melanocytes from Black and White Donors Have Different Sunlight and Ultraviolet A Radiation Sensitivities. *J. Invest. Dermatol.* 99:454-459.

You, Y.-H., D.-H. Lee, J.-H. Yoon, S. Nakajima, A. Yasui, and G.P. Pfeifer. 2001. Cyclobutane Pyrimidine Dimers Are Responsible for the Vast Majority of Mutations Induced by UVB Irradiation in Mammalian Cells. *J. Biol. Chem.* 276:44688-44694.

Yuan, J., G. Ghosal, and J. Chen. 2012. The HARP-like Domain-Containing Protein AH2/ZRANB3 Binds to PCNA and Participates in Cellular Response to Replication Stress. *Mol. Cell*. 47:410-421.

Yusufzai, T., X. Kong, K. Yokomori, and J.T. Kadonaga. 2009. The annealing helicase HARP is recruited to DNA repair sites via an interaction with RPA. *Genes Dev.* 23:2400-2404.

Zachos, G., E.J. Black, M. Walker, M.T. Scott, P. Vagnarelli, W.C. Earnshaw, and D.A.F. Gillespie. 2007. Chk1 Is Required for Spindle Checkpoint Function. *Developmental Cell*. 12:247-260.

Zachos, G., and D. Gillespie. 2007. Exercising Restraints: Role of Chk1 in Regulating the Onset and Progression of Unperturbed Mitosis in Vertebrate Cells. *Cell Cycle*. 6:810-813.

Zachos, G., M.D. Rainey, and D.A.F. Gillespie. 2003. Chk1-deficient tumour cells are viable but exhibit multiple checkpoint and survival defects. *EMBO J.* 22:713-723.

Zachos, G., M.D. Rainey, and D.A.F. Gillespie. 2005. Chk1-Dependent S-M Checkpoint Delay in Vertebrate Cells Is Linked to Maintenance of Viable Replication Structures. *Mol. Cell. Biol.* 25:563-574.

Zeng-Rong, N., J. Paterson, L. Alpert, M.-S. Tsao, J. Viallet, and M.A. Alaoui-Jamali. 1995. Elevated DNA Repair Capacity Is Associated with Intrinsic Resistance of Lung Cancer to Chemotherapy. *Cancer Res.* 55:4760-4764.

Zhang, J., S. Bao, R. Furumai, K.S. Kucera, A. Ali, N.M. Dean, and X.-F. Wang. 2005a. Protein Phosphatase 5 Is Required for ATR-Mediated Checkpoint Activation. *Mol. Cell. Biol.* 25:9910-9919.

Zhang, Y.-W., D.M. Otterness, G.G. Chiang, W. Xie, Y.-C. Liu, F. Mercurio, and R.T. Abraham. 2005b. Genotoxic Stress Targets Human Chk1 for Degradation by the Ubiquitin-Proteasome Pathway. *Mol. Cell*. 19:607-618.

Zhang, Y., and Y. Xiong. 2001. A p53 Amino-Terminal Nuclear Export Signal Inhibited by DNA Damage-Induced Phosphorylation. *Science*. 292:1910-1915.

Zhao, H., and H. Piwnica-Worms. 2001. ATR-Mediated Checkpoint Pathways Regulate Phosphorylation and Activation of Human Chk1. *Mol. Cell. Biol.* 21:4129-4139.

Zharkov, D.O. 2008. Base excision DNA repair. *Cell. Mol. Life Sci.* 65:1544-1565.

Zhou, B.-B.S., and S.J. Elledge. 2000. The DNA damage response: putting checkpoints in perspective. *Nature*. 408:433-439.

Ziegler, A., D.J. Leffell, S. Kunala, H.W. Sharma, M. Gailani, J.A. Simon, A.J. Halperin, H.P. Baden, P.E. Shapiro, A.E. Bale, and D.E. Brash. 1993. Mutation Hotspots Due to Sunlight in the p53 Gene of Nonmelanoma Skin Cancers. *Proc. Natl. Acad. Sci. U. S. A.* 90:4216-4220.

Zimmermann, S., and K. Moelling. 1999. Phosphorylation and Regulation of Raf by Akt (Protein Kinase B). *Science*. 286:1741-1744.

Zlatanou, A., E. Despras, T. Braz-Petta, I. Boubakour-Azzouz, C. Pouvelle, Grant S. Stewart, S. Nakajima, A. Yasui, Alexander A. Ishchenko, and Patricia L. Kannouche. 2011. The hMsh2-hMsh6 Complex Acts in Concert with Monoubiquitinated PCNA and Pol eta in Response to Oxidative DNA Damage in Human Cells. *Mol. Cell*. 43:649-662.

Zou, L., and S.J. Elledge. 2003. Sensing DNA Damage through ATRIP Recognition of RPA-ssDNA Complexes. *Science*. 300:1542-1548.

Appendix

This section outlines (i) funding awards and scholarships supporting the research presented in this thesis, and (ii) details of presentation of this research at scientific meetings.

Funding

- *Postgraduate Research Scholarship,* Irish Research Council (IRC, formally IRCSET) (2009-2012). Awarded to S. Conmy
- *Skin Cancer Research Fund,* (2009). Awarded to Dr. M.P. Carty
- *Thomas Crawford Hayes Trust fund Scholarship,* National University of Ireland, Galway (2010). Awarded to S. Conmy
- *Beckman Fund Scholarship,* National University of Ireland, Galway (2011). Awarded to S. Conmy
- *Thomas Crawford Hayes Trust fund Scholarship,* National University of Ireland, Galway (2011). Awarded to S. Conmy
- *Thomas Crawford Hayes Trust fund Scholarship,* National University of Ireland, Galway (2012). Awarded to S. Conmy
- *Thomas Crawford Hayes Trust fund Scholarship-Travel award,* National University of Ireland, Galway (2012). Awarded to S. Conmy
- *Skin Cancer Research Fund,* (2012). Awarded to Dr. M.P. Carty
- *Beckman Fund Scholarship,* National University of Ireland, Galway (2013). Awarded to S. Conmy

Presentations (presenting author underlined)

Oral presentations:

- Conmy, S. and Carty, M.P. *Induction of DNA damage response pathways in primary normal human epidermal melanocytes exposed to long wavelength UVA radiation.* Irish Radiation Research Society conference, Sligo IT, September 2011. (Prize winning presentation)
- Conmy, S and Carty, M.P. *"Skin cancer: The dark side of UV light"* Martin Ryan Institute, Environment and Health Seminar Series, NUI, Galway, May 2012.

Poster presentations:

- Conmy, S and Carty, M.P. *Long-wavelength UVA radiation activates the DNA damage response in primary normal human melanocytes.* DNA Damage Response and Human Disease conference, IRB, Barcelona, May 2012.
- Conmy, S and Carty, M.P. *Long-wavelength UVA radiation activates the DNA Damage Response in cultured primary normal human epidermal melanocytes.* Royal Academy of Medicine in Ireland, Section of Biomedical science, Annual meeting, NUI, Galway, June 2012.